SYNTHETIC AND SPECTROSCOPIC INVESTIGATIONS OF THE 1,3 – DIPYRIDYLAZAALLYL "SMIF" ANION WITH 2^{ND} AND 3^{RD} ROW TRANSITION METALS AND A SERIES OF DIARYLIMINE IRON BIS-PHOSPHINE COMPLEXES THAT SELECTIVELY EXTRACT DINITROGEN FROM AIR

A Dissertation

Presented to the Faculty of the Graduate School

of Cornell University

in Partial Fulfillment of the Requirements for the Degree of

Doctor of Philosophy

by

Erika Rose Bartholomew

August 2013

SYNTHETIC AND SPECTROSCOPIC INVESTIGATIONS OF THE 1,3 – DIPYRIDYLAZAALLYL "SMIF" ANION WITH 2^{ND} AND 3^{RD} ROW TRANSITION METALS AND A SERIES OF DIARYLIMINE IRON PHOSPHINE COMPLEXES THAT SELECTIVELY EXTRACT DINITROGEN FROM AIR

Erika Rose Bartholomew, Ph.D.

Cornell University, 2013

Aryl-based chelates containing oxazoline or imine donors were synthesized, and their reactivity with 1^{st} -row transition metals were investigated in an attempt to generate metal complexes containing strong field ligands. Successful arylation of nickel was accomplished with a bis-methylated benzyl-oxazoline aryl anion. The reactivity of the dipyridyl imine ligand, 1,3-di-(2-pyridyl)-2-azapropene (**smifH),** was investigated with Ru, Rh, Ir, Mo and Pd. The d^6 bis-smif metal complexes were successfully generated with Ru, Rh and Ir, while carbon-carbon bond formation was observed with Mo and Pd. Treatment of *cis*-$(Me_3P)_4FeMe_2$ with *ortho*-substituted diarylimines afforded two equivalents of CH_4, PMe_3, and generated tris-PMe_3 Fe(II) complexes. Exposure to O_2 caused rapid degradation, but substitution of the unique PMe_3 with N_2 occurred upon exposure to air or N_2, yielding iron-dinitrogen compounds; CO, CNMe and N_2CPh_2 derivatives were also prepared. Dihydrogen or ammonia binding was found comparable to N_2, while PMe_3 and pyridine adducts were unfavorable. Protolytic conditions were modeled using primary acetylenes as weak acids, and *trans*-{κ-C,N-(3,4,5-$(F)_3$-C_6H_2)CH_2N=CH(3,4,6-$(F)_3$-C_6H-2-yl)}$Fe(PMe_3)_3$(CCR) (R = Me, Ph) were generated from *tris*-PMe_3 complexes. Reactions of *tris*-PMe_3 Fe(II)

with N_2O or tosyl azide generated iron-dinitrogen complexes and Me_3PO or $Me_3P{=}N(SO_2)tol$, respectively. Calculations revealed Fe-N_2 to be thermodynamically and kinetically favored over the calculated Fe(III) superoxide complex.

BIOGRAPHICAL SKETCH

Erika Bartholomew was born to Lee and Christine Bartholomew in Colorado Springs, CO. She was lucky enough to grow up on the lake in the small, southern town of Norwood, NC, with her brother, Joshua. Following in the footsteps of her big brother, she began her undergraduate career at the University of North Carolina at Charlotte. As a chemistry major at UNC Charlotte, Erika soon began undergraduate research with Dr. Brian Cooper exploring bioanalytical techniques, such as protein purification and capillary electrophoresis. The next year she was exposed to another area of research working for Dr. Craig Ogle. In his research group, she identified a passion for solving chemical puzzles and investigating chemical reactivity using NMR spectroscopy. Upon taking her first inorganic chemistry course with Dr. Tom Dubois, she discovered a subject she was excited to pursue further. In 2008, Erika decided to leave the warmth of the south, and continue her education at Cornell University. The decision to join the Wolczanski group was made from a desire to gain a synthetic skill set and a fundamental knowledge of inorganic/organometallic chemistry. Along with these attributes, it was clear from the beginning that this was a close-knit group where she would find many great friends and an incredible support system. After obtaining her Ph.D., Erika will be moving to Cranford, NJ to begin an exciting, albeit slightly puzzling adventure in the Basic Pharmaceutical Sciences group at Merck.

To my loving family,

Joshua, Christine and Lee Bartholomew

ACKNOWLEDGMENTS

I have been fortunate to be given the opportunity and experience to study at Cornell University, and though I am being granted this degree, I have not earned it on my own. It has been with the guidance, mentorship, support and love of many people that have helped me reach this point.

I would like to sincerely thank Peter T. Wolczanski for providing me with the opportunity to spend the last five years in his lab. It has certainly been a unique and growing experience, where I have been provided with years of direction, leadership, mentorship, patience (more than I deserve) and stern motivation when necessary. I have learned a great deal about teaching, chemistry, research and life in this lab and will continue to carry that with me. I would also like acknowledge Paul Chirik and Serena DeBeer, who provided me with guidance and support through my first 2 years of graduate school. The last few years of my graduate experience would certainly not have been the same without Kyle Lancaster; the many insightful conversations and friendly banter have been enjoyable and stress-relieving. Special thanks are due to Kyle Lancaster and Geoff Coates for stepping in and agreeing to serve on my committee; I am especially grateful. Tom Ruttledge also belongs on this long list of mentors I have been lucky to call upon. I sincerely value the many honest conversations we have shared, as well as the shoulder to lean on and invaluable advice.

I have been incredibly fortunate to follow in the footsteps of some amazing lab mates, who not only taught me about life in the Wolczanski lab, but who I am lucky to call close friends to this day. I have looked up to Elliott Hulley, Emily Sylvester and

Brenda Kuiper, who all significantly shaped my experience here, and I am lucky to have had them pave the way for me. I am also indebted to those who have been in the trenches with me for the last few years, and who have brought laughter and camaraderie into the daily lab life. Team Estrogen, Wesley Morris and Valerie Williams, have been immensely helpful and supportive teammates. Whether it has been with bad jokes or serious conversations about life and/or chemistry, Wes has been someone I have counted on day in and day out. It has been with much pleasure that I have spent the last 4 years with Valerie. She has an obvious passion for science, and I know it will take her far. I am only sorry that I will be leaving her all alone with Team Testosterone, though I know she is strong and can put the boys in their place. And finally, it has been a delight to share the lab with Brian Lindley for the last year. Brian is not only an extremely gifted scientist, but has a unique ability to diffuse situations with laughter, which has proven valuable on many occasions. I have no doubt the future of the lab is in very capable hands with him.

In these last few years, I have found exceptional friends and unwavering support. My experience has been both greatly enriched and exacerbated by the friendship, comfort and even occasional support of Jonathan Darmon. He has challenged, annoyed, and pushed me to the limits of sanity, and deserves plenty of acknowledgment (and blame) for this. I am forever grateful for the friendship of my fellow classmates, Megan Sikowitz and Angela DiCiccio. The countless nights of Northstar, movies and wine provided me with a miniature escape whenever needed.

There are plenty of Cornell staff members that have made a huge impact on my time here, as well. I owe a debt of gratitude to Dave Neish, Larry Stull, and Josh

Wakeman for being so attentive with the numerous issues our lab has faced. I must thank Pat Hine for her patience and help with the endless paperwork that seems to accompany graduate school, and for always empathizing with us graduate students when we need to vent. Without their hard work and friendliness, Cornell would be a much colder place.

Lastly, but most importantly, I must thank my family. My mom, whom I have relied on heavily for “warm wishes and happy thoughts”, who has taught me what hard work is, and the value therein, has been my rock. My dad, who has listened to my ups and downs nearly every day for the last five years (and the preceding 21 years, to be honest), has always believed in me, and without him, I would not have made it to this point. Finally, to my brother, Joshua, who has always cheered me on, and also put me in my place. I could not be luckier to have him on my side.

TABLE OF CONTENTS

LIST OF FIGURES

LIST OF TABLES

CHAPTER 1

SYNTHETIC INVESTIGATIONS OF 4,4-DIMETHYL-2-(2-PHENYLPROPAN-2-YL)OXAZOLINE WITH NICKEL[1]

I. Introduction

Synthetic targets frequently require organic transformations which necessitate the use of transition metal catalysts, and often the best catalysts contain 2nd or 3rd-row transition metals. Olefin metathesis chemistry is dominated by commercially available ruthenium and molybdenum catalysts,[2-4] whereas certain palladium complexes are incredibly competent cross coupling catalysts. Suzuki,[5,6] Heck[7-9] and Sonogarshira[10,11] cross-coupling reactions are responsible for enabling C-C transformations, and the Buchwald-Hartwig[12,13] catalysts are valuable for C-N and C-O coupling reactions, most of which rely on palladium (Fig. 1.1).

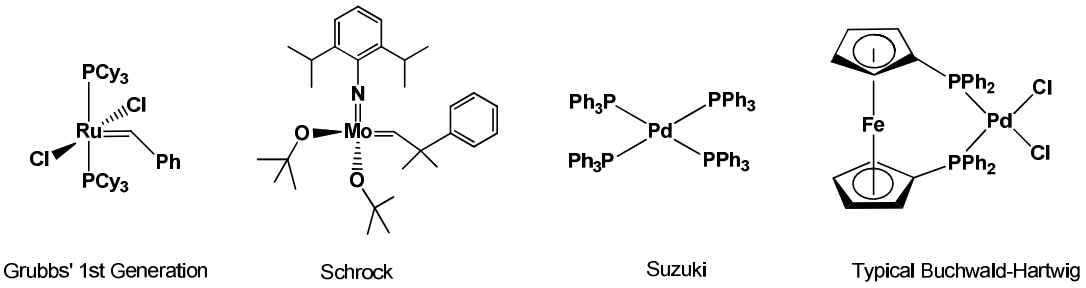

Figure 1.1. Examples of 2nd- and 3rd- row catalysts.

The ideal transition metal catalyst should be cost effective, non-toxic, and easily prepared. Generally, ligand modifications are used to alter and enhance the properties of a catalyst depending on desired reactivity. Proposed catalytic cycles for the transformations enabled by catalysts shown in Fig 1.1 invoke two electron

processes, such as oxidative addition and reductive elimination. First-row transition metals may look like an attractive alternative to 2^{nd} and 3^{rd}- row metals, as they are often cheaper and less toxic, yet first-row transition metal compounds are not used as frequently for catalysis. This is due, in part, to the weak fields exhibited by these complexes, which often lead to one-electron chemistry that can be unproductive for bond-making and bond-breaking processes. An on-going challenge remains to generate 1^{st}-row transition metal complexes with fields strong enough to effectively undergo the same two-electron processes invoked for the 2^{nd} and 3^{rd}-row metal catalysts.

First-row transition metal complexes containing metal-carbon bonds have stronger fields than those containing metal-nitrogen or metal-oxygen bonds.[14] Metal-aryl bonds are particularly appealing and should impart strong fields since carbon-based ligands have better orbital overlap than corresponding O- and N-based ligands ($S_C > S_N > S_O$). Aryls are also an attractive choice for carbon-based ligands because they do not undergo β-H eliminations, which are prevalent in sp^3 carbon-based ligands, and aryls form intrinsically stronger metal-carbon bonds. Angular overlap theory shows stronger fields arise from a more favorable interaction energy (Fig. 1.2), which is dependent on better orbital overlap, S, between metal 3d orbitals and ligands, and β.[15] A better energy match between metal-based orbitals and ligand-based orbitals, ΔE_{ML}, results in a larger β, and an overall larger interaction energy.

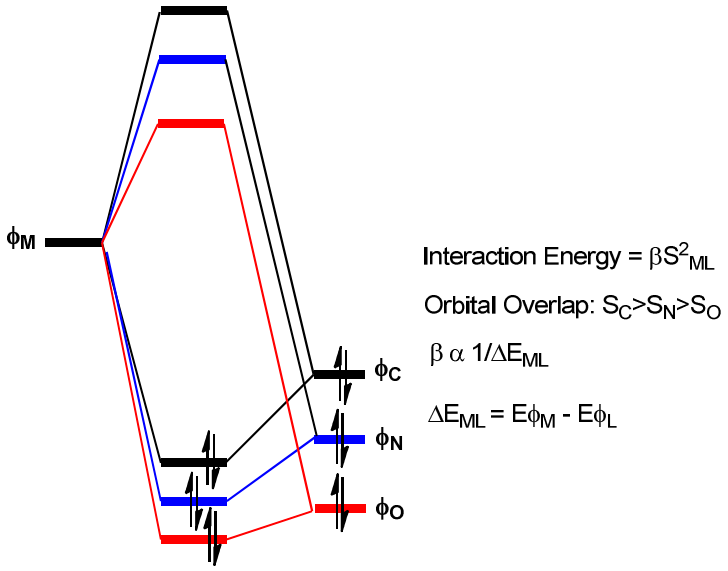

Figure 1.2. Angular overlap arguments that predict that C-based ligands should generate stronger fields than O- and N-based ligands based on β and S.

The preparation of oxazoline ligands are well known in the literature for their versatility and facile syntheses. Carboxylic acids or nitriles can be treated with amino alcohols to generate a wide variety of ligands. Aryl oxazolines are currently employed as ligands for 2nd- and 3rd- row transition metal catalysts,[16-21] and manganese,[22] nickel[23] and copper[24,25] oxazoline complexes have also been synthesized. The preparation of new low-spin, nickel oxazoline complexes was targeted with goals for cheaper and less toxic catalysts in mind.

II. Results and Discussion

A. Ligand Synthesis

The oxazoline ligand, 4,4-dimethyl-2-(2-bromophenylpropan-2-yl)-2-oxazoline (**BrPhCMe$_2$Ox**), was prepared according to modified literature procedures.

Dimethyl substitution on the methylene bridge inhibited the simple condensation generally used in oxazoline syntheses, so alternate routes were considered. The *ortho*-brominated 2-phenyl-2-methylpropionic acid was synthesized from double methylation of *o*-bromophenylacetic acid in two steps. The first methylation involved deprotonation with KOH, followed by treatment with methyl iodide. A stronger base, $LiN(^{i}Pr)_2$, was necessary for removal of the second proton and the final methylation. Heating to reflux in neat $SOCl_2$ converted the carboxylic acid to the acid chloride, which was subsequently treated with 2-amino-2-methyl-1-propanol and base to afford the corresponding amide. Cyclization of the amide using triethylamine and catalytic 4-DMAP generated **BrPhCMe$_2$Ox**. Lithium-halogen exchange of **BrPhCMe$_2$Ox** with ^{n}BuLi afforded **LiPhCMe$_2$Ox,** which was unstable above -78 °C.

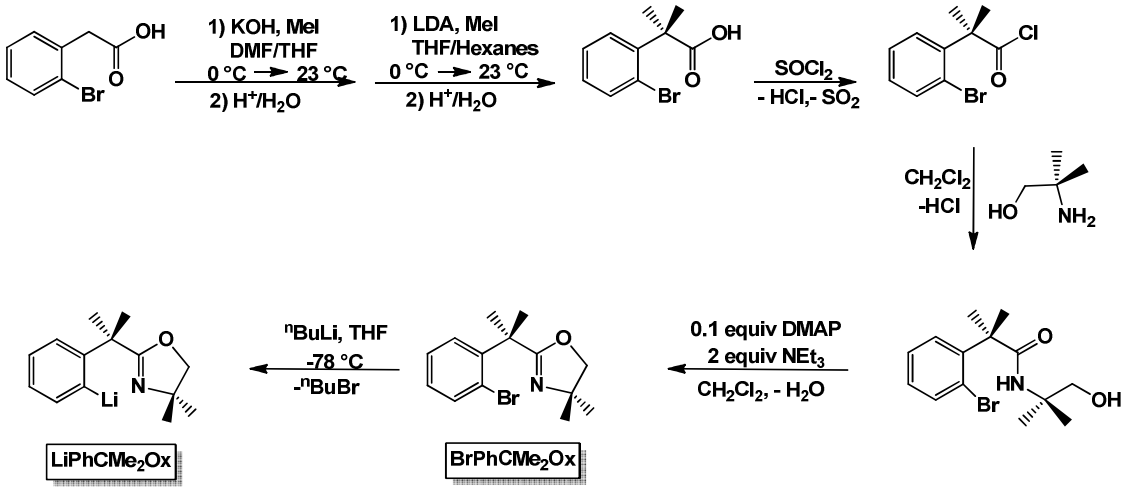

Scheme 1.1. Synthesis of **BrPhCMe$_2$Ox** and **LiPhCMe$_2$Ox**

B. Reactivity of 4,4-dimethyl-2-(2-phenylpropan-2-yl)oxazoline with Nickel.

1. Oxidative addition with nickel.

Previous heterolytic C-H activation attempts with $Ni(OTf)_2$ and **$HPhCMe_2Ox$** were unsuccessful, therefore the halide-substituted **$BrPhCMe_2Ox$** was used in attempt to oxidatively add to nickel, instilling a metal-carbon bond.

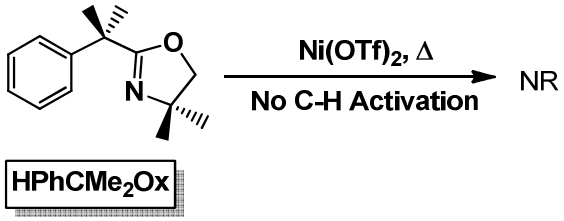

Scheme 1.2. Attempted C-H Activation of $HPhCMe_2Ox$ with $Ni(OTf)_2$.

As shown in Eq. 1.1, oxidative addition of $Ni(COD)_2$ to **$BrPhCMe_2Ox$** in toluene was successful, and dimeric $[\{\kappa\text{-C,N-}(o\text{-}C_6H_4)CMe_2(COCH_2CMe_2N)\}Ni]_2(\mu\text{-Br})_2$ (**1**) was isolated as an insoluble fuchsia solid in 80% yield. Although the dimeric species showed slight solubility in toluene, THF and CH_2Cl_2, **1** readily dissolved in acetonitrile to give a yellow-orange solution, which is likely indicative of the monomeric acetonitrile adduct.

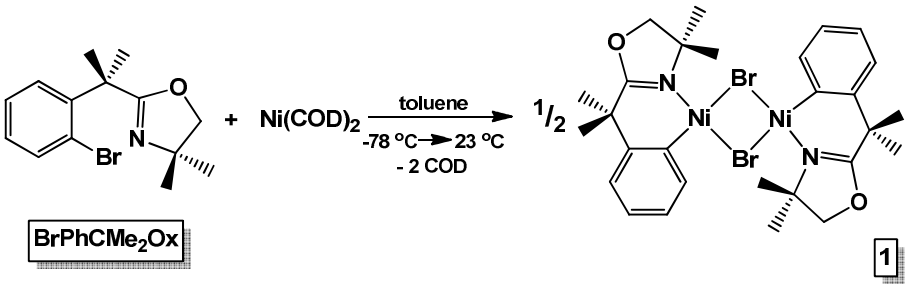

(1.1)

2. **Synthesis of $(PhCMe_2Ox)_2Zn$.**

As shown in Scheme 1.2, lithium-halogen exchange of **$BrPhCMe_2Ox$** successfully generated **$LiPhCMe_2Ox$**. Due to its observed degradation above -78 °C, a more convenient way to store and transfer the anionic **$PhCMe_2Ox$** ligand was targeted. If the lithiated ligand, **$LiPhCMe_2Ox$**, was held at or below -78 °C, then addition of ½ equiv of $ZnCl_2$ led to the organozinc complex, **$(PhCMe_2Ox)_2Zn$,** in 78% yield (Scheme 1.2).

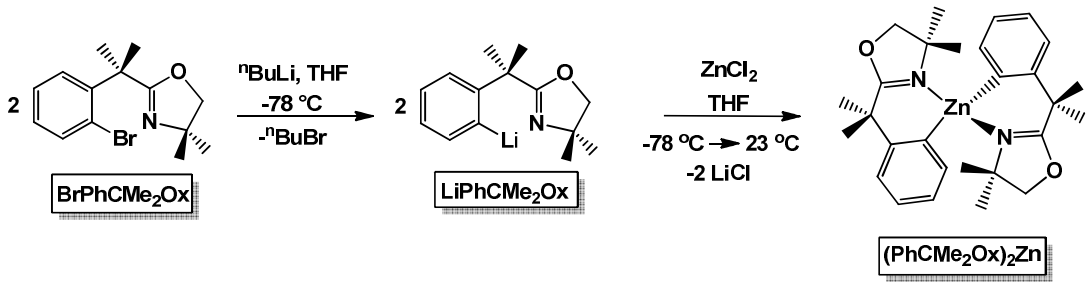

Scheme 1.2. Synthesis of **$(PhCMe_2Ox)_2Zn$**

3. **Synthesis of $\{\kappa$-C,N-(o-C_6H_4)$CMe_2(COCH_2CMe_2N)\}_2Ni$ (2).**

Transfer of two phenyloxazoline ligands was observed for the reaction of **$(PhCMe_2Ox)_2Zn$** with nickel. Treatment of $NiCl_2$(DME) with one equiv of **$(PhCMe_2Ox)_2Zn$** resulted in formation of $\{\kappa$-C,N-(o-C_6H_4)$CMe_2(COCH_2CMe_2N)\}_2Ni$ (**2**), albeit in a modest 25% yield after crystallization from THF/Et_2O. The ^1H NMR spectrum revealed resonances consistent with a diamagnetic complex consistent with the structure shown in Eq 1.2, including diastereotopic methylene and methyl protons.

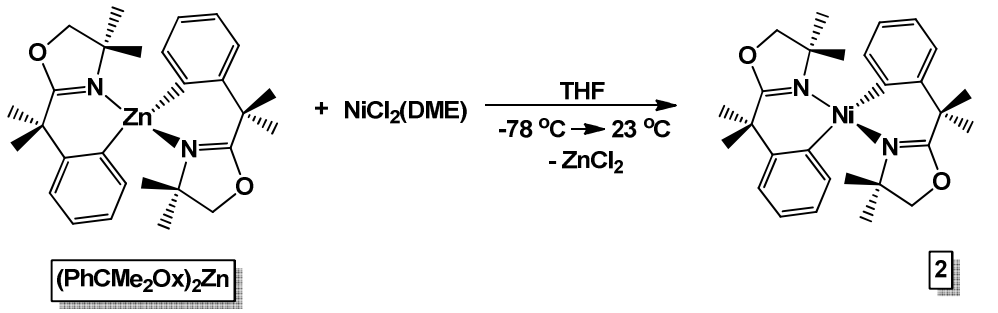

(1.2)

III. Conclusions

The synthesis of an oxazoline nickel dimer (**1)** was accomplished by oxidative addition of **BrPhCMe$_2$Ox** to Ni(COD)$_2$, however generation of the monomeric bis-oxazoline nickel complex, **2**, required a different strategy. *Ortho*-lithiation of the oxazoline ligand to form **LiPhCMe$_2$Ox** produced an anionic ligand. Due to temperature sensitivity, **LiPhCMe$_2$Ox** could be effectively stored in a stable zinc complex, (**PhCMe$_2$Ox)$_2$Zn,** and subsequently transferred to nickel. The installation of metal-aryl bonds resulted in relatively strong fields and generated low-spin complexes in the case of **1** and **2**, which both had ^{1}H NMR spectra consistent with diamagnetic complexes.

IV. Experimental

A. General Considerations

For metal complexes, manipulations were performed using either glovebox or high-vacuum techniques. Ligand syntheses were performed under argon using Schlenk techniques. Hydrocarbon and ethereal solvents were dried over and vacuum transferred from sodium benzophenone ketyl (with 3-4 mL of tetraglyme/L added to hydrocarbons). Methylene chloride was distilled from and stored over CaH_2. Benzene-

d_6 was sequentially dried over sodium and stored over sodium. THF-d_8 was dried over sodium benzophenone keyl. Acetonitrile-d_3 was dried over CaH_2 and stored over 4 Å molecular sieves. The compounds Ni(COD),[26] $NiCl_2$(DME)[27] were prepared according to literature procedures. $SOCl_2$ (Aldrich) was used immediately or distilled prior to use; NEt_3 (Aldrich) was dried and stored over 4Å molecular sieves; $ZnCl_2$ was dried according to a literature procedure;[28] all other reagents were purchased and used as received. All glassware was oven-dried.

^{1}H and ^{13}C{1H}NMR spectra were obtained using Mercury-300, Inova-400, and Inova-500 spectrometers, and chemical shifts are reported relative to benzene-d_6 (^{1}H δ 7.16; ^{13}C{1H} δ 128.39), THF-d_8 (^{1}H δ 3.58; ^{13}C{^{1}H} δ 67.57), and acetonitrile-d_3 (^{1}H δ 1.94; ^{13}C{1H} δ 1.79). Combustion analyses were performed by Complete Analysis Laboratories, Parsippany, NJ.

B. Procedures

1. 4,4-dimethyl-2-(2-phenylpropan-2-yl)oxazoline (BrPhCMe$_2$Ox).

A 50 mL three-neck round-bottom flask fitted with a reflux condenser and external oil bubbler was flushed with argon and charged with 15 mL of $SOCl_2$. A 13 mmol amount of R,R-dimethylbromophenylacetic acid was added, and the solution was heated to reflux for 3 h. The cooled mixture was then concentrated and triturated with CH_2Cl_2 (2 x 5 mL). The oily product was dissolved in 15 mL of CH_2Cl_2. A solution of 2-amino-2-methyl-1-propanol (1.39 g, 15.6 mmol) and NEt_3 (2.72 mL, 19.5 mmol) in 20 mL of CH_2Cl_2 was cooled to 0 °C. The acid chloride solution was added dropwise under argon. The reaction was allowed to warm slowly to 23 °C over

4 h and stirred for an addition 10 h. The mixture was washed first with H_2O (20 mL) then with brine (20 mL), and the organics were dried over $MgSO_4$, filtered, and concentrated. The crude product was recrystallized from 6:1 hexanes/ethyl acetate to yield a white, crystalline solid (90% after 3 crops). A 10 mmol amount of the above amide, 4-(dimethylamino)-pyridine (110 mg, 0.9 mmol), and NEt_3 (3.1 mL, 22 mmol) were dissolved in 30 mL of CH_2Cl_2. A solution of p-toluenesulfonyl chloride in 20mL of CH_2Cl_2 was added via syringe under argon. After stirring at 23 °C for 2 days, the reaction mixture was diluted with CH_2Cl_2 and extracted with saturated NH_4Cl followed by aqueous $NaHCO_3$. The organic layer was dried over $MgSO_4$, treated with decolorizing carbon, filtered, and concentrated. The crude product was purified by flash chromatography (6:1 hexanes/ethyl acetate) to give a clear oil (65%). ^{1}H NMR (400 MHz, benzene-d_6): δ 7.45 (d, J = 8.0, 1H), 7.18 (d, J = 8.0, 1H), 6.93 (t, J = 8, 1H), 6.66 (t, J = 8, 1H), 3.63 (s, 2H), 1.72 (s, 6H), 1.19 (s, 6H). ^{13}C{^{1}H} NMR (400 MHz, benzene-d_6): δ 170.24, 144.75, 135.31, 128.59, 128.22, 127.81, 124.84, 79.82, 67.73, 42.86, 28.58, 27.94.

2. [{κ-C,N-(*o*-C_6H_4)CMe_2($COCH_2CMe_2N$)}Ni]$_2$(μ-Br)$_2$ (1).

A solution of $BrPhCMe_2Ox$ (108 mg, 0.365 mmol) in 5 mL of toluene was added to $Ni(COD)_2$ (100 mg, 0.365 mmol) at -78 °C. Warming slowly to room temperature led to the formation of a pink precipitate. After stirring at 23 °C for ~4 h, the resulting dark pink solid was isolated by filtration and washing several times with toluene (49 mg, 80%). The compound is only sparingly soluble in toluene, THF, or dichloromethane, but dissolves in acetonitrile to give an orange-yellow solution, which is presumably {κ-C,N-(o-C_6H_4)CMe_2($COCH_2CMe_2N$)}NiBr-(NCMe). ^{1}H

NMR (500 MHz, acetonitrile-d_3): δ 7.17 (br s, 1H), 6.89 (d, J = 5.5, 1H), 6.83 (t, J = 7.2, 1H), 6.72 (t, J = 6.3, 1H), 4.01 (s, 2H), 2.43 (s, 6H), 1.38 (s, 6H). ^{13}C NMR (500 MHz, acetonitrile-d_3): δ 179.13, 149.04, 143.95, 138.62, 124.76, 124.45, 123.10, 82.60, 68.62, 44.59, 28.94, 27.70. Anal. Calcd for $C_{28}H_{36}Br_2N_2O_2Ni$: C, 47.38; H, 5.11; N, 3.95. Found: C, 46.92; H, 4.92, N, 3.70.

3. (PhCMe$_2$Ox)$_2$Zn.

^{n}BuLi (0.42 mL, 1.6 M in hexanes) was added to a solution of BrPhMe$_2$Ox (200 mg, 0.676 mmol) in 40 mL of THF at -78 °C under argon. After 3 h at -78 °C, $ZnCl_2$ (46.0 g, 0.338 mmol) was added via addition finger. The reaction was kept at -78 °C for at least 4 h and warmed to 23 °C over 4 h. The reaction mixture was stripped, triturated with benzene, and filtered, and the salt cake washed several times (4 x 30 mL). The mixture was stripped and triturated with pentane, yielding 131 mg (78%) of white solid, which was collected by filtration. ^{1}H NMR(500 MHz, benzene-d_6): δ 8.09 (dd, J = 6.5, 2.0, 1H), 7.49 (d, J = 7.0, 1H), 7.38-7.25 (m, 2H), 3.31 (s, 2H), 1.85 (s, 6H), 0.89 (s, 6H). ^{13}C NMR (500 MHz, benzene-d_6): δ 177.88, 162.09, 151.94, 140.46, 125.79, 125.28, 123.59, 78.79, 68.34, 43.80, 31.00, 28.01.

4. {κ-C,N-(*o*-C$_6$H$_4$)CMe$_2$(COCH$_2$CMe$_2$N)}$_2$Ni (2).

To a mixture of $NiCl_2$(DME) (0.880 mg, 0.282 mmol) and Zn(PhCMe$_2$Ox)$_2$ (200 mg, 0.282 mmol) was distilled 25 mL of THF at -78 °C. The yellow suspension was stirred at -78 °C for 5 h and slowly warmed to room temperature. The resulting orange solution was stripped, triturated with ether, and filtered to give a peach-colored solid. The solid was recrystallized from an ether/THF mixture to give a pale orange crystalline solid (34 mg, 25%). ^{1}H NMR (500 MHz, benzene-d_6): δ 7.23 (d, J = 7.2,

1H), 7.13 (d, *J* = 7.7, 1H), 6.98 (t, *J* = 7.3, 1H), 6.85 (t, *J* = 7.1, 1H), 3.66 (s, 3H), 3.36 (d, *J* = 8.1, 1H), 3.12 (d, *J* = 8.1, 1H), 1.81 (s, 3H), 0.94 (s, 3H), 0.69 (s, 3H). ^{13}C NMR(500 MHz, benzene-d_6): δ 177.82, 171.46, 148.36, 143.17, 124.28, 121.62, 121.20, 79.35, 68.97, 45.03, 35.51, 27.91, 25.47, 23.19). Anal. Calcd. for $C_{28}H_{36}N_2O_2Ni$: C, 68.45; H, 7.39; N, 5.70. Found: C, 68.36; H, 7.30; N, 5.62.

REFERENCES

(1) Volpe, E. C.; Manke, D. R.; Bartholomew, E. R.; Wolczanski, P. T.; Lobkovsky, E. B. *Organometallics* **2010**, *29*, 6642.

(2) Samojlowicz, C.; Bieniek, M.; Grela, K. *Chem. Rev. (Washington, DC, U. S.)* **2009**, *109*, 3708.

(3) La, D. S.; Sattely, E. S.; Ford, J. G.; Schrock, R. R.; Hoveyda, A. H. *J. Am. Chem. Soc.* **2001**, *123*, 7767.

(4) Alcaide, B.; Almendros, P.; Luna, A. *Chem. Rev. (Washington, DC, U. S.)* **2009**, *109*, 3817.

(5) Suzuki, A. *Angew. Chem., Int. Ed.* **2011**, *50*, 6722.

(6) Yin, L.; Liebscher, J. *Chem. Rev. (Washington, DC, U. S.)* **2007**, *107*, 133.

(7) Beletskaya, I. P.; Cheprakov, A. V. *Chem. Rev. (Washington, D. C.)* **2000**, *100*, 3009.

(8) Le, B. J.; Muzart, J. *Chem. Rev. (Washington, DC, U. S.)* **2011**, *111*, 1170.

(9) Weck, M.; Jones, C. W. *Inorg. Chem.* **2007**, *46*, 1865.

(10) Chinchilla, R.; Najera, C. *Chem. Rev. (Washington, DC, U. S.)* **2007**, *107*, 874.

(11) Doucet, H.; Hierso, J.-C. *Angew. Chem., Int. Ed.* **2007**, *46*, 834.

(12) Abaev, V. T.; Serdyuk, O. V. *Russ. Chem. Rev.* **2008**, *77*, 177.

(13) De, F. R. M.; Campagne, J. M.; Prim, D.; John Wiley & Sons, Inc.: 2012, p 77.

(14) Carnes, M.; Buccella, D.; Chen, J. Y. C.; Ramirez, A. P.; Turro, N. J.; Nuckolls, C.; Steigerwald, M. *Angew. Chem., Int. Ed.* **2009**, *48*, 290.

(15) Figgis, B. N. H., M. A. *Ligand Field Theory and Its Applications*; Wiley-VCH: New York, 2000.

(16) Bonnardel, P. A.; Parish, R. V.; Pritchard, R. G. *J. Chem. Soc., Dalton Trans.* **1996**, 3185.

(17) Chen, X.; Li, J.-J.; Hao, X.-S.; Goodhue, C. E.; Yu, J.-Q. *J. Am. Chem. Soc.* **2006**, *128*, 78.

(18) Davies, D. L.; Al-Duaij, O.; Fawcett, J.; Giardiello, M.; Hilton, S. T.; Russell, D. R. *Dalton Trans.* **2003**, 4132.

(19) Davies, D. L.; Al-Duaij, O.; Fawcett, J.; Singh, K. *Organometallics* **2010**, *29*, 1413.

(20) Giri, R.; Chen, X.; Yu, J.-Q. *Angew. Chem., Int. Ed.* **2005**, *44*, 2112.

(21) Yuan, K.; Zhang, T. K.; Hou, X. L. *J Org Chem* **2005**, *70*, 6085.

(22) Djukic, J.-P.; Michon, C.; Heiser, D.; Kyritsakas-Gruber, N.; De, C. A.; Doetz, K. H.; Pfeffer, M. *Eur. J. Inorg. Chem.* **2004**, 2107.

(23) Stol, M.; Snelders, D. J. M.; Godbole, M. D.; Havenith, R. W. A.; Haddleton, D.; Clarkson, G.; Lutz, M.; Spek, A. L.; Van, K. G. P. M.; Van, K. G. *Organometallics* **2007**, *26*, 3985.

(24) Berman, A. M.; Johnson, J. S. *J Org Chem* **2006**, *71*, 219.

(25) Wehman, E.; Van, K. G.; Jastrzebski, J. T. B. H.; Rotteveel, M. A.; Stam, C. H. *Organometallics* **1988**, *7*, 1477.

(26) Krysan, D. J.; Mackenzie, P. B. *J. Org. Chem.* **1990**, *55*, 4229.

(27) Ward, L. G. L. *Inorg. Syn.* **1971**, *13*, 154.

(28) Pray, A. R. *Inorg. Synth.* **1990**, *28*, 321.

CHAPTER 2

SYNTHETIC AND SPECTROSCOPIC INVESITGATIONS OF 1,3-DI-(2-PYRIDYL)-2-AZAALLYL ANION WITH 2ND- AND 3RD-ROW TRANSITION METALS

I. Introduction

Alfred Werner was the first to propose the octahedral configuration of transition metal complexes, and his contributions to inorganic chemistry earned him the Nobel Prize in 1913.[1,2] Since his work in the early 20th century, coordination chemistry has been a large focus of inorganic chemistry, and significant contributions have come from the investigation of amines and N-donor heterocycles.

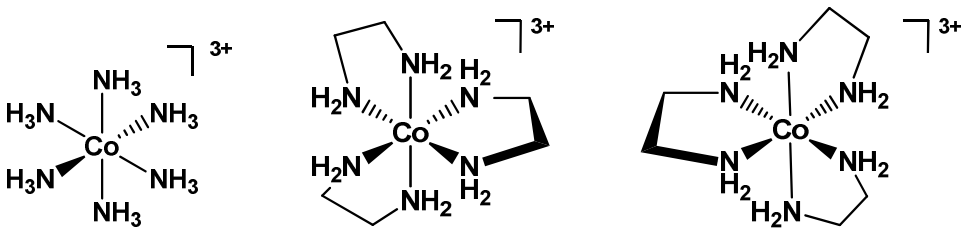

Figure 2.1. Examples of Werner complexes

Early work with N-based chelates focused on 2,6-bis(2-pyridyl)pyridine, commonly referred to as terpy, and 2,2'-bipyridine (bipy). Coordination of two molecules of terpy, bipy, or related derivatives around a metal center resulted in cationic species in most cases,[3-10] however neutral complexes have been synthesized where the metal has a formal oxidation state of zero.[11,12] Lower oxidation states of metals can be stabilized by terpy due to its electron accepting abilities, a circumstance where the ligand is considered redox non-innocent.[13]

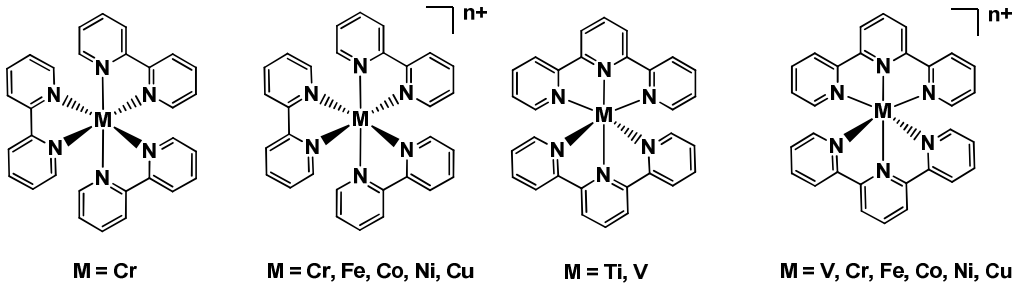

Figure 2.2. Examples of terpy and bipy complexes.

Metal complexes of terpy and bipy are of interest as they exhibit interesting optical and redox properties. For example, $[Ru(bpy)_3]^{2+}$ has been the center of much attention due to its photochemistry. Absorption of visible light by $[Ru(bpy)_3]^{2+}$ leads to the formation of the charge transfer excited state, which subsequently undergoes radiative decay, primarily phosphorescence, back to the ground state (Eq 2.1 and Eq 2.2).[14] $Ru(bpy)_3^{2+}$ and its derivatives have potential applications for photovoltaics and organic light-emitting diodes.[15,16]

$$Ru(bpy)_3^{2+} + hv \longrightarrow Ru(bpy)_3^{2+*} \quad (2.1)$$

$$Ru(bpy)_3^{2+*} \longrightarrow Ru(bpy)_3^{2+} + hv' \quad (2.2)$$

Many variations on terpy ligands have been studied since the original $M(terpy)_2$ complexes were prepared. Figure 2.3. shows examples of other tridentate N-donor ligands, whose corresponding metal complexes have also been prepared and well studied. Similar to terpy metal complexes, these ligands produced mostly cationic species, however (2-py)CH=NNH(2-py) can be easily deprotonated to form an anionic chelate and generate neutral metal complexes.[17]

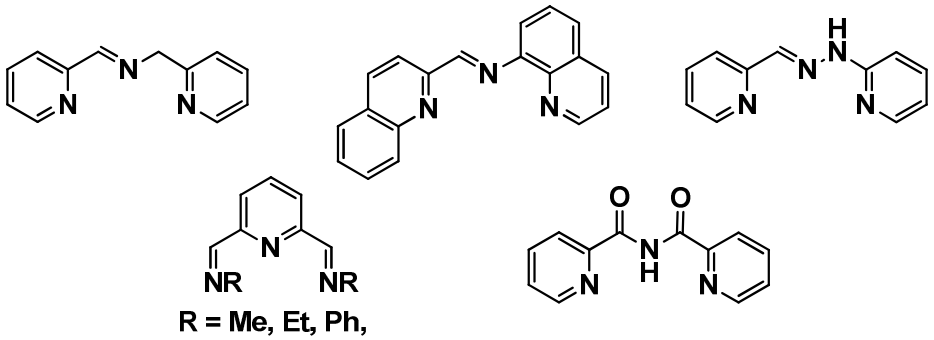

Figure 2.3. Examples of tridentate N-donor ligands

Metal (II) complexes of Mn,[18] Fe,[19] Ni,[20] Cu,[21] and Zn[18] coordinated with two bis(2-pyridylcarbonyl)aminate (bpca) ligands have been synthesized (Figure 2.4), and M(III) species have been prepared for Cr,[22] Fe,[19,20] and Co.[20,22] These complexes are generally isolated from aqueous solutions and have been used to generate multi-nuclear chains by chelation from the oxygen as well as the nitrogen.

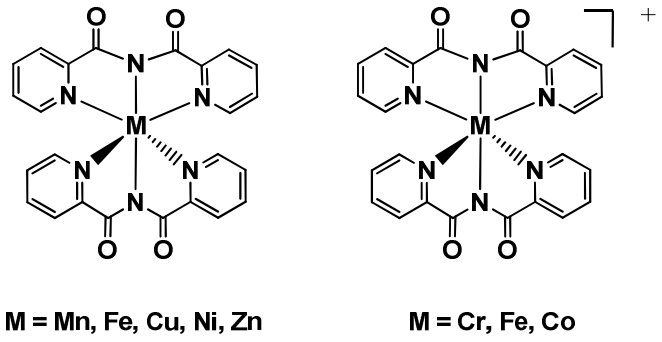

Figure 2.4. M(II) and M(III) bpca complexes.

While investigating another N-donor ligand, *N*-(2-bromo-4-*tert*-butylbenzyl)-1-(pyridine-2-yl)-*N*-(pyridine-2-ylmethyl)methanamine (**BrArpy$_2$N**), as a ligand for first row transition metals, a degradation occurred during the metallation reaction that

resulted in the formation of (smif)CrN(TMS)$_2$, where smif = 1,3-di-(2-pyridyl)-2-azaallyl).[23]

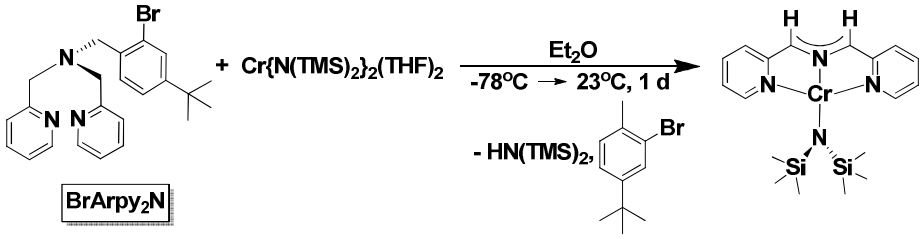

(2.3)

The smif ligand, (2-py)CHNCH(2-py), shown in Eq. 2.3, was originally discovered by Westerhausen and Kniefel in 2004 (Eq. 2.4).[24] This mono-anionic tridentate N-based chelate was the degradation product resulting from heating a mixture of $ZnMe_2$ and di-(2-picolyl)amine.[24] Since the formation of (smif)$_2$Zn was not the desired result, neither the complex nor the ligand were studied further by Westerhausen and Kniefe.

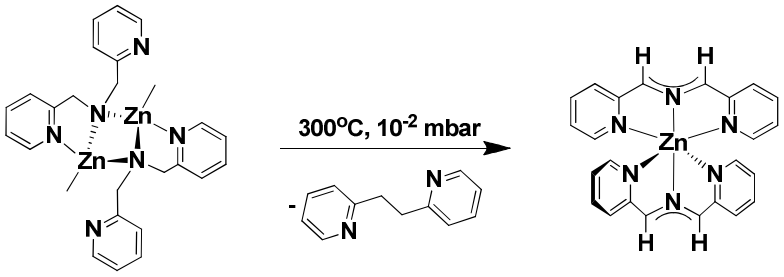

(2.4)

In the formation of (smif)CrN(TMS)$_2$, the chromium amide functioned as an internal base. With this understanding, an alternative synthetic route for its preparation was approached. The protonated ligand, **smifH**, could be treated with Cr{N(TMS)$_2$}$_2$THF$_2$, to afford (smif)$_2$Cr with concomitant loss of two equivs of HN(TMS)$_2$.[23] Alternatively, **smifH** could be deprotonated *in situ* and treated with M(II) halides in a salt metathesis reaction. Several first-row transition metal (smif)$_2$M

complexes were synthesized and revealed to possess remarkable optical properties. UV-Vis spectra for these complexes have intense intraligand charge transfer bands with molar absorptivities ranging from ~10,000 cm^{-1} to ~ 60,000 cm^{-1}.[25]

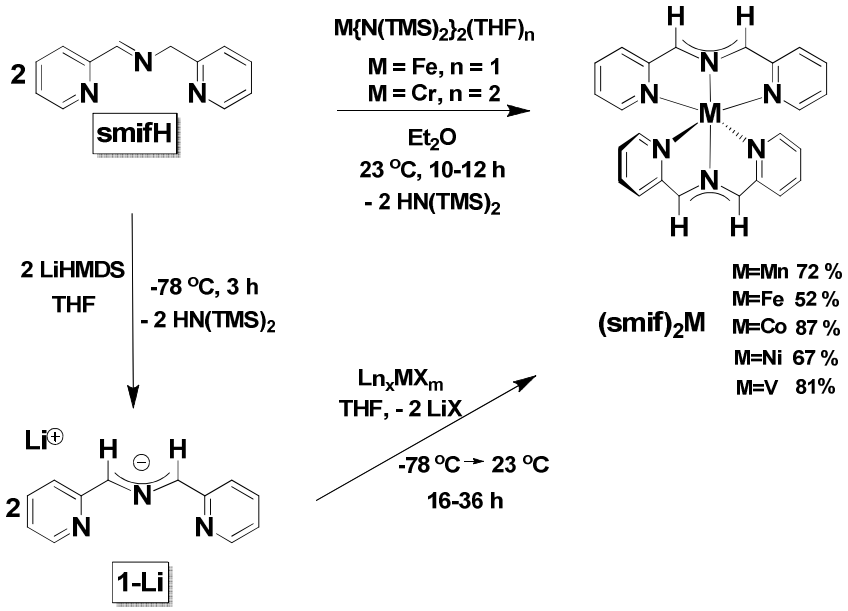

Scheme 2.1. Synthesis of $(smif)_2M$ complexes where M = V, Mn, Fe, Co, and Ni.

Research goals stemming from these discoveries focused on generating a series of $(smif)_2M$ complexes with 2nd and 3rd-row transition metals analogous to those prepared within the first row. Given the remarkable optical properties observed in the first row $(smif)_2M$ series, the possibility for observing photon emission from these complexes was of interest. Although photon emission from first-row transition metal complexes is rare, there is a greater possibility of detecting emission from second and third row transition metals. In addition to investigating the physical and optical properties for the targeted second row $(smif)_2M$ complexes, emission spectroscopy was used in order to observe any luminescence.

II. Results and Discussion

A. Synthesis of ligands.

Condensation of 2-pyridinecarboxaldehyde with 2-(aminomethyl)pyridine afforded 1,3-di-(2-pyridyl)-2-azapropene, **smifH**, according to literature procedures in quantitative yields (Eq. 2.5).[26]

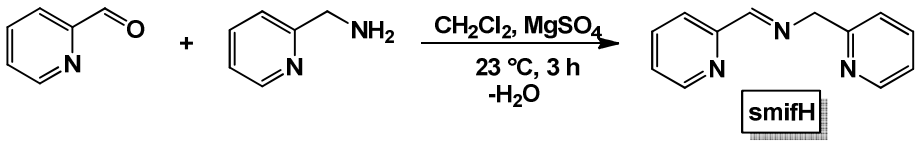

(2.5)

Deprotonation of the acidic benzylic methylene group on **smifH** generated the delocalized, anionic 1,3-di-(2-pyridyl)-2-azaallyl ligand, smif. As shown in Eq. 2.6, treatment of sodium hexamethydisilazide (NaHMDS) with a solution of **smifH** in THF produced a deep magenta solution from which sodium 1,3-di-(2-pyridyl)-2-azapropenide, **1-Na**, was isolated as a metallic-gold solid in 96% yield. The lithium analogue, **1-Li**, was generated by an identical procedure in 90% yield. Unique optical properties of the smif ligand were indicated by intensely colored solutions that were solvent dependent; benzene solutions generated a dark purple color, while Et_2O and THF solutions were deep magenta.

(2.6)

B. Synthesis of $[(smif)_2M]^{n+}$ Complexes [M = Ru, n = 0; M = Rh, Ir, n = 1].

First-row $(smif)_2M$ complexes were generated by a number of methods: internal base of metal amides with **smifH,** salt metathesis of M(II) halides with **1-Li**, and salt metathesis under reducing conditions. Efforts toward synthesizing 2nd- and 3rd-row $(smif)_2M$ complexes were made with salt metathesis of 2nd- and 3rd- row M(II) and M(III) halides and **1-Na.**

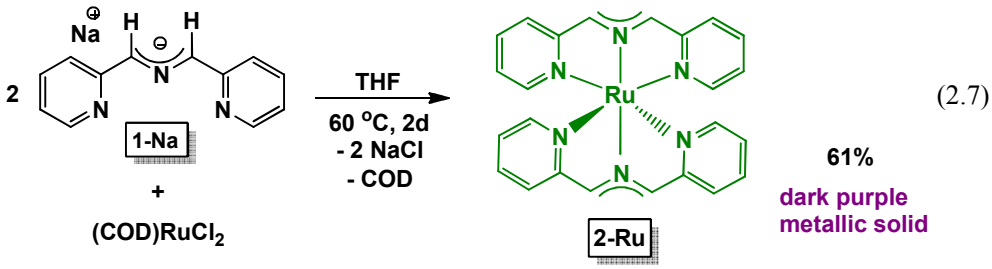

(2.7)

As depicted in Eq. 2.7, treatment of $(COD)RuCl_2$ in THF with two equivalents of **1-Na** yielded the corresponding $(smif)_2Ru$ (**2-Ru)** complex. From the intense forest green solution dark purple crystalline material was isolated (**2-Ru)** in 61% yield. ^1H NMR spectroscopy revealed characteristic "smif" resonances in the diamagnetic region similar to those observed from diamagnetic first-row $(smif)_2M$ complexes.[25]

Attempts to generate $(smif)_2Ir$ could not be made by a simple salt metathesis due to a dearth of Ir(II) starting materials. Instead, a more common starting material, $IrCl_3(THT)_3$,[27] was treated with 2 equivs of **1-Na** and one equiv of $NaBPh_4$ to generate a brilliant turquoise solution from which $[(smif)_2Ir][BPh_4]$ (**2-Ir**$^+$) was isolated as a dark purple crystalline solid in 50% yield.

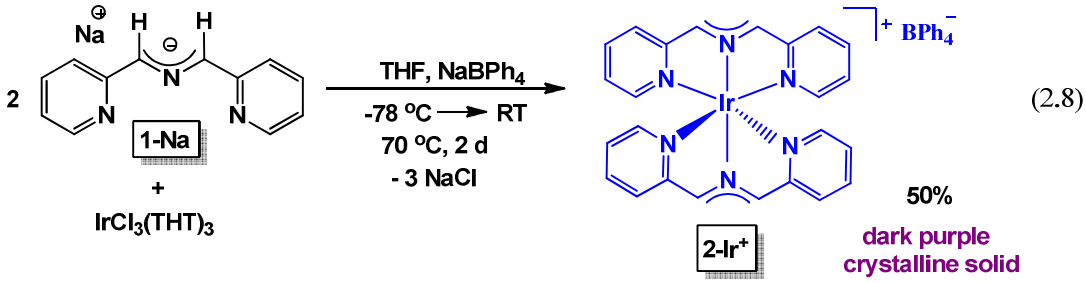

(2.8)

Similar to **2-Ir**$^{+}$, **2-Rh**$^{+}$ was not synthesized directly because addition of 4 equivs of **1-Na** to $[Rh(TFA)_2]_2$ failed to react, even with prolonged heating. The d^6-cation, **2-Rh**$^{+}$**,** could be prepared by treatment of the Rh(II) starting material with 2 equivs of ligand per rhodium in the presence of an oxidant. Addition of AgOTf to $[Rh(TFA)_2]_2$ and 4 equivs of **1-Na** at -78 °C, generated an intense purple solution. Upon heating, a color change to bright blue was observed and red crystalline material, $[(smif)_2Rh^{III}][OTf]$ (**2-Rh**$^{+}$), was isolated in 53% yield.

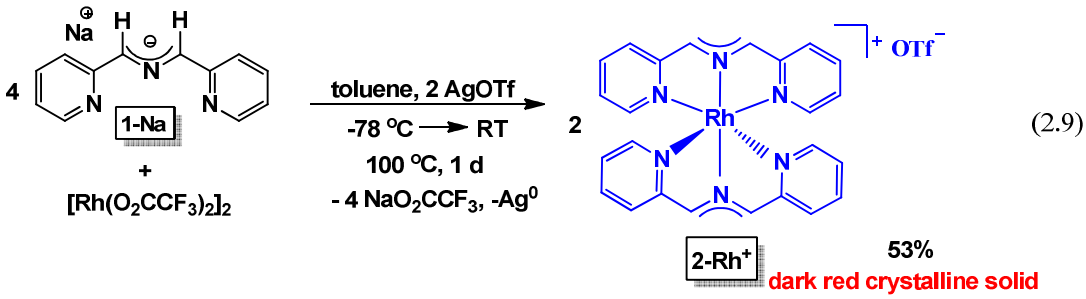

(2.9)

Remarkably, simultaneous addition of **1-Na** and an oxidant (AgOTf) did not prevent the desired formation of **2-Rh**$^{+}$ by an unproductive redox process. In a separate experiment, combination of AgOTf and **1-Na** resulted in rapid oxidation of **1-Na.** It is possible that the oxidation of the Rh(II) starting material by AgOTf proceeds faster than the oxidation of **1-Na**, allowing for the successful formation of **2-Rh**$^{+}$**.**

B. Characterization of 2-Rh$^+$ and 2-Ir$^+$

1. Electrochemical Studies of 2-Rh$^+$ and 2-Ir$^+$

The redox properties of **2-Rh$^+$ and 2-Ir$^+$** were investigated by electrochemical and synthetic methods in an attempt to generate corresponding neutral $(smif)_2M$ complexes. Cyclic voltammograms (CV) were obtained using a 0.1 M $^tBu_4NPF_6$, TBAP, solution in THF at a Pt electrode, and stated reduction or oxidation potentials were referenced relative to Ag with respect to NHE. Prior to this work, the smif ligand (**1-Li**) was electrochemically analyzed, and revealed two reversible ligand reductions at -1.59 V and -1.94 V.[28] An irreversible ligand oxidation occurred at 0.48 V, which resulted in a new irreversible reduction at -0.79 V.[28] The reversible reductions observed for **1-Li** suggested the ligand was capable of accepting an extra electron.

Cyclic voltammetry on **2-Rh$^+$** in THF revealed quasi-reversible waves at -1.2 V and -1.6 V and irreversible oxidations at 0.92 V and 1.38 V. Similarly, measurements on **2-Ir$^+$** in THF showed quasi-reversible waves at -1.18 V and -1.6 V, and an irreversible oxidation at 1.28 V among other minor waves. The quasi-reversible nature of the electrochemical reductions of **2-Rh$^+$** and **2-Ir$^+$** indicated potential for chemical reduction to the corresponding neutral complexes. Synthetic attempts toward isolation of neutral $(smif)_2M$ (M = Rh, Ir) complexes were made.

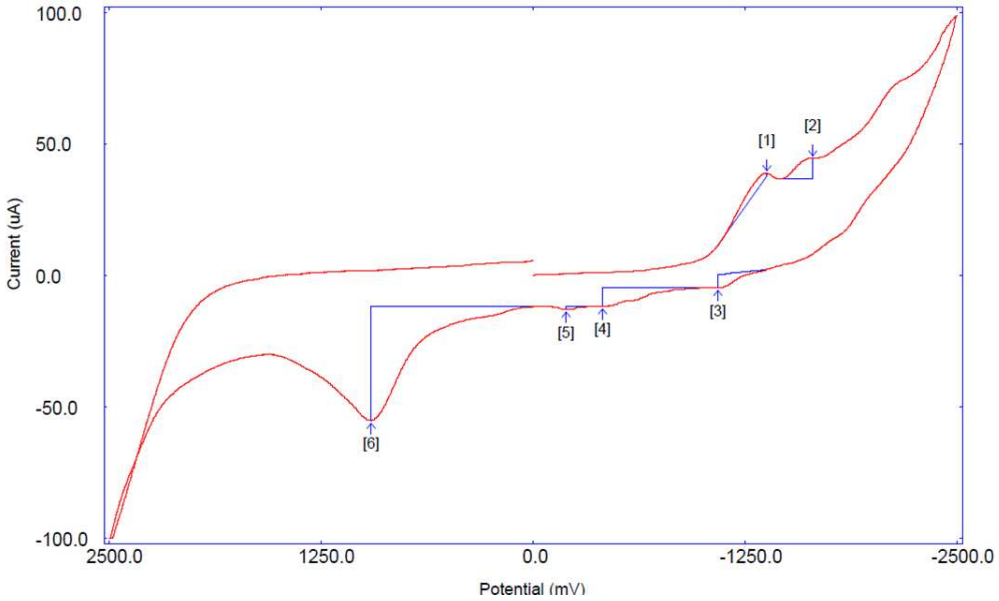

Figure 2.5. Electrochemical reduction of **2-Rh**$^{+}$.

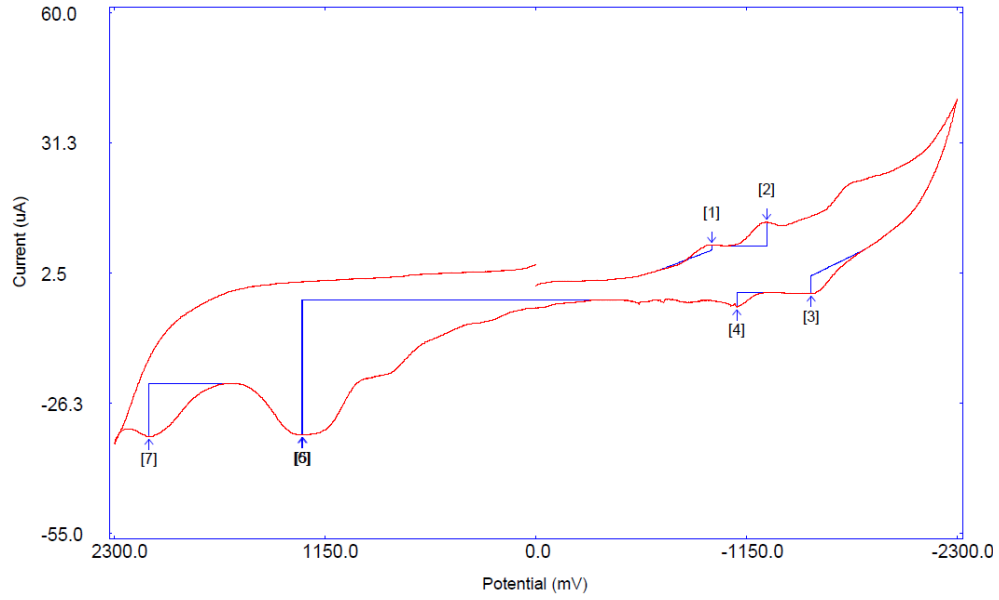

Figure 2.6. Electrochemical reduction of **2-Ir**$^{+}$

2. Synthetic Attempts toward Reduction

While electrochemical measurements of the free ligand suggested that smif could accomodate an additional electron, attempts to chemically reduce **2-Rh**$^{+}$ and **2-**

Ir^{+} to neutral species formally containing a smif dianion failed. Scheme 2.2 depicts the various reducing agents employed to generate neutral $(smif)_2Ir$ and $(smif)_2Rh$. Cobaltocene, with a reduction potential of -1.33 V,[29] did not reduce **2-Ir**$^{+}$ or **2-Rh**$^{+}$**.** Stronger reducing agents, potassium graphite (-2.38 V[29]) and sodium amalgam (-3.08 V[29]), were also used, but upon treatment of **2-Ir**$^{+}$ and **2-Rh**$^{+}$ with KC_8 or Na/Hg, formation of potassium and sodium smif ligands (**1-K**, and **1-Na**) was observed.

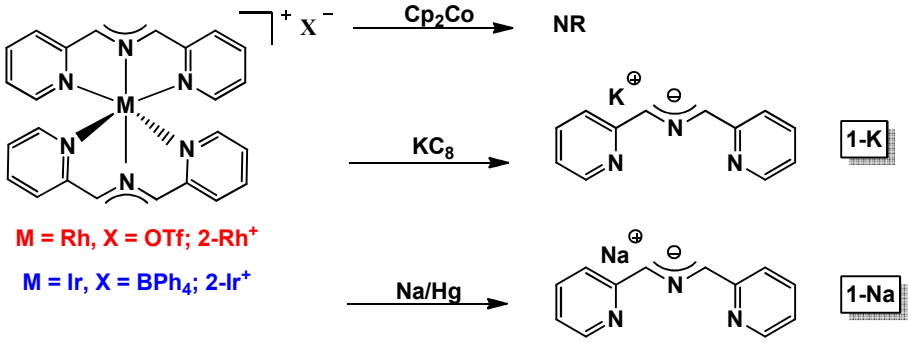

Scheme 2.2. Attempts toward chemical reduction of **2-Rh**$^{+}$ and **2-Ir**$^{+}$**.**

3. UV-Vis Measurements of 2-Ru, 2-Rh^{+}, and 2-Ir^{+}

All smif-containing complexes have remarkably intense colors in solution, separating them from other nitrogen-based tridentate chelates, such as terpyridine. A UV-Vis spectrum of **1-Li** was reported in previous work[28] and revealed two major features: absorption at 420 nm ($\varepsilon \sim 7{,}000\ M^{-1}\ cm^{-1}$) and 583 nm ($\varepsilon \sim 18{,}000\ M^{-1}\ cm^{-1}$), which may be attributed to intraligand (IL) transitions between azaallyl CNC^{nb} orbitals to pyridine π^* orbitals based upon calculations for related first-row smif-containing complexes.

DFT calculations on $(smif)_2Fe$[25] (**2-Fe**) were used to assist in the analysis of spectra obtained for second and third row smif complexes. Figure 2.7 shows the

HOMO and HOMO-1 orbitals corresponding to two linear combinations (b_1 and a_2) of the azaallyl nonbonding orbital (CNC^{nb}). Beneath these are the fully occupied set of metal-based orbitals, e (d_{xz}, d_{yz}) and b_1 (d_{xy}).

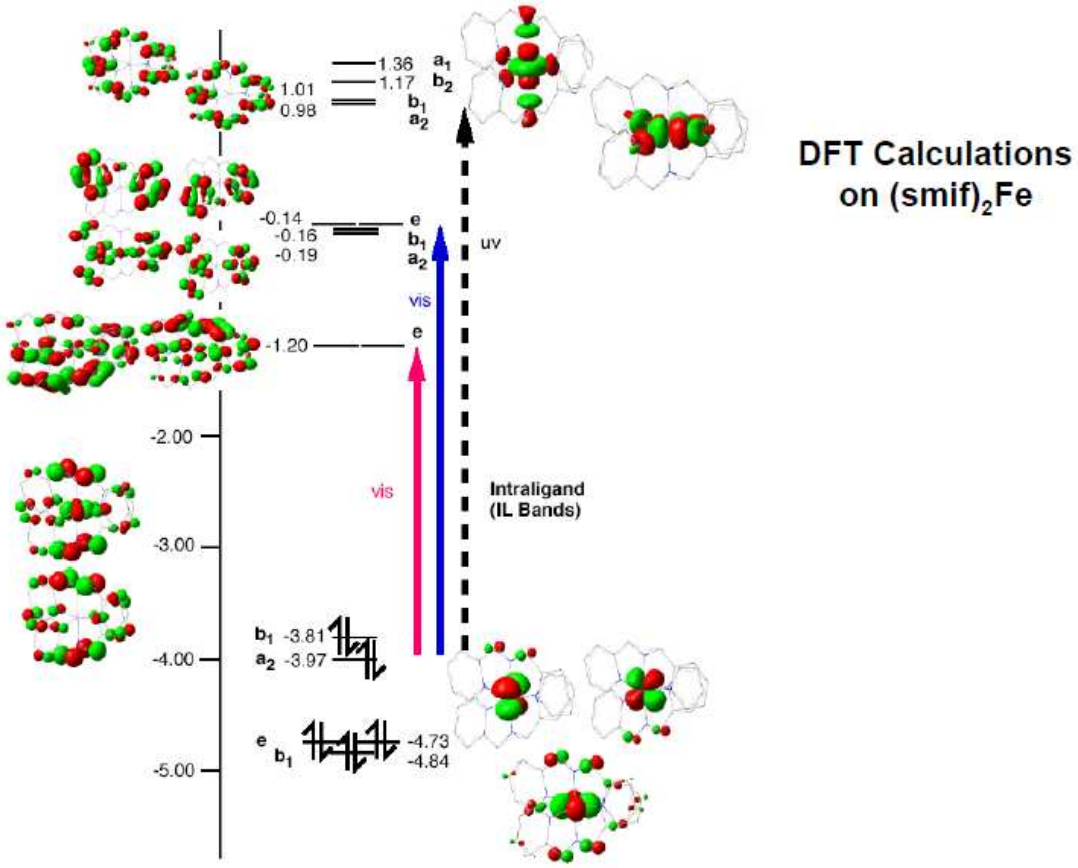

Figure 2.7. DFT calculations for **2-Fe**.

Charge is transferred from the CNC backbone to the pyridines by allowed transitions from the CNC^{nb} orbitals to an e set of ligand π^* orbitals at -1.20 eV, resulting in a large change in electric dipole (the "red" IL bands). A second set of intraligand (IL) transitions from the CNC^{nb} orbitals to a group of ligand π^* orbitals also transfers charge from the CNC backbone to the pyridines ("blue" IL bands).

Experimentally, large intensities from these transitions were observed, as expected from intraligand bands of this type.

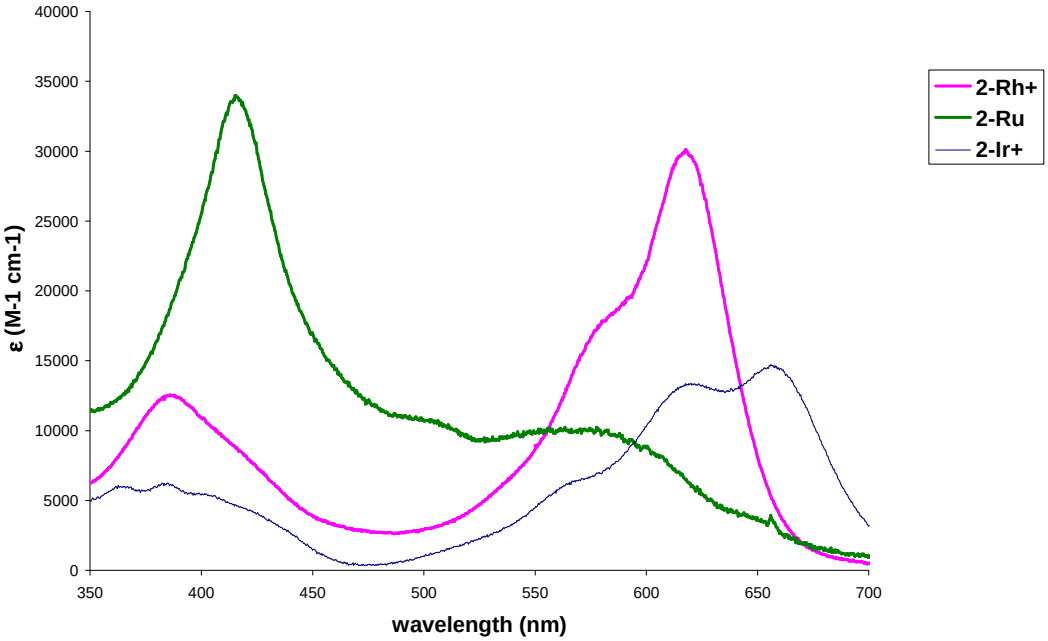

Figure 2.8 UV-vis spectra for **2-Ru, 2-Rh**$^{+}$**,** and **2-Ir**$^{+}$

Similar to the UV-Vis spectrum for **2-Fe**,[25,28] the spectrum of **1-Ru** reveals an IL band ("red band") at 566 nm ($\varepsilon \approx 10{,}000\ M^{-1}\,cm^{-1}$) as a broad and featureless absorbance with a small shoulder at 650 nm ($\varepsilon \approx 3{,}600\ M^{-1}\,cm^{-1}$). An intense transition is observed at 416 nm ($\varepsilon \approx 33{,}000\ M^{-1}\,cm^{-1}$), which most likely corresponds to the "blue IL" band. At 505 nm ($\varepsilon \approx 10{,}500\ M^{-1}cm^{-1}$), a band is observed that is likely a metal to ligand charge transfer (MLCT) transition or another IL component.

The higher energy "blue" bands are significantly less intense than the "red" bands observed in the spectrum for **2-Rh**$^{+}$ and **2-Ir**$^{+}$ relative to **2-Ru**. This trend was also observed in the comparison of first-row complexes **2-Fe**, $(smif)_2Co$ (**2-Co**) and

[(smif)$_2$Co]OTf (**2-Co$^+$**).[25] For **2-Rh$^+$**, the 618 nm ($\varepsilon \approx 30{,}000$ M^{-1} cm^{-1}) absorption has a shoulder at 580 nm ($\varepsilon \approx 17{,}600$ M^{-1} cm^{-1}), which could be the result of a vibronic progression, and the less intense intraligand band appears at 385 nm ($\varepsilon \approx 12{,}400$ M^{-1} cm^{-1}) possessing a shoulder at 425 nm ($\varepsilon \approx 7{,}300$ M^{-1} cm^{-1}). The typical IL features are less intense overall in **2-Ir$^+$**, whose major absorption occurs at 658 nm ($\varepsilon \approx 14{,}700$ M^{-1} cm^{-1}), with apparent vibrational components at 623 nm ($\varepsilon \approx 12{,}900$ M^{-1} cm^{-1}) and 570 nm ($\varepsilon \approx 5{,}800$ M^{-1} cm^{-1}), which corresponds to a vibronic progression of ~1170 cm^{-1}. Its "blue IL band" also appears to have vibrational components with absorptions of similar intensity ($\varepsilon \approx 5000$ M^{-1} cm^{-1}) at 405, 386, 366, and 346 nm, corresponding to a vibronic progression of ~ 1400 cm^{-1}. The vibronic progression is a result of the population of vibrational levels of the excited state upon increasing energy.[30-32]

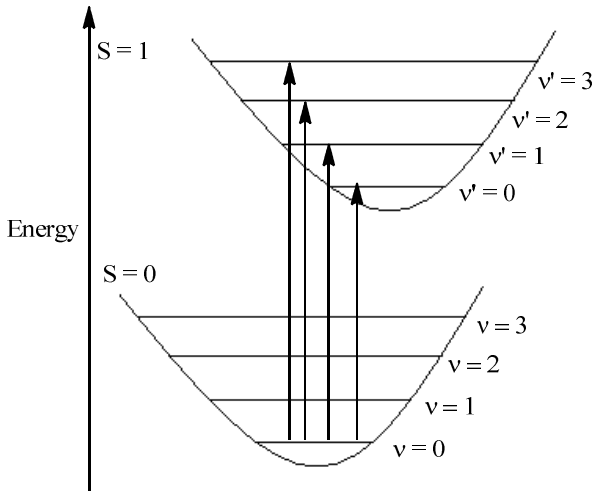

Figure 2.9. Population of vibrational levels of the excited state upon increasing energy, resulting in a vibronic progression

4. Emission Experiments

With the unusual intensity displayed in the UV-Vis spectra by $(smif)_2M$ complexes, there was significant interest in emission spectroscopy. Many 2nd and 3rd row transition metal complexes known for fluorescent properties have N-chelating ligands.[15,16] For example, $[Ru(bipy)_3]^{2+}$, is a well studied compound with phosphorescent lifetimes ranging from 650 – 890 ns.[33] Emission from first-row transition metal complexes is typically more challenging than second and third row transition metal complexes due to various pathways for non-radiative relaxation. Higher instances of non-radiative decay may be a consequence of first row metals having higher density of states.[34] Second and third row transition metals have a lower density of states, therefore **2-Ru, 2-Rh$^+$,** and **2-Ir$^+$** were examined for phosphorescent or fluorescent behavior.

Emission spectra were collected for solutions of **2-Ru**, **2-Rh$^+$** and **2-Ir$^+$** in THF. The emission spectrum for **2-Ru** was obtained by excitation at λ_{max} (417 nm), and subsequently scanned from 445 nm to 1550 nm to detect any radiative decay. Emission spectra for **2-Rh$^+$** and **2-Ir$^+$** were recorded in similar experiments in which each sample was excited at λ_{max}, 619 nm (**2-Rh$^+$**) and 658 nm (**2-Ir$^+$**), and scanned from 650 nm to 1550 nm. Unfortunately, the absence of any observable peaks in the emission spectrum indicated **2-Ru, 2-Rh$^+$** and **2-Ir$^+$** failed to fluoresce or phosphoresce.

C. Attempted Synthesis of $(smif)_2Pd$ and Observed C-C Coupling

The smif ligand has been shown to stabilize unusual electron counts by exhibiting redox non-innocent behavior, such as in $[(smif^{1-})(smif^{2-})]Cr(III)$.[25] Prior work led to the synthesis of $(smif)_2Ni$ (**2-Ni**), a formally 20 e^- species,[25] and it was plausible the analogous $(smif)_2Pd$ could be synthesized in a similar manner.

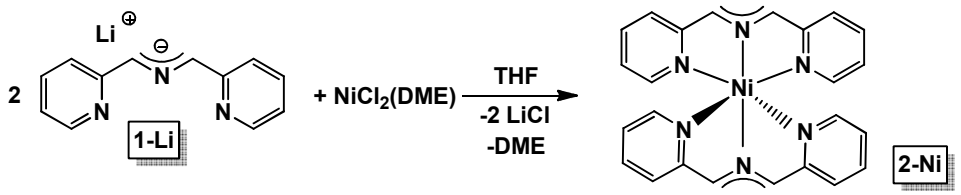

(2.10)

Initially, $(smif)_2Pd$ was targeted by a similar metathesis reaction that resulted in the successful preparation of **2-Ni**. Unfortunately, treatment of anhydrous $PdCl_2$ with two equivs of **1-Na** resulted in an orange/brown solution devoid of the intense colors expected from smif compounds. The ^1H NMR spectrum revealed the presence of several products, none of which were isolated or identified. The next approach involved treatment of $Pd(OAc)_2$ with two equivs of **smifH** to form the smif-coordinated Pd(II) dication, which in the presence of base could deprotonate to generate $(smif)_2Pd$ (Scheme 2.3). This method resulted in a bright blue-green solution and the formation of solid. Interestingly, treatment of $Pd(OAc)_2$ with two equivs of **smifH** in the absence of base generated similar observations.

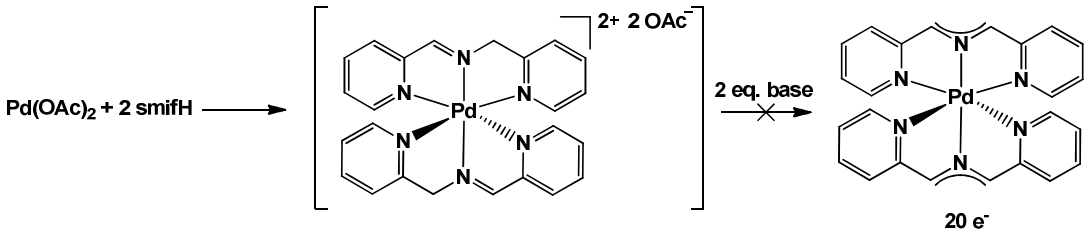

Scheme 2.3 Attempt toward a stable $(smif)_2Pd$ complex.

A bimetallic species where a C-C coupling event and a dehydrogenation had taken place at the backbone of two smif ligands (Eq 2.11), was identified by ^1H NMR and 2-D NMR spectroscopic techniques.

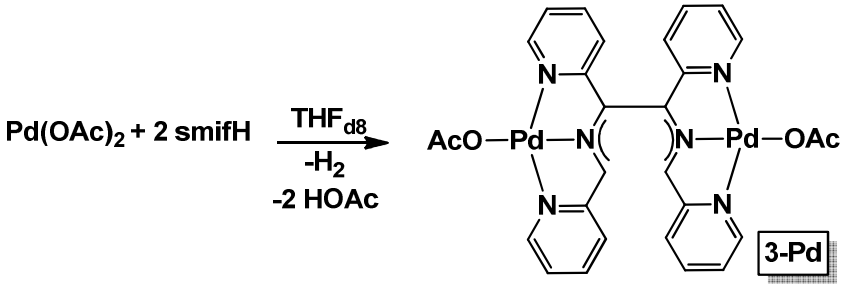

(2.11)

A proposed mechanism, depicted in Scheme 2.4, shows initial formation of [(smifH)Pd(OAc)][OAc] and subsequent loss of acetic acid to form (smif)Pd(OAc). Another equiv of [(smifH)Pd(OAc)][OAc] can undergo attack by (smif)Pd(OAc) to generate [(OAc)Pd(smifH-dpma)Pd(OAc)] [OAc] . Deprotonation by acetate would form the neutral (OAc)Pd(smif-dpma)Pd(OAc), which can undergo β-H elimination to give (OAc)Pd(smif)(smifH)Pd(OAc)(H). Oxidative addition to Pd followed by reductive elimination of H_2 would generate the observed product. Production of acetic acid was verified in the ^1H NMR spectrum of the reaction mixture, but hydrogen was not observed in the ^1H NMR spectrum. As the stoichiometry suggests, this reaction

did not form products cleanly and **3-Pd** was not isolated. Unfortunately, treatment of one equiv of **smifH** with one equiv of $Pd(OAc)_2$ did not cleanly proceed either, and the formation of **3-Pd** along with other unidentified products was observed.

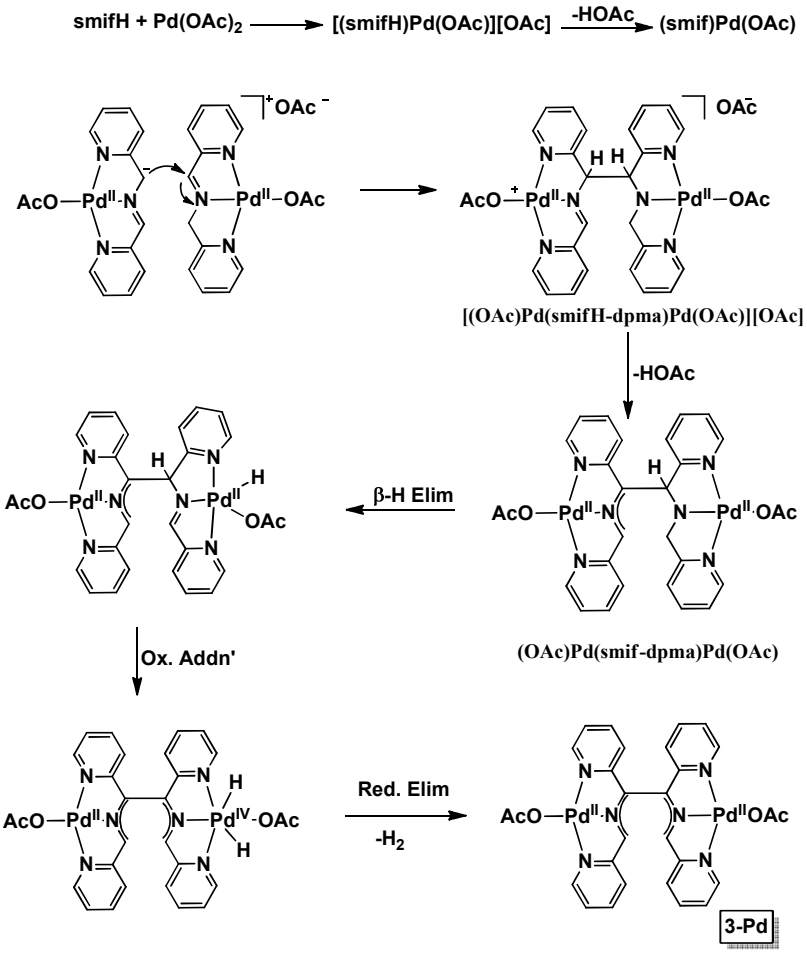

Scheme 2.4. Proposed mechanism for the formation of **3-Pd.**

An alternative mechanism is shown in Scheme 2.5 where acetic acid is reductively eliminated to generate a Pd(0)-Pd(II) cycle, rather than invoking Pd(IV). Once acetic acid is lost, oxidative addition would generate the azaallyl palladium hydride. Protonation via heterolytic H-OAc activation to give H_2 would form **3-Pd.**

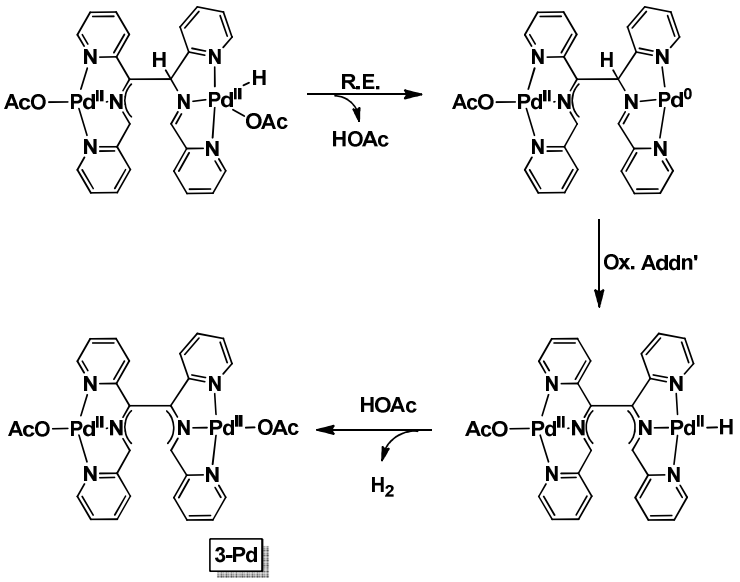

Scheme 2.5. Alternative mechanism for the formation of **3-Pd.**

Attempts to stabilize the formation of $(smif)_2Pd$ by oxidation to generate 18 e^- $(smif)_2Pd$ (IV) were also made. As shown in Eq. 2.12, $Pd(OAc)_2$ was treated with two equivs of **1-Na** and one equiv of $Tl^{III}(TFA)_3$. A major product, tetrapyridyl pyrazine (tppz), was identified from the reaction mixture as the result of 2 anionic smif ligands that C-C coupled with one another at the ligand backbone (Eq. 2.12).

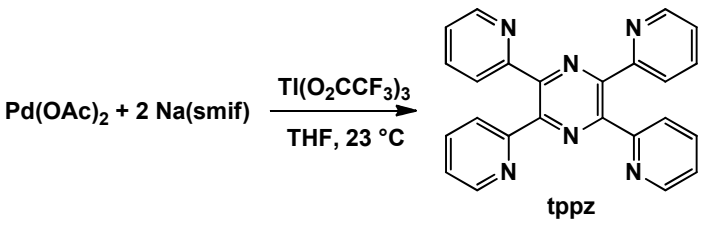

(2.12)

Reports of known routes to tetrapyridyl pyrazine (tppz) involve 2-pyridylmethylamine with $CoCl_2$ in water or ethanol. Although a mechanism was not proposed by Okamoto, it is plausible tppz is generated through a smif-type intermediate.[35] Goodwin and Lions also report a metal-free synthesis of tppz by

refluxing pyridoin and ammonium acetate for 2 hours until the crystalline product crashes out of the melted mixture.[36]

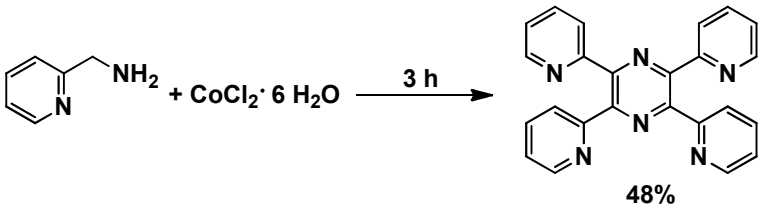

(2.13)

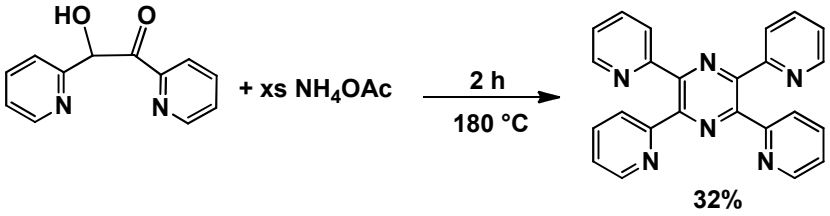

(2.14)

D. Synthesis and Characterization of H(smif-smif)(smif)Mo

Syntheses of $(smif)_2M$ complexes could be generated by salt metathesis under reducing conditions in instances where M(II) starting materials were not readily available (Eq 2.15).

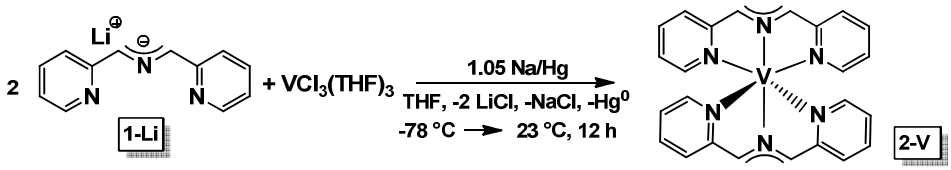

(2.15)

This method worked well for vanadium,[25] but when attempted with titanium several products were identified. The major product, displayed in Fig. 2.10, shows two smif ligands that have C-C coupled and coordinated to a smif-containing titanium center.[37] This may be rationalized by a comparison of the covalent radii of Ti (1.32 Å)[38] and V (1.22 Å).[38] Titanium, with a significantly larger covalent radius, is capable of

coordinating three smif ligands in the hepta-valent structure shown in Fig 2.10. It was plausible molybdenum, with a covalent radius slightly smaller than titanium (1.30 Å vs. 1.32 Å),[38] was capable of forming a stable $(smif)_2Mo$ complex.

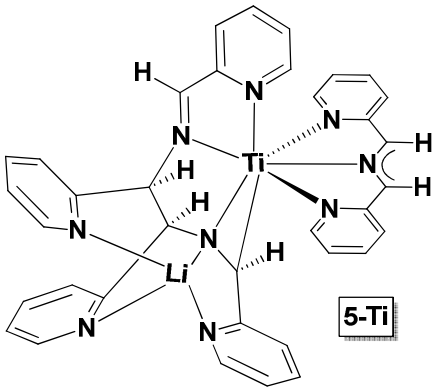

Figure 2.10. Structure of Li(smif)(smif-smif)Ti (**5-Ti)**.

Treatment of $MoCl_3(THF)_3$ with **1-Na** in the presence of Na/Hg generated a cherry red solution from which a dark red metallic solid was isolated (Eq. 2.16.). The ^1H NMR spectrum revealed many more resonances in the diamagnetic region than expected for a symmetric $(smif)_2M$ complex. Two-dimensional NMR experiments, COSY, HSQC, HMBC and TOCSY were employed to determine the structure of the new product, H(smif-smif)(smif)Mo (**4-Mo**). Similarly to titanium (**5-Ti)**, three smif ligands were required to make the product, and the reaction was rerun with the appropriate stoichiometry to yield **4-Mo** in 40% yield.

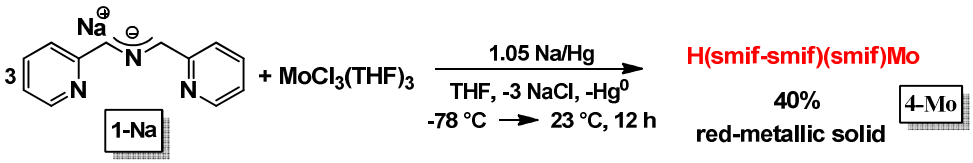

(2.16)

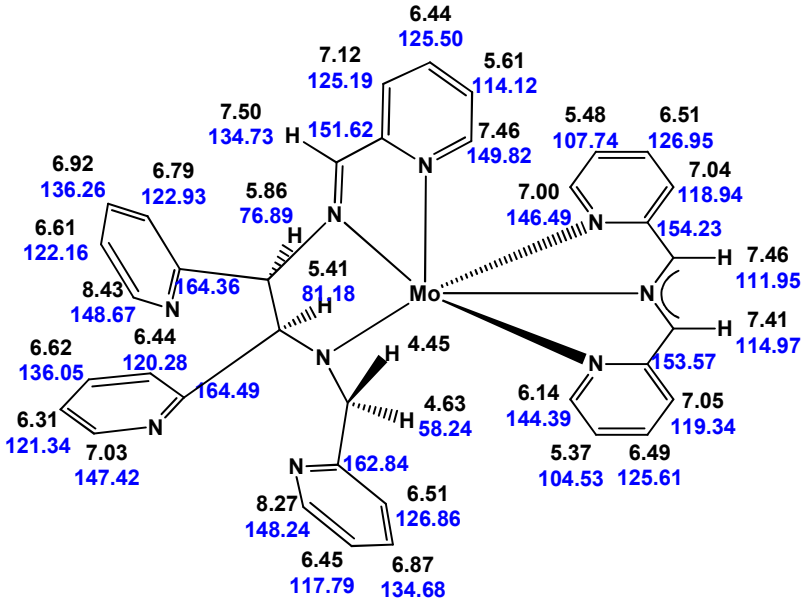

Figure 2.11. Structure of H(smif-smif)(smif)Mo (**4-Mo**).

The two dimensional TOCSY, Total Correlation Spectroscopy, allowed for the determination of the connectivity of the product by correlating all of the spins in a set of mutually coupled spins.[39] ^{1}H-^{13}C HSQC, Heteronuclear Singular Quantum Correlation, uses through-bond coupling to identify protons attached to each carbon, and HMBC, Heteronuclear Mutiple Bond Correlation, uses through bond coupling to correlate protons and carbons that are multiple (~ 3) bonds apart.[39] Although Figure 2.11 shows **4-Mo** as a six-coordinate structure, it is possible the complex forms as a seven coordinate species, similar to its titanium pseudo-analogue, **5-Ti**.

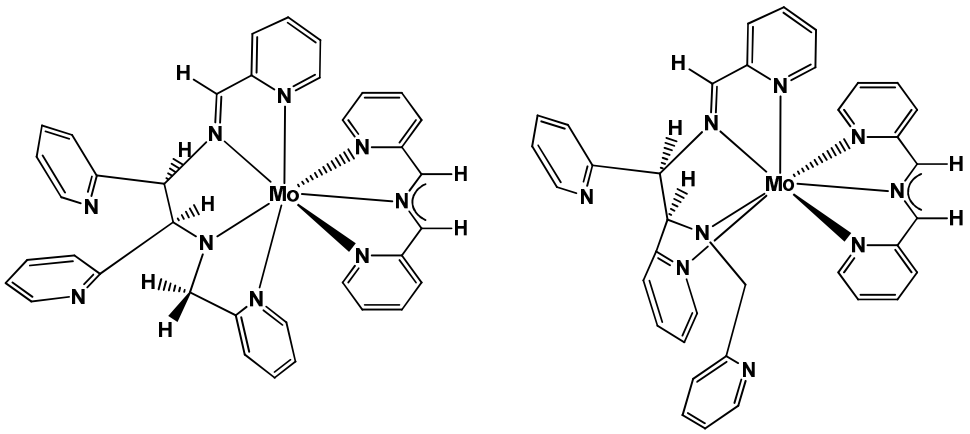

Figure 2.12. Alternative 7-coordinate structures for **4-Mo.**

According to either of the possible structures depicted in Figs. 2.11 and 2.12, three equivs of **1-Na** are required to generate **4-Mo**, and a proposed mechanism for its formation is illustrated in Scheme 2.6. Two equivs of **1-Na** may react with $MoCl_3(THF)_3$ in the presence of Na/Hg to initially form $(smif)_2Mo$. The third equivalent of **1-Na** may be protonated followed by attack at its CNC backbone by the newly formed $(smif)_2Mo$, which subsequently coordinates to the Mo center from the amide nitrogen. In order to generate **4-Mo**, a proton must be picked up from somewhere within the system, either solvent, glassware or other starting materials.

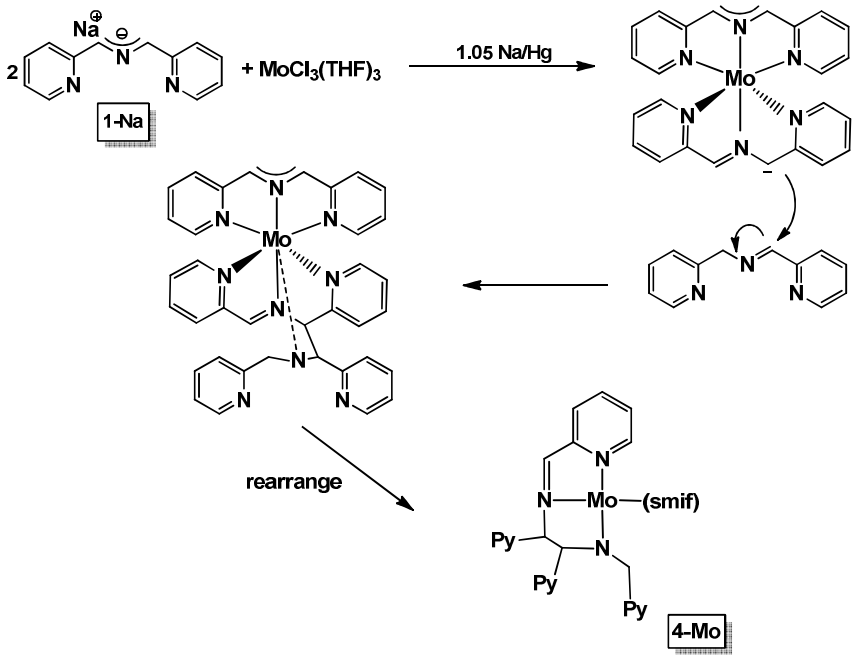

Scheme 2.6. Proposed mechanism for the formation of **4-Mo**.

E. Carbon-Carbon Coupling of the smif CNC Backbone.

The reactivity of the smif backbone may be better understood by examining the electronic features associated with the CNC^{nb} orbital. As shown in Figure 2.13, a simplified wavefunction, Ψ, can be written using the CNC^{nb} orbital. Expansion of the orbital component of Ψ leads to ionic and covalent electronic descriptions, which may be indicative of heterolytic and diradical reactivity, respectively. Either component could be responsible for C−C bond formation at the CNC backbone of the smif ligand.

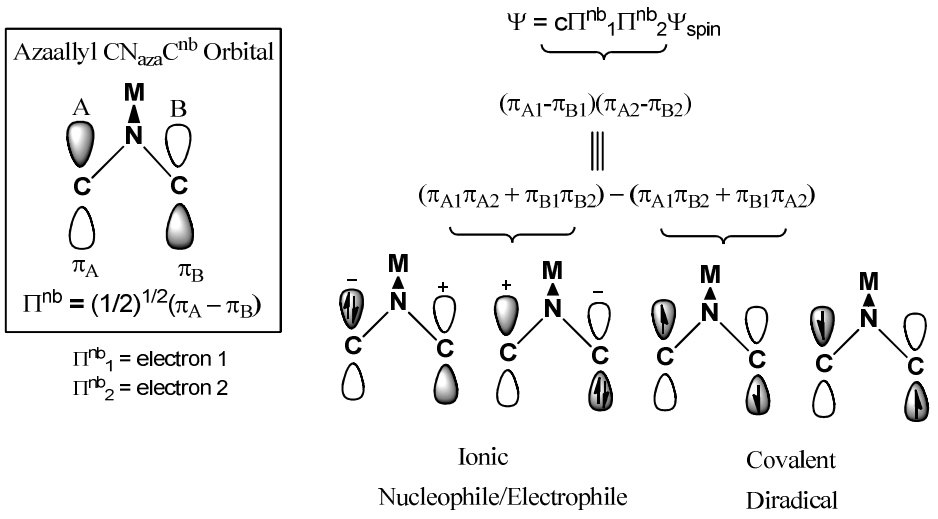

Figure 2.13. Expansion of a smif CNC^{nb} orbital showing ionic and covalent diradical components.

Given the electronic description of the smif backbone, the reactivity of **3-Pd** and **4-Mo** described may be considered either an electrophile-nucleophile process or a diradical coupling event. Other examples of C−C bond formation derived from backbone coupling reactions have been seen in the dimerization of smif-containing iron complexes, as well as the attempted synthesis of $(smif)_2Ti$ (Scheme 2.7).[40,41]

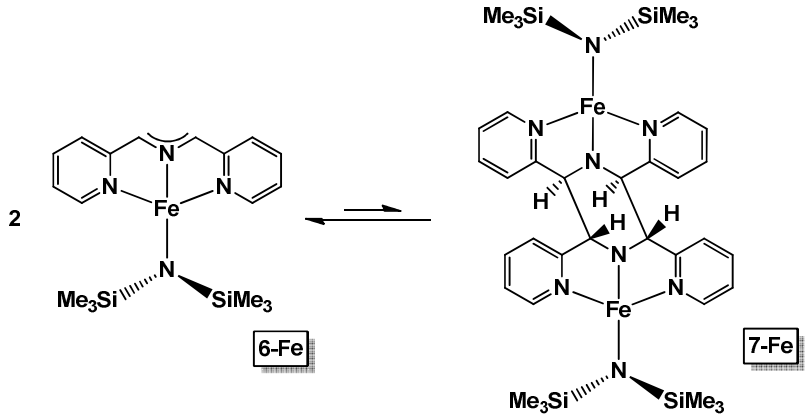

Scheme 2.7. Example of C-C bond formation in a smif-containing iron species, **6-Fe,** to form **7-Fe.**

III. Conclusions

Diamagnetic, d^6 $(smif)_2M^{n+}$ (n = 0, M = Ru (**2-Ru**); n = 1, M = Rh (**2-Rh**$^+$), Ir (**2-Ir**$^+$)) complexes analogous to the first row $(smif)_2M$ (M = V, Cr, Mn, Fe, Co, Ni) series were synthesized in order to investigate their optical properties. Chemical reduction of **2-Rh**$^+$ and **2-Ir**$^+$ in efforts to generate neutral Rh(II) and Ir(II) species were not met with success, even though electrochemical studies indicated reduction was possible. Reducing agents strong enough to reduce **2-Rh**$^+$ and **2-Ir**$^+$ resulted in the regeneration of the smif ligand.

Intense optical properties for **2-Ru, 2-Rh**$^+$ and **2-Ir**$^+$ were observed in the UV-Vis spectra where the dominant transitions were due to IL charge transfer bands. Molar absorptivities ranged from ~14,000 cm^{-1} to ~30,000 cm^{-1} and were similar to those observed for first row transition metal $(smif)_2M$ complexes reported.[25] Unfortunately, attempts to detect emission from these second row $(smif)_2M$ analogues did not result in the observation of any fluorescence or phosphorescence.

Chemical reactivity of the smif CNC backbone to generate **3-Pd** and **4-Mo** is consistent with the description of the CNC^{nb} orbital as having covalent diradical and/or ionic character. This behavior has been reported in related iron compounds (**6-Fe** and **7-Fe**) as well as in the synthesis of (smif)Li(smif-smif)Ti (**5-Ti**).[37,42]

IV. Experimental

A. General Considerations

All manipulations were performed using either glovebox or high vacuum line techniques. Hydrocarbon and ethereal solvents were dried over and vacuum

transferred from sodium benzophenone ketyl (with 3-4 mL of tetraglyme/L added to hydrocarbons). THF-d_8 was dried over sodium benzophenone keyl. Benzene-d_6 was dried over sodium, vacuum transferred and stored under N_2. Literature procedures were used for the preparation of **smifH.**[26,43] $IrCl_3(THT)_3$,[27] $[Rh(TFA)_2]_2$,[44] $Ru(COD)Cl_2$,[45] and $MoCl_3(THF)_3$[46] were all prepared according to literature procedures. Lithium- and sodium- bis(trimethylsilyl)amides were purchased from Aldrich and recrystallized from hexanes prior to use. All other chemicals were commercially available and used as received. All glassware was oven dried.

NMR spectra were obtained using INOVA 400 and INOVA 600 spectrometers. Chemical shifts are reported relative to benzene-d_6 (^{1}H δ 7.16; ^{13}C{^{1}H} δ 128.39) and THF-d_8 (^{1}H δ 3.58, 1.72; ^{13}C{^{1}H} δ 67.21, 25.31). All coupling constants (*J)* are reported in Hz.

B. Procedures

1. Li(smif) (1-Li).

To a solution of lithium bis(trimethylsilyl)amide (1.273 g, 7.60 mmol) in 50 mL THF was slowly added a solution of **smifH** (1.50 g, 7.60 mmol) in 50 mL THF at -78 °C under argon. The solution immediately turned magenta and was stirred at -78 °C for 2 h prior to warming to 23 °C. After stirring at 23 °C for 2 h, the volatiles were removed *in vacuo*. The solid was triturated with Et_2O and filtered. **1-Li** was isolated as a metallic gold solid (1.389 g, 90 %). ^{1}H NMR (C_6D_6, 400 MHz): δ 5.98 (t, py-C^5*H*, 1 H, *J* = 8 Hz), 6.50 (d, py-C^3*H*, 1 H, *J* = 8 Hz), 6.84 (t, py-C^4*H*, 1 H, *J* = 8 Hz), 7.16 (s, C*H*, 1 H), 7.66 (d, py-C^6*H*, 1 H, *J* = 4 Hz). ^{13}C{^{1}H} NMR (C_6D_6, 100 MHz): δ 113.20

(*C*H), 117.95 (py-*C*^{3}H), 118.65 (py-*C*^{5}H), 136.18 (py-*C*^{4}H), 148.90 (py-*C*^{6}H), 159.44 (py-*C*^{2}).

2. Na(smif) (1-Na).

To a solution of sodium bis(trimethylsilyl)amide (1.395 g, 7.60 mmol) in 50 mL THF was slowly added a solution of **smifH** (1.500 g, 7.60 mmol) in 50 mL THF at -78 °C under argon. The solution immediately turned magenta and was stirred at -78 °C for 2 h before warming to 23 °C. After stirring at 23 °C for 2 h, the volatiles were removed *in vacuo*. The solid was triturated with Et_2O (3 x 15 mL) prior to filtering. **1-Na** was isolated as a metallic gold solid (1.602 g, 96 %). ^{1}H NMR (C_6D_6, 400 MHz): δ 6.19 (t, py-C^5*H*, 1 H, *J* = 5.6 Hz), 6.55 (d, py-C^3*H*, 1 H, *J* = 8 Hz), 6.97 (t, py-C^4*H*, 1 H, *J* = 7.2 Hz), 7.04 (s, C*H*, 1 H), 7.72 (d, py-C^6*H*, 1 H, *J* = 4 Hz). ^{13}C{^{1}H} NMR (C_6D_6, 100 MHz): δ 112.19 (*C*H), 115.70 (py-*C*^{3}H), 119.05 (py-*C*^{5}H), 135.62 (py-*C*^{4}H), 149.81 (py-*C*^{6}H), 160.23 (py-*C*^{2}).

3. (smif)$_2$Ru (**2-Ru**).

To a small bomb reactor charged with Na(smif) (0.400 g, 1.82 mmol) and (COD)$RuCl_2$ (0.256 g, 0.946 mmol) was vacuum transferred 15 mL THF at −78 °C. After warming to 23 °C, the bomb was heated in a 60 °C oil bath for 2 d as the magenta solution became dark green with dark purple solids. The reaction mixture was filtered cold in THF, and all volatiles were removed in vacuo. The resulting dark purple, metallic solid was washed with pentane, and 0.276 g **2-Ru** were isolated (61%). ^{1}H NMR (C_6D_6, 400 MHz): *δ* 5.64 (t, py-C$_5$*H*, 1 H, *J* = 6.4 Hz), 6.07 (d, py-C$_3$*H*, 1 H, *J* = 8.3 Hz), 6.81 (s, C*H*, *1* H), 6.31 (t, py-C$_4$*H*, 1 H, *J* = 7.6 Hz), 7.80 (d, py-C$_6$*H*, 1 H, *J* = 5.1 Hz). ^{13}C{^{1}H} NMR (C_6D_6, 125 MHz): *δ* 113.66 (*C*H), 113.73

(py-C_3H), 115.03 (py-C_5H), 134.77 (py-C_4H), 151.24 (py-C_6H), 167.54 (py-C_2). Anal. Calcd. $H_{24}C_{20}N_6Ru$: C, 58.41; H, 4.08; N, 17.03. Found: C, 58.48; H, 4.22; N, 13.28.

4. [(smif)2Rh][OTf] (2-Rh$^+$).

To a small bomb reactor charged with Na(smif) (0.072 g, 0.328 mmol), AgOTf (0.042 g, 0.163 mmol) and $Rh_2(TFA)_4$ (0.054 g, 0.082 mmol) was vacuum transferred 5 mL toluene at −78 °C. After it was warmed to 23 °C, the solution turned from magenta to purple and was placed in a 100 °C oil bath for 1 d. The bright blue reaction mixture was filtered and washed with toluene. All volatiles were removed in vacuo leaving a bright red metallic solid **2-Rh$^+$** (0.028 g, 53%). ^{1}H NMR (THF-*d*8, 400 MHz): δ 6.51 (t, py-C_5H, 1 H, J = 6.4 Hz), 6.87 (d, py-C_3H, 1 H, J = 8.1 Hz), 6.85 (s, C*H*, *1* H), 7.29 (t, py-C_4H, 1 H, J = 7.5 Hz), 7.77 (d, py-C_6H, 1 H, J = 5.6 Hz). $^{13}C\{^1H\}$ NMR (THF-d_8, 125 MHz): δ 114.72 (*C*H), 118.20 (py-C_3H), 138.70 (py-C_5H), 148.20 (py-C_4H), 148.29 (py-C_6H), 165.22 (py-C_2). Anal. Calcd. $H_{20}C_{25}N_6O_3F_3SRh$: C, 46.60; H, 3.13; N, 13.04. Found: C, 44.39, 44.89; H, 4.95, 3.66; N, 8.87, 9.28.

5. [(smif)$_2$Ir][BPh$_4$] (2-Ir$^+$).

To a small bomb reactor charged with Na(smif) (0.195 g, 0.889 mmol), $NaBPh_4$ (0.152 g, 0.444 mmol) and $IrCl_3(THT)_3$ (0.250 g, 0.444 mmol) was vacuum transferred 5 mL THF at −78 °C. Upon warming to 23 °C, the magenta solution quickly turned navy blue. The bomb was placed in a 70 °C oil bath for 2 d after which the solution was turquoise. The reaction mixture was filtered and washed in THF. All volatiles were removed *in vacuo* leaving dark purple metallic solid **2-Ir$^+$** (0.200 g, 50%). ^{1}H NMR (THF-d_8, 400 MHz): δ 6.36 (t, py-C_5H, 1 H, J = 6.7 Hz), 6.53 (d, py-

C_3H, 1 H, J = 8.3 Hz), 6.30 (s, CH, *1* H), 7.03 (t, py-C_4H, 1 H, J = 7.7 Hz), 7.60 (d, py-C_6H, 1 H, J = 6.0 Hz). $^{13}C\{^1H\}$ NMR (THF-d_8, 125 MHz): δ 116.08 (CH), 138.08 (py-C_3H), 140.52 (py-C_5H), 149.47 (py-C_4H), 163.36 (py-C_6H), 169.14 (py-C_2). Anal. Calcd. $H_{40}C_{48}N_6BRh$: C, 63.78; H, 4.46; N, 9.30. Found: C, 62.22, 65.03; H, 4.84, 4.82; N, 8.02, 8.14.

6. OAc-Pd(smif)Pd-OAc, 3-Pd

To a J-Young NMR tube was added 0.010 g $Pd(OAc)_2$ (0.040 mmol) and a solution of 0.016 mg **smifH** (0.080 mmol) in 0.6 mL THF-d_8, The reaction was shaken, and after a day the reaction had gone to completion, leaving **4-Pd** as a green solution. No attempts toward scale-up and isolation were made. ^1H NMR (400 MHz, THF-d_8): δ 7.47 (d, J = 5.7, 4H), 7.32 (tt, J = 6.2, 3.1, 4H), 6.80 (d, J = 8.3, 2H), 6.51 (td, J = 6.5, 2H), 6.41 (t, J = 7.2, 2H), 6.34 (d, J = 8.4, 2H), 5.49 (s, 2H), 1.92 (s, 6H). $^{13}C\{^1H\}$ NMR (600 MHz, THF-d_8): δ 165.47, 163.40, 148.86, 148.42, 139.52, 139.08, 118.08, 117.95, 117.44, 115.90, 115.60, 114.04, 24.41.

7. H(smif-smif)Mo(smif), 4-Mo

A 100 mL 3-neck round-bottom flask containing 0.236 g **1-Na** (1.1 mmol) and 0.911 g (0.376 mmol) 0.95% Na/Hg was equipped with an addition finger charged with 0.150 g (0.347 mmol) $MoCl_3(THF)_3$. THF (~30 mL) was transferred under vacuum at -78 °C. $MoCl_3(THF)_3$ was slowly added to the cold solution and then allowed to slowly warm to room temperature. After 24 h, all volatiles were removed *in vacuo*. Diethyl ether (~20 mL) was transferred under vacuum and the solution was filtered to remove any NaCl and mercury. Diethyl ether was removed *in vacuo* to leave a dark red metallic solid, **H(smif-smif)Mo(smif)**, in 40% yield (0.100 g). ^1H

NMR (400 MHz, benzene-d_6): δ 8.43 (d, *J* = 7.2, 1H), 8.27 (d, *J* = 5.3, 1H), 7.50 (s, 1H), 7.46 (d, *J* = 5.2, 1H), 7.46 (s, 1H) 7.41 (s, 1H), 7.13 (d, *J* = 7.7, 1H), 7.05 (d, *J* = 6.9, 1H), 7.04 (d, 5.2, 1H), 7.03 (d, *J* = 7.7, 1H), 6.98 (t, *J* = 7.3, 1H), 6.92 (t, *J* = 7.5, 1H), 6.87 (t, *J* = 6.7, 1H), 6.79 (d, *J* = 7.2, 1H), 6.61-6.62 (m, 2H), 6.49-6.51 (m, 3H), 6.44-6.45 (m, 3H), 6.31 (t, *J* = 5.7, 1H), 6.14 (d, *J* = 6.3, 1H), 5.86 (br s, 1H), 5.61 (t, *J* = 5.7, 1H), 5.48 (t, *J* = 6.2, 1H), 5.41 (br s, 1H) 5.37 (t, *J* = 5.3, 1H), 4.63 (d, *J* = 14.9, 1H), 4.49 (d, *J* = 14.9, 1H). $^{13}C\{^1H\}$ NMR (600 MHz, benzene-d_6): δ 164.49, 162.84, 154.23, 153.57, 151.62, 149.82, 148.67, 148.24, 147.42, 144.39, 136.26, 136.05, 134.73, 134.68, 126.95, 126.86, 125.61, 125.20, 125.19, 122.93, 122.16, 121.34, 120.28, 119.34, 118.94, 117.79, 114.97, 114.12, 111.95, 107.74, 104.53, 81.18, 76.89, 58.24.

REFERENCES

(1) Kauffman, G. B. *Spectrum (Pretoria)* **1987**, *25*, 5.

(2) Pascal, P. *Rev. Chim. Miner.* **1966**, *3*, 741.

(3) Braterman, P. S.; Song, J. I.; Peacock, R. D. *Inorg. Chem.* **1992**, *31*, 555.

(4) Harris, C. M.; Patil, H. R. H.; Sinn, E. *Inorg. Chem.* **1969**, *8*, 101.

(5) Henke, W.; Reinen, D. *Z. Anorg. Allg. Chem.* **1977**, *436*, 187.

(6) Hogg, R.; Wilkins, R. C. *J. Chem. Soc.* **1962**, 341.

(7) Hughes, M. C.; Macero, D. J. *Inorg. Chem.* **1976**, *15*, 2040.

(8) Kremer, S.; Henke, W.; Reinen, D. *Inorg. Chem.* **1982**, *21*, 3013.

(9) Bennett, L. E.; Taube, H. *Inorg. Chem.* **1968**, *7*, 254.

(10) Braterman, P. S.; Song, J. I.; Wimmer, F. M.; Wimmer, S.; Kaim, W.; Klein, A.; Peacock, R. D. *Inorg. Chem.* **1992**, *31*, 5084.

(11) Behrens, H.; Brandl, H.; Lutz, K. *Z. Naturforsch., B: Anorg. Chem., Org. Chem., Biochem., Biophys., Biol.* **1967**, *22*, 99.

(12) Behrens, H.; Brandl, H. *Z. Naturforsch.* **1967**, *22*, 1216.

(13) Das, A.; Ghosh, T. K.; Dutta, C. A.; Mobin, S. M.; Lahiri, G. K. *Polyhedron* **2013**, *52*, 1130.

(14) Huynh, M. H. V.; Dattelbaum, D. M.; Meyer, T. J. *Coord. Chem. Rev.* **2005**, *249*, 457.

(15) Li, H.-J.; Han, S.; Hu, L.-Z.; Xu, G.-B. *Fenxi Huaxue* **2009**, *37*, 1557.

(16) Zeitler, K. *Angew. Chem., Int. Ed.* **2009**, *48*, 9785.

(17) Geldard, J. F.; Lions, F. *J. Am. Chem. Soc.* **1962**, *84*, 2262.

(18) Marcos, D.; Folgado, J. V.; Beltran-Porter, D.; Do, P.-G. M. T.; Pulcinelli, S. H.; De, A.-S. R. H. *Polyhedron* **1990**, *9*, 2699.

(19) Wocadlo, S.; Massa, W.; Folgado, J.-V. *Inorg. Chim. Acta* **1993**, *207*, 199.

(20) Davidson, R. B.; Sienerth, K. D.; American Chemical Society: 2013, p INOR.

(21) Marcos, D.; Martinez-Manez, R.; Folgado, J. V.; Beltran-Porter, A.; Beltran-Porter, D.; Fuertes, A. *Inorg. Chim. Acta* **1989**, *159*, 11.

(22) Kajiwara, T.; Sensui, R.; Noguchi, T.; Kamiyama, A.; Ito, T. *Inorg. Chim. Acta* **2002**, *337*, 299.

(23) Frazier, B. A.; Wolczanski, P. T.; Lobkovsky, E. B. *Inorg. Chem.* **2009**, *48*, 11576.

(24) Westerhausen, M.; Kneifel, A. N. *Inorg. Chem. Commun.* **2004**, *7*, 763.

(25) Frazier, B. A.; Bartholomew, E. R.; Wolczanski, P. T.; DeBeer, S.; Santiago-Berrios, M. e.; Abruna, H. D.; Lobkovsky, E. B.; Bart, S. C.; Mossin, S.; Meyer, K.; Cundari, T. R. *Inorg. Chem.* **2011**, *50*, 12414.

(26) Incarvito, C.; Lam, M.; Rhatigan, B.; Rheingold, A. L.; Qin, C. J.; Gavrilova, A. L.; Bosnich, B. *J. Chem. Soc., Dalton Trans.* **2001**, 3478.

(27) John, K. D.; Salazar, K. V.; Scott, B. L.; Baker, R. T.; Sattelberger, A. P. *Organometallics* **2001**, *20*, 296.

(28) Frazier, B. A.; Wolczanski, P. T.; Lobkovsky, E. B.; Cundari, T. R. *J. Am. Chem. Soc.* **2009**, *131*, 3428.

(29) Connelly, N. G.; Geiger, W. E. *Chem. Rev. (Washington, D. C.)* **1996**, *96*, 877.

(30) Endicott, J. F.; Schlegel, H. B.; Uddin, M. J.; Seniveratne, D. S. *Coord. Chem. Rev.* **2002**, *229*, 95.

(31) Endicott, J. F.; Uddin, M. J.; Schlegel, H. B. *Res. Chem. Intermed.* **2002**, *28*, 761.

(32) Hitchman, M. A.; Riley, M. J.; John Wiley & Sons, Inc.: 1999; Vol. 1, p 213.

(33) Montalti, M. A. C., Luca Prodi, M. Teresa Gandolfi *Handbook of Photochemistry*; 3rd edition ed.; CRC press Taylor & Francis Group: 6000 Broken Sound Prkway NW, Suite 200 Boca Raton, FL, 2006.

(34) Figgis, B. N. H., M. A. *Ligand Field Theory and Its Applications*; Wiley-VCH: New York, 2000.

(35) Ogura, K.; Kurasawa, Y.; Yamaguchi, Y.; Okamoto, Y. *Heterocycles* **2003**, *59*, 283.

(36) Goodwin, H. A.; Lions, F. *J. Am. Chem. Soc.* **1959**, *81*, 6415.

(37) Frazier, B. A.; Wolczanski, P. T.; Keresztes, I.; DeBeer, S.; Lobkovsky, E. B.; Pierpont, A. W.; Cundari, T. R. *Inorg. Chem.* **2012**, *51*, 8177.

(38) Miessler, G. L.; Tarr, D. A. *Inorganic Chemistry, Second Edition*; Prentice Hall, 1999.

(39) Claridge, T.; Editor *High-Resolution NMR Techniques in Organic Chemistry*; Pergamon, 2000.

(40) Frazier, B. A.; Williams, V. A.; Wolczanski, P. T.; Bart, S. C.; Meyer, K.; Cundari, T. R.; Lobkovsky, E. B. *Inorg Chem* **2013**, *52*, 3295.

(41) Frazier, B. A.; Wolczanski, P. T.; Keresztes, I.; DeBeer, S.; Lobkovsky, E. B.; Pierpont, A. W.; Cundari, T. R. *Inorg Chem* **2012**, *51*, 8177.

(42) Frazier, B. A.; Williams, V. A.; Wolczanski, P. T.; Bart, S. C.; Meyer, K.; Cundari, T. R.; Lobkovsky, E. B. *Inorg. Chem.* **2013**, *52*, 3295.

(43) Skaria, S.; Ghadge, V. B.; Ravishanker, R.; Rajan, C. K. M. R.; Ponrathnam, S.; Council of Scientific and Industrial Research, India . 2009, p 18pp.

(44) Johnson, S. A.; Hunt, H. R.; Neumann, H. M. *Inorg. Chem.* **1963**, *2*, 960.

(45) Albers, M. O.; Ashworth, T. V.; Oosthuizen, H. E.; Singleton, E. *Inorg. Synth.* **1989**, *26*, 68.

(46) Dilworth, J. R.; Zubieta, J. *Inorg. Synth.* **1986**, *24*, 193.

CHAPTER 3

SELECTIVE EXTRACTION OF NITROGEN FROM AIR BY DIARYLIMINE FE(II) BIS-PHOSHINE COMPLEXES[1]

I. Introduction

Nitrogen fixation, the process by which dinitrogen is converted to ammonia, is of incredible importance, as reactive or fixed nitrogen is necessary to sustain life on this planet. Despite the atmosphere containing ~ 78% nitrogen, N_2 is nutritionally unavailable due to its inert, non-polar triple bond. Dinitrogen must be activated and reduced in order to become available in sources that can be utilized, such as ammonia or hydrazine. The triple bond, with a dissociation energy of 226 kcal/mol,[2] makes nitrogen relatively unreactive, requiring complex means of accomplishing this vital activation. Biology has overcome this obstacle with nitrogenase, and industrially, nitrogen fixation has been accomplished with the Haber-Bosch process. There is also much attention being given toward the discovery of molecular catalysts that can bind and activate dinitrogen efficiently, at ambient temperatures and low pressures.

The discovery of the Haber-Bosch process in 1909 made nitrogen fixation on an industrial scale a reality.[3-6] By heating nitrogen and hydrogen at temperatures ranging from 300 - 500 °C at very high pressures (145-250 atm)[7] with a catalyst, nitrogen is activated and reduced to ammonia.[8] This procedure involves passing the gases over four beds of catalysts, and although each cycle has only a 15% conversion, unreacted gases are recycled and a 97 % total conversion is possible.[6,8,9] Annually, 100 million tons of ammonia are produced from the Haber-Bosch process, while 300-400 millions tons of nitrogen are harvested for use as fertilizer and hydrazine.[3,6]

$$N_2 + 3\,H_2 \xrightarrow[300 - 550\ ^\circ C]{\sim 200\ atm,\ Fe_3O_4} 2\,NH_3 \qquad \begin{matrix}\Delta H = -22.04\ kcal/mol \\ \Delta S = -49.5\ eu \\ \Delta G\ (623\ K) = +7.64\ kcal/mol\end{matrix} \tag{3.1}$$

Haber-Bosch catalysts are typically iron-based, although some utilize ruthenium, which permits milder operating conditions. In industrial operations, the iron catalyst is prepared by exposing iron oxide to the hot hydrogen feedstock, reducing the iron oxide to metallic iron, and removing oxygen in the process. The result is a material with a very large surface area that enhances its effectiveness as a catalyst. Other components of the catalyst include calcium and aluminum oxides, which help the iron maintain its surface area over time, and potassium, which increases the electron density of the catalyst to improve its activity. These catalyst systems are responsible for providing the electrons necessary to reduce the nitrogen.

$$N_{2(g)} \longrightarrow N_2\ (adsorbed) \tag{3.2}$$

$$N_2\ (adsorbed) \longrightarrow 2\ N\ (adsorbed) \tag{3.3}$$

$$H_{2(g)} \longrightarrow H_2\ (adsorbed) \tag{3.4}$$

$$H_2\ (adsorbed) \longrightarrow 2\ H\ (adsorbed) \tag{3.5}$$

$$N\ (adsorbed) + H\ (adsorbed) \longrightarrow NH\ (adsorbed) \tag{3.6}$$

$$NH\ (adsorbed) + H\ (adsorbed) \longrightarrow NH_2\ (adsorbed) \tag{3.7}$$

$$NH_2\ (adsorbed) + H\ (adsorbed) \longrightarrow NH_3\ (adsorbed) \tag{3.8}$$

$$NH_3\ (adsorbed) \longrightarrow NH_{3(g)} \tag{3.9}$$

* Reproduced with permission from Bartholomew, E. R.; Volpe, E. C.; Wolczanski, P. T.; Lobkovsky, E. B.; Cundari, T. R. *J. Am. Chem. Soc.* **2013**, *135*, 3511. Copyright 2013, American Chemical Society.

Equations 3.2 – 3.9 outline the proposed mechanism of dinitrogen activation with the Haber-Bosch process.[4,5] The reaction between absorbed nitrogen and absorbed hydrogen is hypothesized to involve three steps: formation of NH, NH_2 and finally NH_3.[4,5] Even though this process successfully generates significant amounts of ammonia every year, a catalyst, high temperatures and high pressures are required to overcome an activation energy of 100 kcal/mol.[8] The discovery of more energy efficient alternatives is an important goal towards stabilizing the cost of ammonia in the future.

Biologically, nitrogen fixation is accomplished with an enzyme, nitrogenase, which requires 8 protons and 8 electrons to generate ammonia and hydrogen (Eq 3.10).[10-21]

$$N_2 + 8\,H + 8\,e^- + 16\,ATP \longrightarrow 2\,NH_3 + H_2 + 16\,ADP + 16\,P_i \quad (3.10)$$

$$\Delta G = -153.2 \text{ kcal/mol}$$

Although the formation of ammonia from nitrogen, as depicted in Eq 3.10, is enthalpically favored, the reaction has a high activation energy, requiring additional energy to overcome the barrier. The hydrolysis of each equiv of ATP provides ~ 7 kcal/mol,[22] and in doing so provides the system with enough energy to overcome the activation energy.[23,24] The conversion of dinitrogen to ammonia as depicted in Eq. 3.10 is highly exergonic with a total free energy of $\Delta G°$ of -153.2 kcal/mol.[23,24]

Nitrogenase comprises of two proteins that each contain iron-sulfur clusters. One of these proteins is a molybdenum-iron containing heterotetramer subunit (FeMo protein) which is the site of nitrogen reduction, and the other contains only iron and is

referred to as the nitrogenase reductase (Fe protein).[12,13,20] The iron protein is a homodimer that contains two ATP binding sites and a single [4Fe-4S] cluster bridged between each monomer through cysteine ligands. Its main function is to serve as an electron donor to the FeMo cofactor during catalysis. This electron transfer is vital for nitrogen reduction, and without repeated association and dissociation with the reduced iron protein, ammonia production would not be possible.

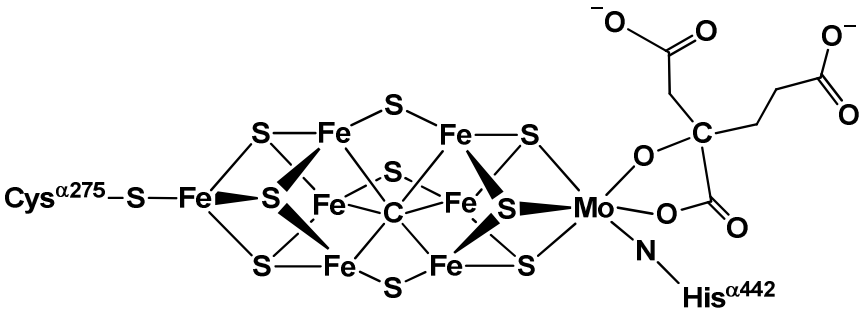

Figure 3.1. FeMo cofactor

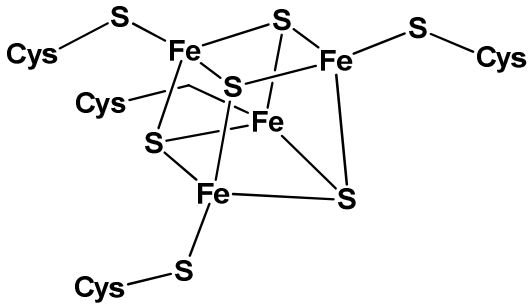

Figure 3.2. [4S-4Fe] cluster of Fe protein

Cycles of association and dissociation are responsible for this electron transfer, and the energy to do so is provided by ATP. The reduction potential of each electron transferred to the iron-molybdenum tetramer is sufficient to break one of the nitrogen-nitrogen bonds.[16,19]

The lack of understanding of how nitrogenase operates to activate nitrogen is likely due to the resting state of the FeMo protein not binding dinitrogen, and also because the FeMo protein requires several electron transfers to perform the catalysis.[16,19] It is understood that dioxygen irreversibly inhibits nitrogenase activity by oxidation and degradation of the Fe-S cofactors.[25,26] Typically, *in vitro* studies are done in the absence of dioxygen, while *in vivo* the FeMo cofactor is delivered to its operational nitrogenase protein in a reducing environment.[25,26]

An area of intense research has been focused on finding catalysts that mimic the operation of nitrogenase, enabling nitrogen activation while avoiding the energy intensive, harsh conditions currently employed in the Haber-Bosch process. Strategies to avoid high pressures and elevated temperatures have involved finding molecular catalysts capable of dinitrogen activation.

Information on the mode of binding and chemistry of dinitrogen at synthetic Fe/S or Mo/Fe/S clusters, which possess at least some of the structural features of the FeMo cofactor, would shed light on how the enzyme operates. Unfortunately, syntheses of well-defined cluster systems which bind dinitrogen and catalyze its reduction have yet to be accomplished, although there have been advances with molecular systems.

Progress in the area of dinitrogen complexation and activation are evidenced by an astounding number of synthesized and characterized dinitrogen complexes,[27-37] and modest success toward ammonia production from a molecular site has been achieved.[30,38-55] Given that nitrogen fixation occurs at a molybdenum center, many of the initial efforts toward designing catalysts for nitrogen reduction at a molecular site

began with molybdenum complexes. Chatt, Hidai and Schrock have shown ammonia formation from molybdenum and tungsten dinitrogen complexes, shown in Figure 3.3, invoking cycles involving reduction from the metal or exogenous sources, and protonation.[56-59]

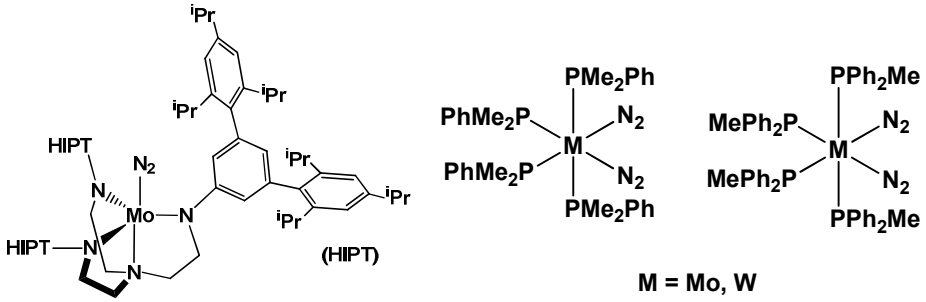

Figure 3.3. Ammonia producing dinitrogen systems

Scheme 3.1 illustrates the original proposed mechanism for dinitrogen reduction at a molybdenum site of a molecular catalyst. The Chatt-cycle, first proposed by Chatt and co-workers in the early 1970's,[60] invokes a heterolytic reduction process that invokes oxidation of Mo (0) to Mo (III). The cycle starts with dinitrogen binding to the $MoLP_4$ scaffold. A series of protons and electrons are introduced step-wise to generate the diazenido, hydrazido, and hydrazidium intermediates. Loss of ammonia generates the Mo (III) nitride, which, by the same addition of protons and electrons, produces another molecule of ammonia. Dinitrogen adduct formation regenerates the initial Mo (0) starting material.

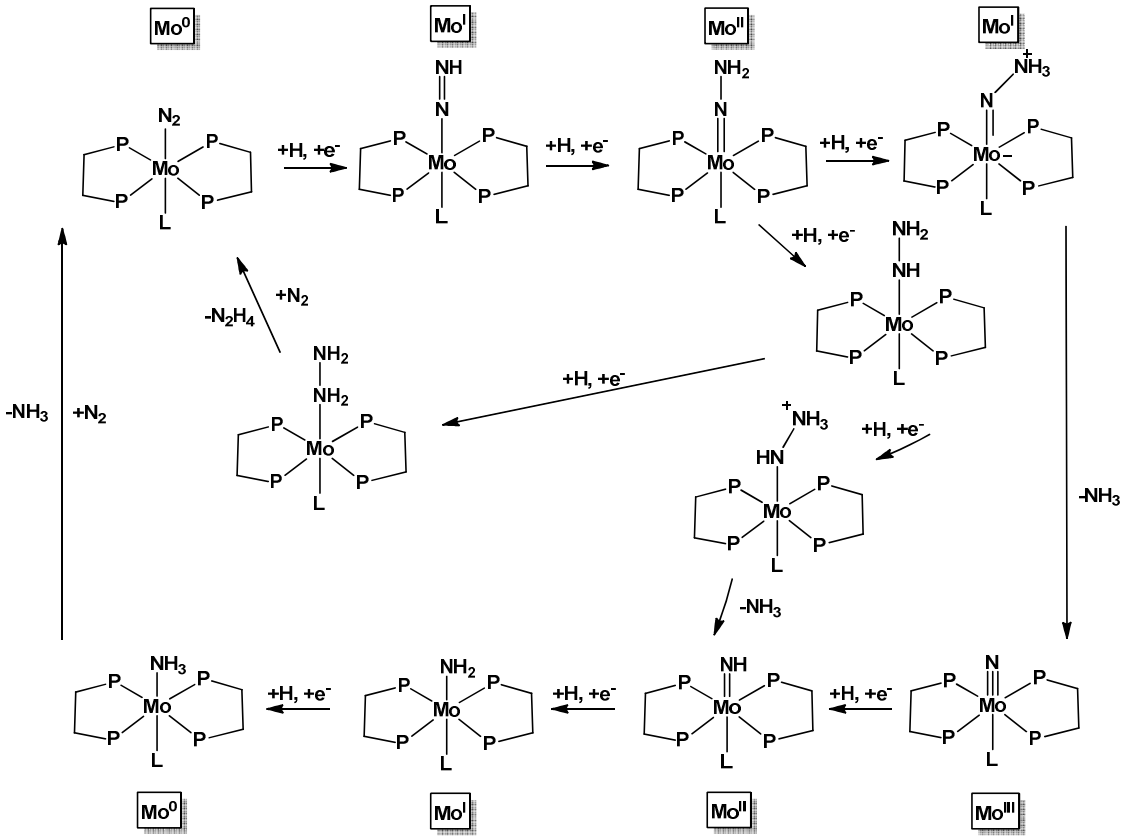

Scheme 3.1 The original Chatt-cycle.

An alternative pathway, shown in the middle of the scheme, generates a Mo(0)-N_2H_3 species upon H-atom transfer to the α- nitrogen of the hydrazido intermediate. This pathway avoids nitride formation, as releasing ammonia generates the Mo (II) imide. If the proton transfer occurs at the α-nitrogen again, the hydrazine intermediate, Mo(0)-N_2H_4, is formed and would account for the formation of hydrazine sometimes observed as a product of nitrogen reduction.

Similar to Chatt, Schrock et. al synthesized the molybdenum catalyst shown in Figure 3.3 along with many of the intermediates (1-6) proposed in the cycle displayed in Scheme 3.2. As many as 12 intermediates have been proposed in this catalytic cycle

of nitrogen reduction, and alternatively to Chatt, Schrock invokes oxidation states of 3 to 6 for the molybdenum site.[56,57,61]

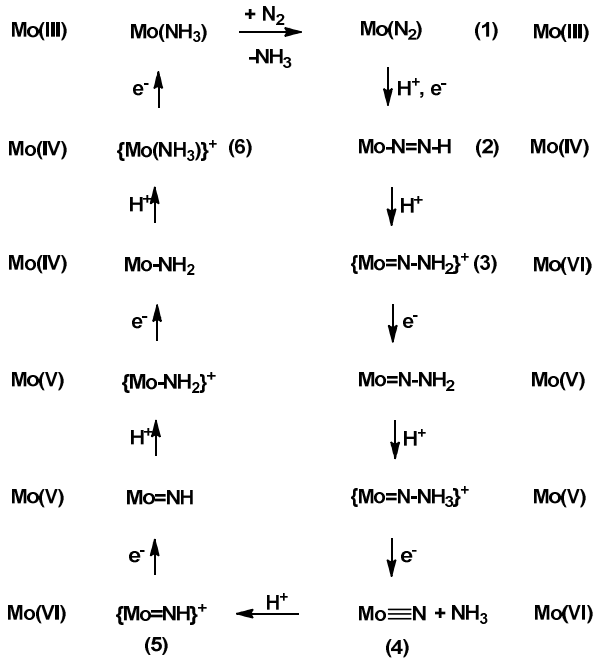

Scheme 3.2 Schrock's Proposed catalytic cycle and intermediates in the reduction of N_2 at a molecular site.

Chirik et.al. were also able to generate ammonia from the reduction of $[(\eta^5\text{-}C_5Me_4H)_2ZrH]_2N_2H_2$ (Scheme 3.3) with hydrogen.[41,42] Even though progress in N_2 reduction has been made, reduction at room temperature is still an extraordinarily difficult reaction. In terms of catalysis, barriers for industrial scale applications of these systems stem from high costs, low yields, and catalyst recovery.

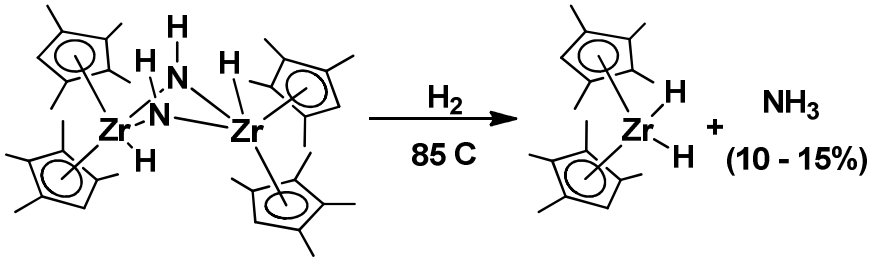

Scheme 3.3. Ammonia production by addition of hydrogen to $[(\eta^5\text{-}C_5Me_4H)_2ZrH]_2N_2H_2$.

First-row transition metals are generally a more attractive option for catalysis as they are more cost-efficient due to higher abundance and availability. Iron, in particular, has been the center of a large effort toward designing and synthesizing iron-dinitrogen systems with activation and reduction in mind, thanks to the iron-containing enzyme, nitrogenase.[13,18,20]

Many iron-dinitrogen systems have been synthesized,[39,62-77] and a few examples where nitrogen reduction, in the form of hydrazine or ammonia, were observed upon exposure to acid and reducing conditions, are shown in Figure 3.4.[34,39,66-68,71,78,79] Most iron-dinitrogen systems contain strong σ-donors such as phosphine ligands or N-heterocyclic carbenes, and Fe-N_2 complexes containing redox non-innocent, pyridine diimines have also been synthesized. These ligands likely contribute to better π-backbonding with the dinitrogen ligand, enhancing dinitrogen binding.

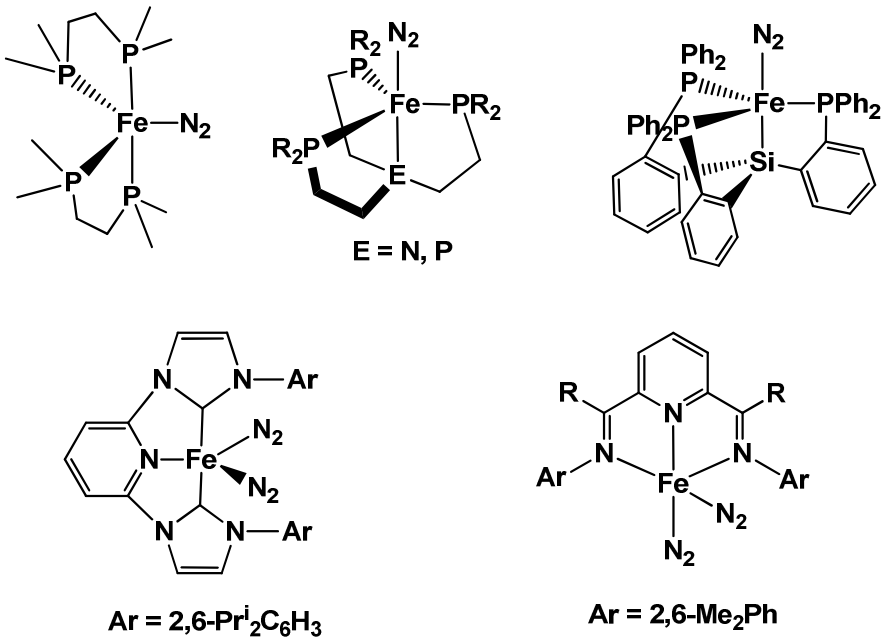

Figure 3.4. Examples of known iron-dinitrogen complexes.[34]

Similar to nitrogenase, the oxidative properties of dioxygen are usually detrimental to organometallic systems, and without excess reducing agent around, dinitrogen binding is unlikely to occur. There are a few exceptions of stability toward dioxygen within organometallic systems, including the formation of $(H_3N)_5RuN_2^{2+}$ in the presence of dioxygen,[36,37] and more interestingly, $[HFe(dppe)_2(THF)]^{+}$[80,81] and $H_2(H_2)Fe(\{PEtPh_2\}_3)$,[80,81] which form dinitrogen complexes upon exposure to air (Eq 3.11 and 3.12).

$$FeH_4(PEtPh_2)_3 \xrightarrow[\text{toluene}]{\text{air}} FeH_2(N_2)(PEtPh_2)_3 + H_2 \qquad (3.11)$$

$$FeH(dppe)_2^{+} \xrightarrow[\text{THF}]{\text{air}} FeH(N_2)(dppe)_2^{+} \qquad (3.12)$$

Since understanding the properties and reactivity of metal-dinitrogen systems is of significant interest, the Fe-N_2 complex, *trans*-{mer-κ-C,N,C'-(Ar-2-yl)CH_2N=CH(Ar-2-yl)}Fe(PMe_3)$_2$(N_2) (**2b**),[82] which contains two iron-carbon bonds, was investigated while cognizant of the potential for nitrogen activation. As discussed in Chapter 1, carbon-based ligands generate strong fields due to better orbital overlap between carbon and 3d metal orbitals, which may have interesting implications for dinitrogen binding and reactivity. Recently, Lancaster and Spatzal et al. proved the long-debated central atom of the FeMo cofactor to be carbon,[83,84] and there may be a related influence of the dinitrogen binding and properties associated with nitrogenase. A greater understanding of iron-dinitrogen complexes was sought while investigating the impact of strong-field ligands within this system.

II. Results and Discussion

A. Discovery of FeN_2

Diarylimine iron (III) compounds were previously prepared in order to access related azaallyl complexes via deprotonation. Unfortunately, deprotonation to generate the azaallyl consistently led to regeneration of the corresponding iron (II) derivatives. If the deprotonation occurred, the resulting high energy CNC^{nb} orbital of the azaallyl was likely to transfer an electron to the Fe (III) center, generating a radical on the azaallyl fragment as shown in Figure 3.5. Hydrogen atom transfer to the azaallyl radical would regenerate the Fe (II) product observed. If this theory is correct, a potential solution could be achieved by lowering the CNC^{nb} orbital beneath at least

one of the t_{2g} orbitals with electron withdrawing ligands. Initial attempts were made with a highly fluorinated system.

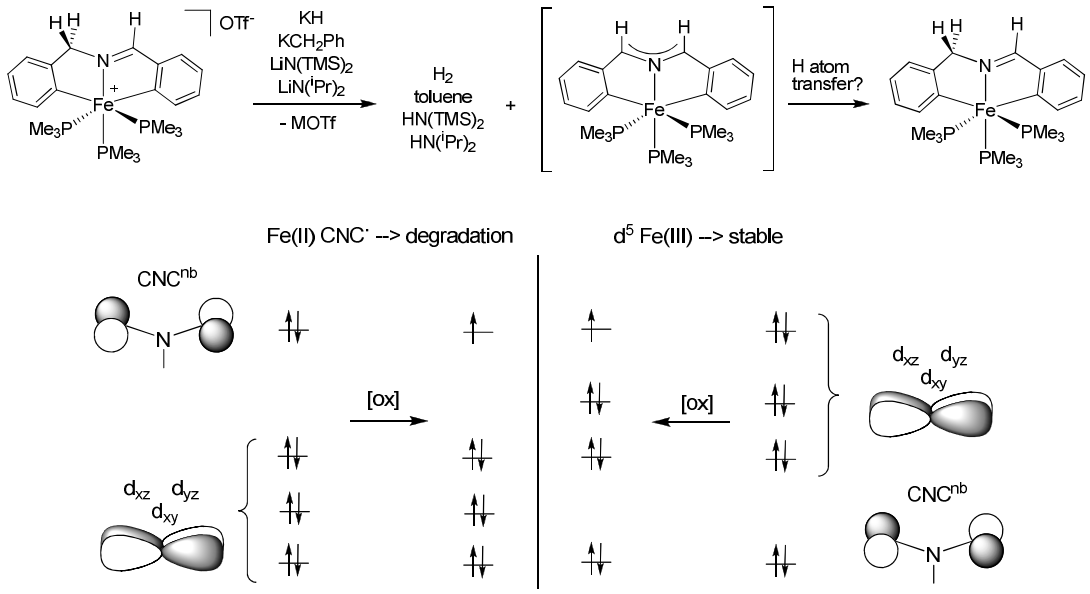

Figure 3.5. Proposed molecular orbital description for the formation of stable and unstable iron (III) species.

The fluorinated imine (**Im-b)** shown in Eq. 3.13, was chosen for initial experiments. Simple condensation of 2,4,5-trifluorobenzaldhyde with 3,4,5-trifluorobenzylamine resulted in the formation of **Im-b** in nearly quantitative yields. The particular substitution pattern shown was chosen due to the inexpensive starting materials available.

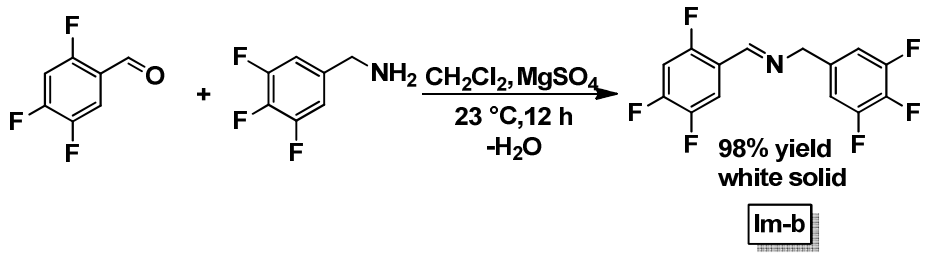

(3.13)

Addition of one equiv of **Im-b** to the iron (II) precursor, *cis*-$Fe(PMe_3)_4Me_2$,[85] in benzene led to the expected loss of two equiv of methane and one equiv of PMe_3, and formation of *trans*-{mer-κ-C,N,C'-(3,4,5-$(F)_3$-C_6H-2-yl)CH_2N=CH(3,4,6-$(F)_3$-C_6H-2-yl)}$Fe(PMe_3)_3$ (**1b**). Upon transferring to a nitrogen glovebox, only the corresponding N_2 complex, *trans*-{mer-κ-C,N,C'-(3,4,5-$(F)_3$-C_6H-2-yl)CH_2N=CH(3,4,6-$(F)_3$-C_6H-2-yl)}$Fe(PMe_3)_2(N_2)$ (**2b**), was observed (Scheme 3.4). Analysis by ^{31}P NMR revealed the equivalent phosphines of **2b** as a singlet at 19.96 and the IR showed a stretching frequency for the dinitrogen ligand at 2107 cm^{-1}. X-ray crystallography confirmed the structure of **2b** (Figure 3.8).

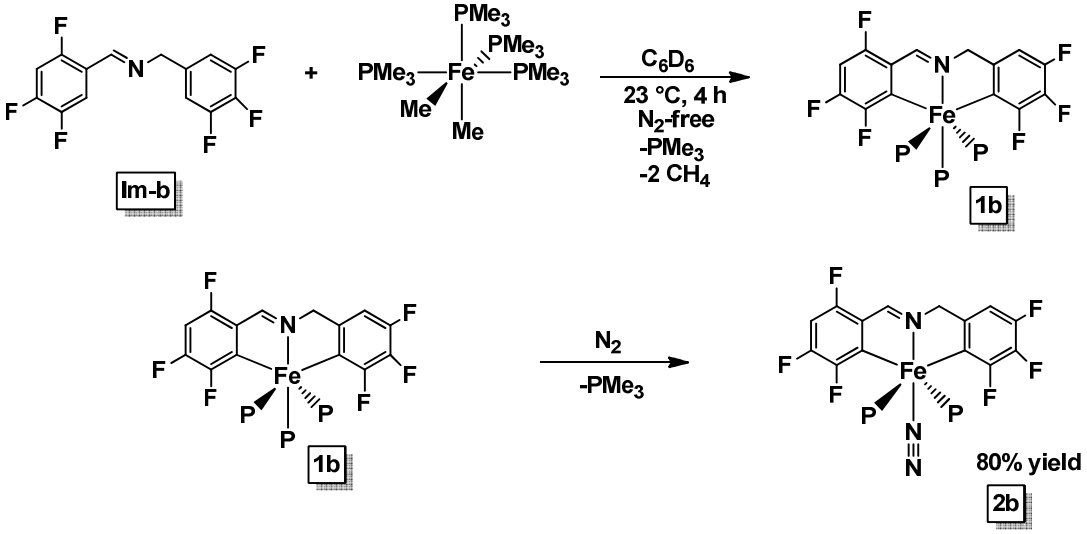

Scheme 3.4. Formation of trans-{mer-κ-C,N,C'-(3,4,5-$(F)_3$-C_6H-2-yl)CH_2N=CH(3,4,6-$(F)_3$-C_6H-2-yl)}$Fe(PMe_3)_2(N_2)$ (**2b**).

As mentioned, an analogous system was studied using an unsubstituted diarylimine where the trisphosphine complex was isolated as shown in Scheme 3.5.[82]

Various aryl pyridine-imines were also activated by *cis*-Fe(PMe_3)$_4$$Me_2$ to generate the corresponding trisphosphine complexes (Scheme 3.5).

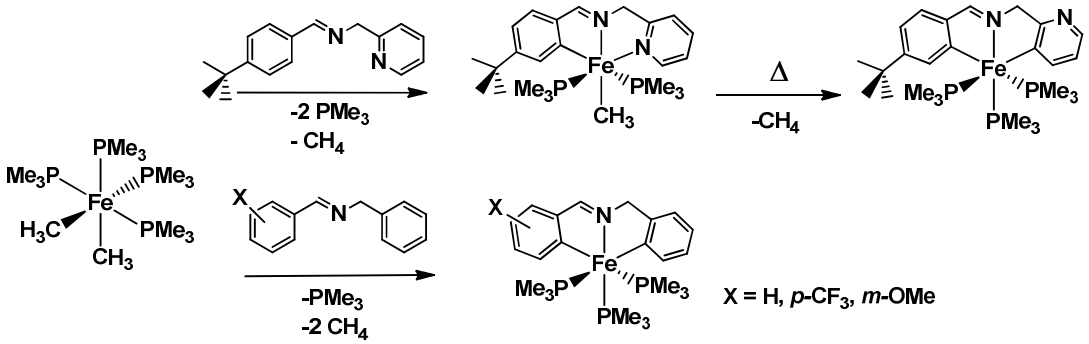

Scheme 3.5. Synthesis of trisphosphine complexes, {*mer*-κ-C,N,C'-Ar-2-yl)CH_2N=CH-(Ar-2-yl)}Fe(PMe_3)$_3$

It was anticipated that this system would be no different, yet the presence of the fluorine substitution seemed to play a substantial role in the loss of the second equiv of PMe_3 and uptake of dinitrogen.

In efforts toward the initial goal of a stabilized iron (III) azaallyl, **2b** was successfully oxidized to **12b**. Subsequent deprotonation attempts with a variety of bases reliably failed to yield a clean, isolable product.

B. Ligand Syntheses

To probe the effects of substituents on reactivity, different substituted diarylimines were prepared and they are illustrated in Figure 3.6. Alteration of the substituents *ortho* to the sites of aryl C-H activation made it possible to compare the resulting steric effects. Likewise, by altering the electron-withdrawing and electron-donating capabilities of the diarylimine, a conclusion about the electronic effects due to each imine could be made.

Diarylimine ligands were synthesized following general literature procedures, or slightly modified literature procedures (Eq 3.13).[86,87] Condensation of one equiv of substituted benzylamine with one equiv of the appropriate benzaldehyde in CH_2Cl_2 generated the imine as yellow oils or white solids in nearly quantitative yields. All were isolated and used without further purification (purity > 95%).

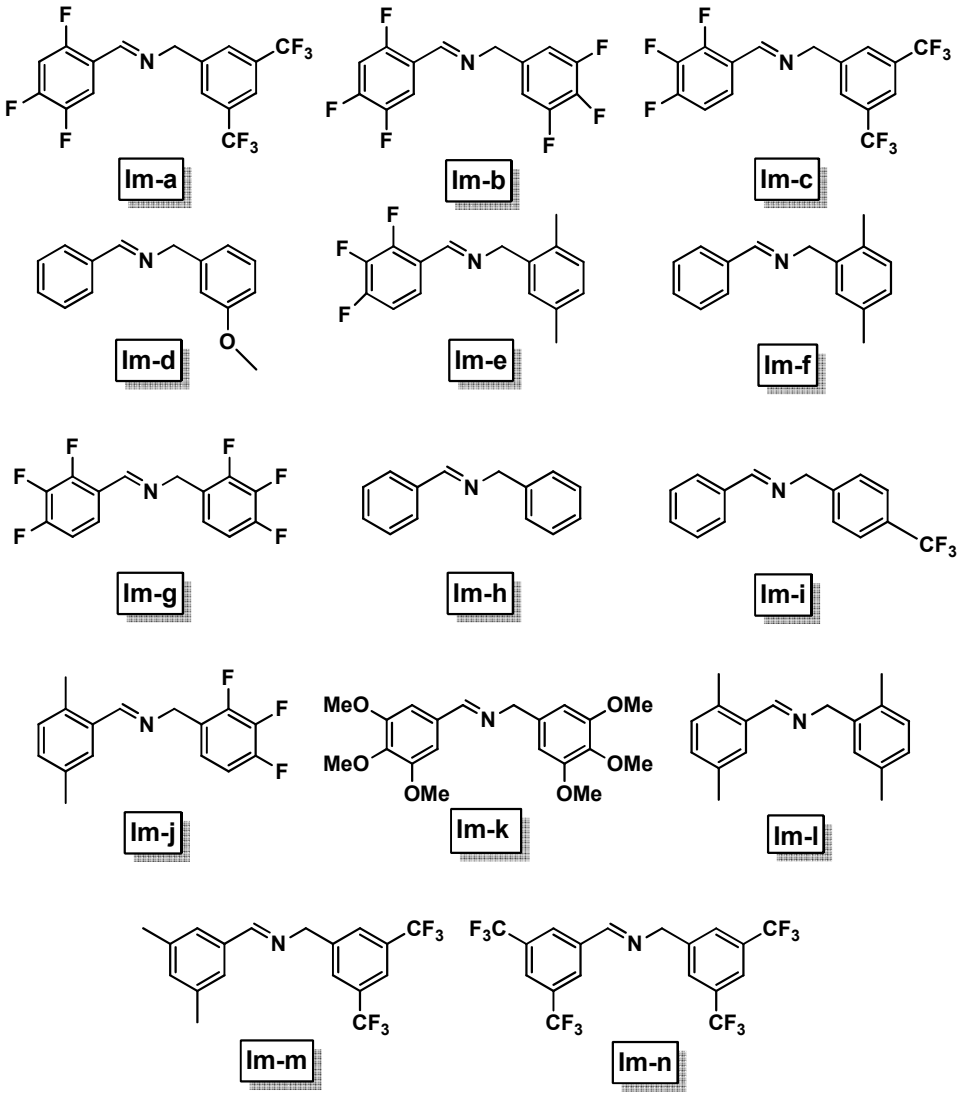

Figure 3.6. Various substituted diarylimine ligands.

C. Ligand Effects

To probe the effect the fluorinated substitution had on the formation of iron-dinitrogen complexes, a variety of diarylimines were synthesized as shown in Figure 3.6. Electron-withdrawing substituents on the aryl rings should weaken the backbonding to the nitrogen and could impede iron-dinitrogen formation. In contrast, the initial results suggested that there was some electronic feature of the fluorine-substituted diarylimine that permitted phosphine loss and subsequent dinitrogen binding. When a diarylimine ligand with similar electron withdrawing capability, but no *ortho*-fluorines to the metal-carbon bonds was investigated (**Im-g)**, it was quickly demonstrated that the electronic features of the fluorine were not responsible for the dinitrogen binding. **Im-g**, (2,3,4,-$(F)_3$-C_6H_2)CH_2N=CH(2,3,4-$(F)_3$-C_6H_2), was treated with *cis*-$Fe(PMe_3)_4Me_2$ to form the expected trisphosphine complex, {mer-κ-C,N,C'-(4,5,6-$(F)_3$-C_6H-2-yl)CH_2N=CH(4,5,6-$(F)_3$-C_6H-2-yl)}$Fe(PMe_3)_3$ (**1g**). Upon exposure to an atmosphere of nitrogen, no reaction was observed. This is in agreement with previous results reported in the formation of {mer-κ-C,N,C'-C_6H_4-2-yl)CH_2N=CH-(C_6H_4-2-yl)}$Fe(PMe_3)_3$ (**1h**) and {mer-κ-C,N,C'-5-(CF_3)-C_6H_2-2-yl)CH_2N=CH(C_6H_4-2-yl)}$Fe(PMe_3)_3$ (**1i**), which were unreactive towards a nitrogen atmosphere.[82]

Given that the electron-withdrawing features of the diarylimine were not substantially affecting dinitrogen binding, several different imines were investigated in attempts to find a trend in reactivity.

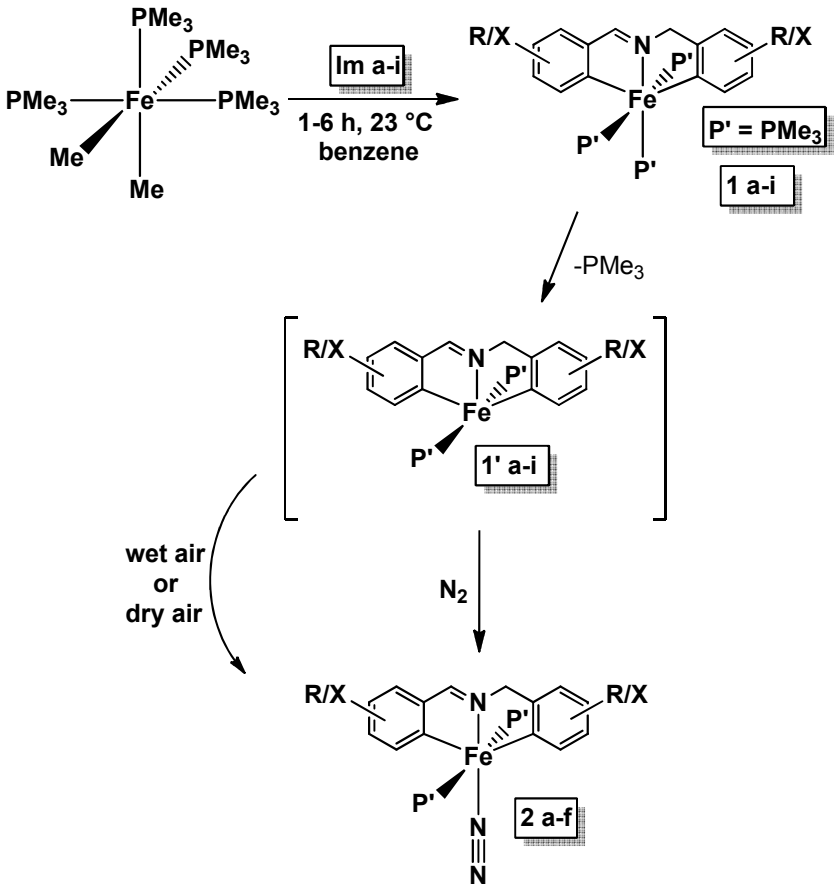

Scheme 3.6. Formation of trisphosphine complexes **1 a-i** and subsequent reaction with dinitrogen (N_2 atmosphere, dry air and wet air).

Organometallic compounds, in particular those containing iron-carbon bonds, are often unstable to air. Rapid degradation upon exposure to air is often indicated by a drastic change in color as the complex undergoes oxidation and/or hydrolysis. Upon removing reaction flasks of **2b** from the nitrogen glovebox and exposing them to air, no such change was visible. The apparent stability of **2b** led to us to question the stability of the trisphosphine precursor, **1a,** and to inquire about the potential selective binding of dinitrogen by these complexes. **Im-b** was combined with *cis*-$(Me_3P)_4FeMe_2$ in a J. Young NMR tube into which benzene-d_6 was vacuum transferred. ^1H, ^{19}F, and

^{31}P NMR spectroscopy confirmed the formation of **1b** after 1-6 h. Air was admitted to the tube and was forcefully shaken, resulting in a mixture of **1b** and **2b** as observed in subsequent NMR spectra. Upon repeated exposure to air, complete conversion to the dinitrogen complex **2b** was noted.

Shown in Scheme 3.6 are the imines which generated trisphosphine iron complexes that form dinitrogen complexes upon exposure to wet air, dry air or an atmosphere of dinitrogen. Previously, the reaction of a substantially more electron-donating methoxy substituted derivative, **Im-d,** with *cis*-$Fe(PMe_3)_4Me_2$ had been investigated and was prepared in-situ in a J.Young tube. The iron trisphosphine, {mer-κ-C,N,C'-6-(OCH_3)-C_6H_2-2-yl)CH_2N=CH(C_6H_4-2-yl)}$Fe(PMe_3)_3$ (**1d**), was generated, but the reaction mixture was never exposed to a nitrogen atmosphere. The reaction was rerun under a blanket of nitrogen, and *trans*-{mer-κ-C,N,C'-6-(OCH_3)-C_6H_2-2-yl)CH_2N=CH(C_6H_4-2-yl)}$Fe(PMe_3)_2(N_2)$ (**2d**) was generated in 80% yield. The imines that reacted to form complexes **2 a-f** ranged from the most electron-withdrawing (**Im-a)** to electron-donating (**Im-b)**. These imines have a substituent other than hydrogen at the position *ortho* to the metallation, and only one *ortho* substituent seems necessary for iron-dinitrogen formation. The relationship between the stretching frequency of the dinitrogen and the electron withdrawing capability of the diarylimines was determined by measuring IR spectra of **2 a-f**. The more electron withdrawing diarylimines (**Im a-c)** led to relatively electron-poor iron centers, attenuating iron π-backbonding with the dinitrogen ligand. This weaker π-backbonding led to weaker Fe-N bonds, and resulted in higher NN stretching frequencies. In contrast, substantially more electron donating imines, such as **Im d,f**,

resulted in lower stretching frequencies due to the enhanced backbonding between the iron and nitrogen. The expected inverse correlation of dinitrogen stretching frequencies versus electron withdrawing capacity of each diarylimine is displayed in Table 3.1.

Table 3.1: Stretching frequencies of {*mer*-κ-C,N,C'-(Ar-$_2$-yl)CH_2N=CH(Ar-2-yl)}Fe$(PMe_3)_2$(L), L= N_2, CO.

Compound P'=PMe_3		L = N_2 ν(NN), cm^{-1}		L = CO ν(CO), cm^{-1}	
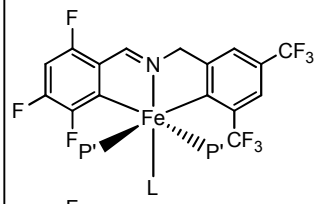	2a	2121	3a	1950
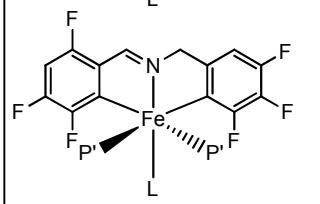	2b	2107	3b	1936
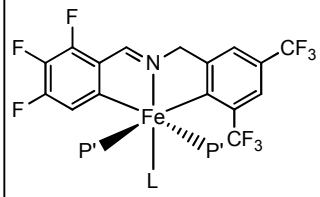	2c	2102	3c	1921
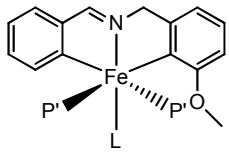	2d	2067	3d	1896
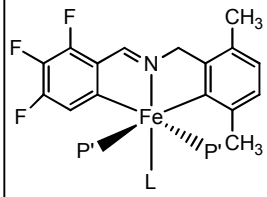	2e	2058	3e	
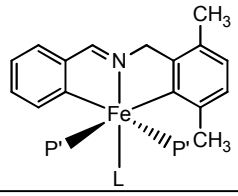	2f	2046	3f	1882

D. *Tris*-PMe_3 Iron (II) Complexes

1. Synthesis of Trisphosphine complexes 1 a-f.

Trisphosphine iron intermediates (**1 a-f**) were formed by treating *cis*-$Fe(PMe_3)_4Me_2$ with one equiv of imines **Im-a-f** in the absence of any nitrogen source (Scheme 3.6). The reactions were run on an NMR tube scale, and were followed by ^1H, ^{19}F and ^{31}P NMR spectroscopy. Complexes {*mer*-κ-C,N,C'-(Ar-2-yl)CH_2N=CH(Ar-2-yl)}$Fe(PMe_3)_3$ **1b** and **1d** gave characteristic diamagnetic shifts similar to that of **1g, 1i** and **1h**. The ^{31}P NMR revealed the expected splitting for an A_2B pattern with coupling constants (J_{PP}) of 58 (**1b**), 62 (**1d)** and 61(**1g)** Hz. Although **1b** and **1g** were diamagnetic, ^1H NMR spectra of trisphosphine complexes **1 a,c,e,f,g** were consistent with paramagnetic species. DFT calculations show the singlet and triplet ground states to be close in energy (Table 3.2), and Evans method measurements gave μ_{eff} values ranging from 3.0-3.3 μ_B, revealing S = 1 ground states with contributions from spin-orbit coupling.[88,89]

DFT calculations support triplet ground states for phosphine-dissociated intermediates, **1' a-f**, so it was conceivable that dissociation to the five-coordinate species had occurred. The ^1H NMR spectrum of **1a** revealed *cis*- and *trans*-phosphines as two unique signals at δ -11.64 ppm and δ -4.86 ppm respectively, along with the presence of free PMe_3, a byproduct from the *in situ* synthesis. The ^1H NMR spectra for **1c,e,f** showed broad features and overlapping PMe_3 signals. In addition to broad and overlapping signals, the spectrum for **1-c** also showed free PMe_3. The observation of free PMe_3 suggests that phosphine binding is strong enough to prevent exchange with free PMe_3 on the NMR timescale.

2. Activation of Imines (Im a-i) by *cis*-Fe(PMe$_3$)$_4$(Me)$_2$ for Formation of ({*mer*-κ-C,N,C'-(Ar-2-yl)CH$_2$N=CH(Ar-2-yl)}Fe(PMe$_3$)$_3$).

The ability of *cis*-Fe(PMe$_3$)$_4$(Me)$_2$ to perform two aryl C-H activations has been vital for the aforementioned investigations. From observations of CH-bond activation, some conclusions can be made regarding the mechanism of aryl activations by the iron starting material. As shown in Scheme 3.5, *cis*-Fe(PMe$_3$)$_4$(Me)$_2$ is able to activate aryl pyridine-imines as well as the imines **Im–a-j**. In the case of the aryl pyridine-imine, an initial chelation by the pyridine and imine along with one aryl C-H activation is observed. Upon heating, a second activation occurs as the pyridine rearranges. This illustrates the importance of the initial imine chelation prior to activation, and the two-step process likely required for both aryl activations.

As discussed, treatment of *cis*-Fe(PMe$_3$)$_4$(Me)$_2$ with one equiv of **Im–a-j**, resulted in the formation of the corresponding trisphosphine complexes. The rapid formation of **1 a-i** indicates the ease with which these aryl C-H activations occur. Surprisingly, not all diarylimines could be activated. Treatment of imines **Im–j-n** with *cis*-Fe(PMe$_3$)$_4$(Me)$_2$ resulted in no reaction. Due to the temperature sensitivity of the iron starting material, heating the reaction in efforts to initiate C-H activation led to decomposition of *cis*-Fe(PMe$_3$)$_4$(Me)$_2$.

The inability to form {*mer*-κ-C,N,C'-(Ar-2-yl)CH$_2$N=CH(Ar-2-yl)}Fe(PMe$_3$)$_3$ with imines **Im–j-n** suggests a steric barrier to forming the anticipated C-H activated complexes, as these imines all have larger substituents *ortho* to the site of activation. All diarylimines activated by *cis*-Fe(PMe$_3$)$_4$(Me)$_2$ have aryl-imine substitutions of either a hydrogen or fluorine at the position ortho to the metallation (Scheme 3.7).

Once that position is substituted with a methyl, methoxy, or CF_3 group, the imposing sterics prevented activation and no reaction was observed. Alternatively, substitutions at the analogous position on the aryl-amine unit did not present the same issues toward activation.

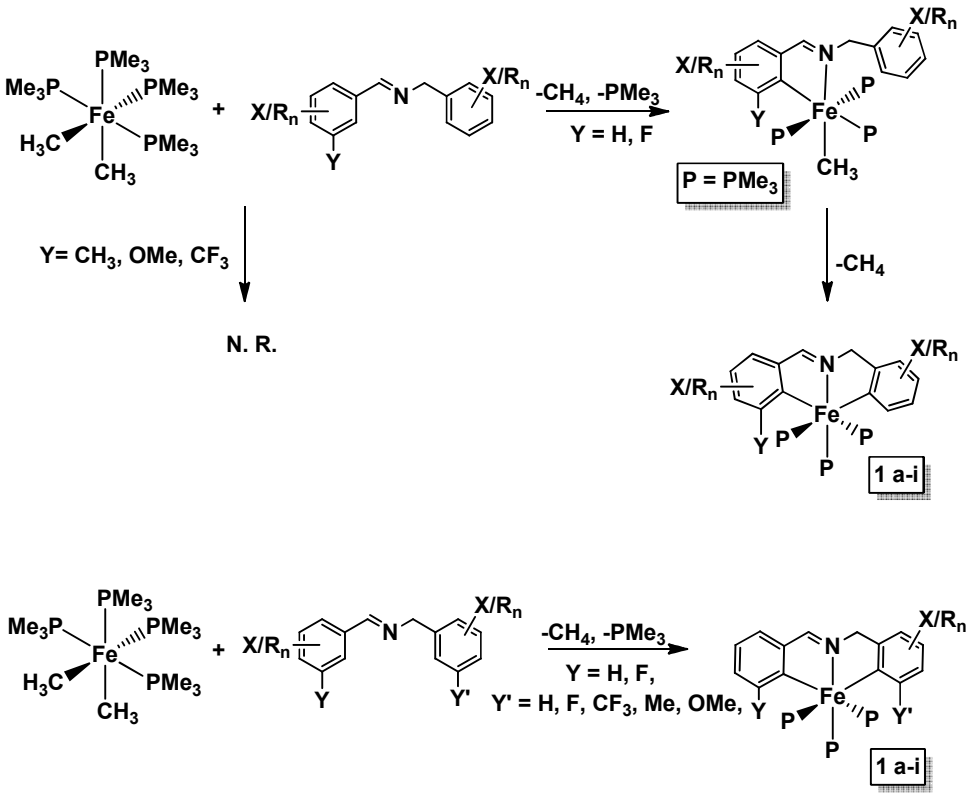

Scheme 3.7. Activation of substituted diarylimines by *cis*-$Fe(PMe_3)_4(Me)_2$.

It is reasonable to conclude that the *cis*-$Fe(PMe_3)_4(Me)_2$ initiates reactivity with the ligands by binding the imine followed by C-H activation of the aryl group attached to the imine side (arylCH=N) (Scheme 3.7). This preference in aryl activation could be due to the shorter bond distance of the C=N double bond. Once the first

activation has occurred, the second aryl group is poised to swing in and undergo the second activation.

2. Various Spin-States of Trisphosphine Complexes 1 a-g.

Complexes {*mer*-κ-C,N,C'-(Ar-2-yl)CH_2N=CH(Ar-2-yl)}Fe(PMe_3)$_3$, **1 a-f,** were generated and investigated as precursors for the preparation of the corresponding dinitrogen complexes **2 a-f**. In complexes where the *ortho* substituents were two fluorines (**1b)** or one methoxy group (**1d**), NMR spectra with diamagnetic resonances were recorded. When the *ortho* substituents were one fluorine and one CF_3 group (**1a**), only one CF_3 group (**1c**), or one CH_3 group (**1 e,f)**, NMR spectra with paramagnetic resonances were recorded. If the methoxy group can be considered smaller than a methyl group in the position *ortho* to activation, sterics may play a role in influencing the electronic structure. Smaller substituents allow for shorter Fe-P_{trans} bond distances, which results in a stronger field that and low spin. A longer Fe-P_{trans} bond results in intermediate spin.

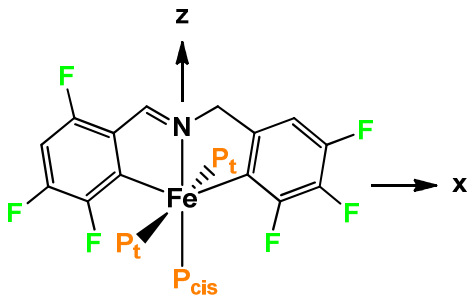

Table 3.2 Calculated metric parameters for the singlet, triplet and quintet states of {*mer*-κ-C,N,C'-(3,4,5-(F)$_3$-C$_6$H-2-yl)CH$_2$N=CH(3,4,6-(F)$_3$-C$_6$H-2-yl)}Fe(PMe$_3$)$_3$ (**1b**).

Spin State		***S* = 0**	***S* = 1**	***S* = 2**
	d(Fe-C)	2.07, 2.08	2.04, 2.06	2.20, 2.21
Å	d(Fe-P$_{tr}$)	2.26, 2.29	2.26, 2.26	2.57, 2.59
	d(Fe-P$_{cys}$)	2.36	3.18	2.69
	d(Fe-N)	1.96	2.15	2.20
	<C-Fe-C	159.7	155.8	150.8
	<C-Fe-N	80.1, 80.1	77.9, 77.9	72.5, 75.7
(°)	<P$_{tr}$-Fe-P$_{cis}$	89.6, 93.6	87.0, 87.0	89.5, 91.0
	<P$_{tr}$-Fe-P$_{tr}$	173.8	172.8	176.9
	<P$_{tr}$-Fe-N	86.6, 90.7	83.1, 93.4	88.7, 91.1
	<P$_{cis}$-Fe-N	173.5	175.8	174.9
	<P$_{tr}$-Fe-C	85.9, 88.2, 90.5, 94.5	89.1, 89.4, 92.2, 92.2	87.9, 89.1, 91.3, 91.6
	<P$_{cis}$-Fe-C	95.1, 105.1	97.9, 106.2	99.7, 109.5
	Δ E$_{rel}$	-7.0	-3.0	0.0
(kcal/mol)	Δ H$_{rel}$	-4.7	-2.3	0.0
	Δ G$_{rel}$	3.9	2.3	0.0

Table 3.2 lists the bond distances, angles, and relative energies for {*mer*-κ-C,N,C'-(3,4,5-(F)$_3$-C$_6$H-2-yl)CH$_2$N=CH(3,4,6-(F)$_3$-C$_6$H-2-yl)}Fe(PMe$_3$)$_3$ (**1b**) when calculated as a singlet (*S* = 0), triplet (*S* = 1) and quintet (*S*=2). In the comparison of bond distances and angles from singlet to triplet, there is an overall trend of bond elongation. The difference in d(Fe-P$_{cys}$) in the calculated singlet and triplet state is particularly dramatic. The calculated free energy of the singlet is 1.6 kcal/mol higher than the triplet, and 3.9 kcal/mol higher in energy than the quintet state. This clearly does not match experimental observations for diamagnetic complex **1b.** Even though

the calculations differ from experiment, the calculated relative energies for the singlet, triplet and quintet are all quite similar. Since DFT methods do not always generate reliable energies for comparison of open shell (S = 1, 2) and closed shell systems (S = 0), [90-93] relatively similar values for all of the calculated states is significant. Although the free energies do not correlate with experiment for predicting diamagnetic vs. paramagnetic behavior in this case, the values for ΔE_{rel} and ΔH_{rel} do predict a singlet ground state for **1b**.

Upon changing from S = 0 to S = 1, there is a remarkable increase in the bond length of Fe-P_{cys}, the iron-phosphorus bond trans to the imine, from 2.36 to 3.18 Å.

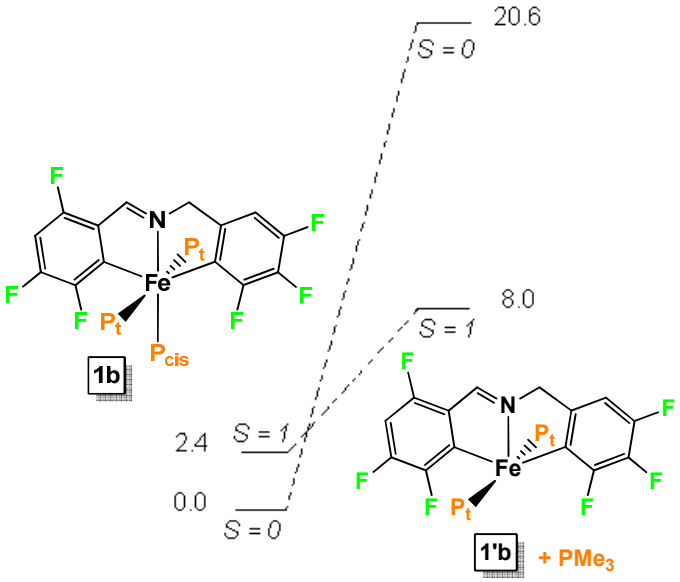

Figure 3.7. Calculated phosphine dissociation from **1b** along the reaction coordinate to generate **1'b**.

This occurs as one electron populates the dz^2 orbital in the triplet state. Since the hypothesized five-coordinate species, **1'b**, is calculated to be a triplet, the dissociation of phosphine (P_{cys}) likely occurs along a reaction coordinate by an intersystem

crossing event from a singlet surface to that of a triplet. As the Fe-P_{cys} bond elongates, transition to the five-coordinate species, **1'b,** is achieved through phosphine loss (Figure 3.7). The barrier to **1'b** is calculated to be at least 8.0 kcal/mol, and could correlate to the binding energy of PMe_3 (Figure 3.7). Franke et. al. discussed similar observations in their investigation of five-coordinate iron (II) complexes ($[FeX(depe)_2]BPh_4$, X = Cl, Br) which have triplet ground states.[94,95] They also observe reactivity with dinitrogen to form the analogous six-coordinate complexes that have singlet ground states.

E. Structure of *trans*-{*mer*-k-C,N,C'-(3,4,5-$(F)_3$-C_6H-2-yl)CH_2N=CH(3,4,6-$(F)_3$-C_6H-2-yl)}Fe $(PMe_3)_2(N_2)$ (2b).

The molecular structure of *trans*-{*mer*-k-C,N,C'-(3,4,5-$(F)_3$-C_6H-2-yl)CH_2N=CH(3,4,6-$(F)_3$-C_6H-2-yl)}Fe$(PMe_3)_2(N_2)$ (**2b**) was determined by single crystal X-ray diffraction techniques, and is shown in Fig. 3.8.

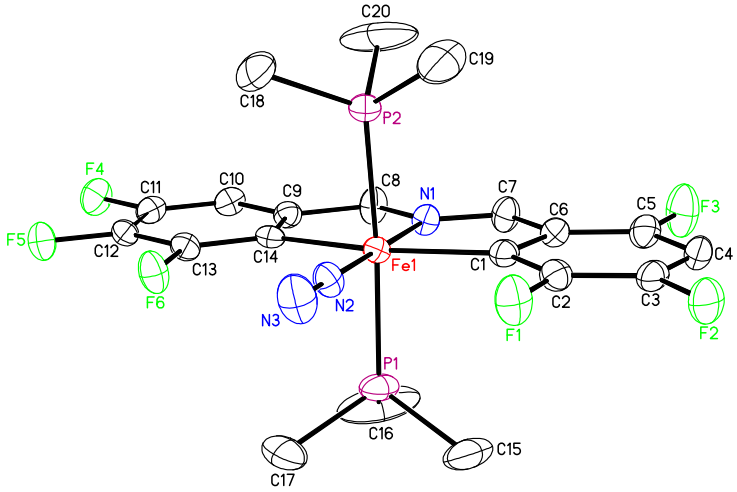

Figure 3.8. Molecular view of *trans*-{*mer*-κ-C,N,C'-(3,4,5-$(F)_3$-C_6H-2-yl)CH_2N=CH(3,4,6-$(F)_3$-C_6H-2-yl)}$Fe(PMe_3)_2(N_2)$ (**2b**).

Crystallographic details and pertinent bond distances and angles for **2b** are given in Tables 3.2 and 3.3, respectively. Core bond lengths are very similar to previously studied aryl pyridyl-imine and diarylimines complexes[82] derived from aryl-activation by *cis*-$Fe(PMe_3)_4Me_2$. Specifically, the similarities are highlighted in the Fe-N_{im} (Fe1-N1) distance of 1.9347(19) Å, the iron-carbon distances of 1.996(2) and 2.014(2) Å, and iron-phosphorus distances of 2.2292(7), and 2.2389(7) Å. With an N2-N3 distance of 1.104(3), the dinitrogen is only slightly elongated from the molecular dinitrogen N-N distance of 1.0977 Å.[34,96] The relatively short N2-N3 distance is consistent with an IR stretching frequency of 2107 cm^{-1}. The N1-C7 and N1-C8 bond distances of 1.308(3) Å and 1.459(3) Å show substantial differences in the imine C=N and C-N bonds, as expected.

Table 3.3. Crystallographic data for *trans*-{*mer*-k-C,N,C'-(3,4,5-$(F)_3$-C_6H-2-yl)CH_2N=CH(3,4,6-$(F)_3$-C_6H-2-yl)}$Fe(PMe_3)_2(N_2)$ (**2b**) and *trans*-{*mer*-κ-C,N,C'-(3,4,5-$(F)_3$-C_6H-2-yl)CH_2N=CH(3,4,6-$(F)_3$-C_6H-2-yl)}$Fe(PMe_3)_2Cl$ (**12b**).

	2b	**12b**
Formula	$C_{20}H_{23}F_6N_3P_2Fe$	$C_{20}H_{23}ClF_6FeNP_2$
Formula weight	537.20	544.63
Crystal System	Monoclinic	Monoclinic
Space group	Cc	P2(1)/c
Z	4	4
a, Å	19.0597(7)	10.6916(9)
b, Å	9.1733(4)	8.1275(7)
c, Å	15.7972(10)	26.737(2)
α, deg	90	90
β, deg	121.8450(10)	100.653(4)
γ, deg	90	90
V, $Å^3$	2346.2(2)	2283.3(3)
r_{calc}, $g \cdot cm^{-3}$	1.521	1.584
μ, mm^{-1}	0.839	0.974
Temperature, K	173(2)	173(2)
λ(Å)	0.71073	0.71073
R indices	R_1 = 0.0364	R_1 = 0.0370
$[I > 2\sigma(I)]^{a,b}$	wR_2 = 0.0815	wR_2 = 0.0903
R indices	R_1 = 0.0434	R_1 = 0.0528
(all data)^{a,b}	wR_2 = 0.0858	wR_2 = 0.1004
Goodness-of-fit^c	1.024	1.023

$^a R_1 = \Sigma||F_o| - |F_c||/\Sigma|F_o|$. $^b wR_2 = [\Sigma w(|F_o| - |F_c|)^2/\Sigma wF_o^2]^{1/2}$. ^{c}*GOF* (all data) = $[\Sigma w(|F_o| - |F_c|)^2/(n - p)]^{1/2}$, n = number of independent reflections, p = number of parameters.

Core angles of **2b** show a slightly distorted octahedron with an N1-Fe-N2 angle of 178.17(10) °, a phosphorus-iron-phosphorus angle of 176.04(03) °, an aryl-iron-aryl angle of 163.06(9) °, N1-Fe-C angles of 81.82(9) ° and 81.25(9) °, and an average N2-Fe-P angle of 90.11(7) °. A small difference in binding of the aryl rings is indicated by the difference in the inner and outer Fe-C-C angles. This difference is slightly larger for the imine-containing chelate (Fe-C1-C6 = 111.81 (15) °; Fe-C1-C2 = 134.17(19) °) than for the other (Fe-C14-C9 = 113.79(18) °; Fe-C14-C13 =

131.84(16) °). The C1-Fe-C14 of 163.06(9) ° is perhaps the most interesting feature of the structure. This bite angle is significant because it is key to σ^*/d_{xz} mixing within the diarylimine plane, which allows for better orbital overlap and energy match with the N(π^*) orbitals (Figure 3.9). Unsurprisingly, the Fe-N2-N3 angle of 178.9(2) ° indicates a linear dinitrogen.

Table 3.4. Selected distances (Å) and angles (°) for *trans*-{*mer*-k-C,N,C'-(3,4,5-$(F)_3$-C_6H-2-yl)CH_2N=CH(3,4,6-$(F)_3$-C_6H-2-yl)}Fe$(PMe_3)_2(N_2)$ (**2b**) and *trans*-{*mer*-κ-C,N,C'-(3,4,5-$(F)_3$-C_6H-2-yl)CH_2N=CH(3,4,6-$(F)_3$-C_6H-2-yl)}Fe$(PMe_3)_2$Cl (**12b**).

	2b	**12b**
Fe1-N1	1.9347(19)	1.9389(17)
Fe1-C1	1.996(2)	2.031(2)
Fe1-C8		2.028(2)
Fe1-C14	2.014(2)	
Fe1-P1	2.2292(7)	2.2602(6)
Fe1-P2	2.2389(7)	2.2463(6)
Fe1-N2	1.811(2)	
Fe1-Cl		2.2306(6)
N1-C7	1.308(3)	1.299(3)
N1-C8	1.459(3)	
N1-C14		1.460(3)
N2-N3	1.104(3)	
C6-C7	1.443(3)	1.434(3)
C14-C13		1.497(3)
C8-C9	1.501(4)	
N1-Fe-N2	178.17(10)	
N1-Fe-Cl		178.04(5)
C1-Fe-C8		160.70(9)
C1-Fe-C14	163.06(9)	
P1-Fe-P2	176.04(3)	174.29(2)
N1-Fe-C1	81.25(9)	79.80(8)
N1-Fe-C8		80.96(8)
N1-Fe-C14	81.82(9)	
P1-Fe-N1	91.47(6)	91.90(5)
P2-Fe-N1	91.32(6)	93.74(5)
P1-Fe-Cl		86.64(2)
P2-Fe-Cl		87.75(2)
P1-Fe-N2	89.54(7)	

	2b	12b
P2-Fe-N2	87.74(7)	
C1-Fe-P1	91.62(7)	89.88(6)
C8-Fe-P1		89.23(6)
C14-Fe-P1	89.13(7)	
C1-Fe-P2	91.59(7)	92.02(6)
C8-Fe-P2		90.74(6)
C14-Fe-P2	88.49(6)	
C1-Fe-Cl		98.88(7)
C8-Fe-Cl		100.31(6)
C1-Fe-N2	97.20(9)	
C14-Fe-N2	99.73(9)	
Fe-C1-C2	134.17(19)	133.60(18)
Fe-C1-C6	111.81(15)	111.90(16)
Fe-C14-C13	131.84(16)	
Fe-C8-C9		131.47(17)
Fe-C14-C9	113.73(18)	
Fe-C8-C13		114.41(15)

F. Molecular Orbital View of π-backbonding to N_2.

A DFT calculation was performed for *trans*-{*mer*-k-C,N,C'-(3,4,5-$(F)_3$-C_6H-2-yl)CH_2N=CH(3,4,6-$(F)_3$-C_6H-2-yl)}Fe$(PMe_3)_2(N_2)$ (**2b**) and the truncated molecular orbital diagram generated is displayed in Figure 3.9. The extent of σ^*/d_{xz} mixing within the diarylimine plane is a consequence of the 163.06(9) ° bite angle. This mixing is responsible for better overlap and a greater energy match with the N(π*) orbitals. The results are seen in enhanced backbonding, even with the electron-withdrawing ligand, **Im-b.** The bite angle is presumed similar in the other Fe-N_2 complexes, **2 a,c-f**, which are likely to have similarly efficient backbonding with dinitrogen. While these calculated energies are given in eV, they should not be taken as absolute values[90-93] because the energies of virtual vs. filled orbitals are relatively accurate within each set, but are probably imprecise in relation to each other.

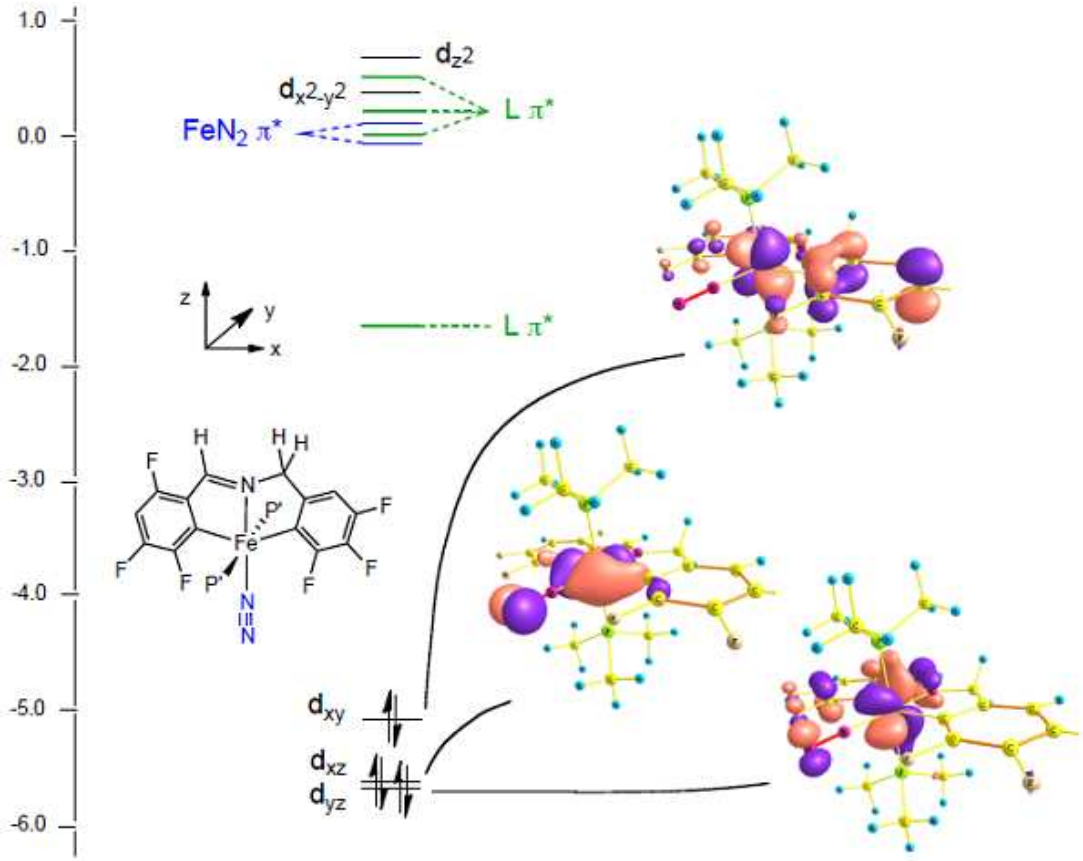

Figure 3.9. Truncated molecular orbital diagram of *trans*-{*mer*-κ-C,N,C'-(3,4,5-$(F)_3$-C_6H-2-yl)CH_2N=CH(3,4,6-$(F)_3$-C_6H-2-yl)}$Fe(PMe_3)_2(N_2)$ (**2b**) showing the greater π-backbonding from the d_{xz} orbital relative to d_{yz} as a consquence of σ^*/d_{xz}-mixing.

G. Half-Life Studies for Decomposition of 2 b-f in Air and Oxygen.

As described in section C, complexes **2 b-f** failed to show any visible signs of degradation immediately upon exposure to air. In order to investigate the degree of stability toward air, studies to determine half-life values for each Fe-N_2 complex (**2a-2f)** were conducted. Table 3.5 shows $t_{1/2}$ values for each complex in air (wet and dry) and pure dioxygen, all under 1 atmosphere. Each experiment was conducted by placing compounds **2 a-f** in a J.Young tube with 0.6 mL benzene-d_6, exposing the sample to the specified conditions, shaken, and monitored via ^{1}H NMR. For air

experiments, no visible change or degradation was noticed immediately. After refreshing the atmosphere over the samples periodically, a remarkable stability was noted in the dry air experiments. Treatment of **2 a-f** with pure dioxygen resulted in the solution changing from yellow/brown in color to red/orange.

The most stable of the iron-dinitrogen complexes (**2 a,b,f)** did not degrade in "dry air", atmospheric air that had been run through a dry-ice/acetone trap, for over 2 weeks; other complexes (**2 c,e)** were only stable for a few hours. In "wet air", the complexes had much shorter half-lives of 1-2 hours, which suggested protolytic degradation in the presence of water. This hypothesis was corroborated by the observation of free ligand growing in during the decomposition of Fe-N_2 in "wet air". Addition of 1 atm of pure dioxygen led to the shortest half-life values ranging from 10 – 30 min. In the O_2 experiments, no trend was associated with the diarylimine ligands and $t_{1/2}$ values, as complexes with both electron-donating and -withdrawing imines showed similar stability.

Table 3.5. Stability $t_{1/2}$ values for **2 a-f** under various conditions (wet air = atmosphere conditions; dry air = atmospheric conditions with water removed; $p(H_2O)$ ~ 22-30 torr).

Compound P' = PMe_3	$T_{1/2}$ 1 atm air	$t_{1/2}$ 1 atm dry air	$t_{1/2}$ 1 atm O_2
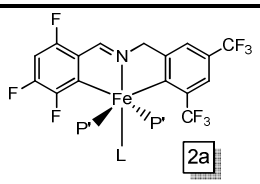 2a	2h	>2 weeks	<10 min
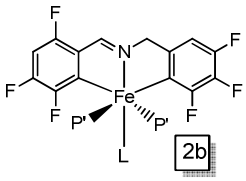 2b	1.5 h	>2 weeks	30 min
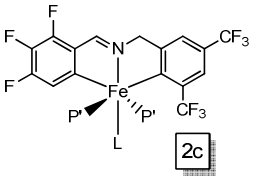 2c	1.5 h	2 h	30 min
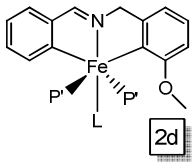 2d	2 h	1 week	30 min
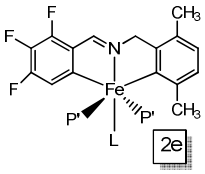 2e	1 h	2 h	<10 min
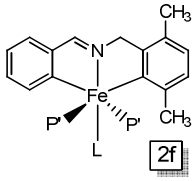 2f	2 h	<2 weeks	30 min

Half-life values for degradation in 1 atm of dioxygen were remarkably shorter than in dry air. Although the concentration of oxygen in air (~0.2 atm) is roughly five times less than 1 atm of pure dioxygen, the average rate difference was roughly 1000 times. If the only factor for degradation was oxygen concentration, the dry air experiments would yield $t_{1/2}$ values that were four times larger than dioxygen experiments. Only for **2 c** did half-life values for dry air and dioxygen show similar degradation rates once the difference in concentration was taken into account. These results imply a kinetic preference for dinitrogen over dioxygen association with the 5-coordinate iron diphosphine intermediate. If initial loss of dinitrogen is the first step, selective and reversible binding of dinitrogen could be a reasonable explanation for the observed stabilities. A sample of **2b**-$^{15}N_2$ was prepared by generating **1b** in a J.Young tube and subsequently exposing the tube to $^{15}N_2$. **2b**-$^{15}N_2$ was observed by ^{15}N NMR spectroscopy (Figure 3.10), and the spectrum shows resonances at δ 369.55 (N_α) and δ 334.15 (N_β) relative to $NH_3(l)$.[97] The resolved N-N coupling, $^1J_{15N15N}$, of 4 Hz indicates there is no rapid and reversible dissociation of dinitrogen on the NMR timescale, nor is there scrambling at N_α and N_β.

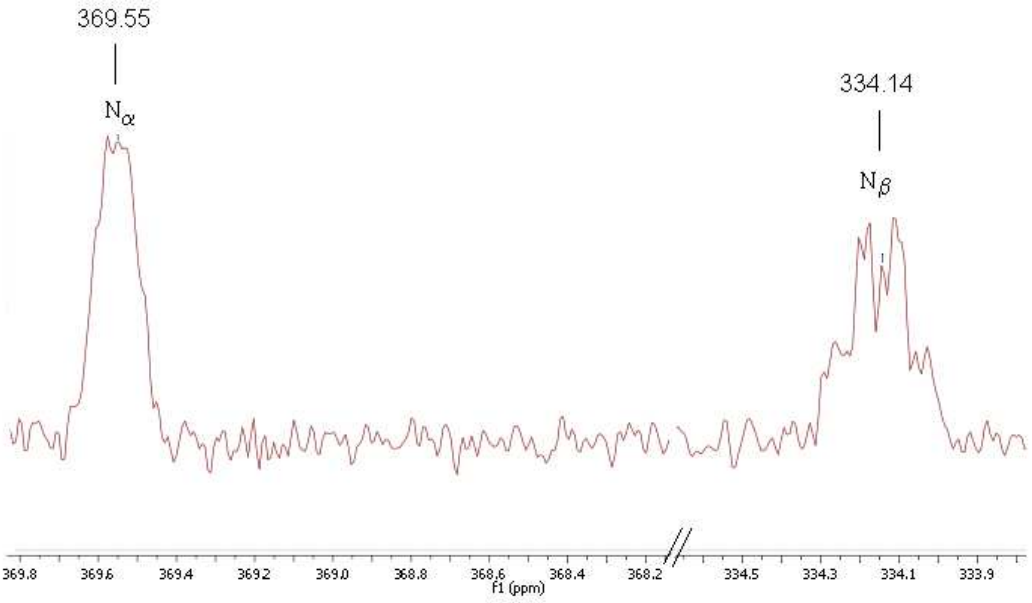

Figure 3.10. ^{15}N NMR spectrum for **2b** showing resolved signals for N_α and N_β.

Rapid degradation under an atmosphere of dioxygen could be the result of irreversible loss of dinitrogen. If the mechanism of degradation were purely dissociative, it would be easy to correlate the strength of the Fe-N binding by comparing ν(NN) to rates of degradation. This does not appear to be the case since **2e** has a relatively low stretching frequency of 2058 cm^{-1}, suggesting stronger Fe-N backbonding, and yet it is one of the fastest to degrade under an atmosphere of dioxygen. With a stretching frequency of 2102 cm^{-1}, **2c** is one of the slowest to degrade under identical conditions. There also seems to be no correlation between degradation rates of **2a-2c** and the electron transfer to dioxygen. The more electron-rich complexes (**2d-2f)** appear to degrade at similar rates as the more electron-deficient species (**2a-2c)**.

Determining the path of degradation in dioxygen is not trivial. It is clear that **2 b-f** disappear under these conditions, but there are no other organic materials or NMR-active species observed that identify the outcome of the reaction. It is not unusual for signals in NMR spectroscopy to broaden in the presence of dioxygen, but it is strange for paramagnetic signals to vanish completely. Evans method experiments on crude samples of **1 a-i** gave μ_{eff} values ranging from 3.1-3.5 μ_B, indicating formation of an *S* = 1 material was possible. Calculations also suggested the possibility of an iron (III) superoxide with a triplet ground state. The generation of paramagnetic {*mer*-κ-C,N,C'-Ar-2-yl)CH_2N=CH(Ar-2-yl)}Fe(PMe_3)$_2$-(O_2) was initially considered as an option (Fig 3.11), however the expected O-O bands and Fe-O bands were not observed in the infrared spectrum.[98-100] Other potential products that could possess triplet ground states are presented in Figure 3.11, including an iron (IV)-oxo and a bridging μ-oxo complex.

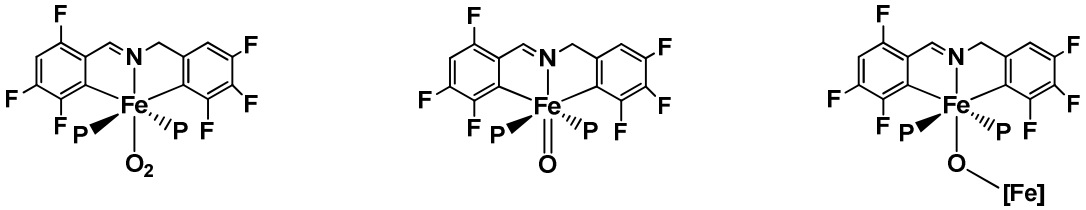

Figure 3.11. Possible products of **2b** after treatment with 1 atm of dioxygen (P = PMe_3).

Attempts to crystallize and structurally characterize the unknown product resulted in crystallization of trimethylphosphine oxide, indicative of oxidative destruction. The unknown product of **2b** and O_2 was quenched with water, and the

formation of **Im-b,** $OPMe_3$ and black solid was observed. It is possible that the Fe-N_2 complexes generate aggregates of L_nFeO_x upon exposure to an atmosphere of dioxygen. These paramagnetic aggregates could sufficiently broaden NMR spectroscopic signals making it difficult to see organic products.

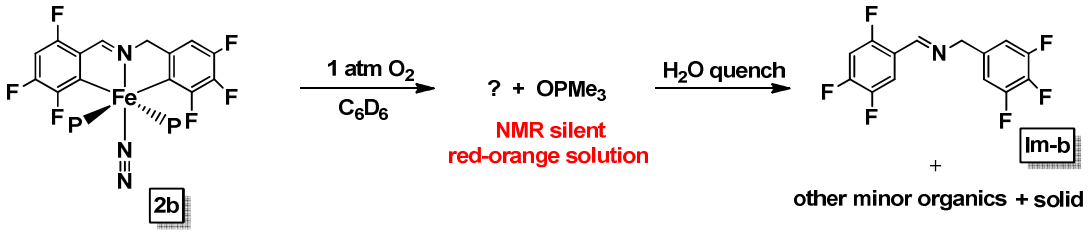

Scheme 3.8. Treatment of **2b** with dioxygen to form unknown products and subsequent regeneration of **Im-b** in the presence of water.

Treatment of {*mer*-κ-C,N,C'-(3,4,5-$(F)_3$-C_6H-2-yl)CH_2N=CH(3,4,6-$(F)_3$-C_6H-2-yl)}$Fe(PMe_3)_3$ (**1b**) with 1 atm of O_2 resulted in similar formation of black solid, but without $OPMe_3$ or free ligand (**Im-b)**. Trimethylphosphine oxide can be challenging to see by ^{31}P NMR spectroscopy in the presence of paramagnetic species, so not observing $OPMe_3$ by NMR spectroscopy does not necessarily rule out its presence.

H. Primary Alkynes as Weak Acids to Model Protolytic Degradation

From Table 3.5, the degradation of compounds **2 b-f** is more rapid in "wet air" than "dry air" for most cases. The formation of free ligand (**Im b-f)** upon exposure to "wet air", suggested protolytic degradation was likely. One equiv of H_2O was added to *trans*-{*mer*-κ-C,N,C'-(3,4,5-$(F)_3$-C_6H-2-yl)CH_2N=CH(3,4,6-$(F)_3$-C_6H-2-yl)}$Fe(PMe_3)_3$ (**1b**) in hopes of observing hydrolysis intermediates, however such procedures consistently led to decomposition of the starting complex to form black solid and free ligand (**Im-b)**. Primary alkynes, thought of as weakly acidic substrates,

were considered as another means toward observing intermediates generated during protolytic degradation. Trisphosphine complexes **1a** and **1b** were treated with one equiv of HCCR (R = Me, Ph), to afford *trans*-{κ-C,N-(3,5-$(CF_3)_2$-C_6H_3)CH_2N=CH(3,4,6-$(F)_3$-C_6H-2-yl)}Fe$(PMe_3)_3$(CCR) (R = Me, **4a**-Me; R = Ph, **4a**-Ph) and *trans*-{κ-C,N-(3,4,5-$(F)_3$-C_6H_2)CH_2N=CH(3,4,6-$(F)_3$-C_6H-2-yl)}Fe$(PMe_3)_3$(CCR) (R = Me, **4b**-Me; R = Ph, **4b**-Ph). IR spectra revealed acetylide CC stretching frequencies of 2077 cm^{-1} for **4a**-Me, and 2044 cm^{-1} for **4a**-Ph. Similar bands were observed at 2081 cm^{-1} for **4b**-Me, and 2050 cm^{-1} for **4b**-Ph. Dark red solids of **4b**-Me and **4b**-Ph were isolated in 69% and 79%, respectively. Reactions of **1a** with HCCR (R = Me, Ph) were run in J.Young tubes, and no attempts at isolation of **4a**-Me or **4a**-Ph were made.

As shown in Scheme 3.9, the primary acetylenes protonate one of the aryls to generate a free-hanging "arm". In both cases, protonation occurs on the benzylamine (CH_2-Ar-2-yl) side. It is not surprising that protonation occurs at the longer iron-aryl site (2.014(2) vs. 1.996(2) Å), but it was not determined if this was a kinetic or thermodynamic preference. The ^{31}P NMR shows the characteristic A_2B spin-system[95] present in all of the diamagnetic trisphosphine complexes, giving rise to a triplet for the unique PMe_3 and a doublet for the *trans*- phosphines, P'.

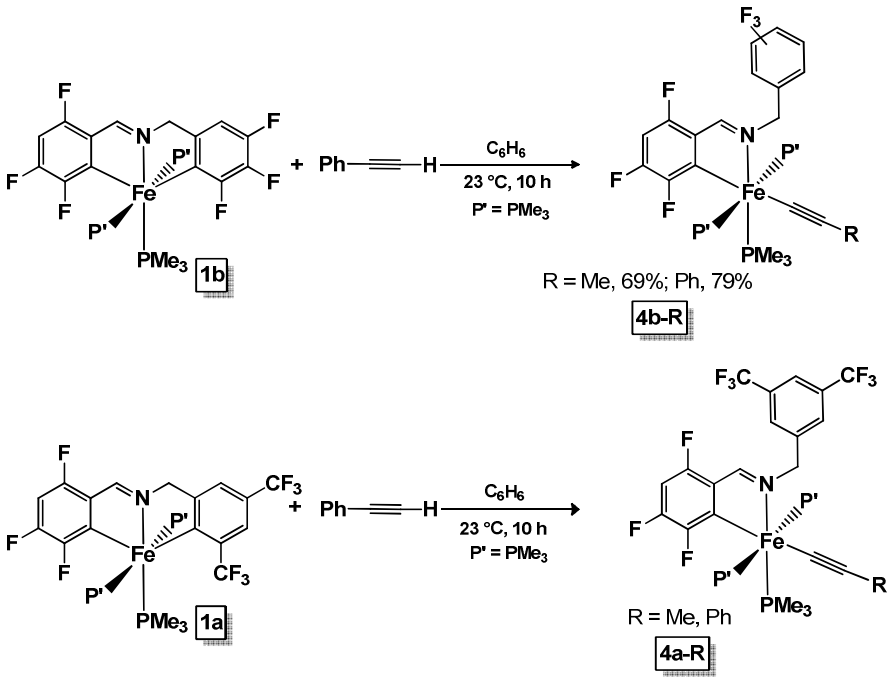

Scheme 3.9. Modeling protolytic degradation with weak acids (primary alkynes).

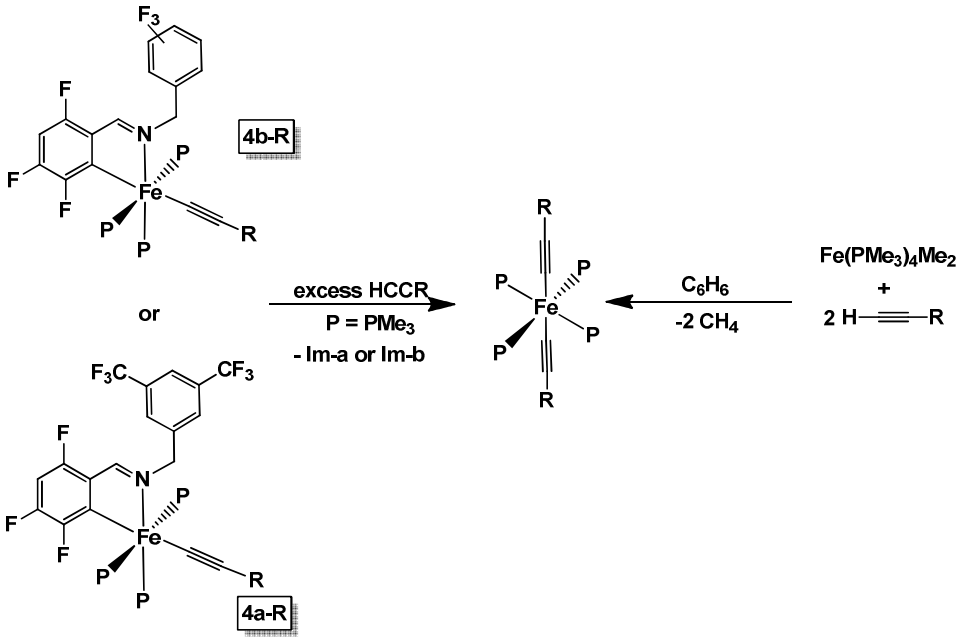

Scheme 3.10. Liberation of **Im-a** and **Im-b** upon addition of access HCCR to **4a**-R and **4b**-R, and formation of *trans*-$(Me_3P)_4Fe(CCR)_2$ via *cis*-$Fe(PMe_3)_4Me_2$ and 2 equiv of HCCR.

As indicated in Scheme 3.10, when **4a-**R and **4b-**R were treated with additional equivalents of primary alkyne, the diarylimine ligand was completely protonated off and *trans*-$(Me_3P)_4Fe(CCR)_2$ was generated. The identity of *trans*-$(Me_3P)_4Fe(CCR)_2$ was confirmed by an independent synthesis from *cis*-$Fe(PMe_3)_4Me_2$ and two equivalents of HCCR.

J. Routes to new Fe-N_2 Complexes via Reactivity with N_2O and Tosyl Azide

In an attempt to generate diarylimine diphosphine iron (II) adducts with nitrous oxide (N_2O), {*mer*-κ-C,N,C'-(3,4,5-$(F)_3$-C_6H-2-yl)CH_2N=CH(3,4,6-$(F)_3$-C_6H-2-yl)}$Fe(PMe_3)_3$ (**1b**) and *trans*-{*mer*-κ-C,N,C'-(3-OMe)-C_6H_3-2-yl)CH_2N=CH(C_6H_4-2-yl)}$Fe(PMe_3)_3$ (**1d**) were generated in J.Young tubes and treated with N_2O. As Scheme 3.11 illustrates, **2b** and **2d** were observed instead of adduct formation, and the formation of $OPMe_3$ indicated an oxygen-atom transfer (OAT) from N_2O to PMe_3.

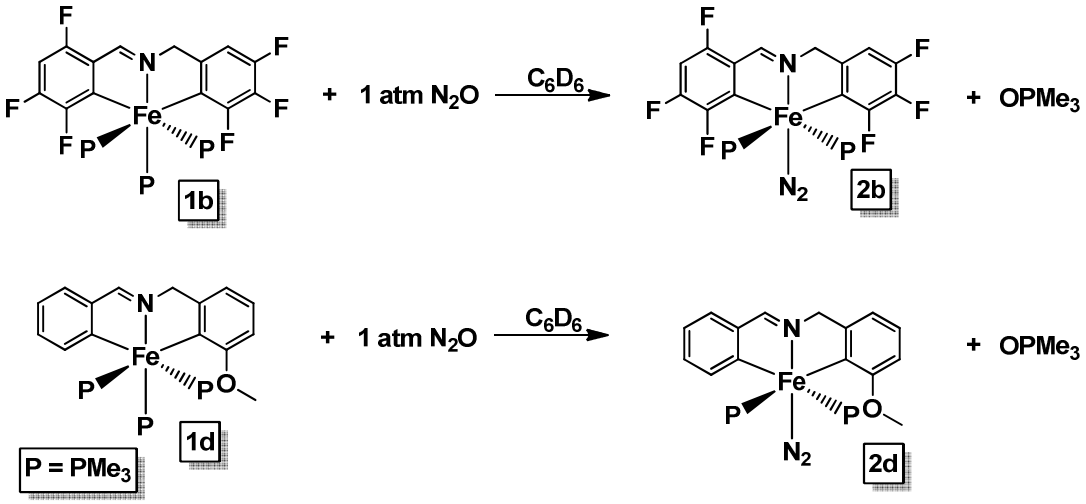

Scheme 3.11. Observed OAT with N_2O to generate **2b** and **2d** from **1b** and **1d.**

Transition-metal catalyzed substrate oxidation using nitrous oxide as an inexpensive oxidant is of significant interest, especially for industrial-scale processes.[101-105] Upon further examination, **2b** was found to have modest catalytic activity for OAT to PMe_3 under pseudo-first order conditions, with a rate constant of ~4 x $10^4 s^{-1}$ at 23 °C (Scheme 3.12). Uncatalyzed conversion to form $OPMe_3$ under otherwise identical conditions was determined to have a rate constant of ~8 x 10^{-7} s^{-1}.

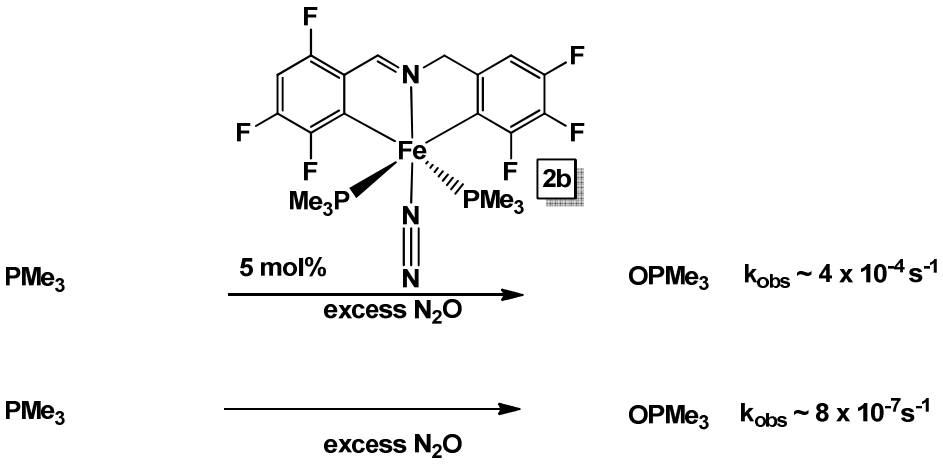

Scheme 3.12. Oxidation of PMe_3 via OAT from N_2O, catalyzed by 5 mol% **2b**.

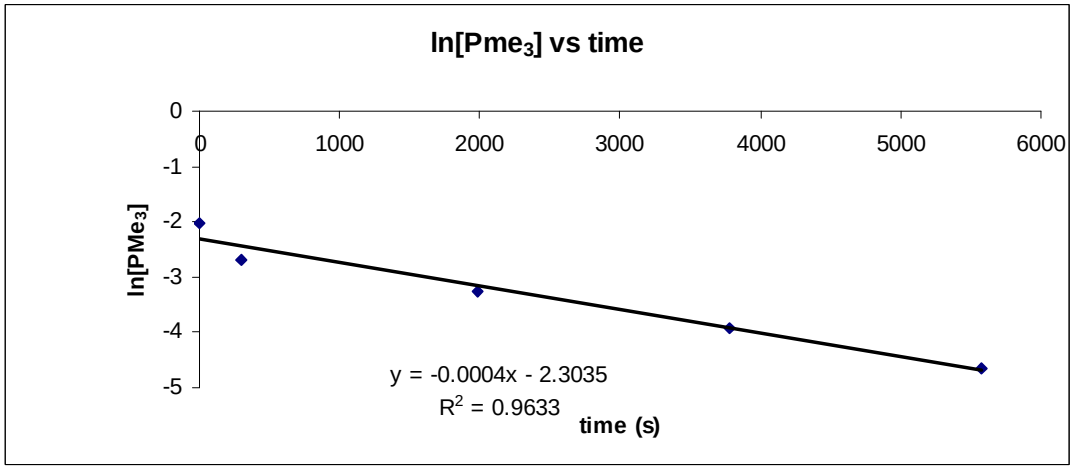

Figure 3.12: Catalyzed OAT from N_2O following the disappearance of PMe_3 with time under pseudo-first order conditions.

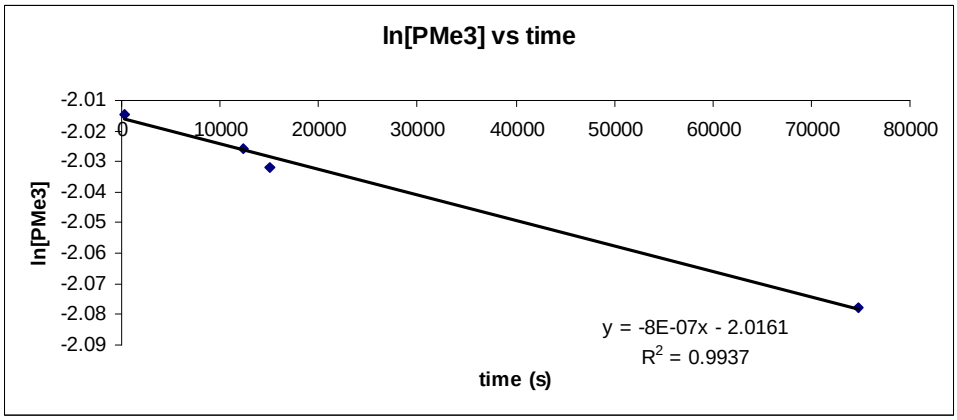

Figure 3.13: Uncatalyzed OAT from N_2O following the disappearance of PMe_3 with time under pseudo-first order conditions.

Many early transition metals utilize N_2O for OAT (Ti, V, Mo, Cr, Ta and W),[101-105] however its use is less widespread with late transition metals. Scheme 3.13 shows a possible catalytic cycle for the formation of $OPMe_3$, where N_2O initially displaces N_2. Oxidation of PMe_3, and subsequent loss of $OPMe_3$, is followed by N_2 binding to regenerate **2b**. Attempts to generate a new Fe-N_2 species via OAT to {mer-κ-C,N,C'-(4,5,6-(F)$_3$-C_6H-2-yl)CH_2N=CH(4,5,6-(F)$_3$-C_6H-2-yl)}Fe(PMe_3)$_3$ (**1g),** were unsuccessful.

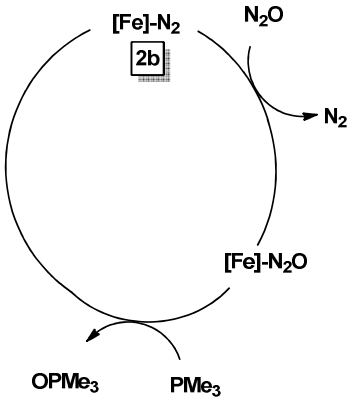

Scheme 3.13. Possible mechanism for OAT from N_2O to PMe_3.

Given the interest in using N_2O as an inexpensive and environmentally friendly oxygen-atom source, a modest amount of time was spent trying to oxidize more useful substrates such as olefins. Failure to oxidize anything other than trimethylphosphine ended our brief foray into oxygen atom transfer. Instead, focus was placed on using nitrene transfer from tosyl azide to generate iron-nitrogen multiple bonds. Two equiv of tosyl azide were initially used; one equiv could react with PMe_3 to form $TsN{=}PMe_3$, leaving the second equiv available to form the iron-nitrene. Unfortunately, treatment of **1b** with 2 equiv of tosyl azide only led to formation of **2b** (Scheme 3.14).

Attempts toward generating previously unmade dinitrogen complex, **2g,** with N_2O was ineffective, however addition of tosyl azide to **1g** afforded *trans*-{*mer*-κ-C,N,C'-(4,5,6-$(F)_3$-C_6H-2-yl)$CH_2N{=}CH$(4,5,6-$(F)_3$-C_6H-2-yl)}$Fe(PMe_3)_2(N_2)$ (**2g**) on an NMR tube scale. The IR spectrum for **2g** revealed a ν(NN) of 2070 cm^{-1}, which highlights the effects of the *ortho*-fluorine substituents. When compared to the stretching frequency of **2b** (2107 cm^{-1}), the electron-withdrawing capability of **Im-b** is influenced by the *ortho*-fluorines, rendering it more inductively electron withdrawing than **Im-g**. Subsequent treatment of **2b** with an excess of tosyl azide at elevated temperatures did not yield any further reactivity (Scheme 3.14).

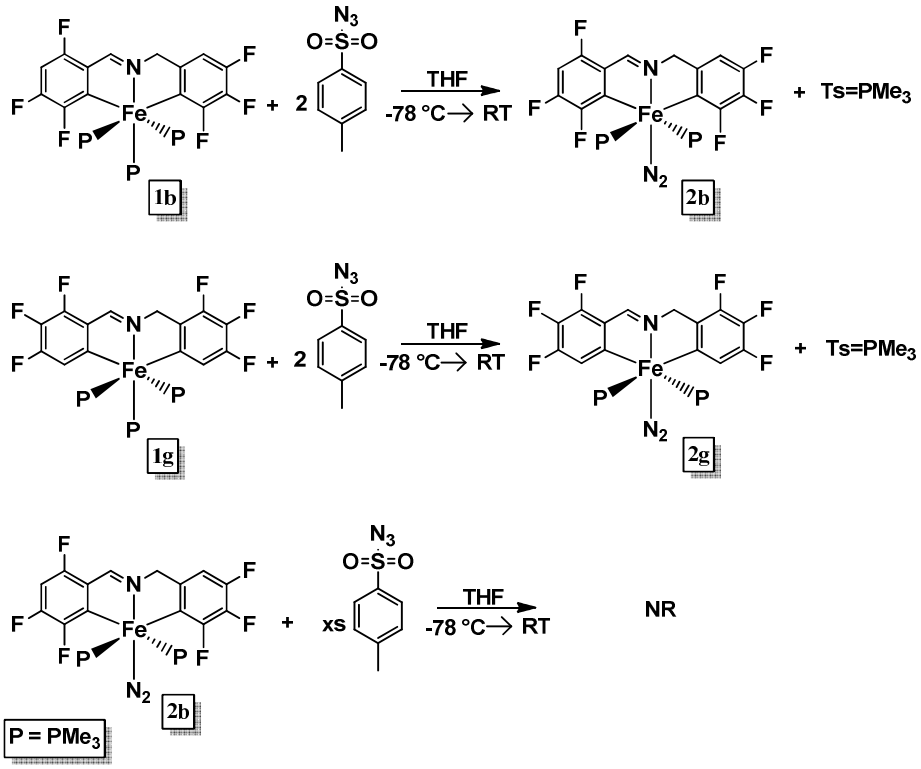

Scheme 3.14. Formation of **2b** and **2g** from treatment of **1b** and **1g** with tosyl azide.

K. Related Diarylimine Fe (II) Adducts and Dinitrogen Displacement

1. Synthesis of Carbonyl Derivatives

Select diarylimine iron (II) carbonyl complexes (**3 a-d,f)** were synthesized as shown in Scheme 3.15 from addition of one atm of CO to the trisphosphine precursors, **1 a-d,f,** in benzene.

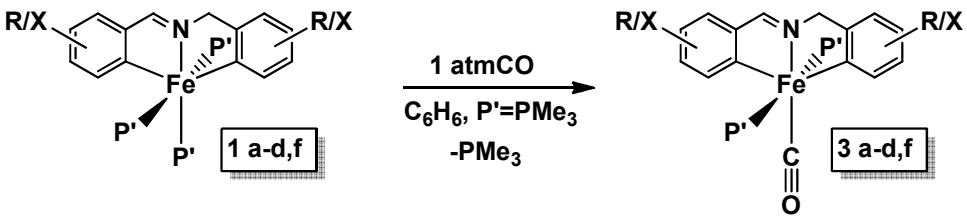

Scheme 3.15. Synthesis of carbonyl derivatives, **3 a-d,f,** by treatment of **1 a-d,f** with CO.

Similarly to the dinitrogen complexes, **2 a-f**, effects of the substituted imines on the CO stretching frequency in the infrared spectrum were observed. Table 3.1 reveals the electron-withdrawing imines to have higher CO stretching frequencies, and more electron-donating ligands have lower CO stretches due to better back bonding. The enhanced backbonding described in Figure 3.9 is illustrated again by the relatively low CO stretching frequencies, which range from 1950 to 1882 cm^{-1}.[106-109]

2. Binding Studies of H_2, NH_3, PMe_3

a.) Syntheses and equilibrium studies of H_2, NH_3, and PMe_3 adducts

The binding of other ligands, such as hydrogen and ammonia, were possible via dinitrogen displacement. Fe(II)-L complexes, *trans*-{*mer*-κ-C,N,C'-(3,4,5-$(F)_3$-C_6H-2-yl)CH_2N=CH(3,4,6-$(F)_3$-C_6H-2-yl)}Fe$(PMe_3)_2$(L) (L = H_2, NH_3, PMe_3), were placed under N_2 and upon reaching equilibrium, values for K_c were determined. Henry's constants were used to determine solubility of the gases in benzene.[110,111] From the solubility, the concentrations of H_2 and N_2 at a given pressure were calculated, and equilibrium constants were determined.

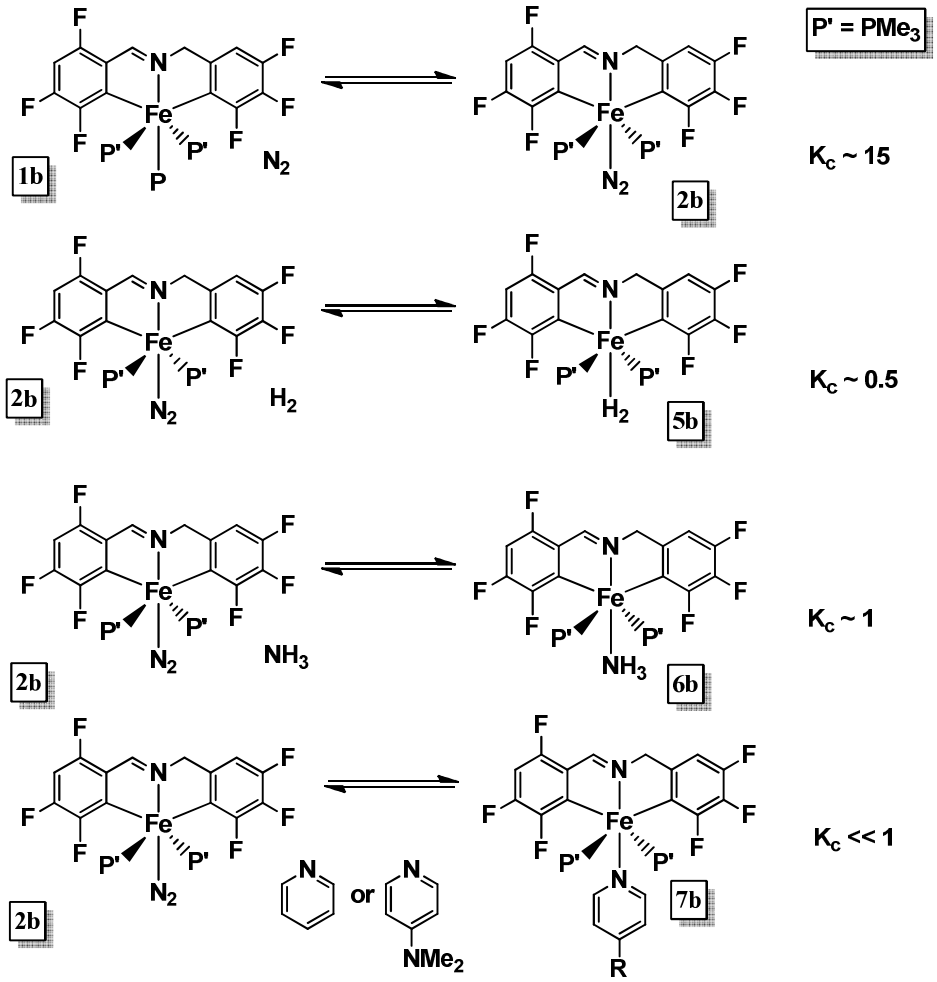

Scheme 3.16: Equilibrium constants for formation of **2b** from **1b,** and formation of **5b, 6b** and **7b.**

Initial displacement of PMe_3 in *mer*-κ-C,N,C'-(3,4,5-$(F)_3$-C_6H-2-yl)CH_2N=CH(3,4,6-$(F)_3$-C_6H-2-yl)}Fe(PMe_3)$_3$ (**1d**) to generate *trans*-{*mer*-κ-C,N,C'-(3,4,5-$(F)_3$-C_6H-2-yl)CH_2N=CH(3,4,6-$(F)_3$-C_6H-2-yl)}Fe(PMe_3)$_2$(N_2) (**2b**) was found to have a K_c of ~15, as shown in Scheme 3.16. The dihydrogen complex, **5b,** was generated *in situ* by repeated exposure of *trans*-{*mer*-κ-C,N,C'-(3,4,5-$(F)_3$-C_6H-2-yl)CH_2N=CH(3,4,6-$(F)_3$-C_6H-2-yl)}Fe(PMe_3)$_2$(N_2) (**2b**) with dihydrogen, and a K_c of ~0.5 was determined.

Characterization of **5b** via ^{1}H NMR spectroscopy revealed the H_2 resonance as a broad triplet at δ -13.88 with J_{PH} = 12 Hz. The T_1 of any resonance can be measured by a standard inversion-recovery pulse sequence,[112] and it was used to calculate H-H distances. The hydrogen-hydrogen distance of **5b** can be calculated if rapid rotation of the dihydrogen is assumed, and the major contribution to the relaxation of hydrogen is by a dipole-dipole mechanism. Variable temperature T_1 measurements, taken in toluene-d_8, resulted in a T_1(min) of 11 ms at 288 K and an H-H distance of 0.77 Å. Isolation of **5b** was not possible due to the eventual hydrogenation of the iron-aryl bonds to generate free ligand, **Im–b**, trimethylphosphine and black solid. Attempts to generate and characterize H_2 adducts of **2 d,f,** resulted in rapid formation of free ligand without observation of adduct formation (Scheme 3.17). Lack of adduct formation suggests the slightly more electron-rich iron center, due to the electron-donating imines, is more prone to undergo an oxidative addition of H_2 , and subsequent reductive elimination to generate **Im–d,f**.

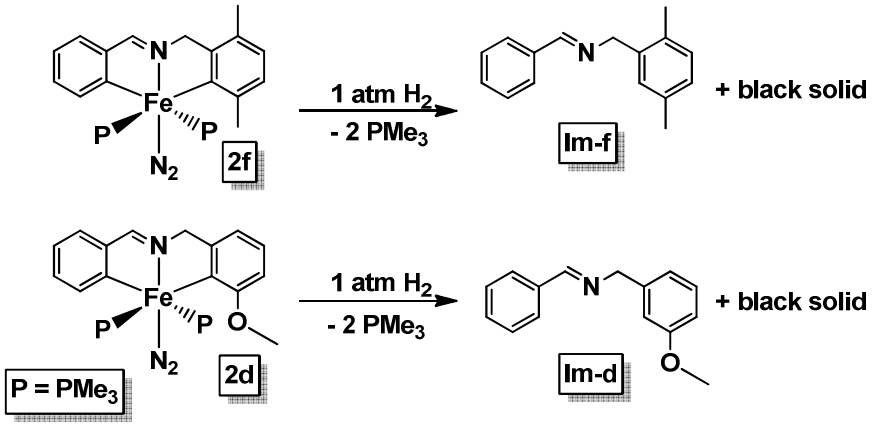

Scheme 3.17. Hydrogenation of **2f** and **2d** under 1 atm of H_2 to generate **Im–f,d.**

The ammonia adduct, *trans*-{*mer*-κ-C,N,C'-(3,4,5-$(F)_3$-C_6H-2-yl)CH_2N=CH(3,4,6-$(F)_3$-C_6H-2-yl)}$Fe(PMe_3)_2NH_3$ (**6b),** was isolated in 98% yield as a bright purple solid after repeated exposure of **2b** to NH_3 in benzene. As shown in Scheme 3.16, with a K_c of ~1, **6b** consistently regenerated **2b** upon exposure to N_2.

The pyridine adduct, **7b**, could not be generated by simple dinitrogen displacement by pyridine**.** Addition of pyridine n-oxide to **1b** resulted in the successful generation of **7b** as red microcrystals in 70% yield (Eq. 3.14). The pyridine complex rapidly reverted back to **2b** upon exposure to dinitrogen, and conditions suitable for K_c determination could not be found. The oxide of the pyridine derivative, dimethylaminopyridine (DMAP), could also be used to generate the iron-DMAP complex. Again, the rapid conversion back to **2b** prevented determination of the equilibrium constant.

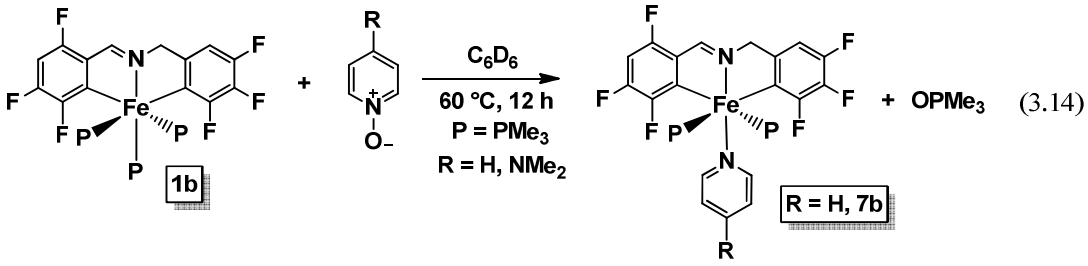

(3.14)

b.) Calculation of equilibrium constants.

Upon exposure of 0.0203 mmol of **1b** to 1 atm N_2, the reaction was allowed to equilibrate until the NMR spectrum showed no change. The K_c was calculated by direct integration of **2b**, **1b** and PMe_3, and the amount of N_2 in solution was estimated from the Henry's Law constant of N_2 in benzene. There are 0.102 mmol of N_2 present at 1 atm in a 2.5 mL J.Young tube. After subtracting the amount of N_2 required to

generate the Fe-N_2 formed there is approximately 0.874 atm N_2, and with a Henry's Law constant of 2260 atm in benzene,[111] there are 0.0022 mmol of N_2 in 0.6 mL of C_6D_6.

$$\mathbf{X_{N2} = \frac{P}{K_{H,N2}} = \frac{0.874\ atm}{2260\ atm} = 3.87 \times 10^{-4}}$$ **where $K_{H,N2}$ is Henry's Law Constant for N_2 in benzene**

$$\mathbf{X_{N2} = \frac{mol\ N_2}{mol\ N_2 + mol\ C_6D_6}}$$ **where mol C_6D_6 = 5.64 mmol**

mol N_2 = 0.0022 mmol

Scheme 3.19. Calculation for K_c determination using Henry's Law Constant for N_2 solubility in benzene.

After equilibration, [**2b**] = 0.0205 M, [**1b**] = 0.0124 M, [PMe_3] = 0.0333 M and [$N_{2soln'}$] = 0.00367 M, resulting in K_c = 15.0. K_c for NH_3 displacement was found by treatment of **6b** with 1 atm N_2. The reaction was allowed to equilibrate until the NMR spectrum remained unchanged. The K_c was calculated by direct integration of **1b**, **2b** and NH_3, and the amount of N_2 in solution was estimated from the Henry's Law constant of N_2 in benzene. After equilibration, [**2b**] = 0.011 M, [**6b**] = 0.0265 M, [NH_3] = 0.0106 M, [$N_{2soln'}$] = 0.004 M, and K_c = 1.1

3. Methyl isocyanide and Diphenyldiazomethane Adducts

Attempts toward iron (IV) species containing pi-donating ligands were made with azo and azide reagents.[113] Diazo compounds were initially chosen because of their ability to lose dinitrogen and potentially form an iron-carbon double bond. Inspiration for this type of transformation came from precendence shown by Chirik et. al, where a kinetically stable iron alkylidene, (PDI)Fe=CPh_2, was observed.[114]

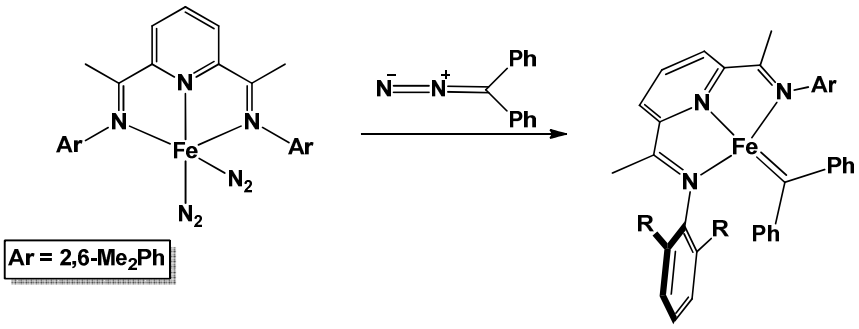

Scheme 3.20. Precedence for N_2 loss from N_2CPh_2 to generate an iron-alkylidene.

Treatment of *trans*-{*mer*-κ-C,N,C'-(3,4,5-$(F)_3$-C_6H-2-yl)CH_2N=CH(3,4,6-$(F)_3$-C_6H-2-yl)}$Fe(PMe_3)_2(N_2)$ (**2b**) with N_2CPh_2 formed the adduct, *trans*-{*mer*-κ-C,N,C'-(3,4,5-$(F)_3$-C_6H-2-yl)CH_2N=CH(3,4,6-$(F)_3$-C_6H-2-yl)}$Fe(PMe_3)_2(NN\text{-}CPh_2)$ (**9b),** as a dark purple crystalline material in 76% yield as shown in Eq 3.15. Efforts to activate dinitrogen loss with light and heat were unsuccessful.

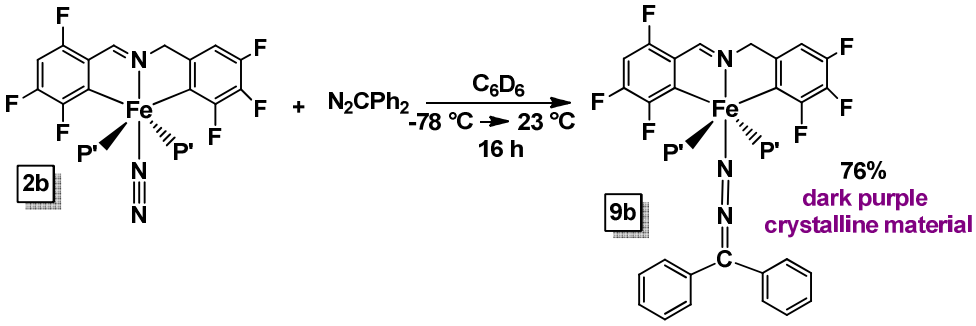

(3.15)

A methyl isocyanide adduct, **8b** (ν(CN) = 2073 cm^{-1}), was generated in 69% yield by treating {*mer*-κ-C,N,C'-(3,4,5-$(F)_3$-C_6H-2-yl)CH_2N=CH(3,4,6-$(F)_3$-C_6H-2-yl)}$Fe(PMe_3)_3$ (**1b**) with methyl isocyanide at room temperature (Eq. 3.15). Attempts toward protonation were made with triflic acid, which led to the formation of a bright green solution, and a multitude of organic products were seen by ^1H NMR

spectroscopy. Given the propensity of the iron-aryl bonds toward protonation, it is likely the acid protonated the aryl-iron bonds, liberating **Im-b** from iron. Subsequent protonation with triflic acid could have generated an iminium salt.

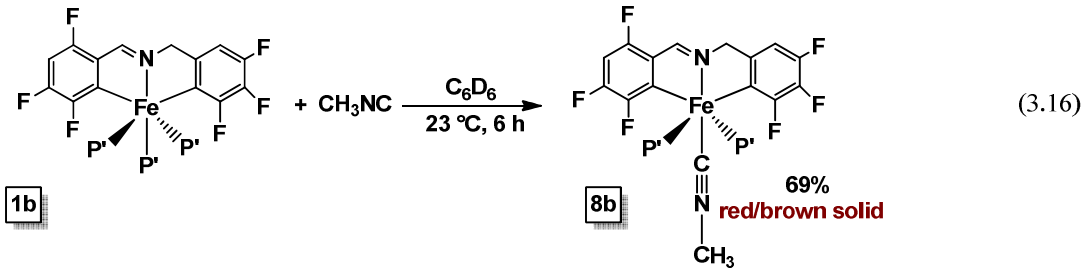

(3.16)

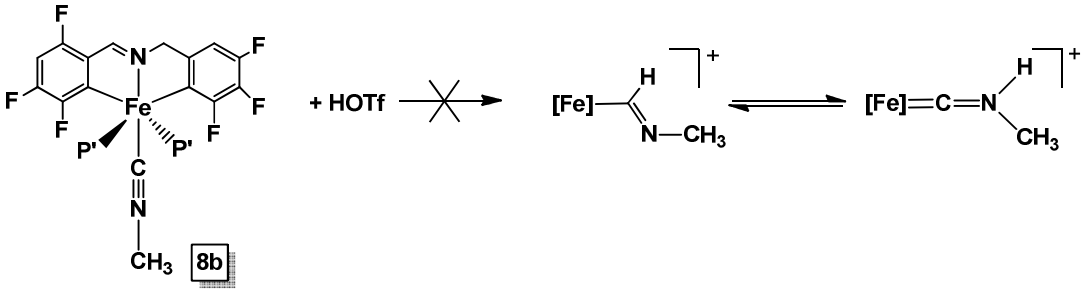

Scheme 3.21. Protonation attempt of 8b with triflic acid.

4. Calculated Binding Energies

To evaluate the steric and electronic properties inherent to **Im-b**, calculations on the binding energies of L (L = N_2, NH_3, PMe_3, H_2) to the presumed transient five-coordinate *trans*-{*mer*-κ-C,N,C'-(3,4,5-$(F)_3$-C_6H-2-yl)CH_2N=CH(3,4,6-$(F)_3$-C_6H-2-yl)}$Fe(PMe_3)_2$ (**1'b**) were performed, and the results are given in Table 3.6.

Table 3.6. Calculated (M06/6-311+G(d)) binding energies for *trans*-{*mer*-κ-C,N,C'-(3,4,5-$(F)_3$-C_6H-2-yl)CH_2N=CH(3,4,6-$(F)_3$-C_6H-2-yl)}Fe$(PMe_3)_2$ (**1'b**) + L (L = N_2, NH_3, PMe_3, H_2) and related reactions (P' = PMe_3).

Compound	L		$\Delta H°_{calc}$ kcal/mol	$\Delta S°_{calc}$ eu	$\Delta G°_{calc}$ (298K) kcal/mol	$\Delta G°_{calc}$ (298K) kcal/mol	$\Delta\Delta G°_{exp}$ (298K) kcal/mol
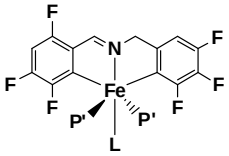	N_2	**2b**	-27.6	-43.0	-14.8	2.6	0.0
	NH_3	**6b**	-31.2	-46.3	-17.4	0.0	0.0
	PMe_3	**1b**	-27.2	-59.5	-9.4	8.0	1.6
	H_2	**5b**	-18.6	-37.0	-7.5	9.9	0.4
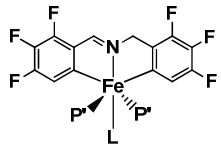	N_2	**2g**	-30.5	-37.3	-19.4		
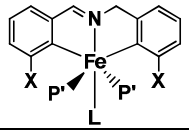	N_2 X = H		-31.6	-37.6	-20.4	0.0	
	N_2 X = F		-26.0	-45.0	-12.6	7.8	

Initially, B3LYP calculations predicted results contrary to experimental observations, therefore M06[115]/6-311+G(d)[116] functional[117] was used to better account for van der Waals interactions. Table 3.6 reports similar binding energies for the dinitrogen and ammonia, while binding of PMe_3 and dihydrogen are substantially less favorable. Comparison to the experimental binding studies reveal dihydrogen to be the outlier, as it was calculated to be 7.3 kcal/mol less favorable than dinitrogen binding. Experimentally, dihydrogen was found to be roughly equal to dinitrogen and ammonia, which is in agreement with other reports finding dinitrogen and dihydrogen as comparable ligands.[112,118,119] PMe_3 was shown to be unfavorable experimentally, and the calculation overestimates its unfavorable relative binding energy. From Table 3.6, it appears the difference in binding energies of N_2 vs. PMe_3 to be mostly entropic, as the relative binding of PMe_3 was calculated to have a $\Delta\Delta S°$ of 16.5. Such a large

ΔΔS° likely represents the steric penalty for the phosphine being adjacent to *ortho*-fluorine substituents.

Dinitrogen binding to a five-coordinate diarylimine iron (II) species with no *ortho*-fluorines, *trans*-{*mer*-κ-C,N,C'-(4,5,6-$(F)_3$-C_6H-2-yl)CH_2N=CH(4,5,6-$(F)_3$-C_6H-2-yl)}$Fe(PMe_3)_2$ (**1'g**), was then calculated. The effect of the *ortho*-fluorines is apparent, as the binding of dinitrogen ($\Delta G°_{calc}$ = -19.4 kcal/mol) was more favorable entropically (5.7 eu) and enthalpically (-2.9 kcal/mol) than dinitrogen binding to **1'b**. The *ortho*-fluorines impact binding by inductively destabilizing dinitrogen binding and they also introduce increased sterics, as revealed in the calculated ΔS° of -43.0 eu for **1'b**, as compared to only ΔS° = -37.3 eu in **1'g**. The binding of dinitrogen to the hypothetical five-coordinate unsubstituted diarylimine iron to give the corresponding Fe-N_2 complex was calculated and compared to the binding of N_2 to a diarylimine iron complex with only *ortho*-fluorines. The results, as shown in Table 3.6, are very similar to the calculations of N_2 binding to **1'b** and **1'g**, ensuring these arguments are not compromised by the nature of the additional fluorine substituents.

L. Oxidation Attempts

1. Synthesis of *trans*-{κ-C,N,C'-(3,4,5-$(F)_3$-C_6H-2-yl)CH_2N=CH(3,4,6-$(F)_3$-C_6H-2-yl)}$Fe(PMe_3)_2I$ (11b), *trans*-{κ-C,N,C'-(3,5-$(CF_3)_2$-C_6H_3)-CH_2N=CH(2,4,5-$(F)_3$-C_6H_2)}$Fe(PMe_3)_2$ Cl (12a), and *trans*-{κ-C,N,C'-(3,4,5-$(F)_3$-C_6H-2-yl)CH_2N=CH(3,4,6-$(F)_3$-C_6H-2-yl)}$Fe(PMe_3)_2$ Cl (12b).

Initially, synthesis of a neutral iron (III) azaallyl species, analogous to the smif complexes described in Chapter 2, was targeted by one electron oxidation and

subsequent deprotonation of **2b**. Oxidation of **2b** was also of interest because iron (III) species containing metal-carbon bonds are rare,[120-123] and iron (III) derivatives have not been shown to bind dinitrogen. While oxidation of an analogous system was achieved with AgOTf to afford ([*mer*-κ-C,N,C'-{(Ph-2-yl)CH_2N=CH(Ph-2-yl)}Fe(PMe_3)$_3$]OTf),[82] **2b** was unaffected by the same reagent. Treatment of **2b** with [Cp_2Fe]BF_4 in the presence of LiI (Scheme 3.22) resulted in bubbling, signaling loss of dinitrogen, and the neutral iron (III) complex, *trans*-{κ-C,N,C'-(3,4,5-$(F)_3$-C_6H-2-yl)CH_2N=CH(3,4,6-$(F)_3$-C_6H-2-yl)}Fe(PMe_3)$_2$I (**11b**), was isolated as a dark green solid in 42% yield. When the reaction was run in the absence of LiI, a dark orange-red solution formed and IR spectroscopy confirmed the loss of dinitrogen. It is plausible that the orange-red solution formed was the THF adduct (**10b**, Scheme 3.22), as subsequent addition of LiI generated **11b.**

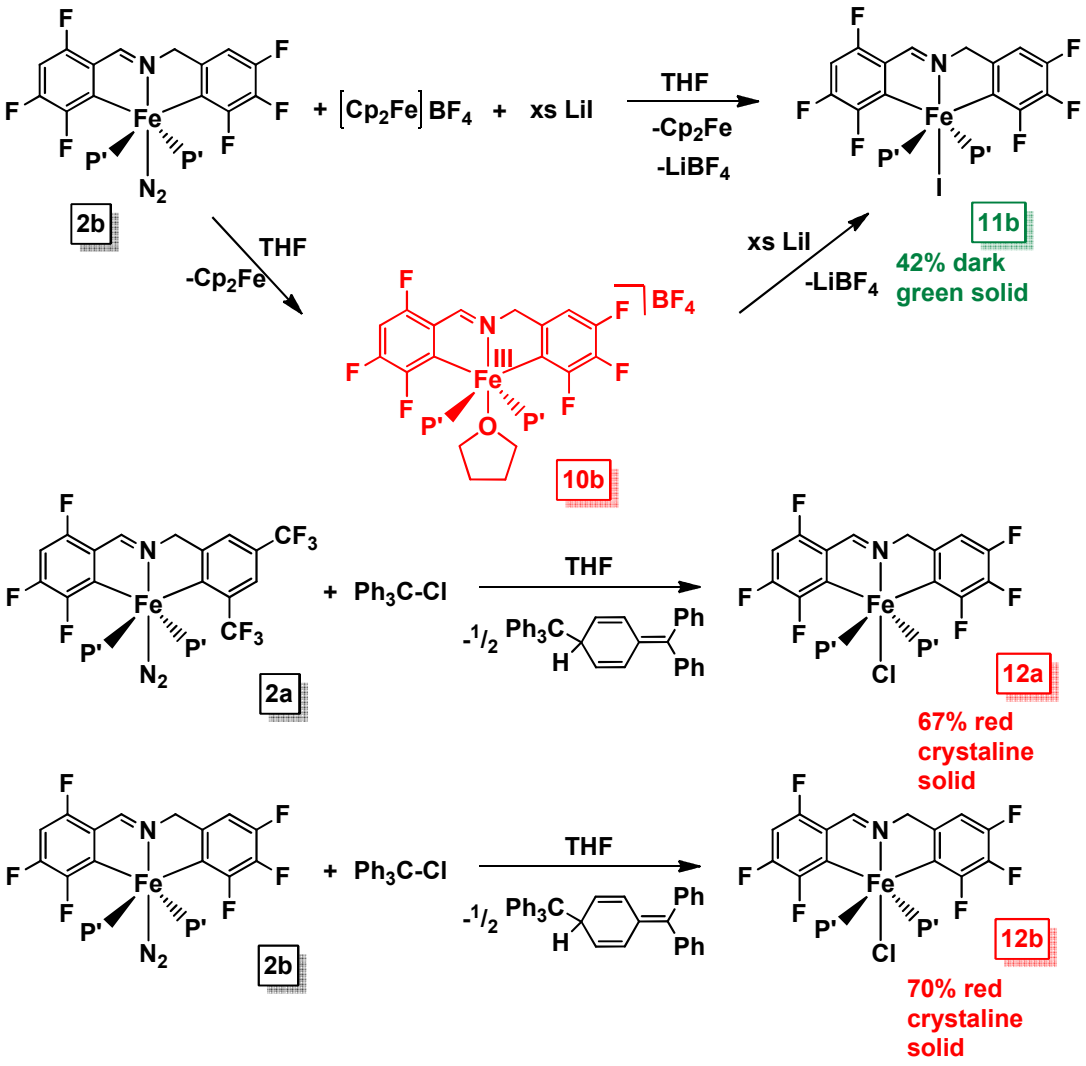

Scheme 3.22. Inner and outer sphere electron transfers to generate neutral iron (III) halides, **11b, 12a** and **12b**.

The neutral iron (III) iodide complex, **11b,** was generated via outer sphere electron transfer, but inner sphere paths were a viable option as well, due to the possible lability of the dinitrogen ligand in complexes **2 a-f**. Treatment of **2a** and **2b** with trityl chloride led to the corresponding iron (III) chloride derivatives, **12a** and **12b**, in 67% and 70% yield, respectively. Evans method[124] measurements for **11b, 12a**

and **12b,** revealed each complex to have an $S = ½$ ground state with a significant spin-orbit contribution.[92] **11b**, μ_{eff} = 2.0(1) μ_B; **12a**, μ_{eff} = 2.1(1) μ_B; **12b**, μ_{eff} = 2.0(1) μ_B.

2. Structure of *trans*-{κ-C,N,C'-(3,4,5-(F)$_3$-C$_6$H-2-yl)CH$_2$N=CH(3,4,6-(F)$_3$-C$_6$H-2-yl)}Fe(PMe$_3$)$_2$ Cl (12b).

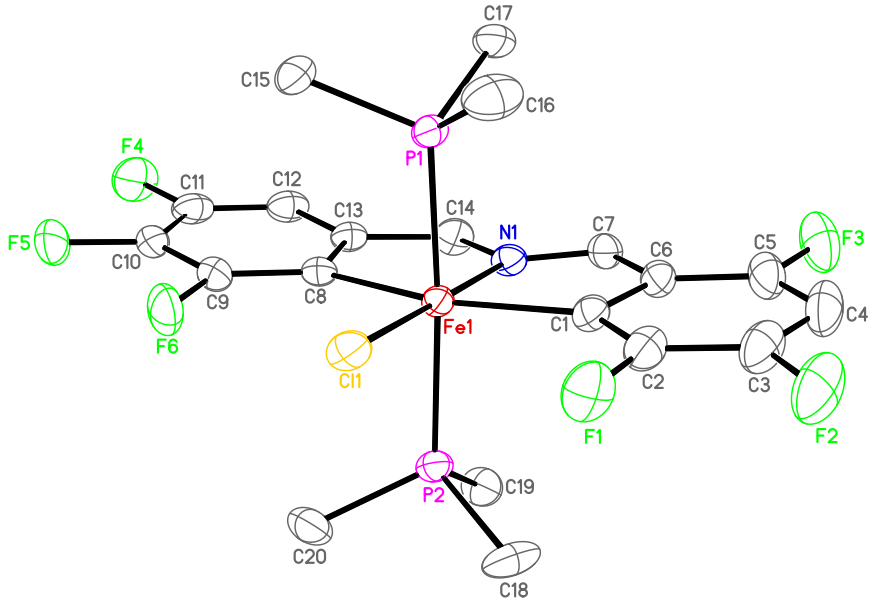

Figure 3.14. Molecular view of *trans*-{κ-C,N,C'-(3,4,5-(F)$_3$-C$_6$H-2-yl)CH$_2$N=CH(3,4,6-(F)$_3$-C$_6$H-2-yl)}Fe(PMe$_3$)$_2$ Cl (**12b**).

Crystallographic details and pertinent bond distances and angles for **12b** are given in Tables 3.3 and 3.4. The Fe-N$_1$ distance of 1.9389(17) Å is remarkably similar to that of **2b**, but the Fe-C1 and Fe-C8 bonds are slightly elongated to 2.031(2) and 2.028(2) Å, as are the Fe-P bonds with distances of 2.2602(6) and 2.2463(6) Å. While oxidation usually causes bond distances to shorten in complexes with greater ionic

character, contraction of 3d orbitals in the ferric complex likely resulted in bond lengthening due to decreased orbital overlap.[82] The core of **12b** is quite similar to that of **2b** with N1-Fe-Cl and P1-Fe-P2 angles of 178.04(5) and 174.29(2) Å, respectively. As the iron-carbon distances increase, the C1-Fe-C8 bite angle decreases to 160.70(9)°, and the related N1-Fe-C angles decrease to 79.80(8)° and 80.96(8)°, while the C1-Fe-Cl and C8-Fe-Cl angles are 98.88(7)° and 100.31(6)°.

L. Fe-NH_3 Reactivity

Attemps were made toward utilizing *trans*-{*mer*-κ-C,N,C'-(3,4,5-$(F)_3$-C_6H-2-yl)CH_2N=CH(3,4,6-$(F)_3$-C_6H-2-yl)}Fe$(PMe_3)_2NH_3$ (**6b)** to observe the microscopic reverse of dinitrogen reduction at a molecular site (Scheme 3.23). As many as 14 intermediates have been proposed by Chatt, Hidai and Shrock, for the catalytic cycle,[58,59,61] and it seemed possible that by oxidation and deprotonation of **6b,** the dinitrogen complex, **2b,** could be generated.

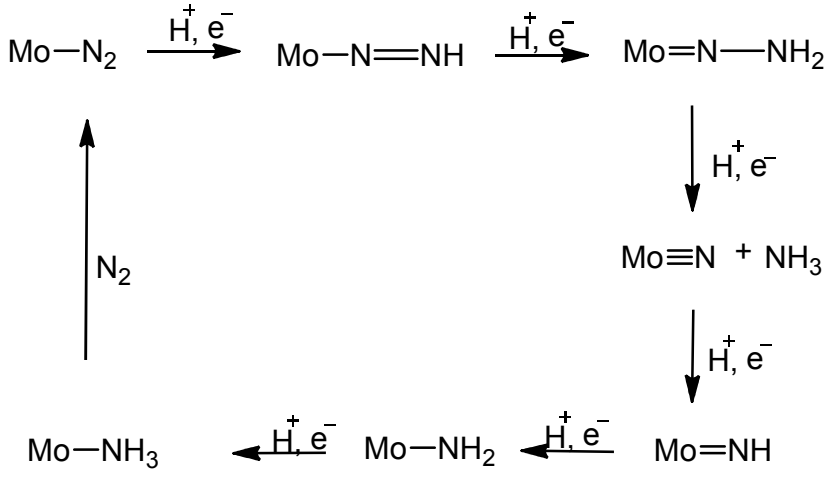

Scheme 3.23. Proposed catalytic cycle and intermediates in the reduction of N_2 at a molecular site.[58,59,61]

Treatment of **6b** with AgOTf and triethylamine led to the formation of a product with paramagnetic resonances in the ^{1}H NMR spectrum, an intractable mixture of products observed in the diamagnetic region of the ^{1}H NMR spectrum, and black solid. While it is possible the paramagnetic product was the sought-after iron (III) amide species, the numerous other products present made isolation unfeasible, so other approaches were considered.

Another potential route involved treating the iron (III) halide, **11b**, with sodium amide and ammonia as illustrated in Scheme 3.24. In both cases, reduction resulted in the observation of the ferrous derivatives, **2b** and **6b.**

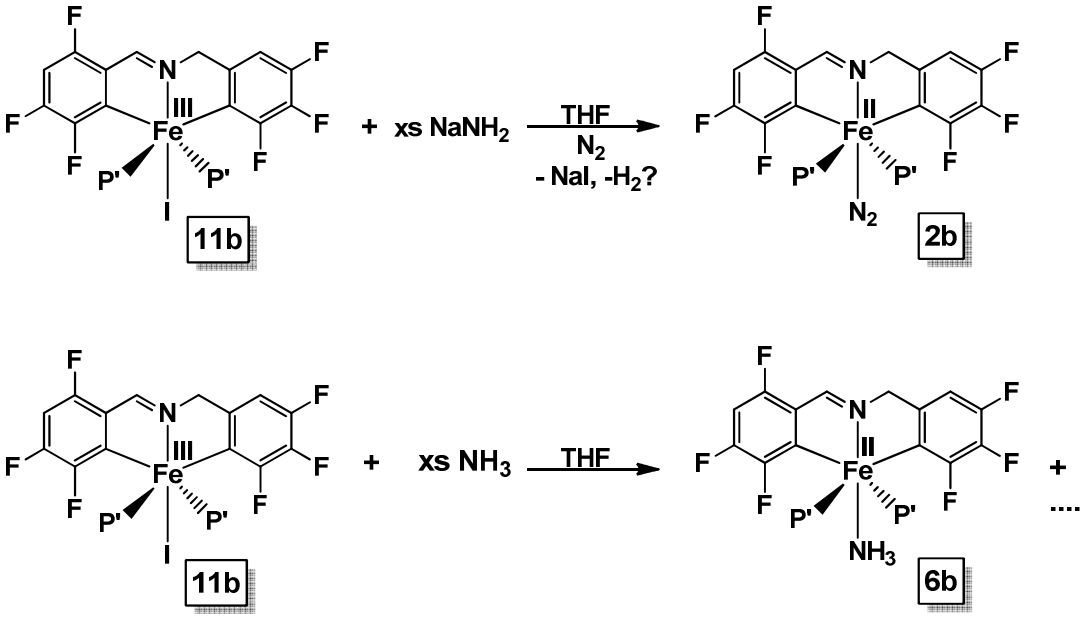

Scheme 3.24. Treatment of **11b** with $NaNH_2$ and NH_3 which resulted in reduction to **2b** and **6b,** respectively.

M. Attempts Toward Proton Delivery

One potentially useful application would be to alter the existing ligand framework such that proton delivery to the dinitrogen ligand of **2b** would be possible.

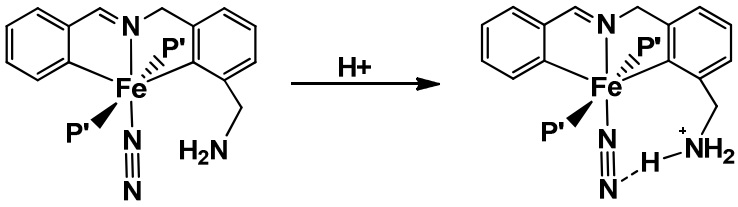

Scheme 3.25. Potential proton-delivery system.

Conceivably, this could be accomplished by one of two ways: condensation of one equiv of benzaldehyde with an equiv of 1,3-bis(aminomethyl)benzene, or two condensations of benzaldehyde with an equiv of 1,3-bis(aminomethyl)benzene to form the bis-imine ligand (**Im-o**). In either case, the nitrogen not bound to iron (N_{im} or NH_2) could be protonated to then deliver the proton to dinitrogen (Scheme 3.25). As shown in Scheme 3.26, the first approach of condensing one equiv of benzaldehyde with one equiv of 1,3-bis(aminomethyl)benzene, led to a mixture of single and double condensation products. Therefore, the second approach was used to isolate a single product (**Im-o**) in 84% yield.

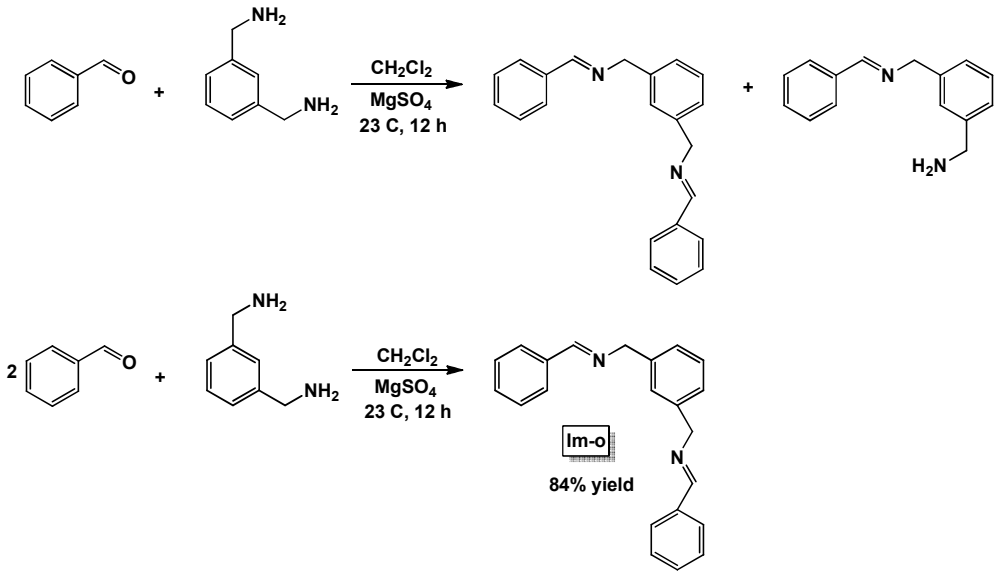

Scheme 3.26. Formation of double condensation product, **Im-o**, as a ligand for proton-delivery.

Under an atmosphere of dinitrogen, treatment of *cis*-Fe(PMe_3)$_3$$Me_2$ with one equiv of **Im-o** led to a mixture of three products in a 1:1:0.25 ratio. Two of the products were identified as the anticipated dinitrogen species, and the related trisphosphine complex. The third product was a different trisphosphine species generated by aryl activation at the sterically unhindered position of the aryl-amine (Scheme 3.27). No attempts toward isolation were made.

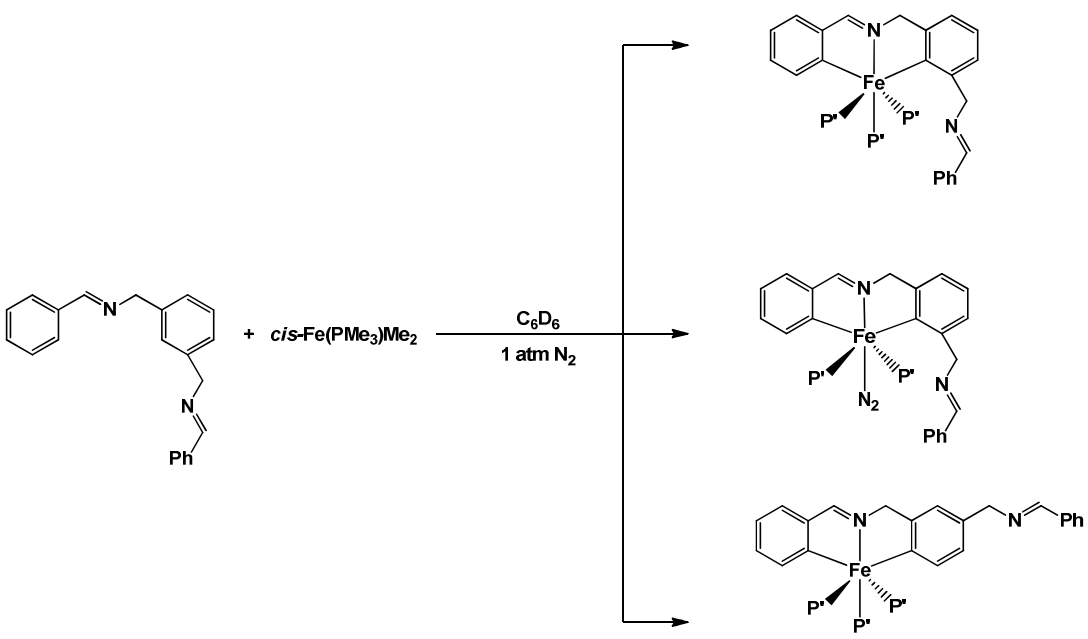

Scheme 3.27. Activation of **Im-o** to afford a mixture of two trisphosphine complexes and dinitrogen complex.

A few complications have stunted the progress of the efforts presented in this section. Competition for activation at the second *ortho* site is detrimental to the formation of the Fe-N_2 sought. Starting materials where the unwanted site of activation is protected are costly and thus have not been pursued. It is also likely that the "arm" designed for proton delivery proposed was too short to reach the N_2. Perhaps, a different aryl substituent can be designed with the appropriate length to reach around and deliver a proton to the dinitrogen ligand.

I. Selectivity of N_2 Extraction over O_2 from Air

Selectivity for dinitrogen over dioxygen binding to five-coordinate complexes, **1' a-f**, appears to be kinetic since exposure to dioxygen over time resulted in decomposition. Failure to isolate or identify products formed upon Fe-N_2 exposure to dioxygen, along with observation of $OPMe_3$ and black solid, is consistent with

irreversible binding of O_2 and subsequent degradation. In air, significant stability was observed, suggesting reversible binding by dinitrogen and irreversible decomposition by dioxygen.

To gain insight on this unusual stability, calculations on the binding of N_2 vs. O_2 to *trans*-{*mer*-κ-C,N,C'-(3,4,5-$(F)_3$-C_6H-2-yl)CH_2N=CH(3,4,6-$(F)_3$-C_6H-2-yl)}$Fe(PMe_3)_2$ (**1'b**) were performed, and the results are illustrated in Figure 3.15. First, the Fe-N_2 complex, written as $^1[FeN_2]$, is calculated to be 4.9 kcal/mol lower in energy than the dioxygen species, $^3[FeO_2]$, which is best described as an iron (III)-superoxide. The 5-coordinate precursor, ^{3}[Fe] (**1'b**), has a triplet ground state (GS) and must intersystem cross to form either $^1[FeN_2]$ or $^3[FeO_2]$. The GS has d_{xy} and d_{z2} each populated with one electron, which in orbital symmetry terms is written as a $\pi^1\sigma^1$. Since the product, $^1[FeN_2]$, has an electron configuration of $(d_{xz})^2(N\sigma)^2$ which can be written as $\pi^2\sigma^2$, the conversion of **1'b** + $^1N_2$ ($\pi^1\sigma^1 + \sigma^2$) to **2b** is not orbital symmetry allowed or spin allowed. The combination of ^{3}[Fe] with $^1N_2$ correlates to an excited state on the left side of Fig. 3.15 that is 20.9 kcal/mol above $^1[FeN_2]$. The ^{1}[Fe] configuration ($(d_{xz})^2$) of **1'b** is only 12.6 kcal/mol above the GS, and thus the energy of the intersystem crossing point (ICP) to give **2b** ($^1[FeN_2]$) from **1'b** (^{3}[Fe] + $^1N_2$) is the lowest. The conversion of HS Fe(II) to LS Fe(II) is the main electronic barrier to overcome in order to form **2b**. Intersystem crossing events in other examples of N_2 binding have been similarly rationalized.[38,94,95,125]

The binding of dioxyen to GS **1'b** (^{3}[Fe] + $^3O_2$) correlates to an O_2-bound quintet state that could not identified. This can also be expressed as $(d_{xy})^1(d_{z2})^1$ + $\pi^{*1}\pi^{*1}$, or $\pi\ ^1\sigma^1 + \pi^{*1}\pi^{*1}$, along the reaction coordinate but the spin state is not

conserved, and its conversion to the Fe(III) superoxide species, $^3[FeO_2]$ $((d_{xy})^1(O\sigma)^2(O\pi)^1)$, is slightly endergonic by +2.7 kcal/mol. Any additional thermodynamic preference for N_2 binding comes from electronic features, since steric hindrance in dioxygen binding was not observed in the calculations. The lowest energy spin state correlation occurs at 12.6 kcal/mol from $^1[Fe] + {}^3O_2$, whose orbital symmetry state of $(d_{xz})^2(\pi^*\pi^*)$ or $(\pi^2)(\pi^*\pi^*)$, and does not correlate with the orbital symmetry of the Fe-O_2 GS superoxide. The ICP derived from this spin correlation is likely to be only slightly higher in energy than that of N_2 binding, assuming the quintet surface is sufficiently high in energy, and therefore it seems improbable this difference in the two intersystem crossing points would result in the observed kinetic stability. The $^3[FeO_2]$ ground state best correlates with a high energy $^3[Fe] + {}^1O_2$ state in which the singlet oxygen $^1(\pi^{*1}\pi^{*1})$ configuration ($^1\Sigma^+_g$) can be considered $(\pi^{*1}\sigma^1)$ along the reaction coordinate, and spin state is conserved. The calculated ground state for the Fe (III) superoxide species is formed by pairing the Fe ($d_{z2}{}^1$) and O(σ^1) spins. The ICP generated by this correlation is likely to be significantly higher than for N_2 binding, which accounts for the N_2 vs. O_2 selectivity, but this is entirely dependent on the energy of the unoptimized quintet surface.

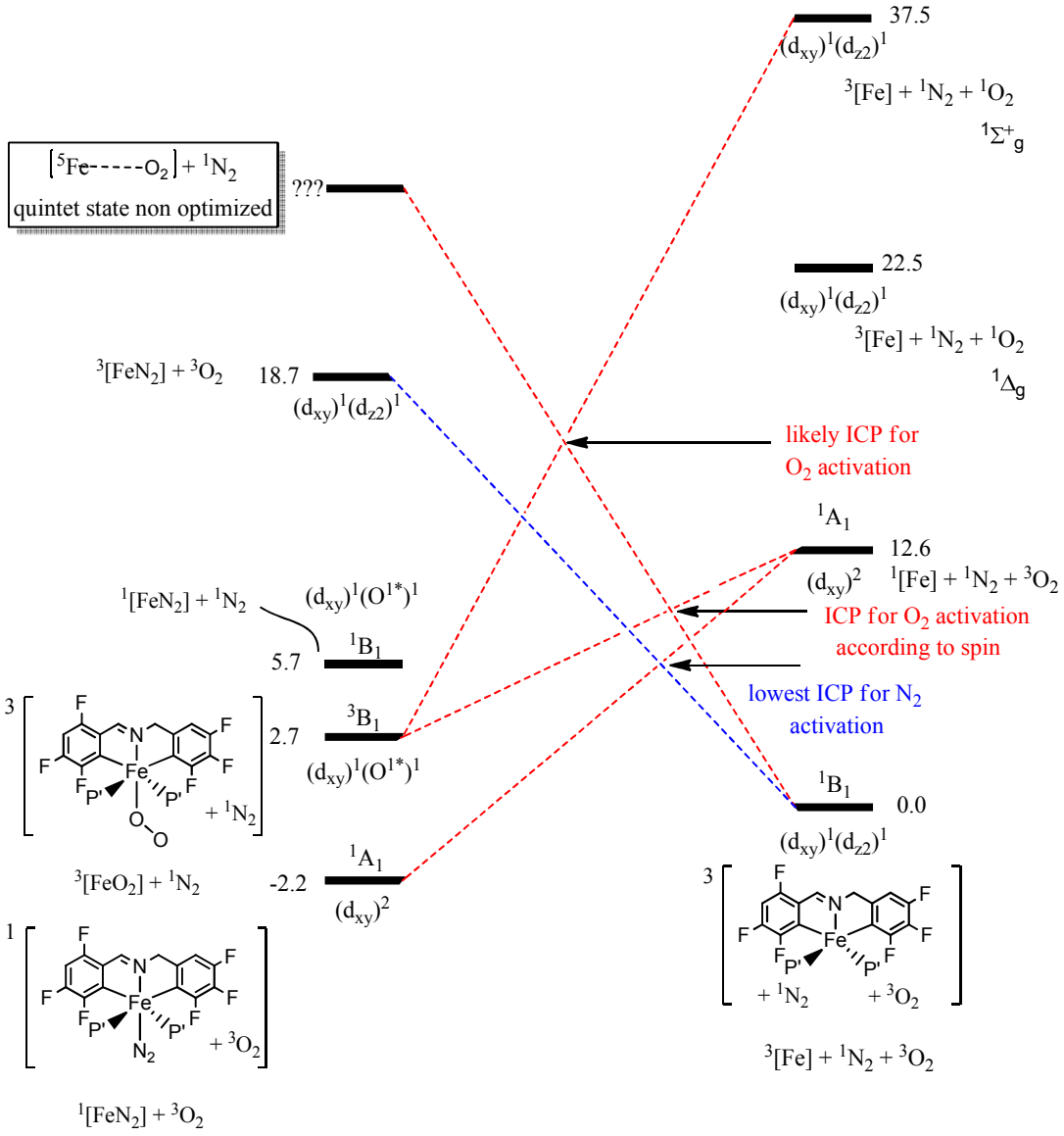

Figure 3.15. Calculated description of kinetic selectivity for N_2 over O_2.

The inability to locate and optimize a quintet surface that would correlate directly with the reactant ^{3}[Fe] + $^3O_2$ surface may indicate that $^3O_2$ cannot bind to ^{3}[Fe]. Without this calculated surface, the ICP is not known, however the orbital symmetry of the calculated superoxide complex, ^{3}[FeO$_2$], correlated with a high-energy reagent surface, so it is likely that the ICP is high in energy.

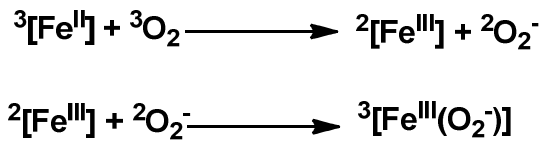

Scheme 3.28. Proposed mechanism for O_2 binding to form calculated superoxide complex.

Scheme 3.28 shows a proposed mechanism for dioxygen binding to form an O_2 adduct, which calculationally looks like an Fe(III) superoxide. Once PMe_3 has dissociated, leaving **1'b**, oxygen can initiate an outer sphere oxidation to generate $^2[Fe^{III}]$ and $^2O_2^-$. The doublet Fe(III) and doublet dioxygen anion can then recombine to form the calculated $^3[Fe^{III}(O_2^-)]$, which subsequently initiates decomposition. Since a dioxygen adduct could not be isolated or observed spectroscopically due to rapid degradation, this analysis is based upon the calculated initially formed dioxygen species, Fe(III) superoxide ($^3[FeO_2]$).

III. Conclusions

A number of Fe-N_2 complexes (**2 a-f**) were synthesized, characterized and shown to have a very unique kinetic stability toward air. *Ortho*-substituted diarylimine ligands (**Im a-f**) caused dissociation of PMe_3 from {*mer*-κ-C,N,C'-Ar-2-yl)CH_2N=CH(Ar-2-yl)}Fe(PMe_3)$_3$ (**1 a-f**) complexes as a result of steric interactions, and the resulting 5-coordinate species, {*mer*-κ-C,N,C'-Ar-2-yl)CH_2N=CH(Ar-2-yl)}Fe(PMe_3)$_2$ (**1'a-f**), were shown to selectively extract dinitrogen from air. Complexes **2 a-f** eventually degraded, rapidly in wet air by protolytic pathways, but far less quickly in dry air. The ability of the five-coordinate species and dinitrogen to

recombine resulted in significant stability in the presence of dioxygen. Calculations show the dinitrogen complexes, {*mer*-κ-C,N,C'-Ar-2-yl)CH_2N=CH(Ar-2-yl)}Fe(PMe_3)$_2N_2$ (**2 a-f**), are kinetically and thermodynamically preferred over the calculated dioxygen adduct, while experiments are consistent with rapid degradation of the diarylimine iron complex upon dioxygen binding.

Dinitrogen, ammonia, and dihydrogen bind similarly to the five-coordinate species **1'b**, while PMe_3 and pyridine are disfavored, due to the aforementioned steric features. Ligands with π-accepting capability (N_2, CO, CNMe) bind strongly, but attempts to generate iron multiple bonds were unsuccessful. Neutral iron (III) derivatives were generated via inner and outer sphere oxidations, but these complexes did not bind dinitrogen.

Obvious applications for Fe-N_2 chemistry involve dinitrogen reduction but this is typically approached via initial protonation. Since the Fe-N_2 complexes (**2 a-f**) were not stable to acid, the usual methods to generate ammonia were impractical. Attempts to observe the microscopic reverse of N_2 reduction with this system also failed since efforts toward Fe(III)-NH_2 or Fe(III)-NH_3 resulted in reduction to Fe(II)-N_2 and Fe(II)-NH_3.

Another potential application involves a chemical means to remove dinitrogen from hydrocarbon feed streams. Complexes **2 a,b** that have been shown to bind and release dinitrogen depending on oxidation state, could aid in dinitrogen removal, even with trace dioxygen present.

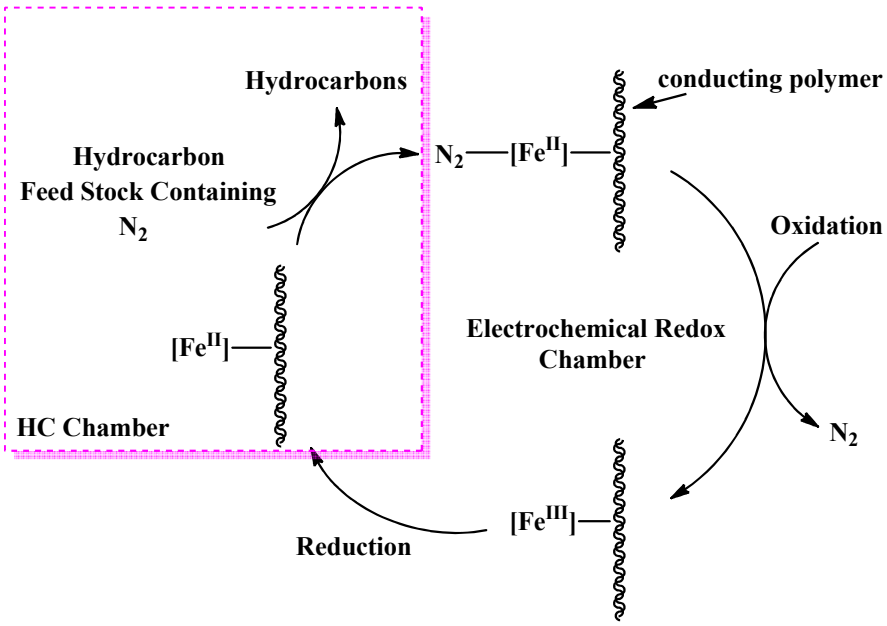

Figure 3.16. Two-chamber system for dinitrogen removal from hydrocarbon feed stocks.

If the Fe-N_2 complex is coordinated to a conducting polymer that can be subjected to electrochemical oxidation to release dinitrogen, it could then be electrochemically reduced to generate the Fe (II), which can capture dinitrogen from a hydrocarbon feed.

Perhaps insight gained from these Fe-N_2 complexes can be applied to the way nitrogenase is considered. Biologically, dinitrogen is converted to ammonia with the enzyme, requiring 8 protons, 8 electrons and the hydrolysis of 16 equivs of ATP.[14,16,19,20] The FeMo cofactor is accepted to be the site of N_2 binding and reduction, and it is possible the μ_6-carbide present at the center of the cluster (Figure 3.17)[83,84] helps impart a strong field and an electronic influence on dinitrogen binding. Nitrogenase is thought to operate anaerobically, and in the absence of reducing conditions, dioxygen can oxidize and degrade the Fe-S cofactors, but perhaps the

strong field imparted by the μ_6-carbide offers some stability even in the presence of dioxygen.

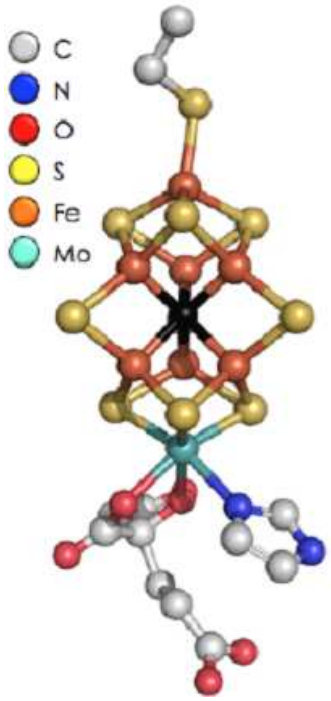

Figure 3.17. The μ_6-carbide present in the operational cluster of nitrogenase.

IV. Experimental

A. General Considerations.

All manipulations were performed using either glovebox or high vacuum line techniques. Hydrocarbon solvents containing 1-2 mL of added tetraglyme, and ethereal solvents were distilled under nitrogen from purple sodium benzophenone ketyl and vacuum transferred from same prior to use. Benzene-d_6 and toluene-d_8 were dried over sodium, vacuum transferred and stored under N_2. THF-d_8 was dried over sodium benzophenone ketyl. Methylene chloride-d_2 was dried over CaH_2, vacuum transferred and stored over activated 4 Å molecular sieves. $Fe(PMe_3)_4Me_2$ was

prepared according to a literature procedure.[85] Compounds **1d,h,I** were previously reported.[82] All other chemicals were commercially available and used as received. All glassware was oven dried.

NMR spectra were obtained using Mercury-300, INOVA 400, 500 and 600 MHz spectrometers. Chemical shifts are reported relative to benzene-d_6 (^{1}H δ 7.16; ^{13}C{^{1}H} δ 128.39), THF-d_8 (^{1}H δ 3.58; ^{13}C{^{1}H} δ 67.57), and CD_2Cl_2 (^{1}H δ 5.32; ^{13}C{^{1}H} δ 54.00). Infrared spectra were recorded on a Nicolet Avatar 370 DTGX spectrophotometer interfaced to an IBM PC (OMNIC software). UV-Vis spectra were obtained on an Ocean Optics USB2000 spectrometer. Solution magnetic measurements were conducted via Evans' method in benzene-d_6.[124] Elemental analyses were performed by Complete Analysis Laboratories, Inc., Parsippany, New Jersey.

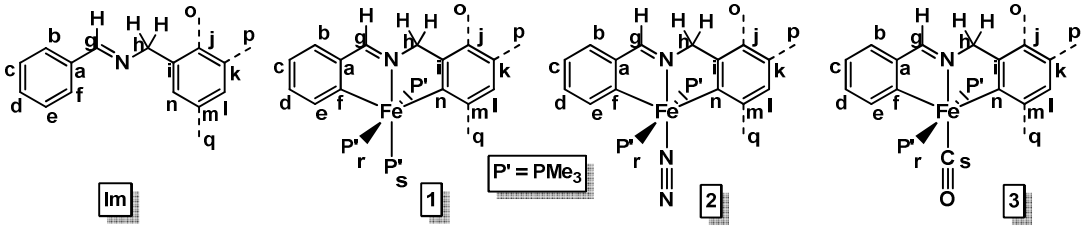

Figure. 3.18. Key for ^{1}H, ^{13}C{^{1}H}, ^{31}P and ^{19}F NMR assignments.

1. General procedures for imines, Im a – Im g

To a suspension of $MgSO_4$ (5-8 equiv) in CH_2Cl_2 were added 1.5 mmol of aldehyde and 1.5 mmol of amine. After stirring for 12 h, the mixture was filtered and concentrated to yield a clear to pale yellow oil in >98% purity (by 1H NMR).

Im-a (*b* = *d* = *e* = CF, *kp* = *mq* = CCF_3)**.** ^{1}H NMR (C_6D_6, 400MHz, mult, *J*(Hz); assmt): δ 6.22 (dt, 10, 9, *c*), 7.66 (m, *f*), 8.02 (s, *g*), 3.99 (s, *h*), 7.50 (s, *j*, *n*), 7.69 (s, *l*). ^{13}C{^{1}H} NMR (C_6D_6, 500 MHz, mult, J_{CF} (Hz); assmt): δ 125.07 (*a*), 157.80 (d, 250, *b*), 105.79 (*c*), 147.80 (d, 250, *d*), 152.35 (d, 250, *e*), 115.14 (*f*), 153.77 (*g*), 63.28 (*h*), 122.89 (*i*), 142.21 (*j*, *n*), 120.45 (*k*, *m*), 121.03 (*l*), 131.79 (q, 32, *o*, *p*). ^{19}F NMR (C_6D_6 400 MHz): δ -124.06 (m, *a*), -140.96 (m, *c*), -128.26 (m, *d*), -62.67 (d, 4.5, *l*).

Im-b (*b* = *d* = *e* = *k* = *l* = *m* = CF)**.** ^{1}H NMR (C_6D_6, 400MHz, mult, *J*(Hz); assmt): δ 7.71 (td, 9,7, *c*), 6.24 (td, 10,6, *f*), 7.98 (s, g), 3.91 (s, *h*), 6.51 (dd, 8,7, *j*,*n*). ^{13}C{^{1}H} NMR (C_6D_6, 500 MHz, mult, J_{CF} (Hz); assmt): δ 135.89 (*a*), 157.63 (d, 250, *b*), 105.89 (d, 250, *c*), 151.63 (d, 250, *d*), 152.37 (d, 250, *e*), 115.25 (*f*), 153.35 (*g*), 62.91 *h*), 120.47 (*i*), 111.64 (*j*,*n*), 147.70 (d, 250, *k*,*m*), 139.02 (d, 250, *l*). ^{19}F NMR (C_6D_6 400 MHz): δ -123.84 (ddd, 16,11,6, *b*), -128.48 (dtd, 22,9,5, *d*), -134.76 (dd, 21,8, *m*,*k*), -141.26 (tdd, 20,14,7, *e*), -163.20 (tt, 21,7, *l*).

Im-c (*b* = *c* = *d* = CF, *kp* = *mq* = CCF_3)**.** ^{1}H NMR (C_6D_6, 400MHz, mult, *J*(Hz); assmt): δ 6.26 (m, *e*), 7.44 (m, *f*), 7.99 (s, *g*), 4.02 (s, *h*), 7.54 (s, *j*, *n*), 7.70 (s, *l*). ^{13}C{^{1}H} NMR (C_6D_6, 500 MHz, mult, J_{CF} (Hz); assmt): δ 125.12 (*a*), 153.06 (d, 250, *b*), 140.06 (d, 250, *c*), 151.54 (d, 250, *d*), 112.45 (*e*), 121.05 (*f*), 153.73 (*g*), 62.80

(*h*), 122.88 (*i*), 142.45 (j, *n*), 121.27 (m, *k*), 121.87 (*l*), 131.86 (q, 33, *o*, *p*). ^{19}F NMR (C_6D_6 400 MHz): δ -143.16 (dt, 20, 7, *b*), -160.90 (td, 20, 7, *c*), -130.10 (m, *d*), -62.66 (s, *p*, *q*).

Im-d (*mq* = $COCH_3$). ^{1}H NMR (C_6D_6, 400MHz, mult, *J*(Hz); assmt): δ 7.75 (d, 2, *b*), 7.12-7.10 (m, *c*, *e*), 6.67 (dd, 8, 2, *d*), 7.76 (d, 2, *f*), 7.99 (s, *g*), 4.62 (s, *h*), 7.13 (d, 4, *j*), 7.07 (t, 2, *k*), 6.99 (d, 8, *l*), 3.34 (s, o), proton *n* obscured by solvent. ^{13}C{^{1}H} NMR (C_6D_6, 500 MHz; assmt): δ 136.66 (*a*), 128.36 (*b*, *f*), 128.28 (*c*, *e*), 130.34 (*d*), 161.08 (*g*), 64.74 (*h*), 141.44 (*i*) 120.22 (*j*), 129.22 (*k*), 113.69 (*l*), 160.11 (*m*), 112.37 (*n*), 54.33 (*o*).

Im-e (*b* = *c* = *d* = CF, *jo* = *mq* = CCH_3). ^{1}H NMR (C_6D_6, 400MHz, mult, *J*(Hz); assmt): δ 6.27 (m, *e*), 7.57 (m, *f*), 8.22 (s, *g*), 4.48 (s, *h*), 7.01 (d, 8, *k*), 6.93 (d, 8, *l*), 7.09 (s, *n*), 2.21 (s, *q*), 2.17 (s, *o*). ^{13}C{^{1}H} NMR (C_6D_6, 500 MHz mult, J_{CF} (Hz); assmt): δ 137.34 (*a*), 152.71 (d, 254, *b*), 140.01 (d, 254, *c*), 151.38 (d, 254, *d*), 112.26 (*e*), 121.63 (*f*), 152.30 (*g*), 63.25 (*h*), 135.62 (*i*), 133.29 (*j*), 130.46 (*k*), 128.15 (*l*), 133.29 (*m*), 129.58 (*n*), 18.52 (*q*), 20.84 (*o*). ^{19}F NMR (C_6D_6 400 MHz): δ -143.57 (dt, 20, 7, *b*), -161.39 (td, 20, 7, *c*), -131.53 (m, *d*).

Im-f (*jo* = *mq* = CCH_3). ^{1}H NMR (C_6D_6, 400MHz, mult, *J*(Hz); assmt): δ 7.76 (dd, 7, 2, *b*, *f*), 7.10 (s, broad, *c*, *e*), 7.22 (s, broad, *d*), 8.05 (s, *g*), 4.63 (s, *h*), 6.95 (s, broad, *k*), 7.03 (s, broad, *l*), 7.12 (s, *n*), 2.16 (s, *q*), 2.24 (s, *o*). ^{13}C{^{1}H} NMR (C_6D_6, 500 MHz; assmt): δ 139.59 (*a*), 128.28 (b, *f*), 126.00 (c, *e*), 128.40-128.43 (d, *n*), 160.98 (*g*), 65.04 (*h*), 139.58 (*i*), 130.30 (*j*), 128.36 (k, *l*), 136.75 (*m*), 21.01 (*o*), 18.94 (*o*).

Im-g (*b* = *c* = *d* = *jo* = *kp* = *l* = CF). ^{1}H NMR (C_6D_6, 400 MHz, mult, *J*(Hz); assmt): δ 6.54 (m, *e*), 7.47 (m, *f*), 8.04 (s, *g*), 4.23 (s, *h*), 6.40 (m, *m*), 6.27 (m, *n*). ^{13}C{^{1}H} NMR (C_6D_6, 500 MHz mult, J_{CF} (Hz); assmt): δ 124.11 (*a*), 152.97 (d, 250, *b*), 140.07 (d, 250, *c*), 150.75 (d, 250, *d*), 123.46 (*e*), 121.87 (*f*), 153.80 (*g*), 57.56 (*h*), 115.95 (*i*), 151.51 (d, 250, *j*), 140.61 (d, 250, *k*), 149.78 (d, 250, *l*), 111.95 (*m*), 112.70 (*n*). ^{19}F NMR (C_6D_6 400 MHz): δ -139.40 (dt, 21, 7, *b*), -160.96 (td, 20, 7, *c*), -130.48 (m, *d*), - 142.95 (dt, 20, 8, *j*), -161.07 (td, 20, 7, *k*), -136.31 (m, *l*).

2. General Procedure for *tris*-PMe_3 Complexes. Since **1a-f** cannot be exposed to dinitrogen, spectral assays of the (diarylimine)Fe(PMe_3)$_3$ complexes were conducted on NMR tube scale reactions. In a typical reaction, ~8 mg (0.020 mmol) $(Me_3P)_4FeMe_2$ and 0.020 mmol of imine were loaded into a J-Young NMR tube into which ~0.6 mL C_6D_6 was vacuum transferred. The reactions went to completion in 1-6 h, and the contents were never exposed to dinitrogen. Evans' method measurements were conducted on the crude paramagnetic compounds generated *in situ.*

1a (*b* = *d* = *e* = CF, *kp* = *mq* = CCF_3)**.** ^{1}H NMR (C_6D_6, 400 MHz): δ 66.13 (2H), 34.01 (2H), 32.57 (2H), -4.86 (18H), -11.46 (9H). Free PMe_3 was noted at δ 0.80. ^{31}P{^{1}H} NMR (400 MHz): δ -60.0 (br s, free PMe_3); no other resonances were noted. μ_{eff} (296 K) = 3.0 μ_B, 3.3 μ_B.

1b (*b* = *d* = *e* = *k* = *l* = *m* = CF)**.** ^{1}H NMR (C_6D_6, 400 MHz): δ 6.39 (s, *c*, *j*), 8.27 (s, *g*), 4.24 (s, *h*), 0.46 (s, *r*) 1.36 (s, *s*). ^{13}C{^{1}H} NMR (C_6D_6, 500 MHz, mult, J_{CF} (Hz); assmt): δ 117.39 (a), 161.49 (d, 230, *b*), 103.11 (*c*), 157.94 (d, 230, *d*), 159.10 (d, 250, *e*), 111.40 (*f*), 163.13 (*g*), 65.59 (*h*), 111.77 (*i*), 96.50 (*j*), 146.44 (d, 250, *k*),

144.97 (d, 250, *l*), 157.54 (d, 250, *m*), 111.26 (*n*), 16.97 (t, 10, *r*), 16.08 (d, 13, *s*). ^{19}F NMR: (C_6D_6, 400 MHz): δ -106.35 (d, 32, *b*), -147.15 (br s, *d*), -120.42 (dd, 21, 7, *e*) -166.60 (dd, 33, 20, *k*), -116.08 (t, 26 *l*), -133.28 (dd, 32, 9, *m*). ^{31}P{^{1}H} NMR (400 MHz): 14.14 (d, 58, o), 9.60 (t, 58, p).

1c (*b* = *c* = *d* = CF, *kp* = *mq* = CCF_3)**.** ^{1}H NMR (C_6D_6, 400 MHz): δ 64.36 (3H), 34.91 (2H), 13.91 (1H), -2.57 (27H). μ_{eff} (296 K) = 3.0 μ_B, 3.3 μ_B.

1d (*mq* = $COCH_3$). ^{1}H NMR (C_6D_6, 400 MHz): δ 7.48 (s, b), 7.44 (s, c), 6.98 (s, d), 7.07 (s, e), 8.34 (s, g), 4.87 (s, h), 6.46 (s, j), 6.84 (s, k), 6.87 (s, l), 3.37 (s, o), 0.65 (s, broad, p), 1.46 (s, broad, q). ^{13}C{^{1}H} NMR (C_6D_6, 500 MHz): δ 143.38 (*a*), 126.45 (*b*), 125.90 (*c*), 120.29 (*d*), 118.93 (*e*), 125.96 (*f*), 146.68 (*g*), 66.85 (*h*), 145.32 (*i*), 104.77 (*j*), 112.57 (*k*), 128.08 (*l*), 153.88 (*m*), 119.12 (*n*), 52.50 (*q*), 17.31 (t, 9, *r*), 25.44 (d, 15, *s*). ^{31}P{^{1}H} NMR (C_6D_6, 400 MHz): δ 24.18 (t, 62, q), 19.53 (d, 62, p).

1e (*b* = *c* = *d* = CF, *jo* = *mq* = CCH_3). ^{1}H NMR (C_6D_6, 400 MHz): δ 15.94 (3H), -1.17 (6H), -5.13 (3H), -11.42 (27H). μ_{eff} (296 K) = 3.2 μ_B, 3.3 μ_B.

1f (*jo* = *mq* = CCH_3). ^{1}H NMR (C_6D_6, 400 MHz): δ 16.29 (4H), 13.76 (3H), 12.51 (3H), -4.97 (3H), -11.02 (29H). μ_{eff} (296 K) = 3.0 μ_B, 3.2 μ_B.

1g (*b* = *c* = *d* = *jo* = *kp* = *l* = CF). ^{1}H NMR (C_6D_6, 400 MHz, mult, *J*(Hz); assmt): δ 7.10 (t, 9, *e*), 8.17 (s, *g*), 4.58 (s, *h*), 7.39 (t, 9, *m*), 0.30 (t, 3, *r*), 0.98 (d, 6, *s*). ^{13}C{^{1}H} NMR (500 MHz): δ 135.45 (*a*), 148.73 (d, 250, *b*), 151.00 (d, 250, *c*), 149.54 (d, 250, *d*), 123.01 (*e*), 132.38 (*f*), 162.44 (*g*), 61.14 (*h*), 145.40 (*i*), 133.41 (d, 250, *j*), 134.58 (d, 250, *k*), 144.12 (d, 250, *l*), 125.10 (*m*), 132.56 (*n*), 16.57 (t, 10, *o*), 22.22 (d, 16, *p*). ^{19}F NMR: (C_6D_6, 400 MHz): δ -140.61 (d, 22, *b*, *j*), -172.89 (td, 20, 7, *c*), -

135.29 (ddd, 20, 11, 4, *d*) -173.07 (tt, 20, 3, *k*), -141.86 (dd, 20, 11, *l*). $^{31}P\{^{1}H\}$ NMR (400 MHz): δ 20.15 ("t", 61, *r*), 16.24 (d, 61, *s*).

3. General Procedure for Dinitrogen Complexes. To a 100 mL bomb reactor charged with $Fe(PMe_3)_4Me_2$ (0.200g, 1.02mmol) and imine (1 equiv) was transferred 15 mL of benzene. The mixture was placed under an atmosphere of N_2 at 23 °C. The solution was allowed to stir for 6 h. Upon removal of solvent, the crude mixture was dissolved in Et_2O, filtered, and washed (4x10mL of Et_2O). Crystallization from hexanes at -78 °C afforded product.

2a (*b* = *d* = *e* = CF, *kp* = *mq* = CCF_3)**.** Dark purple microcrystals (0.200 g) of **1a** were obtained in 63% yield. ^{1}H NMR (C_6D_6, 400MHz, mult, *J*(Hz); assmt): δ 6.37 (s, *c*), 8.02 (s, *g*), 3.99 (s, *h*), 7.83 (s, *j*), 6.93 (s, broad, *l*), 0.34 (s, *r*). $^{13}C\{^{1}H\}$ NMR (C_6D_6, 500 MHz, mult, J_{CF} (Hz); assmt): δ 125.32 (*a*), 157.99 (d, 240, *b*), 120.13 (*c*), 159.73 (d, 240, *d*), 156.04 (d, 240, *e*), 123.85 (*f*), 162.25 (*g*), 64.11 (*h*), 129.68 (*i*), 115.83 (*j*), 120.26 (*k*), 124.11 (*l*), 152.14 (*m*), 124.84 (*n*), 141.34 (q, 25, *o*), 127.39 (q, 25, *p*), 13.02 (t, 12, *r*). ^{19}F NMR (400 MHz): δ -131.85 (ddd, 28,10, 4, *b*), -130.25 (td, 25, 4, *d*), -119.16 (ddd, 23, 9, 4, *e*), -61.37 (s, *q*), -59.37 (s, *p*). $^{31}P\{^{1}H\}$ NMR (400 MHz): δ 15.72 (s, *r*). IR (C_6D_6): ν(N_2) = 2121 cm^{-1}.

2b (*b* = *d* = *e* = *k* = *l* = *m* = CF)**.** Dark red crystalline **1b** (0.184 g) was obtained in 67% yield. ^{1}H NMR (C_6D_6, 400MHz, mult, *J*(Hz); assmt): δ 7.79 (s, *g*), 6.36 (m, *c*, *j*), 3.95 (s, *h*), 0.44 (s, *r*). $^{13}C\{^{1}H\}$ NMR (C_6D_6, 500 MHz, mult, J_{CF} (Hz); assmt): δ 133.26 (*a*), 160.4 (d, 230, *b*), 97.34 (*c*), 157.19 (d, 230, *d*), 157.93 (d, 230, *e*), 112.47 (*f*), 161.98 (*g*), 64.04 (*h*), 142.75 (*i*), 104.45 (*j*), 148.17 (d, 240, *k*), 138.46 (d, 240, *l*),

150.80 (d, 240, *m*), 111.07 (*n*), 12.90 (t, 12, *r*). ^{19}F NMR (400 MHz): δ -119.36 (d, 31, *b*), -145.94 (m, *d*), -118.92 (ddd, 3, 9, 23, *e*), -166.13 (dd, 20, 30, *k*), -128.81 (t, 29, *l*), -132.18 (ddd, 3, 10, 30, *m*). ^{31}P{^{1}H} NMR (400 MHz): δ 19.95 (s, *r*). ^{15}N NMR (**1b**-$^{15}N_2$, 600 MHz, referenced to NH_3(*l*)): δ 327.50 (br d, $^{1}J_{15N15N}$ = 4 Hz, $^{3}J_{15NP}$ <1.5 Hz, N_β), 362.90 (q, $^{1}J_{15N15N}$ = 5 Hz, $^{2}J_{15NP}$ = 5 Hz, N_a).[97] IR (C_6D_6): ν(N_2) = 2107 cm^{-1}. Anal. Calcd for $C_{20}H_{23}N_3F_6FeP_2$: C, 44.72; H, 4.32; N, 7.82. Found: C, 44.85; H, 4.22; N, 7.88.

2c (*b* = *c* = *d* = CF, *kp* = *mq* = CCF_3)**.** Dark red/brown solid (0.181g) was isolated in 57% yield . ^{1}H NMR (C_6D_6, 400 MHz): 6.94 (s, e), 8.03 (s, g), 4.00 (s, h), 7.58 (s, j), 7.77 (s, l), 0.15 (s, q). ^{13}C{^{1}H} NMR (C_6D_6, 500 MHz): 134.32 (a), 149.93 (d, 250, b), 134.24 (d, 250, c), 151.98 (d, 250, d), 118.39 (e), 124.14 (f), 161.77 (g), 64.20 (h), 125.47 (i), 119.99 (j), 135.24 (k), 116.10 (l), 133.35 (m), 124.86 (n), 140.87 (q, 30, o, p), 12.24 (t, 12, q). ^{19}F NMR (400 MHz): -138.96 (dd, 20,6, b), -170.81 (td, 20,7, c), -133.03 (ddd, 20,9,6, d), -60.38 (s, o), -61.40 (s, p). ^{31}P NMR (400 MHz): 14.30 (s, q). IR: v (N_2), 2102 cm^{-1}.

2d (*mq* = $COCH_3$). Dark green microcrystals (0.188 g) were isolated in 80% yield. ^{1}H NMR (C_6D_6, 400MHz, mult, *J*(Hz); assmt): δ 7.27 (m, *b*, *c*), 7.63 (t, 7, *d*), 7.45 (d, 7, *e*), 8.35 (s, *g*), 4.57 (s, *h*), 6.57 (d, 7, *j*), 7.08 (t, 7, *k*), 6.79 (d, 7, *l*), 3.71 (s, *q*), 0.56 (s, *r*). ^{13}C{^{1}H} NMR (C_6D_6, 500 MHz): δ 142.97 (*a*), 129.31 (*b*), 128.31 (*c*), 138.74 (*d*), 128.22 (*e*), 126.66 (*f*), 160.98 (*g*), 64.54 (*h*), 144.90 (*i*), 126.40 (*j*), 130.28 (*k*), 112.32 (*l*), 160.07 (*m*), 113.64 (*n*), 54.05 (*q*), 12.51 (t, 9, *r*). ^{31}P{^{1}H} NMR (400 MHz): δ 21.82 (s, *r*). IR (C_6D_6): ν(N_2) = 2067 cm^{-1}. Anal. Calcd for $C_{21}H_{31}N_3P_2OFe$: C, 54.92; H, 6.80; N, 9.15. Found: C, 54.84; H, 6.69, N, 9.24.

2e (*b* = *c* = *d* = CF, *jo* = *mq* = CCH_3). Dark green solid (0.167g) was isolated on a 65% yield. ^{1}H NMR (C_6D_6, 400 MHz): 7.76 (t, 7, e), 7.90 (s, broad, g), 4.28 (s, h), 7.07 (d, 8, k), 6.82 (d, 8, l), 2.06 (s, o), 2.70 (s, p), 0.33 (s, q). $^{13}C\{^1H\}$ NMR (C_6D_6, 500 MHz): 133.26 (a), 151.97 (d, 240, b), 134.02 (d, 240, c), 150.54 (d, 240, d), 117.97 (e), 123.26 (f), 160.72 (g), 63.94 (h), 125.17 (i), 134.46 (j), 123.57 (k, l), 132.55 (m), 130.81 (n), 27.49 (o), 20.17 (p), 12.39 (t, 11, q). ^{19}F NMR (400 MHz): -139.85 (ddd, 20,9,5, b), -172.25 (td, 20,7, c), -134.90 (ddd, 20,9,5, d). IR: v (N_2), 2058 cm^{-1}.

2f (*jo* = *mq* = CCH_3). A dark green solid (0.178 g) was isolated in 76% yield. ^{1}H NMR (C_6D_6, 400MHz, mult, *J*(Hz); assmt): δ 7.48 (br s, *b*), 7.22-7.32 (br s, *c*, *d*), 7.68 (br s, *e*), 8.36 (s, *g*), 4.50 (s, *h*), 6.80-6.95 (s, broad, *k*, *l*), 2.15 (s, *q*), 2.85 (s, *o*), 0.48 (s, *r*). $^{13}C\{^1H\}$ NMR (C_6D_6, 500 MHz): δ 150.16 (*a*), 126.09 (*b*), 137.57 (*c*), 129.93 (*d*), 137.57 (*e*), 126.76 (*f*), 167.40 (*g*), 64.72 (*h*), 151.29 (*i*), 148.54 (*j*), 119.63 (*k*), 118.42 (*l*), 144.30 (*m*), 117.39 (*n*), 27.52 (*q*), 20.88 (*o*), 13.35 (t, 12, *r*). $^{31}P\{^1H\}$ NMR (400 MHz): δ 20.77 (s, *r*). IR (C_6D_6): ν(N_2) = 2046 cm^{-1}. Anal. Calcd for $C_{22}H_{33}N_3P_2Fe$: C, 57.78; H, 7.27; N, 9.19. Found: C, 57.83; H, 7.09, N, 9.08.

2g (*b* = *c* = *d* = *j* = *k* = *l* = CF). To a J-Young NMR tube was added 0.020g (0.034 mmol) **1g** and 0.007g (0.034 mmol) tosyl azide. Benzene-d_6 (~0.6mL) was transferred and the tube warmed to room temperature. After 24 h, the dinitrogen complex was formed in ~50% yield. ^{1}H NMR (C_6D_6, 400 MHz): 7.30 (t, 8, e), 8.20 (s, broad, g), 4.30 (s, h), 7.49 (d, 8, m), 0.20 (s, r). ^{19}F NMR (400 MHz): -126.97 (d, 19, b), -166.27 (t, 20, c), -136.13 (dd, 19,9, d), -128.55 (dd, 17,12, j), -168.06 (t, 18, k). -130.72 (dd, 18,9, l). ^{31}P NMR (400 MHz): 17.69 (s, r). IR: v (N_2), 2070 cm^{-1}.

4. General Procedure for Carbonyl Complexes. To a 100 mL bomb reactor charged with $(PMe_3)_4FeMe_2$ (0.100 g, 0.513 mmol) and imine (1 equiv) was transferred 15 mL of benzene at -78 °C. The solution was allowed to warm to 23 °C and stir for 4 h. Upon removal of solvent and excess PMe_3, the crude mixture was re-dissolved in benzene, placed under an atmosphere of dry CO, and stirred for 12 h. Solvent and excess CO was removed from the bomb reactor via vacuum transfer, and the crude solid was dissolved in Et_2O, filtered and washed (3 x 10 ml). Crystallization from hexanes at -78 °C afforded product.

3a (*b* = *d* = *e* = CF, *kp* = *mq* = CCF_3)**.** Dark red microcrystals (0.140 g) were isolated in 88% yield. ^{1}H NMR (C_6D_6, 400 MHz): δ 7.99 (br s, *c*, *g*), 6.29 (s, *l*), 4.23 (s, *h*), 0.33 (s, *r*). $^{13}C\{^1H\}$ NMR (C_6D_6, 500 MHz, mult, J_{CF} (Hz); assmt): δ 133.96 (*a*), 157.30 (d, 250, *b*), 98.33 (*c*), 156.03 (d, 250, *d*), 155.46 (d, 250, *e*), 122.59 (*f*), 161.48 (*g*), 63.79 (*h*), 149.75 (*i*), 120.59 (*j*), 141.68 (*k*), 116.45 (*l*), 125.21 (*m*), 124.66 (*n*), 124.39 (q, 40, *q*), 124.12 (q, 40, *p*), 14.76 (t, 13, *r*), 193.65 (*s*). ^{19}F NMR: (C_6D_6, 400 MHz): δ -118.71 (ddd, 22, 9, 4, *b*), -122.08 (t, 25, *d*), -130.89 (ddd, 28, 9, 3, *e*), -61.56 (s, *q*), -58.84 (s, *p*). $^{31}P\{^1H\}$ NMR (400 MHz): 16.00 (q). Anal. Calcd for $C_{23}H_{24}F_9P_2NOFe$: C, 44.61; H, 3.91; N, 2.26. Found: C, 44.62; H, 3.92, N, 2.32. IR (C_6D_6): ν(CO) = 1950 cm^{-1}.

3b (*b* = *d* = *e* = *k* = *l* = *m* = CF)**.** Dark red microcrystals were (0.110 g) isolated in 80% yield. ^{1}H NMR (C_6D_6, 400 MHz): δ 6.36 (m, *c*, *j*), 7.96 (s, *g*), 4.18 (s, *h*), 0.44 (s, *r*). $^{13}C\{^1H\}$ NMR (C_6D_6, 500 MHz, mult, J_{CF} (Hz); assmt): δ 149.13 (*a*), 158.93 (d, 240, *b*), 97.81 (*c*), 158.08 (d, 240, *d*), 154.57 (d, 240, *e*), 142.67 (*f*), 160.95 (*g*), 63.40 (*h*), 147.26 (*i*), 104.59 (*j*), 157.15 (d, 240, *k*), 151.83 (d, 240, *l*), 156.24 (d,

240, *m*), 132.88 (n), 14.72 (t, 13, *r*), 190.97 (*s*). ^{19}F NMR (C_6D_6, 400 MHz): δ -110.14 (d, 30, *b*), -145.40 (m, *d*), -118.70 (ddd, 22, 9, 4, *e*), -120.92 (t, 27, *k*), -165.24 (t, 26, *l*), -131.28 (ddd, 30, 10, 4, *m*). ^{31}P{^{1}H} NMR (400 MHz): δ 20.54 (s, *r*). IR (C_6D_6): ν(CO) = 1936 cm^{-1}.

3c (*b* = *c* = *d* = CF, *kp* = *mq* = CCF_3)**.** The reaction was conducted on an NMR tube scale starting from 10 mg *cis*-$(Me_3P)_4FeMe_2$ and 10 mg **Im-c** in ~0.6 mL C_6D_6, giving a dark red solution. ^{1}H NMR (C_6D_6, 400 MHz): δ 6.96 (s, *e*), 7.98 (s, *g*), 4.27 (s, *h*), 7.69 (s, *j*), 7.86 (s, *l*). 0.21 (s, *r*). ^{13}C{^{1}H} NMR (C_6D_6, 500 MHz, mult, J_{CF} (Hz); assmt): δ 134.19 (*a*), 153.81 (d, 230, *b*), 151.61 (d, 250, *c*), 150.05 (d, 250, *d*), 116.66 (*e*), 124.09 (*f*), 160.97 (*g*), 63.87 (*h*), 142.46 (*i*), 121.42 (*j*), 141.00 (*k*), 120.32 (*l*), 141.17 (*m*), 124.77 (*n*), 121.77 (q, 40, *q*), 121.03 (q, 40, *p*), 14.19 (t, 14, *r*), 197.59 (*s*). ^{19}F NMR: (C_6D_6, 400 MHz): δ -132.59 (m, *b*), -170.45 (t, 20, *c*), -138.61 (m, *d*), -59.66 (s, *p*), -61.54 (s, *q*). ^{31}P{^{1}H} NMR (400 MHz): 14.90 (s, *r*). IR (C_6D_6): ν(CO) = 1921 cm^{-1}.

3d (*mq* = $COCH_3$). The reaction was conducted on an NMR tube scale starting from 10 mg *cis*-$(Me_3P)_4FeMe_2$ and 6 mg **Im-c** in ~0.6 mL C_6D_6, giving a dark red solution. ^{1}H NMR (C_6D_6, 400 MHz): δ 7.58 (br m, *b*), 7.40 (br m, *c*), 7.26 (br m, *d*, *e*), 8.00 (br s, *g*), 4.80 (br s, *h*), 6.52 (br m, *j*), 6.85 (br m, *k*, *l*), 3.28 (s, *q*), 0.62 (s, *r*). ^{13}C{^{1}H} NMR (C_6D_6, 500 MHz, assmt): δ 145.46 (*a*), 127.23 (*b*), 123.06 (*c*, *e*), 149.96 (*d*), 126.94 (*f*), 167.08 (*g*), 64.76 (*h*), 143.40 (*i*), 120.09 (*j*), 142.61 (*k*), 105.81 (*l*), 151.06 (*m*), 113.59 (*n*), 54.48 (*q*), 15.05 (t, 13, *r*), 201.54 (*s*). ^{31}P{^{1}H} NMR (C_6D_6, 400 MHz): δ 22.05 (s, *r*). IR (C_6D_6): ν(CO) = 1896 cm^{-1}.

3f (*jo* = *mq* = CCH_3). A dark red solid was (0.075 g) isolated in 64% yield. ^1H NMR (C_6D_6, 400 MHz): δ 7.90 (br s, *b*) 6.83 (br s, *c*), 7.27 (br s, *d*), 7.43 (d, 6, *e*), 8.44 (s, *g*), 4.74 (s, *h*), 7.34-7.39 (br s, *k, l*), 2.29 (s, *q*), 2.10 (s, *o*), 0.56 (s, *r*). $^{13}C\{^1H\}$ NMR (C_6D_6, 500 MHz, assmt): δ 138.01 (*a*), 130.37 (*b*), 126.96 (*c*), 127.19 (*d*), 127.45 (*e*), 125.45 (*f*), 161.10 (*g*), 63.39 (*h*), 141.07 (*i*), 133.29 (*j*), 130.63 (*k*), 120.38 (*l*), 135.55 (*m*), 137.18 (*n*), 20.84 (*q*), 21.14 (*o*), 15.07 (t, 12, *r*). $^{31}P\{^1H\}$ NMR (400 MHz): δ 21.31 (s, *r*). IR (C_6D_6): ν(CO) = 1882 cm^{-1}. Anal. Calcd for $C_{23}H_{33}P_2NOFe$: C, 60.41; H, 7.27; N, 3.06. Found: C, 60.49; H, 7.29, N, 3.23.

5. *trans*-{κ-C,N-(3,4,5-(F)$_3$-C$_6$H$_2$)CH$_2$N=CH(3,4,6-(F)$_3$-C$_6$H-2-yl)}Fe(PMe$_3$)$_3$(CCMe) (4b-Me).

To a 25 mL round-bottom flask charged with $Fe(PMe_3)_4$ Me_2 (0.050g,0.128 mmol) and **Im-b** (0.038g, 0.128 mmol) was transferred an 8 mL amount of benzene. The reaction was allowed to stir for 4 h at 23 °C. Propyne was added to the reaction via gas bulb (0.128 mmol) and the mixture was stirred for 10 h. Upon removal of solvent, the crude solid was filtered and washed with Et_2O (3 x 5 mL). Dark red **4b**-Me was isolated (0.055 g) in 69% yield. ^1H NMR (C_6D_6, 400 MHz): δ 6.30 (m, *c*), 8.23 (s, *g*), 4.79 (s, *h*), 6.96 (t, 7, *j*, *n*), 0.73 (s, *r*), 1.28 (d, 6, *s*), 2.30 (s, CH_3). $^{13}C\{^1H\}$ NMR (C_6D_6, 500 MHz, mult, J_{CF} (Hz); assmt): δ 133.26 (*a*), 157.66 (d, 260, *b*), 96.10 (*c*), 158.32 (d, 260, *d*), 151.54 (d, 260, *e*), 110.75 (*f*), 165.29 (*g*), 62.03 (*h*), 131.79 (*i*), 117.45 (*j*, *n*), 152.16 (d, 260, *k*, *m*), 139.69 (d, 260, *l*), 16.79 (t, 10, *r*), 16.06 (d, 10, *s*), 62.51 (C_α), 103.34 (C_β), 3.43 (s, CH_3). ^{19}F NMR (C_6D_6, 400 MHz): δ -119.52 (d, 20, *b*), -161.31 (m, *d*), -132.76 (dd, 33, 7, *e*), -133.99 (dd, 22, 8, *k*, *m*), -118.35 (t, 29, *l*).

$^{31}P\{^{1}H\}$ NMR (C_6D_6, 400 MHz): δ 16.08 ("d", 62, *r*), 14.12 (td, 62, 11, *s*). Anal. Calcd for $C_{26}H_{36}F_6P_3NFe$: C, 49.94; H, 5.80; N, 2.24. Found: C, 50.04; H, 5.42, N, 2.45. IR ν(CC): 2081 cm^{-1}.

6. *trans*-{κ-C,N-(3,4,5-(F)$_3$-C$_6$H$_2$)CH$_2$N=CH(3,4,6-(F)$_3$-C$_6$H-2-yl)}Fe(PMe$_3$)$_3$(CCPh) (4b-Ph).

To a 25 mL round-bottom flask charged with $Fe(PMe_3)_4Me_2$ (0.050g, 0.128 mmol) and **Im-b** (0.038g, 0.128 mmol) was transferred an 8 mL amount of benzene, and the reaction was allowed to stir for 4 h at 23 °C. Phenylacetylene was added to the reaction via syringe (14 uL, 0.128 mmol), and the reaction was stirred for 10 h at 23 °C. Upon removal of solvent, the crude solid was filtered and washed with Et_2O (3 x 5 mL). Dark red **4b**-Ph was isolated (0.070g) in 79% yield. ^{1}H NMR (C_6D_6, 400 MHz): δ 6.31 (m, *c*), 8.18 (s, *g*), 4.82 (s, *h*), 6.85 (t, 6, *j*, *n*), 0.74 (s, *r*), 1.27 (d, 5, *s*), 7.54 (d, 7, C_oH) , 7.25 (t, 7, C_mH), 7.00 (t, 7, C_pH). $^{13}C\{^{1}H\}$ NMR (C_6D_6, 500 MHz, mult, J_{CF} (Hz); assmt): δ 133.46 (*a*), 160.19 (d, 260, *b*), 96.55 (*c*), 157.76 (d, 260, *d*), 153.53 (d, 260, *e*), 125.97 (*f*), 165.29 (*g*), 62.32 (*h*), 150.11 (*i*), 114.69 (*j*, *n*), 151.62 (d, 250, *k*,*m*), 149.41 (d, 260, *l*), 16.65 (t, 12, *r*), 23.39 (d, 20, *s*), 120.89 (q), 121.30 (r), 130.66 (s), 129.97 (C_o), 128.33 (C_m), 123.35 (C_p). ^{19}F NMR (C_6D_6, 400 MHz): δ -119.0 (d, 20, *b*), -160.97 (m, *d*), -132.10 (dd, 33, 7, *e*), -133.68 (dd, 22, 8, *k*, *m*), -118.30 (t, 30, *l*). $^{31}P\{^{1}H\}$ NMR (C_6D_6, 400 MHz): δ 15.68 ("d", 61, *r*), 13.46 (td, 62, 12, *s*). Anal. Calcd for $C_{31}H_{38}F_6P_3NFe$: C, 54.17; H, 5.57; N, 2.04. Found: C, 54.36; H, 5.41, N, 2.28. IR ν(CC): 2020 cm^{-1}.

7. *trans*-{κ-C,N-(3,5-$(CF_3)_2$-C_6H_3)CH_2N=CH(3,4,6-$(F)_3$-C_6H-2-yl)}Fe$(PMe_3)_3$(CCMe) (4a-Me).

To a J-Young tube containing **1a** (0.010 g, 0.0149mmol), 0.0149 mmol methylacetylene was added via gas bulb. After 8 hours, the reaction was complete leaving **4a-Me** as a dark red solution. ^{1}H NMR (C_6D_6, 400 MHz): 6.88 (s, *c*), 8.33 (s, *g*), 4.88 (s, *h*), 7.31 (s, *l*), 8.10 (s, *j*, *n*), 0.64 (s, *r*), 1.28 (s, *s*), 2.30 (s, CH_3). ^{19}F NMR (C_6D_6, 400 MHz): -119.44 (d, 20, *b*), -118.02 (d, 32, *d*), -132.28 (d, 30, *e*), -62.87 (s, *p*,*q*). ^{31}P NMR (C_6D_6, 400 MHz): 15.24 (d, 63, *r*), 12.52 (t, 63, *s*).

8. *trans*-{κ-C,N-(3,5-$(CF_3)_2$-C_6H_3)CH_2N=CH(3,4,6-$(F)_3$-C_6H-2-yl)}Fe$(PMe_3)_3$(CCPh) (4a-Ph).

To a J-Young tube containing **1a** (0.010 g, 0.0149mmol), 1.6 uL (0.0149 mmol) phenylacetylene was added via syringe under argon. After 8 hours, the reaction was complete leaving **4a-Ph** as a dark red solution. ^{1}H NMR (C_6D_6, 400 MHz): 7.41 (s, *c*), 8.25 (s, *g*), 4.97 (s, *h*), 7.67 (s, *l*), 7.93 (s, *j*, *n*), 0.70 (s, *r*), 1.25 (s, *s*), 7.25-7.30 (broad s, C_m, C_p), 7.03 (broad s, C_o). ^{19}F NMR (C_6D_6, 400 MHz): -119.04 (d, 19, *b*), -118.29 (d, 32, *d*), -131.74 (d, 32, *e*), -62.51 (s, *p*,*q*). ^{31}P NMR (C_6D_6, 400 MHz): 15.02 (d, 59, *r*), 12.50 (t, 59, *s*).

9. *trans*-{*mer*-κ-C,N,C'-(3,4,5-$(F)_3$-C_6H-2-yl)CH_2N=CH(3,4,6-$(F)_3$-C_6H-2-yl)}Fe$(PMe_3)_2(H_2)$ (5b).

a. Observation of 5b. Into a J-Young tube (2.1 mL volume) was added **2b** (20 mg, 0.037 mmol) in C_6D_6 or toluene-d_8. The tube was degassed by multiple freeze-pump-thaw cycles, and dihydrogen (660 torr) was added at 23°C. The reaction was monitored by ^{1}H and ^{19}F NMR spectroscopy. ^{1}H NMR (C_6D_6): δ 8.08 (s, *g*), 6.48

(m, *c*, *j*), 4.24 (s, *h*), 0.22 (t, 3, *r*), -13.88 (t, 12, *s*). ^{19}F NMR (C_6D_6): δ -107.83 (d, 35, *b*), -118.85 (m, *e*,*l*), -133.23 (dd, 8, 30, *m*), -146.57 (br s, *d*), -166.00 (m, *k*). ^{31}P NMR (C_6D_6): δ 20.54. **b. T_1(min) Measurement. 5b** was prepared in toluene-d_8 and allowed to equilibrate for 48 h. ^{1}H NMR spectra were recorded at 500 MHz and temperature calibration was performed for each measurement (T(K), T_1 (ms)): 298, 21; 288, 18; 278; 16; 268, 15; 258, 13; 238, 11; 218, 11; 198, 15. The T_1(min) of 10.7 ms (226 K) was obtained by plotting ln T_1 (ms) vs. 1/T (K^{-1}) and fitting with linear regression. The d(H-H) of 0.77 Å was calculated by assuming rapid rotation of H_2 and using the following equations: dipolar relaxation, $1/T_1 = 0.3\gamma_H^4(h/2\pi)^2(J(\omega) + 4J(2\omega))/r_{HH;}^{112,126}$ spectral density function, $J(\omega) = A\tau/(1 + \omega^2\tau^2)$ where $A = 0.25$ for rapid rotation. The temperature dependence of the correlation time is $\tau = \tau_0\exp[E_a/RT]$, and at T_1, $\tau = 0.62/(2\pi\nu)$; simplifying, $r_{HH} = 4.611\ (T_1(\text{min})/\nu)^{1/6}$.[112,126-128] **c. K_c Measurement. 5b** was prepare from **2b** in C_6D_6 as above and allowed to equilibrate for 48 h. The K_c was calculated by direct integration of **2b**, **5b**, and H_2, and the amount of N_2 in solution was estimated from the Henry's Law constant of N_2 in benzene and assuming the total amount of N_2 (gas and solution) was equal to that of **5b**.

10. *trans*-{*mer*-κ-C,N,C'-(3,4,5-(F)$_3$-C$_6$H-2-yl)CH$_2$N=CH(3,4,6-(F)$_3$-C$_6$H-2-yl)}Fe(PMe$_3$)$_2$NH$_3$ (6b).

To a 100 mL bomb charged with **2b** (0.100g) was transferred 15 mL of benzene at -78 °C. An excess of ammonia dried over sodium was transferred to the bomb at -78 °C. The bomb was slowly warmed to 23 °C and allowed to stir for 0.5 h. The solution turned from yellow/red to bright red and eventually bright purple. The

excess ammonia and benzene were removed *in vacuo*. The addition of benzene and excess ammonia was repeated 3 times. Crude product was assayed by transferring d_6-benzene to an NMR tube in absence of N_2. Bright purple **6b** was isolated (0.096g) in 98% yield. ^{1}H NMR (C_6D_6, 400 MHz): δ 6.44 (s, *c, j*), 8.14 (s, *g*), 3.89 (s, *h*), 0.37 (s, *s*), 0.48 (s, *r*). ^{13}C{^{1}H} NMR (C_6D_6, 500 MHz, mult, J_{CF} (Hz); assmt): δ 150.70 (*a*), 161.64 (d, 240, *b*), 95.29 (*c*), 161.19 (d, 240, *d*), 160.65 (d, 240, *e*), 145.89 (*f*), 163.67 (*g*), 64.93 (*h*), 147.80 (*i*), 103.64 (*j*), 159.87 (d, 230, *k*), 149.31 (d, 230, *l*), 152.57 (d, 230, *m*), 135.51 (*n*), 12.51 (t, 12, *r*). ^{19}F NMR (C_6D_6, 400 MHz): δ -128.99 (d, 35, *b*), -168.31 (m, *d*), -119.72 (dd, 24, 4, *e*), -148.39 (t, 12, *k*), -136.60 (t, 27, *l*), -135.51 (dd, 34, 7, *m*). ^{31}P{^{1}H} NMR (C_6D_6, 400 MHz): δ 21.42 (s, *r*). Anal. Calcd for $C_{20}H_{26}F_6N_2P_2Fe$: C, 45.65; H, 4.98; N, 5.32. Found: C, 45.62; H, 5.09, N, 5.35.

11. *trans*-{*mer*-κ-C,N,C'-(3,4,5-(F)$_3$-C$_6$H-2-yl)CH$_2$N=CH(3,4,6-(F)$_3$-C$_6$H-2-yl)}Fe(PMe$_3$)$_2$py (7b).

To a 50 mL bomb was charged with $(Me_3P)_4FeMe_2$ (0.050 g, 0.128 mmol) and **Im-b** (0.039g, 0.128 mmol) were transferred 8 mL of Et_2O, and the reaction was allowed to stir for >4 h at 23 °C. The Et_2O and PMe_3 were removed *in vacuo*, and the residual was triturated with Et_2O to remove excess PMe_3. Another 8 mL of Et_2O were transferred to the flask, and a solution of pyridine-N-oxide in Et_2O (0.126 M) was added dropwise and allowed to stir for 12 h at 60 °C. Product **7b** was filtered and washed (3 x 5 mL) with Et_2O and crystallized at -78 °C (0.053 g, 70%). The red microcrystalline solid was assayed by transferring C_6D_6 to an NMR tube containing the solid, in the absence of N_2. ^{1}H NMR (C_6D_6, 400 MHz): δ 6.53 (s, *c*), 8.81 (s, *g*), 4.24 (s, *h*), 8.01 (s, *j*), 0.54 (s, *r*), 6.89 (d, 6, C_oH), 7.10 (m, C_mH, C_pH). ^{13}C{^{1}H} NMR

(C_6D_6, 500 MHz, mult, J_{CF} (Hz); assmt): δ 135.03 (*a*), 161.38 (d, 250, *b*), 94.93 (*c*), 158.56 (d, 250, *d*), 153.06 (d, 250, *e*), 129.96 (*f*), 163.67 (*g*), 62.96 (*h*), 138.79 (*i*), 115.11 (*j*), 144.10 (d, 250, *k*), 134.47 (d, 250, *l*), 151.19 (d, 250, *m*), 124.47 (*n*), 12.03 (t, 10, *r*), 141.19 (C_o), 124.96 (C_mH), 135.27 (C_p). ^{19}F NMR: (C_6D_6, 400 MHz): δ -134.48-134.77 (m, *b*, *d*, m), -119.96 (dd, 22, 7, *e*), -162.23 (t, 21, *k*), -127.45 (t, 26, *l*). ^{31}P{^{1}H} NMR (C_6D_6, 400 MHz): 20.15 (s, *r*). Anal. Calcd for $C_{25}H_{28}F_6N_2P_2Fe$: C, 51.04; H, 4.80; N, 4.76. Found: C, 51.02; H, 4.90, N, 4.76.

12. *trans*-{*mer*-κ-C,N,C'-(3,4,5-(F)$_3$-C$_6$H-2-yl)CH$_2$N=CH(3,4,6-(F)$_3$-C$_6$H-2-yl)}Fe(PMe$_3$)$_2$(CNMe) (8b).

To a 50 mL round-bottom flask charged with $(Me_3P)_4FeMe_2$ (0.200 g, 0.512 mmol) and **Im-b** (0.155 g, 0.512 mmol) was transferred 15 mL benzene. The reaction mixture was stirred for 4 h at 23°C. Methyl isocyanide (27 uL, 0.512 mmol) was added to the flask, which continued to stir for 6 h at 23 °C. Solvent was removed *in vacuo*, and the crude solid was filtered and washed in Et_2O (3 x 10 mL). Red/brown solid **8b** was isolated (0.200 g) in 69% yield. ^{1}H NMR (C_6D_6, 400 MHz): δ 6.40 (m, *c*, *j*), 8.18 (s, *g*), 4.32 (s, *h*), 0.53 ("t", 4, *r*), 2.85 (t, 2, CH_3). ^{13}C{^{1}H} NMR (C_6D_6, 500 MHz, mult, J_{CF} (Hz); assmt): δ 139.19 (*a*), 156.94 (d, 250, *b*), 103.73 (*c*), 156.57 (d, 250, *d*), 150.38 (d, 250, *e*), 143.55 (*f*), 159.30 (*g*), 63.78 (*h*), 137.22 (*i*), 133.25 (*j*), 147.68 (d, 250, *k*), 138.53 (d, 250, *l*), 150.00 (d, 250, *m*), 157.33 (*n*), 14.62 (t, 12, *r*), 96.13 (*s*), 29.86 (CH_3). ^{19}F NMR (C_6D_6, 400 MHz): δ -114.16 (d, 31, *b*), -147.14 (m, *d*), -119.94 (ddd, 23, 8, 2, *e*), -166.70 (dd, 32, 19, *k*), -124.57 (t, 27, *l*) -133.85 (ddd, 31, 10, 2, *m*). ^{31}P{^{1}H} NMR (C_6D_6, 400 MHz): δ 24.04 (s, *r*). Anal. Calcd for

$C_{22}H_{26}F_6P_2N_2Fe$: C, 48.02; H, 4.76; N, 5.09. Found: C, 48.09; H, 4.62, N, 5.03. IR v(CN): 2073 cm^{-1}.

13. *trans*-{*mer*-κ-C,N,C'-(3,4,5-(F)$_3$-C$_6$H-2-yl)CH$_2$N=CH(3,4,6-(F)$_3$-C$_6$H-2-yl)}Fe(PMe$_3$)$_2$(N$_2$CPh$_2$) (9b).

To a 10 mL round-bottom flask charged with **2b** (0.045 g, 0.084 mmol) and diphenyldiazomethane (0.017 g, 0.088 mmol) was transferred 5 mL Et_2O at -78 °C. The reaction was allowed to warm to 23 °C and stir for 16 h. The brown solution was filtered and solvent was removed *in vacuo* leaving a dark purple microcrystalline solid (0.045 g, 0.064 mmol) in 76% yield. ^{1}H NMR (C_6D_6): δ 6.37 (m, *c*, *j*), 7.78 (s, *g*), 3.98 (s, *h*), 0.34 (t, 3, *r*), 7.61 (d, 8, C_oH), 7.30 (t, 8, C_mH), 6.98 (t, 8, C_pH). ^{13}C{^{1}H} NMR (C_6D_6, mult, J_{CF} (Hz); assmt): δ 136.38 (*a*), 160.93 (*b*), 97.60 (*c*), 159.40 (*d*), 158.11 (*e*), 120.27 (*f*), 162.21 (*g*), 64.31 (*h*), 131.82 (*i*), 104.71 (*j*), 156.99 (*k*), 141.98 (*l*), 156.08 (*m*), 124.94 (*n*), 13.15 (*r*), 131.83 (*p*), 131.09 (*q*), 132.12 (C_o), 126.02 (C_m), 125.45 (C_p). ^{19}F NMR: (C_6D_6): δ -114.53 (d, 31, *m*), -145.55 (dd, 20, 8, *k*), -119.22 (dd, 22, 9, *b*), -132.42 (dd, 31, 9, *d*), -124.31 (ddd, 30, 23,5, *e*), -165.49 (dd, 31, 20, *l*). ^{31}P NMR (C_6D_6): δ 17.52 (s, *r*). Anal. Calcd for $C_{33}H_{33}F_6P_2N_3Fe$: C, 56.35; H, 4.73; N, 5.97. Found: C, 56.31; H, 4.83, N, 5.91.

14. *trans*-{*mer*-κ-C,N,C'-(3,4,5-(F)$_3$-C$_6$H-2-yl)CH$_2$N=CH(3,4,6-(F)$_3$-C$_6$H-2-yl)}Fe(PMe$_3$)$_2$I (11b).

To a 25 mL round-bottom flask charged with **2b** (0.100 g, 0.186 mmol), $[Cp_2Fe]BF_4$ (0.061g, 0.186 mmol), and excess lithium iodide (0.075 g, 0.560 mmol), was transferred 8 mL of THF at -78 °C. The reaction was allowed to warm to 23 °C and stir for 16 h. Solvent was removed from the olive green solution, and the crude

brown solid was filtered and washed (3 x 5 mL) with toluene. The brown solid was then filtered and washed (3 x 5 mL) with pentane leaving a green/brown paramagnetic **11b** (0.050 g, 0.079 mmol) in 42% yield. ^{1}H NMR (C_6D_6, 400 MHz): 19.95 (2 H), 12.35 (1 H), -10.25 (1 H), -13.49 (1 H), -16.62 (18 H). Anal. Calcd for $C_{20}H_{23}F_6NP_2IFe$: C, 37.76; H, 3.64; N, 2.20. Found: C, 37.62; H, 3.70, N, 2.26. μ_{eff} (296 K) = 1.9 μ_B, 2.0 μ_B.

15. *trans*-{*mer*-κ-C,N,C'-(3,4,5-(F)$_3$-C$_6$H-2-yl)CH$_2$N=CH(3,4,6-(F)$_3$-C$_6$H-2-yl)}Fe(PMe$_3$)$_2$Cl (12b).

To a 25 mL round-bottom flask charged with **2b** (0.085 g, 0.158 mmol) and triphenylmethyl chloride (0.066 g, 0.237 mmol), was transferred 8 mL benzene at -78 °C. The reaction was allowed to warm to 23 °C and stir for 16 h. The solvent was removed *in vacuo* and the crude red solid was filtered and washed (3 x 5 mL) with hexane leaving microcrystalline red **12b** (0.060g, 0.110 mmol) in 70% yield. Single crystals were grown from a concentrated solution in Et_2O at -40 °C. ^{1}H NMR (C_6D_6, 400 MHz): 12.45 (1 H), -4.61 (2 H), -9.86 (2 H), -16.52 (18 H). μ_{eff} (296 K) = 1.9 μ_B, 2.0 μ_B.

16. *trans*-{κ-C,N-(3,5-(CF$_3$)$_2$-C$_6$H$_3$)CH$_2$N=CH(3,4,6-(F)$_3$-C$_6$H-2-yl)}Fe(PMe$_3$)$_3$Cl (12a).

To a 25 mL round-bottom flask charged with **2b** precursor (0.100 g, 0.161 mmol) and triphenylmethyl chloride (0.068 g, 0.242 mmol), was transferred 10 mL benzene at -78 °C. The reaction was allowed to warm to 23 °C and stir for 16 h. The solvent was removed *in vacuo* and the crude red solid was filtered and washed (3 x 5 mL) with hexanes leaving microcrystalline red **12a** (0.068 g, 0.108 mmol) in 67%

yield. ^{1}H NMR (C_6D_6, 400 MHz): 33.75 (2 H), 12.20 (1 H), 10.77 (2 H), -1.86 (1 H), -17.36 (18 H). Anal. Calcd for $C_{22}H_{24}F_9P_2ClNFe$: C, 42.17; H, 3.86; N, 2.24. Found: C, 42.33; H, 4.05, N, 1.98μ_{eff} (296 K) = 2.1 μ_B, 2.1 μ_B.

17. FeP_4(-CCPh)$_2$.

To a 10 mL round-bottom flask charged with 0.100 g of *cis*-Fe(PMe_3)$_4$$Me_2$ (0.256 mmol) was vacuum transferred ~ 5 mL of benzene at 0 °C. Two equivalents of phenylacetylene (0.512 mmol) were syringed into the round bottom under argon. The solution was warmed to 23 °C and allowed to stir for 10 h, after which formation of yellow solid was observed. Upon filtration and washing (3 X 5 mL) in benzene, removal of all volatiles, *in vacuo,* allowed for isolation of FeP_4(-CCPh) (0.090 g, 0.160 mmol) in 63 % yield. ^{1}H NMR (C_6D_6): 6.96 (4, Ph_m, t, 7), 7.41 (6 H, $Ph_{o,\,p}$, m), 1.42 (36 H, PMe_3) ^{31}P NMR (C_6D_6) : 20.73

Single crystal X-ray diffraction studies. Upon isolation, the crystals were covered in polyisobutenes and placed under a 173 K N_2 stream on the goniometer head of a Siemens P4 SMART CCD area detector (graphite-monochromated MoKα radiation, λ = 0.71073 Å). The structures were solved by direct methods (SHELXS). All non-hydrogen atoms were refined anisotropically unless stated, and hydrogen atoms were treated as idealized contributions (Riding model).

17. *trans*-{κ-C,N,C'-(2,4,5-trifluorophen-2-yl)CH=N-CH_2(3,4,5-trifluorophen-2-yl)}Fe(PMe_3)$_2$ (N_2) (2b). A red block (0.25 x 0.20 x 0.15 mm) was obtained from benzene. A total of 9,138 reflections were collected with 5,119 determined to be symmetry independent (R_{int} = 0.0298), and 4,493 were greater than

2σ(I). A semi-empirical absorption correction from equivalents was applied, and the refinement utilized $w^{-1} = \sigma^2(F_o^2) + (0.0437p)^2 + 0.1193p$, where $p = ((F_o^2 + 2F_c^2)/3)$.

18. *trans*-{*mer*-κ-C,N,C'-(3,4,5-(F)$_3$-C$_6$H-2-yl)CH$_2$N=CH(3,4,6-(F)$_3$-C$_6$H-2-yl)}Fe(PMe$_3$)$_2$Cl (X). A red block (0.40 x 0.15 x 0.10 mm) was obtained from diethyl ether. A total of 23,077 reflections were collected with 6,176 determined to be symmetry independent (R_{int} = 0.0321), and 4,841 were greater than 2σ(I). A semi-empirical absorption correction from equivalents was applied, and the refinement utilized $w^{-1} = \sigma^2(F_o^2) + (0.0483p)^2 + 1.1000p$, where $p = ((F_o^2 + 2F_c^2)/3)$.

Computations. Calculations were carried out at the M06[115]/6-311+G(d)[116] level of theory. An ultrafine grid was used for integration in all calculations. Simulations were performed with the Gaussian 09 program.[117] All structures were optimized with restraint of neither symmetry nor geometry. Open-shell complexes were modeled within the framework of the unrestricted Kohn-Sham formalism; spin contamination was deemed to be minimal via calculation of the $<\hat{S}^2>_{UDFT}$ expectation value. Systems were judged to be minima via calculation of the energy Hessian. Quoted energetics are free energies (kcal/mol), unless specified otherwise, and were determined with unscaled vibrational frequencies assuming standard temperature and pressure.

REFERNCES

(1) Bartholomew, E. R.; Volpe, E. C.; Wolczanski, P. T.; Lobkovsky, E. B.; Cundari, T. R. *J. Am. Chem. Soc.* **2013**, *135*, 3511.

(2) Blanksby, S. J.; Ellison, G. B. *Acc. Chem. Res.* **2003**, *36*, 255.

(3) Greenwood, N. N. E., A. *Chemistry of the Elements*; 2nd ed.; Elsevier Science: New York, 1997.

(4) Ertl, G. *Z. Anorg. Allg. Chem.* **2012**, *638*, 487.

(5) Ertl, G. *Angew. Chem., Int. Ed.* **2008**, *47*, 3524.

(6) Erisman, J. W.; Sutton, M. A.; Galloway, J.; Klimont, Z.; Winiwarter, W. *Nat. Geosci.* **2008**, *1*, 636.

(7) Weissman, K. *Chem. World* **2009**, *6*, 46.

(8) Modak, J. M. *Resonance* **2002**, *7*, 69.

(9) Schlogl, R. *Angew Chem Int Ed Engl* **2003**, *42*, 2004.

(10) Wiig, J. A.; Hu, Y.; Lee, C. C.; Ribbe, M. W. *Science (Washington, DC, U. S.)* **2012**, *337*, 1672.

(11) Tuczek, F. *Nachr. Chem.* **2006**, *54*, 1190.

(12) Rubio, L. M.; Ludden, P. W. *J. Bacteriol.* **2005**, *187*, 405.

(13) Rees, D. C.; Tezcan, F. A.; Haynes, C. A.; Walton, M. Y.; Andrade, S.; Einsle, O.; Howard, J. B. *Philos. Trans. R. Soc. London, Ser. A* **2005**, *363*, 971.

(14) Newton, W. E.; John Wiley & Sons, Inc.: 2006; Vol. 17, p 290.

(15) Hu, Y.; Ribbe, M. W. *Microbiol. Mol. Biol. Rev.* **2011**, *75*, 664.

(16) Hu, Y.; Ribbe, M. W. *Acc. Chem. Res.* **2010**, *43*, 475.

(17) Hu, Y.; Lee, C. C.; Ribbe, M. W. *Dalton Trans.* **2012**, *41*, 1118.

(18) Howard, J. B.; Rees, D. C. *Proc. Natl. Acad. Sci. U. S. A.* **2006**, *103*, 17088.

(19) Hoffman, B. M.; Dean, D. R.; Seefeldt, L. C. *Acc. Chem. Res.* **2009**, *42*, 609.

(20) Einsle, O.; Tezcan, F. A.; Andrade, S. L. A.; Schmid, B.; Yoshida, M.; Howard, J. B.; Rees, D. C. *Science (Washington, DC, U. S.)* **2002**, *297*, 1696.

(21) Eady, R. R. *Chem. Rev. (Washington, D. C.)* **1996**, *96*, 3013.

(22) Berg, J. M. T., John L.; Stryer, Lubert *Biochemistry*; 6th ed.; W. H. Freeman: New York, 2007.

(23) Alberty, R. A. *Biophys. Chem.* **2005**, *114*, 115.

(24) Alberty, R. A. *J. Biol. Chem.* **1994**, *269*, 7099.

(25) Ribbe, M.; Gadkari, D.; Meyers, O. *J. Biol. Chem.* **1997**, *272*, 26627.

(26) Oelze, J. *FEMS Microbiol. Rev.* **2000**, *24*, 321.

(27) Weiss, C. J.; Groves, A. N.; Mock, M. T.; Dougherty, W. G.; Kassel, W. S.; Helm, M. L.; DuBois, D. L.; Bullock, R. M. *Dalton Trans.* **2012**, *41*, 4517.

(28) Taube, H. *Coord. Chem. Rev.* **1978**, *26*, 1.

(29) Sellmann, D.; Hille, A.; Heinemann, F. W.; Moll, M.; Reiher, M.; Hess, B. A.; Bauer, W. *Chem.--Eur. J.* **2004**, *10*, 4214.

(30) Richards, R. L. *Coord. Chem. Rev.* **1996**, *154*, 83.

(31) Leigh, G. J. *Can. J. Chem.* **2005**, *83*, 277.

(32) Leigh, G. J. *J. Organomet. Chem.* **2004**, *689*, 3999.

(33) Korobkov, I.; Gambarotta, S.; Yap, G. P. A. *Angew. Chem., Int. Ed.* **2002**, *41*, 3433.

(34) Crossland, J. L.; Tyler, D. R. *Coord. Chem. Rev.* **2010**, *254*, 1883.

(35) Ballmann, J.; Munha, R. F.; Fryzuk, M. D. *Chem. Commun. (Cambridge, U. K.)* **2010**, *46*, 1013.

(36) Allen, A. D.; Senoff, C. W. *Chem. Commun. (London)* **1965**, 621.

(37) Allen, A. D.; Bottomley, F.; Harris, R. O.; Reinsalu, V. P.; Senoff, C. V. *J. Am. Chem. Soc.* **1967**, *89*, 5595.

(38) Studt, F.; Tuczek, F. *J. Comput. Chem.* **2006**, *27*, 1278.

(39) Shaver, M. P.; Fryzuk, M. D. *Adv. Synth. Catal.* **2003**, *345*, 1061.

(40) Pun, D.; Bradley, C. A.; Lobkovsky, E.; Keresztes, I.; Chirik, P. J. *J. Am. Chem. Soc.* **2008**, *130*, 14046.

(41) Pool, J. A.; Lobkovsky, E.; Chirik, P. J. *Nature (London, U. K.)* **2004**, *427*, 527.

(42) Pool, J. A.; Bernskoetter, W. H.; Chirik, P. J. *J. Am. Chem. Soc.* **2004**, *126*, 14326.

(43) Nikiforov, G. B.; Vidyaratne, I.; Gambarotta, S.; Korobkov, I. *Angew. Chem., Int. Ed.* **2009**, *48*, 7415.

(44) Leigh, G. J. *Acc. Chem. Res.* **1992**, *25*, 177.

(45) Laplaza, C. E.; Johnson, M. J. A.; Peters, J.; Odom, A. L.; Kim, E.; Cummins, C. C.; George, G. N.; Pickering, I. J. *J. Am. Chem. Soc.* **1996**, *118*, 8623.

(46) Hanna, T. E.; Keresztes, I.; Lobkovsky, E.; Chirik, P. J. *Inorg. Chem.* **2007**, *46*, 1675.

(47) Gambarotta, S.; Scott, J. *Angew. Chem., Int. Ed.* **2004**, *43*, 5298.

(48) Fryzuk, M. D.; Johnson, S. A. *Coord. Chem. Rev.* **2000**, *200-202*, 379.

(49) Fryzuk, M. D. *Acc. Chem. Res.* **2009**, *42*, 127.

(50) Figueroa, J. S.; Piro, N. A.; Clough, C. R.; Cummins, C. C. *J. Am. Chem. Soc.* **2006**, *128*, 940.

(51) Chirik, P. J. *Dalton Trans.* **2007**, 16.

(52) Bernskoetter, W. H.; Pool, J. A.; Lobkovsky, E.; Chirik, P. J. *J. Am. Chem. Soc.* **2005**, *127*, 7901.

(53) Bernskoetter, W. H.; Olmos, A. V.; Lobkovsky, E.; Chirik, P. J. *Organometallics* **2006**, *25*, 1021.

(54) Bernskoetter, W. H.; Lobkovsky, E.; Chirik, P. J. *J. Am. Chem. Soc.* **2005**, *127*, 14051.

(55) Bazhenova, T. A.; Shilov, A. E. *Coord. Chem. Rev.* **1995**, *144*, 69.

(56) Schrock, R. R. *Angew. Chem., Int. Ed.* **2008**, *47*, 5512.

(57) Schrock, R. R. *Acc. Chem. Res.* **2005**, *38*, 955.

(58) Hidai, M. *Coord. Chem. Rev.* **1999**, *185-186*, 99.

(59) Chatt, J.; Dilworth, J. R.; Richards, R. L. *Chem. Rev.* **1978**, *78*, 589.

(60) *Activation of Small Molecules*; Wiley-VCH: Weinheim, Germany, 2006.

(61) Yandulov, D. V.; Schrock, R. R. *Science (Washington, DC, U. S.)* **2003**, *301*, 76.

(62) Crossland, J. L.; Young, D. M.; Zakharov, L. N.; Tyler, D. R. *Dalton Trans.* **2009**, 9253.

(63) Crossland, J. L.; Zakharov, L. N.; Tyler, D. R. *Inorg. Chem.* **2007**, *46*, 10476.

(64) Danopoulos, A. A.; Wright, J. A.; Motherwell, W. B. *Chem. Commun. (Cambridge, U. K.)* **2005**, 784.

(65) Gilbertson, J. D.; Szymczak, N. K.; Crossland, J. L.; Miller, W. K.; Lyon, D. K.; Foxman, B. M.; Davis, J.; Tyler, D. R. *Inorg. Chem.* **2007**, *46*, 1205.

(66) Gilbertson, J. D.; Szymczak, N. K.; Tyler, D. R. *J. Am. Chem. Soc.* **2005**, *127*, 10184.

(67) Hazari, N. *Chem. Soc. Rev.* **2010**, *39*, 4044.

(68) Hendrich, M. P.; Gunderson, W.; Behan, R. K.; Green, M. T.; Mehn, M. P.; Betley, T. A.; Lu, C. C.; Peters, J. C. *Proc. Natl. Acad. Sci. U. S. A.* **2006**, *103*, 17107.

(69) Holland, P. L. *Can. J. Chem.* **2005**, *83*, 296.

(70) Moret, M.-E.; Peters, J. C. *Angew. Chem., Int. Ed.* **2011**, *50*, 2063.

(71) Rodriguez, M. M.; Bill, E.; Brennessel, W. W.; Holland, P. L. *Science (Washington, DC, U. S.)* **2011**, *334*, 780.

(72) Saouma, C. T.; Kinney, R. A.; Hoffman, B. M.; Peters, J. C. *Angew. Chem., Int. Ed.* **2011**, *50*, 3446.

(73) Saouma, C. T.; Muller, P.; Peters, J. C. *J. Am. Chem. Soc.* **2009**, *131*, 10358.

(74) Smith, J. M.; Sadique, A. R.; Cundari, T. R.; Rodgers, K. R.; Lukat-Rodgers, G.; Lachicotte, R. J.; Flaschenriem, C. J.; Vela, J.; Holland, P. L. *J. Am. Chem. Soc.* **2006**, *128*, 756.

(75) Takaoka, A.; Mankad, N. P.; Peters, J. C. *J. Am. Chem. Soc.* **2011**, *133*, 8440.

(76) Whited, M. T.; Mankad, N. P.; Lee, Y.; Oblad, P. F.; Peters, J. C. *Inorg. Chem.* **2009**, *48*, 2507.

(77) Yuki, M.; Miyake, Y.; Nishibayashi, Y. *Organometallics* **2012**, *31*, 2953.

(78) Crossland, J. L.; Balesdent, C. G.; Tyler, D. R. *Inorg. Chem.* **2012**, *51*, 439.

(79) Crossland, J. L.; Balesdent, C. G.; Tyler, D. R. *Dalton Trans.* **2009**, 4420.

(80) Giannoccaro, P.; Rossi, M.; Sacco, A. *Coord. Chem. Rev.* **1972**, *8*, 77.

(81) Aresta, M.; Giannoccaro, P.; Rossi, M.; Sacco, A. *Inorg. Chim. Acta* **1971**, *5*, 203.

(82) Volpe, E. C.; Wolczanski, P. T.; Lobkovsky, E. B. *Organometallics* **2010**, *29*, 364.

(83) Spatzal, T.; Aksoyoglu, M.; Zhang, L.; Andrade, S. L. A.; Schleicher, E.; Weber, S.; Rees, D. C.; Einsle, O. *Science (Washington, DC, U. S.)* **2011**, *334*, 940.

(84) Lancaster, K. M.; Roemelt, M.; Ettenhuber, P.; Hu, Y.; Ribbe, M. W.; Neese, F.; Bergmann, U.; DeBeer, S. *Science (Washington, DC, U. S.)* **2011**, *334*, 974.

(85) Karsch, H. H. *Chem. Ber*. **1977**, *110*, 2699.

(86) Moonen, K.; Stevens, C. V. *Synthesis* **2005**, 3603.

(87) Liu, L.; Zhang, S.; Fu, X.; Yan, C.-H. *Chem. Commun. (Cambridge, U. K.)* **2011**, *47*, 10148.

(88) Figgis, B. N. H., M. A. *Ligand Field Theory and Its Applications*; Wiley-VCH: New York, 2000.

(89) Carlin, R. L. *Magnetochemistry*; Springer-Verlag: New York, 1986.

(90) Kuiper, D. S.; Douthwaite, R. E.; Mayol, A.-R.; Wolczanski, P. T.; Lobkovsky, E. B.; Cundari, T. R.; Lam, O. P.; Meyer, K. *Inorg. Chem.* **2008**, *47*, 7139.

(91) Sydora, O. L.; Wolczanski, P. T.; Lobkovsky, E. B.; Buda, C.; Cundari, T. R. *Inorg. Chem.* **2005**, *44*, 2606.

(92) Zhang, G.; Musgrave, C. B. *J. Phys. Chem. A* **2007**, *111*, 1554.

(93) Poli, R.; Cacelli, I. *Eur. J. Inorg. Chem.* **2005**, 2324.

(94) Franke, O.; Wiesler, B. E.; Lehnert, N.; Peters, G.; Burger, P.; Tuczek, F. *Z. Anorg. Allg. Chem.* **2006**, *632*, 1247.

(95) Franke, O.; Wiesler, B. E.; Lehnert, N.; Naether, C.; Ksenofontov, V.; Neuhausen, J.; Tuczek, F. *Inorg. Chem.* **2002**, *41*, 3491.

(96) Rayner-Canham, G. O., Tina *Descriptive Inorganic Chemistry*; W. H. Freeman and Company: New York, New York, 2010.

(97) Field, L. D.; Hazari, N.; Li, H. L.; Luck, I. J. *Magn. Reson. Chem.* **2003**, *41*, 709.

(98) Ermakov, A. N.; Borisova, L. V. *Zh. Neorg. Khim.* **1986**, *31*, 2814.

(99) Murray, K. S. *Coord. Chem. Rev.* **1974**, *12*, 1.

(100) Winkler, J. R.; Gray, H. B. *Struct. Bonding (Berlin, Ger.)* **2012**, *142*, 17.

(101) McMullin, C. L.; Pierpont, A. W.; Cundari, T. R. *Polyhedron* **2013**, *52*, 945.

(102) Pierpont, A.; Cundari, T.; American Chemical Society: 2009, p INOR.

(103) Figg, T. M.; Cundari, T. R. *Organometallics* **2012**, *31*, 4998.

(104) Harrold, N. D.; Waterman, R.; Hillhouse, G. L.; Cundari, T. R. *J. Am. Chem. Soc.* **2009**, *131*, 12872.

(105) Yonke, B. L.; Reeds, J. P.; Zavalij, P. Y.; Sita, L. R. *Angew. Chem., Int. Ed.* **2011**, *50*, 12342.

(106) Fedorova, G. R. *Tr. Proekt. Nauch.-Issled. Inst. Gipronikel (Gos. Inst. Proekt. Predpr. Nikelevoi Prom.)* **1968**, *No. 38*, 140.

(107) Haines, L. M.; Stiddard, M. H. B. *Advan. Inorg. Chem. Radiochem.* **1969**, *12*, 53.

(108) Hartwig, J. F. *Organotransition Metal Chemistry*; University Science Books: Mill Valley, California, 2010.

(109) Turner, J. J.; Elsevier: 1977, p 353.

(110) Murad, S.; Gupta, S. *Fluid Phase Equilib.* **2001**, *187-188*, 29.

(111) Pierotti, R. A. *J. Phys. Chem.* **1963**, *67*, 1840.

(112) Szymczak, N. K.; Tyler, D. R. *Coord. Chem. Rev.* **2008**, *252*, 212.

(113) Saouma, C. T.; Peters, J. C. *Coord. Chem. Rev.* **2011**, *255*, 920.

(114) Russell, S. K., Cornell, 2011.

(115) Zhao, Y.; Truhlar, D. G. *Acc. Chem. Res.* **2008**, *41*, 157.

(116) Krishnan, R.; Binkley, J. S.; Seeger, R.; Pople, J. A. *J. Chem. Phys.* **1980**, *72*, 650.

(117) Frisch, M. J. T., G. W.; Schlegel, H. B.; Scuseria, G. E.; Robb,M. A.; Cheeseman, J. R.; Scalmani, G.; Barone, V.; Mennucci, B.; Petersson, G. A.; Nakatsuji, H.; Caricato, M.; Li, X.; Hratchian, H. P.; Izmaylov, A. F.; Bloino, J.; Zheng, G.; Sonnenberg, J. L.; Hada, M.; Ehara, M.; Toyota, K.; Fukuda, R.; Hasegawa, J.; Ishida, M.; Nakajima, T.; Honda, Y.; Kitao, O.; Nakai, H.; Vreven, T.; Montgomery, Jr., J. A.; Peralta, J. E.; Ogliaro, F.; Bearpark, M.; Heyd, J. J.; Brothers, E.; Kudin, K. N.; Staroverov, V. N.; Kobayashi, R.; Normand, J.; Raghavachari, K.; Rendell, A.; Burant, J. C.; Iyengar, S. S.; Tomasi, J.; Cossi, M.; Rega, N.; Millam, J. M.; Klene, M.; Knox, J. E.; Cross, J. B.; Bakken, V.; Adamo, C.; Jaramillo, J.; Gomperts, R.; Stratmann, R. E.; Yazyev, O.; Austin, A. J.; Cammi, R.; Pomelli, C.; Ochterski, J.W.; Martin, R. L.; Morokuma, K.; Zakrzewski, V. G.; Voth, G. A.; Salvador, P.; Dannenberg, J. J.; Dapprich, S.; Daniels, A. D.; Farkas, Ö.; Foresman, J.

B.; Ortiz, J. V.; Cioslowski, J.; Fox, D. J. *Gaussian 09, Revision A.1*; Gaussian, Inc: Wallingford, CT, 2009.

(118) Heinekey, D. M.; Oldham, W. J., Jr. *Chem. Rev.* **1993**, *93*, 913.

(119) Kubas, G. J. *Metal-Dihydrogen and Sigma-Bond Complexes: Struture, Theory, and Reactivity*; Kluwer Academic: New York, 2001.

(120) Balch, A. L.; Olmstead, M. M.; Safari, N.; St, C. T. N. *Inorg. Chem.* **1994**, *33*, 2815.

(121) Doppelt, P. *Inorg. Chem.* **1984**, *23*, 4009.

(122) Goedken, V. L.; Peng, S.-M.; Park, Y.-A. *J. Amer. Chem. Soc.* **1974**, *96*, 284.

(123) Kadish, K. M.; Tabard, A.; Van, C. E.; Aukauloo, A. M.; Richard, P.; Guilard, R. *Inorg. Chem.* **1998**, *37*, 6168.

(124) Evans, D. F. *J. Chem. Soc.* **1959**, 2003.

(125) Leal, A. d. l. J.; Tenorio, M. J.; Puerta, M. C.; Valerga, P. *Organometallics* **1995**, *14*, 3839.

(126) Desrosiers, P. J.; Cai, L.; Lin, Z.; Richards, R.; Halpern, J. *J. Am. Chem. Soc.* **1991**, *113*, 4173.

(127) Bautista, M. T.; Earl, K. A.; Maltby, P. A.; Morris, R. H.; Schweitzer, C. T.; Sella, A. *J. Am. Chem. Soc.* **1988**, *110*, 7031.

(128) Earl, K. A.; Jia, G.; Maltby, P. A.; Morris, R. H. *J. Am. Chem. Soc.* **1991**, *113*, 3027.

CHAPTER 4

SYNTHESIS AND REACTIVITY OF BIS(2-PYRIDYLCARBONYL)AMINE WITH IRON

I. Introduction

Hydrocarbon activation is a significant area of academic research and is practically significant from the perspective of energy production and storage. For example, methane from natural gas is available in large amounts, but gaseous methane cannot be transported easily or economically. Conversion of methane into a transportable liquid, such as methanol, would make inaccessible methane a practical energy source.[1] Unfortunately, selectivity to generate only a desired product such as methanol, is very difficult to achieve. Low reactivity of unactivated hydrocarbons means harsh reaction conditions are generally required, and when RH is methane, over-oxidation occurs to produce CO_2.[1]

$$1/2\ O_2 + RH \longrightarrow ROH \qquad (4.1)$$

Biologically, there are many enzymes responsible for catalyzing difficult oxidations like those in Eq 4.1.[1] For methane, this conversion is catalyzed by methane monooxygenase (MMO),[2-5] which contains a di-iron oxo cluster active site. Cytochrome P450,[6] with a heme iron at its active site, commonly performs similar oxidations (Figure 4.1).

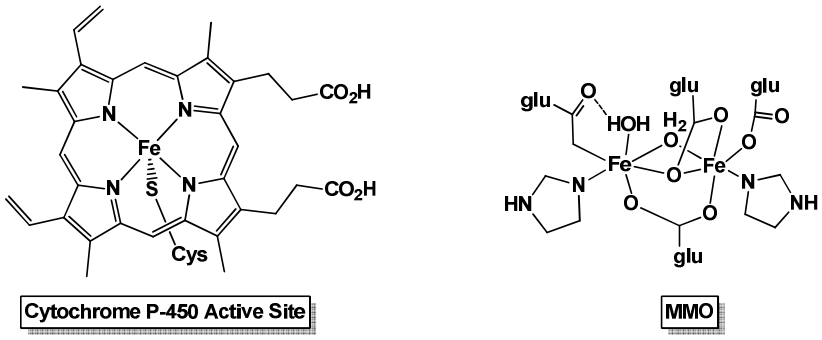

Figure 4.1. Cytochrome P-450 and MMO

These biological oxidations work by a process known as the rebound mechanism (Scheme. 4.1).[7,8] H-atom abstraction from RH occurs via a heteroatom, X, to generate a radical (R·) that also attacks X to generate RXH. If non-biological autoxidations could be designed to proceed by an analogous rebound process, potential for greater hydrocarbon oxidation selectivity would prove useful. Goals in this chapter focused on designing a system which is capable of activating hydrocarbons, transforming RH and X_2 to RX and HX (Scheme 4.1).

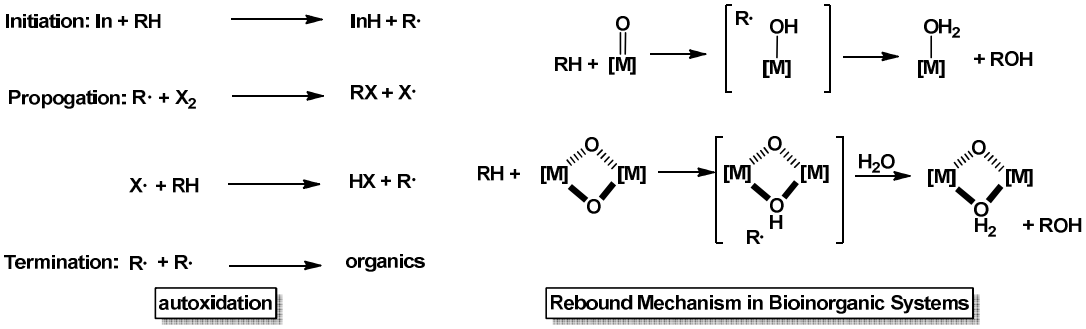

Scheme 4.1. Processes that activate RH, either with bioinorganic systems or via autoxidation.

Chapter 2 discussed investigations of metal complexes containing a tridendate N-donor ligand, **smif**. One derivative of the **smif** ligand, bis(2-pyridylcarbonyl)amine, **Hbpca**, contains two carbonyl groups that have potential for advantageous hydrogen-bonding once the desired H-atom abstraction occurs. Scheme 4.2 presents two cycles with critical activations that illustrate how the system could work using the **bpca** (bis(2-pyridylcarbonyl)aminate) ligand. In the first cycle of Scheme 4.2, $[M]^n$ oxidatively adds X_2 to generate a $[M]^{n+2}$ intermediate, capable of doing an H-atom abstraction, which leaves the radical, R·, to abstract X from M-X to lose RX. Subsequent loss of HX regenerates the $[M]^n$ starting material.

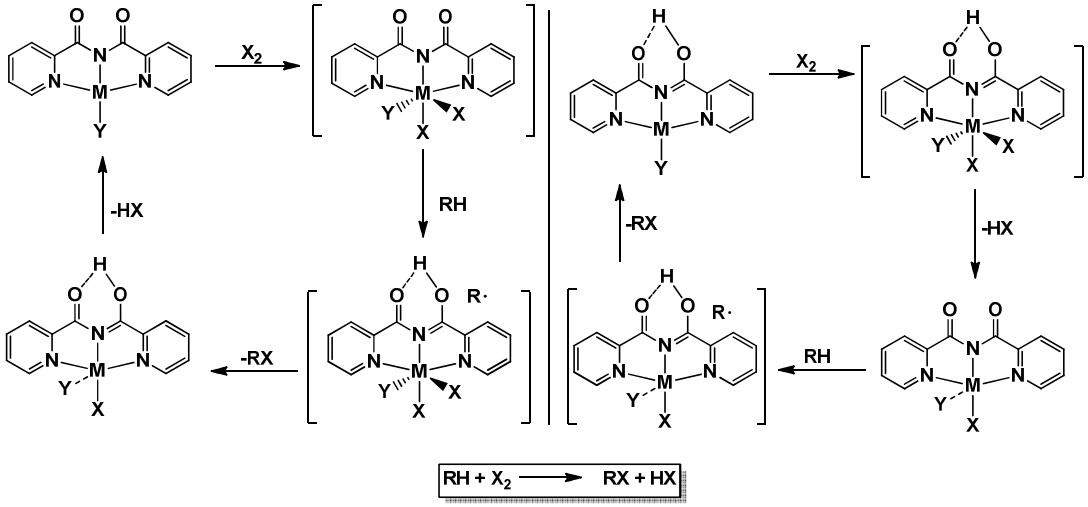

Scheme 4.2. Proposed transformations with M(bpca) systems.

Another way to consider the cycle is to begin with an H-bonded species (Scheme 4.2, cycle on right). Addition of X_2 generates a transient species which subsequently loses HX, and upon reaction with RH, the H-bonded species is regenerated as RX is lost. As

long as the radical, R·, reacts faster with MX than it terminates, these cycles can continue to be productive.

Ideally, various X_2 species can be used in these cycles, such as dihalogens and organic peroxides. Ultimately, success can be measured by comparison to the corresponding autoxidation products, initiated via standard procedures. Significant deviations from the autoxidation product distribution would confirm the success of the proposed systems.

The bpca ligand has been utilized with various 1st row transition metals in aqueous solutions. Metal (II) complexes of Mn,[9] Fe,[10] Co,[11,12] Ni,[13] Cu,[14] and Zn[14] coordinated with two bis(2-pyridylcarbonyl)aminate (bpca) ligands have been synthesized (Fig 4.2), and M(III) species have been prepared for Cr,[12,15] Fe,[10] and Co.[12]

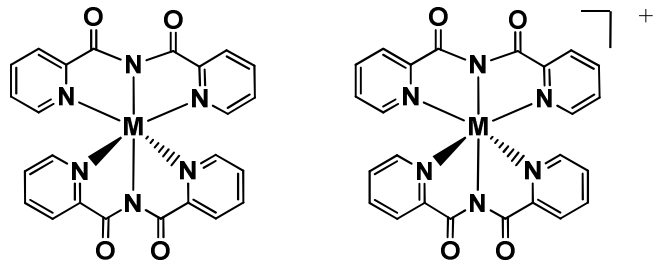

Figure 4.2. M(II) and M(III) bpca complexes.

Initial goals for this project included synthesizing an iron (II) species soluble in organic solvents, coordinating only one bpca ligand, which could be tested for the catalysis of RH activation.

II. Results and Discussion

A. Ligand syntheses

Bis(2-pyridylcarbonyl)amine, **Hbpca**, was prepared following literature procedures.[13] No direct synthesis for **Hbpca** is reported, but free ligand can be isolated by first generating $[Cu(bpca)(H_2O)_2][Cu(bpca)(SO_4)(H_2O)]H_2O$,[13] **$Cu_2(bpca)_2$,** followed by a quench to extract the ligand from copper.

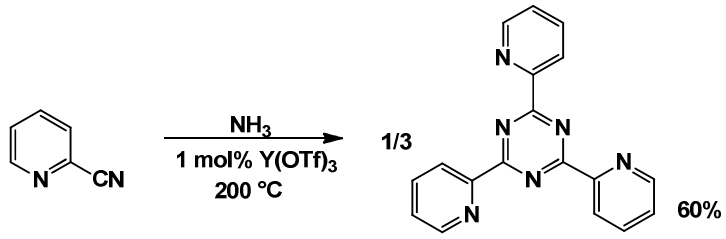

(4.2)

Trimerization of cyanopyridine in the presence of ammonia and catalytic $Y(OTf)_3$ formed 1,3,5-tris(2-pyridyl)triazine,[16] and was subsequently treated with 2 equiv of copper sulfate pentahydrate in water (Eq. 4.2).[13] The resulting suspension was refluxed to form a solution from which blue microcrystals of **$Cu_2(bpca)_2$** were obtained.

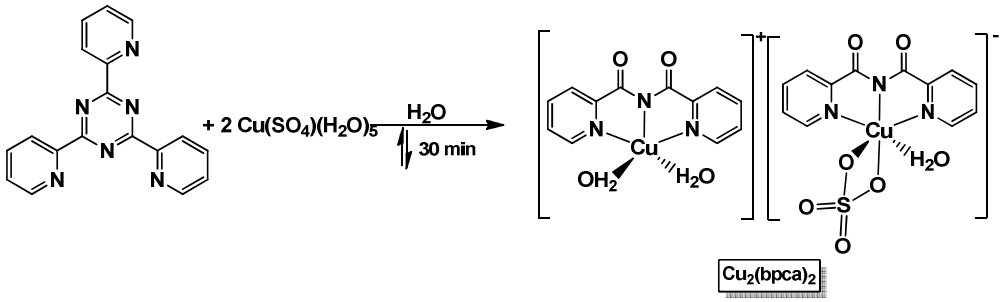

(4.3)

An excess of Na_2H_2EDTA or zinc dust was then treated with the isolated copper (II) complex, and vigorously stirred for several hours in a water/chloroform mixture to

remove the ligand from copper. The resulting light green organic layer was dried over sodium sulfate, and evaporated to dryness to leave slightly colored solids. Upon recrystallization from a hot 1,4-dioxane solution, colorless prisms of **Hbpca** were obtained.

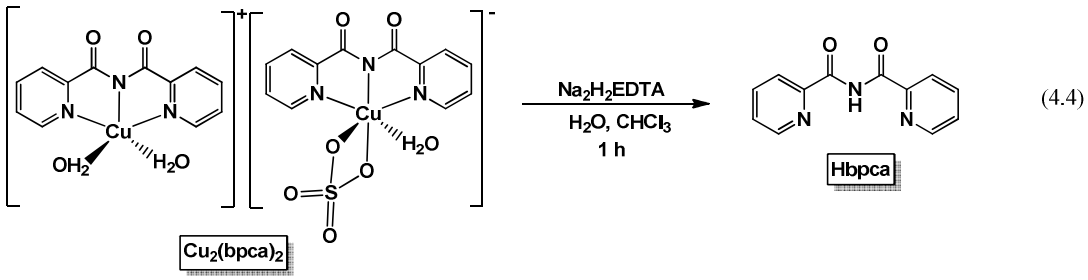

(4.4)

Methyl and *tert*-butyl substituted **bpca** ligands were also targeted with increased solubility in mind. To generate the desired R-substituted (R = Me, ^{t}Bu) bpca ligands, the appropriately substituted 1,3,5-tris(2-pyridyl)triazine was needed. Since the methyl- and *tert*-butyl-substituted triazines were not commercially available, syntheses analogous to those used to prepare the unsubstituted 1,3,5-tris(2-pyridyl)triazine (Eq 4.2) were attempted.[16] Upon treatment of 4-methylpyridine or 4-*tert*-butylpyridine with hydrogen peroxide, the corresponding N-oxide was successfully generated in high yields. Addition of trimethylsilylcyanide, and N,N-dimethyl carbamoyl chloride, to pyridine N-oxide, resulted in formation of the substituted cyanopyridine (Scheme 4.3). Unfortunately, these methyl and *tert*-butyl-substituted cyanopyridines did not undergo the necessary trimerization to form the triazine needed for complexation with copper.

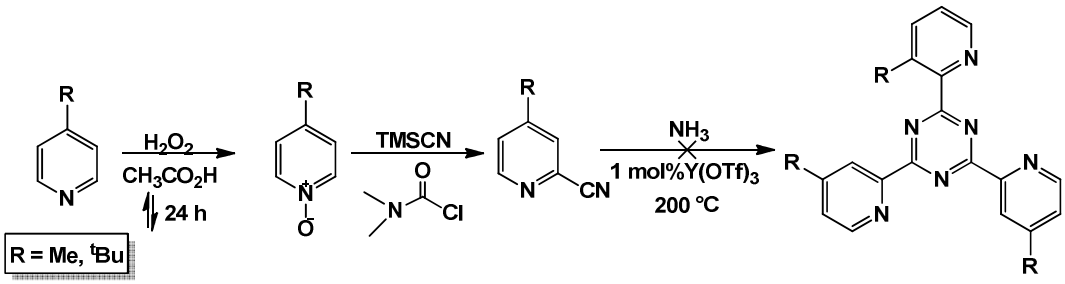

Scheme 4.3. Attempted syntheses of methyl and ^{t}butyl substituted Hbpca derivatives.[17]

B. Attempts Toward M(bpca)$_2$ Complexes in Organic Solvents

Although many metal complexes containing the bpca ligand have been reported,[10-13,15,18-20] they have been generated in aqueous solutions and in many instances form multi-nuclear chains through binding to the pyridines and amide, as well as to the oxygen. In order to promote hydrocarbon (RH) activation, organic solvent-soluble systems were sought . The use of M{N(TMS)$_2$}$_2$THF (M = Cr, Fe, Co) as an internal base had been successful in the synthesis of (smif)$_2$M complexes as discussed in Chapter 2,[21] therefore a logical first attempt toward M(bpca)$_2$ involved treatment of **Hbpca** with Fe{N(TMS)$_2$}$_2$THF (Scheme 4.4). Unfortunately, no reaction was observed between **Hbpca** and Fe{N(TMS)$_2$}$_2$THF, likely due to the insolubility of the ligand which prevented reactivity. The reaction was also run in other organic solvents, such as benzene, chloroform, methylene chloride and acetonitrile, with similarly dissatisfying results. Solubility in organic solvents proved very limited and likely prohibited reactivity of any sort.

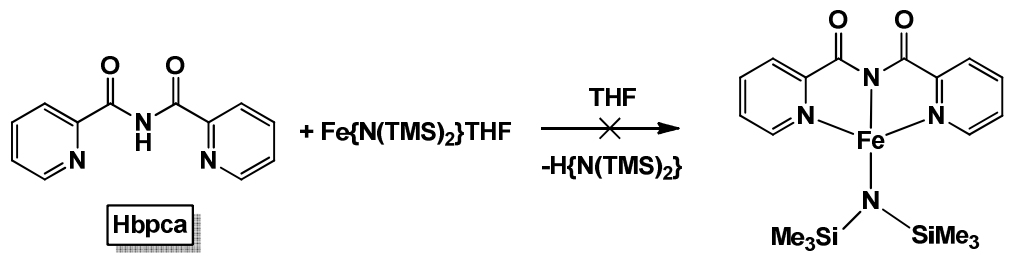

Scheme 4.4. Initial attempts toward (bpca)FeN(TMS)$_2$.

In an effort to make the ligand more soluble in organic solvents, **Hbpca** derivatives were designed with methyl or *tert*-butyl groups on the pyridines (Scheme 4.3). Increased solubility of these new ligands may be the key toward observing desired reactivity, however generation of these derivatives has not proven successful thus far.

III. Conclusions

The ligand, bis(2-pyridylcarbonyl)amine (**Hbpca**), was successfully prepared according to literature procedures, however limited solubility inhibited reactivity to generate the desired bpca-coordinated iron (II) complexes. Attempts to enhance solubility by incorporating 4-*tert*-butyl and 4-methyl-substituted pyridines into the ligand have been unsuccessful thus far. It seems unlikely that the *tert*-butyl and methyl substitutions introduce any consequential steric interference which would inhibit the crucial trimerization reaction from occurring. In fact, there are reports of preparation of the 4-methyl-substituted **bpca** ligand with NaH instead of ammonia.[22] This route for the generation of appropriately substituted triazines could be the key towards successful preparation of soluble ligands.

IV. Experimental

A. General Considerations

For metal complexes, manipulations were performed using either glovebox or high-vacuum techniques. Ligand syntheses were performed under argon using Schlenk techniques. Hydrocarbon and ethereal solvents were dried over and vacuum transferred from sodium benzophenone ketyl (with 3-4 mL of tetraglyme/L added to hydrocarbons). Benzene-d_6 and toluene-d_8 were sequentially dried over sodium and stored over sodium. THF-d_8 was dried over sodium benzophenone keyl. Acetonitrile-d_3 was dried over CaH_2 and stored over 4 Å molecular sieves. Ammonia was dried over sodium metal at -78 °C and transferred under vacuum to the reaction vessel. The iron starting material, $Fe\{N(TMS)_2\}_2THF$,[23,24] was prepared according to literature procedures. Trimethylsilylcyanide was commercially available (Aldrich) and used immediately; NEt_3 and MeCN (Aldrich) were dried and stored over 4 Å molecular sieves; all other reagents were purchased and used as received. All glassware was oven-dried.

^1H NMR spectra were obtained using Mercury-300, Inova-400, and Inova-500 spectrometers, and chemical shifts are reported relative to benzene-d_6 (^1H δ 7.16; $^{13}C\{1H\}$ δ 128.39), and chloroform-d (^1H δ 7.26; $^{13}C\{1H\}$ δ 77.16).

B. Procedures

1. 4 -*R-pyridine-N-oxide (R = Me, ^{t}Bu)*

A stirred mixture of 4-R-pyridine (0.1 mol), glacial acetic acid (100 mL) and H_2O_2 (3% solution, 20 mL) under argon was heated to 80 °C for 3 h. After the initial 3 h, another 20 mL of 3% H_2O_2 was added, and the reaction continued at 80°C for a

final 3 h. The yellow solution was concentrated *in vacuo* and the residue neutralized with aqueous NaOH. Extraction with CH_2Cl_2 followed by drying the organic extract over $MgSO_4$ and removal of the solvent afforded a crude material which was purified by column chromatography (alumina, CH_2Cl_2) to give pure 4-*R*-butyl-pyridine-*N*-oxide as a white microcrystalline solid in 94% yield. R = ^{t}Bu; ^{1}H NMR ($CDCl_3$, 300 MHz, δ ppm): 8.36 (d, J = 7.3, 2H); 7.20 (d, J = 7.3, 2H); 1.34 (s, 9H, ^{t}Bu). R = Me, 90% yield; ^{1}H NMR ($CDCl_3$, 300 MHz, δ ppm): 8.10 (d, J = 6.3, 2H), 7.06 (d, J = 6.3, 2H), 1.91 (s, 3H).

2. 2-Cyano-4-R-Pyridine

To a solution of the appropriate pyridine N-oxide (5 mmol) in 10 mL of CH_2Cl_2 was added 0.55 g (5.5 mmol) of trimethylsilylcyanide, and was stirred at 23 °C for 5 minutes. The solution was then treated with 5 mmol of carbomoyl chloride and stirred at 23 °C for 1 day. A solution of 10% aqueous potassium carbonate (10 mL) was added, and stirring was continued for 5-15 minutes. The organic layer was separated, and the aqueous layer was extracted twice with 5 mL of dichloromethane. The combined dichloromethane layers were dried over anhydrous potassium carbonate. The crude products obtained were purified via column chromatography (5:l hexane-dichloromethane and pure dichloromethane). The side products, acyl cyanide and acid anhydride, were contained in the first fractions when present. Cyanopyridines were eluted with dichloromethane. ^{1}H NMR ($CDCl_3$, 300 MHz, δ ppm): R = ^{t}Bu, 60%; 8.62 (dd, J = 5.2, 0.9,1H); 7.72 (dd, J = 2.0, 0.9, 1H); 7.53 (dd, J = 5.3, 2.0, 1H); 1.36 (s, 9H). R = Me, 70%; 8.55 (d, J = 4.9, 1H), 7.51 (s, 1H), 7.32 (d, J = 4.9, 1H), 2.42 (s, 3H).

3. 1,3,5-tris(2-pyridyl)triazine

To a 500 mL reaction bomb was added 2-cyanopyridine (6.027 g, 58.0 mmol), 1.45 mL NH_3 (0.987 g, 58.0 mmol) and $Y(OTf)_3$ (0.031 g, 0.058 mmol). The bomb was heated at 200 °C for 24 hours, and then allowed to cool to room temperature. The ammonia was carefully bled from the mixture and the product was scraped from the bomb. Unreacted 2-cyanopyridine was removed by washing the crude product with ether. Pure 1,3,4-tris(2-pyridyl)triazine was obtained by recrystallization from water/ethanol (1:1) in 60% yield. ^{1}H NMR ($CDCl_3$, 300 MHz, δ ppm): 8.99 (d, J = 4.9, 1H), 8.92 (d, J = 7.8, 1H), 8.01 (t, J = 7.7, 1H), 7.58 (t, J = 4.9, 1H).

4. [bpcaCu]$_2$

To a 50 mL round-bottom flask charged with 1.25 g of 1,3,5-tris(2-pyridyl)triazine (4.0 mmol) was added a suspension of 2.0 g of copper sulfate pentahydrate (8.0 mmol) in 30 mL of water. The suspension was refluxed for 30 min, and from the resulting solution, blue microcrystals of $[Cu(bpca)(H_2O)_2][Cu(bpca)(SO_4)(H_2O)]H_2O_{17}]$ (**[bpcaCu]$_2$**) were obtained (yield 1.4 g, 70%).

5. Bis(2-pyridylcarbonyl)amine, Hbpca

i) Free organic ligand was isolated from **[bpcaCu]$_2$**. The copper (II) complex (1.0 g, 1.3 mmol) and 2.0 g of Na_2H_2EDTA (5.4 mmol) were vigorously stirred for 10 h in a water (80 mL) and chloroform (50 mL) mixture at 23 °C. The light green organic layer was dried over sodium sulfate and evaporated to dryness to give slightly colored solids. Colorless prisms of 3·Hbpca-1,4-dioxane were obtained by

recrystallization of the residue from hot 1,4-dioxane solution. This compound was filtered and dried *in vacuo* to give white powder of **Hbpca** (yield ~30 %).

ii) Free organic ligand was isolated from **[bpcaCu]$_2$**. The copper (II) complex (1.0 g, 1.3 mmol) and 0.500 g of Zn dust (6.5 mmol) were vigorously stirred for 1 h in a water (80 mL) and chloroform (50 mL) mixture at 23 °C. Once the organic layer was filtered to remove any zinc, it was dried over sodium sulfate and evaporated to dryness to give slightly colored solids. Colorless prisms of 3·Hbpca-1,4-dioxane were obtained by recrystallization of the residue from hot 1,4-dioxane solution. This compound was filtered and dried *in vacuo* to give white powder of **Hbpca** (yield ~70 %). ^{1}H NMR (400 MHz, chloroform-*d*): δ 8.55 (d, J = 7.8, 2H), 8.12 (d, J = 4.5, 2H), 7.91 (t, J = 7.6, 2H), 7.32 (t, J = 4.6, 2H), 1.72 (s, 1H).

REFERENCES

(1) Crabtree, R. H. *J. Chem. Soc., Dalton Trans.* **2001**, 2437.

(2) Howard, J. B.; Rees, D. C. *Chem. Rev. (Washington, D. C.)* **1996**, *96*, 2965.

(3) Lipscomb, J. D. *Annu. Rev. Microbiol.* **1994**, *48*, 371.

(4) Ruettinger, W.; Dismukes, G. C. *Chem. Rev. (Washington, D. C.)* **1997**, *97*, 1.

(5) Siegbahn, P. E. M.; Blomberg, M. R. A. *Chem. Rev. (Washington, D. C.)* **2000**, *100*, 421.

(6) Smith, D. A.; Ackland, M. J.; Jones, B. C. *Drug Discovery Today* **1997**, *2*, 406.

(7) Groves, J. T. *J. Inorg. Biochem.* **2006**, *100*, 434.

(8) Hlavica, P. *Eur. J. Biochem.* **2004**, *271*, 4335.

(9) Marcos, D.; Folgado, J. V.; Beltran-Porter, D.; Do, P.-G. M. T.; Pulcinelli, S. H.; De, A.-S. R. H. *Polyhedron* **1990**, *9*, 2699.

(10) Wocadlo, S.; Massa, W.; Folgado, J.-V. *Inorg. Chim. Acta* **1993**, *207*, 199.

(11) Davidson, R. B.; Sienerth, K. D.; American Chemical Society: 2013, p INOR.

(12) Kajiwara, T.; Sensui, R.; Noguchi, T.; Kamiyama, A.; Ito, T. *Inorg. Chim. Acta* **2002**, *337*, 299.

(13) Kamiyama, A.; Noguchi, T.; Kajiwara, T.; Ito, T. *Inorg. Chem.* **2002**, *41*, 507.

(14) Marcos, D.; Martinez-Manez, R.; Folgado, J. V.; Beltran-Porter, A.; Beltran-Porter, D.; Fuertes, A. *Inorg. Chim. Acta* **1989**, *159*, 11.

(15) Lescoueezec, R.; Marinescu, G.; Vaissermann, J.; Lloret, F.; Faus, J.; Andruh, M.; Julve, M. *Inorg. Chim. Acta* **2003**, *350*, 131.

(16) Bell, Z. R.; Motson, G. R.; Jeffery, J. C.; McCleverty, J. A.; Ward, M. D. *Polyhedron* **2001**, *20*, 2045.

(17) Fife, W. K. *J. Org. Chem.* **1983**, *48*, 1375.

(18) Kajiwara, T.; Ito, T. *J. Chem. Soc., Dalton Trans.* **1998**, 3351.

(19) Paul, P.; Tyagi, B.; Bilakhiya, A. K.; Bhadbhade, M. M.; Suresh, E. *J. Chem. Soc., Dalton Trans.* **1999**, 2009.

(20) Paul, P.; Tyagi, B.; Bilakhiya, A. K.; Bhadbhade, M. M.; Suresh, E.; Ramachandraiah, G. *Inorg. Chem.* **1998**, *37*, 5733.

(21) Frazier, B. A.; Bartholomew, E. R.; Wolczanski, P. T.; DeBeer, S.; Santiago-Berrios, M. e.; Abruna, H. D.; Lobkovsky, E. B.; Bart, S. C.; Mossin, S.; Meyer, K.; Cundari, T. R. *Inorg. Chem.* **2011**, *50*, 12414.

(22) Case, F. H.; Koft, E. *J. Am. Chem. Soc.* **1959**, *81*, 905.

(23) Andersen, R. A.; Faegri, K., Jr.; Green, J. C.; Haaland, A.; Lappert, M. F.; Leung, W. P.; Rypdal, K. *Inorg. Chem.* **1988**, *27*, 1782.

(24) Olmstead, M. M.; Power, P. P.; Shoner, S. C. *Inorg. Chem.* **1991**, *30*, 2547.

CHAPTER 5

SYNTHESIS OF BINUCLEATING N,N'-DIARYLIMINE, $^{DIPP}N_2$(INDIGO), AND REACTIVITY WITH FIRST-ROW TRANSITION METALS

I. Introduction

Hydrogen atom transfer (HAT) is one of the most fundamental chemical reactions (Eq 5.1), and is defined as the concerted transfer of a proton and an electron, a hydrogen atom, in a single step. In HAT, the proton and electron are abstracted from one substrate and transferred to a single product. Proton-coupled electron-transfer (PCET) reactions are one way an HAT can take place, while others involve separation of the proton and electron.[1-5]

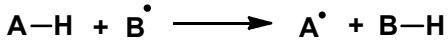

(5.1)

Chapter 4 introduced an idea for the design and synthesis of first-row transition metal complexes that may be used as catalysts for RH activation. In the absence of successful syntheses of soluble **bpca** ligands, other ligand platforms were considered with similar H-atom transfer goals in mind. **Indigo** (2,2'-Bis(2,3-dihydro-3-oxoindolylidne)), an organic compound used as a dye, contains a carbonyl-amine backbone functionality that is hypothesized to be advantageous in the RH activation schemes proposed in Chapter 4, and for other HAT reactions.

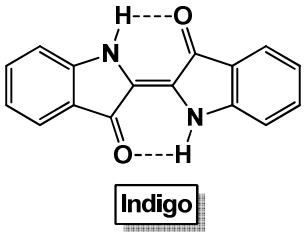

Figure 5.1 Structure of (2,2'-Bis(2,3-dihydro-3-oxoindolylidne)), **indigo.**

Indigo was first synthesized by Baeyer[6-13] who prepared it from isatin in 1870. The production of **indigo** for commercial use was based on a procedure developed by Heumann,[14,15] however a more practical synthesis, created by Pfleger, was implemented shortly thereafter (Eq 5.2).[16] Treatment of *N*-phenylglycine with a molten mixture of sodium hydroxide, potassium hydroxide and sodium amide, generates indoxyl, which is subsequently oxidized in air to form **indigo**.

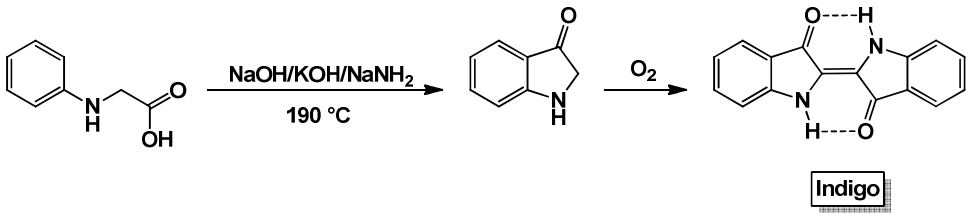

(5.2)

Indigo is a valuable dye, in large part because of its insolubility in most common solvents, however there are some soluble derivatives known. Reduction of **indigo** results in the formation of white indigo (leuco-indigo),[17,18] and treatment with sulfuric acid converts **indigo** into a blue-green derivative called indigo-carmine (sulfonated indigo), shown in Figure 5.2.[19]

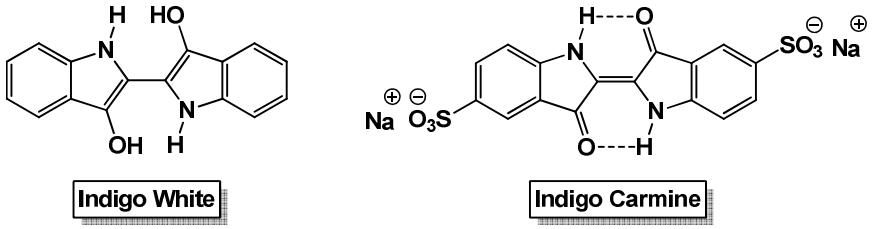

Figure 5.2. Soluble indigo derivatives

Recently, Hicks and co-workers reported the synthesis of binucleating N,N'-diarylimines, or "**Nindigo**," which consist of two coupled iminoindole units (Figure 5.3).[20] These indigo derivatives contain two β-diketiminate motifs that are connected through a central C=C bridge, and similar to other β-diketiminates, the imine substituents of **Nindigo** can be easily modified.

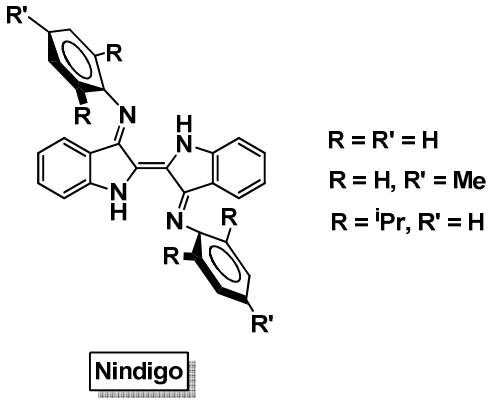

Figure 5.3. Reported **Nindigo** ligands

Hicks et. al. also showed when **Nindigo** is coordinated to Pd(II) (Figure 5.4), the binuclear complex exhibits several electrochemical features that are **Nindigo** ligand-based.[20-22]

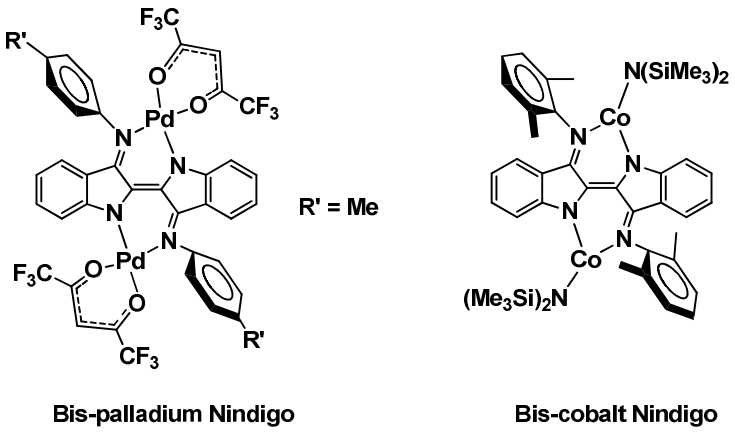

Figure 5.4. Bis-palladium and Bis-cobalt Nindigo complexes.

Caulton and coworkers also took the opportunity to look at the reactivity of **Nindigo** ligands with redox active metals, and recently published the synthesis of a bimetallic **Nindigo** cobalt complex, shown in Figure 5.4.[23] They concluded **Nindigo** is not only a β-diketiminate variant, but also exhibits rich redox chemistry within its indigo-based scaffold. The **Nindigo** system has the capacity for useful redox chemistry, as shown by both Hicks and Caulton, capable of transferring four electrons in its tetraanionic form.[21-23]

While the redox properties of **Nindigo** are undoubtedly important, it also possesses a desirable architecture for H-atom transfer. Jim Mayer has demonstrated proton-coupled electron transfer (PCET) reactions with his $Fe(II)H_2(bim)^2$ and $Fe(II)H_2(bip)^2$ systems (Figure 5.5), which transfer a proton from the ligand and an electron via iron oxidation.[23]

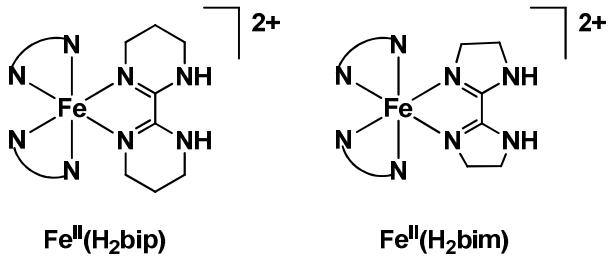

Figure 5.5. Fe(II)H_2bip and Fe(II)H_2(bim) complexes

Goals for this project included the synthesis of **Nindigo**-coordinated first-row transition metal complexes for H-atom transfer, similar to HAT reactions shown my Mayer. These compounds may also have potential for RH activation with X_2 to generate RX and HX, as discussed in Chapter 4.

II. Results and Discussion

A. Ligand Synthesis

The bis-diisopropylphenyl Nindigo ligand, **(^{dipp}N)$_2$indigo,** was synthesized according to literature procedures with slight modifications.[20] Condensation of indigo with 2 equivs of diispropylphenyl aniline generated two β-diketiminate-type coordination environments in the resulting indigo bis(arylimine) structure, shown in Scheme 5.1. Due to the inactivity of the ketone functionalities toward condensation by traditional routes, $TiCl_4$ was used to initiate reactivity.[20] A solution of $TiCl_4$ was added to a heated solution of diisopropyl aniline and DABCO (1,4-diazabicyclo[2.2.2]octane), followed by the addition of indigo. Upon heating to reflux for 24 hours, an intense purple solution was generated, and the insoluble, unreacted indigo was removed via hot filtration. Incomplete conversion resulted in residual aniline and the mono-diisopropyl Nindigo product, **(^{dipp}N)indigo.** Separation attempts

using *n*-butanol, as stated in the literature procedure,[20] were tedious and time-consuming, thus an easier purification process was sought. The crude purple solid was repeatedly dissolved in small volumes of hot methanol and filtered, leaving a purple powder, **(^{dipp}N)$_2$indigo**, in 20 % yield.

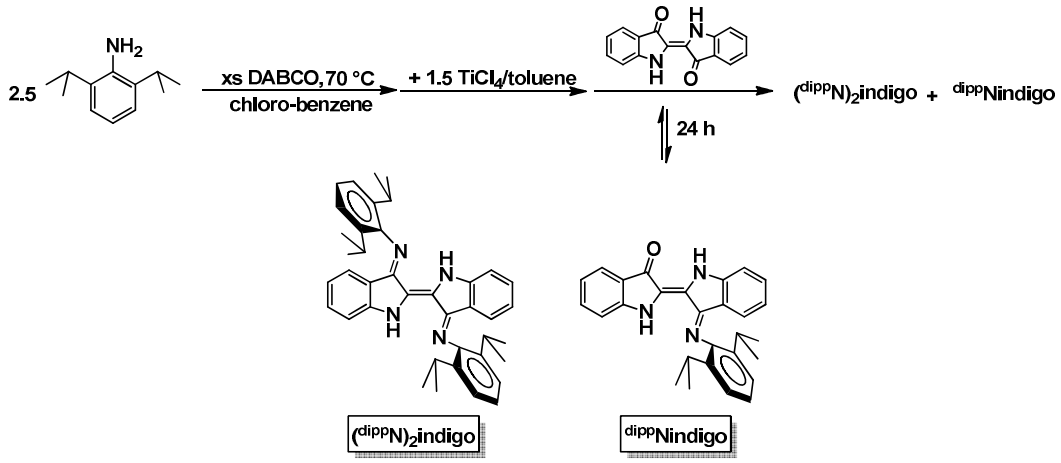

Scheme 5.1. Synthesis of **(^{dipp}N)$_2$indigo** and **^{dipp}Nindigo**

Deprotonation of **(^{dipp}N)$_2$indigo** to generate the lithium salt would present an opportunity for reactivity with MX_2 sources via salt metatheses. Treatment of **(^{dipp}N)$_2$indigo** with LiHMDS successfully generated **Li(^{dipp}N)$_2$indigo** as a blue-green solid in high yields.

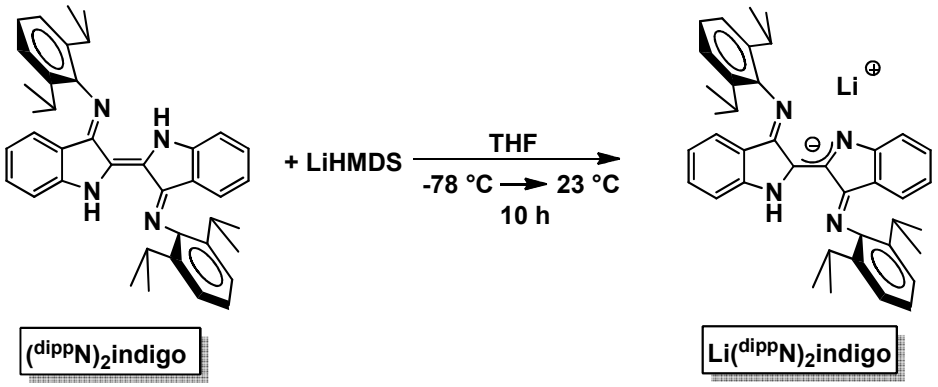

(5.3)

B. Reactivity of Nindigo ligands with Iron

Initially, coordination to first-row transition metals by one or two **(^{dipp}N)$_2$indigo** ligands was targeted, and first attempts toward desired products were made by treatment of Fe{N(TMS)$_2$}$_2$THF with an equivalent of **(^{dipp}N)$_2$indigo**. Ideally, deprotonation of the ligand to lose the amine would generate the mono-ligand metal amide complex (Scheme 5.2).

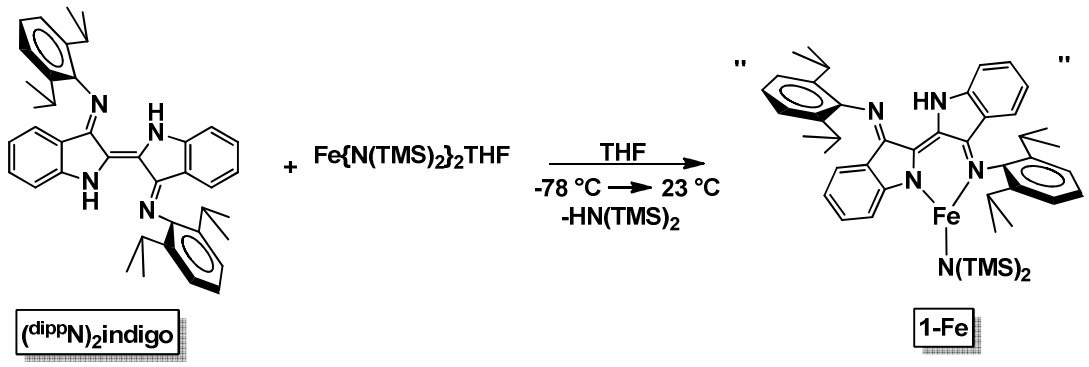

Scheme 5.2. Reactivity of **(^{dipp}N)$_2$indigo** with Fe{N(TMS)$_2$}$_2$THF.

Addition of **(^{dipp}N)$_2$indigo** to Fe{N(TMS)$_2$}$_2$THF resulted in the formation of an intense teal solution that turned dark green over the course of 6 h. The only observable resonances in the ^{1}H NMR spectrum were those associated with H{N(TMS)$_2$} and solvent, indicating a deprotonation from the ligand had occurred. Removal of solvent and residual HN(TMS)$_2$ resulted in a dark blue/purple solid, which was potentially the mono-Nindigo iron complex, **1-Fe**. Scheme 5.2 shows one possible product, but there are a few plausible products, illustrated in Figure 5.6. Due to a lack of informative resonances within the ^{1}H NMR spectrum, the product remains unknown without x-ray or elemental analysis.

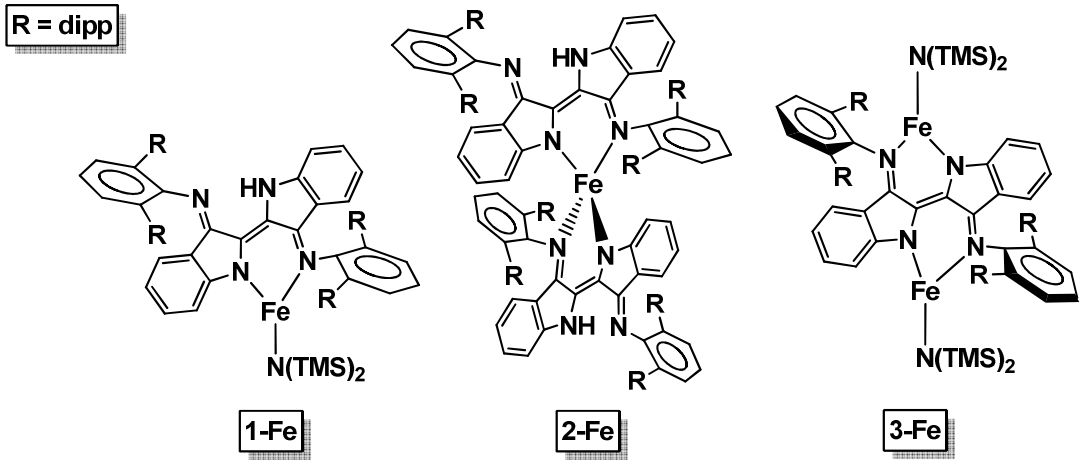

Figure 5.6. Possible reaction products from reaction shown in Scheme 5.2

.

It was plausible two equivalents of **(^{dipp}N)$_2$indigo** could coordinate to iron as shown in Figure 5.6 (**2-Fe)**, and to test this hypothesis, Fe{N(TMS)$_2$}$_2$THF was treated with two equivs of **(^{dipp}N)$_2$indigo.** The resulting dark green solution gave a ^{1}H NMR spectrum that indicated the presence of many products; numerous resonances were observed, spanning the paramagnetic region as well as the diamagnetic region. If two ligands coordinated to an iron center (**2-Fe)**, two more ligand sites would be left open to coordination by two more equivs of iron; it is possible oligomeric chains were formed, generating the complicated ^{1}H NMR spectra observed.

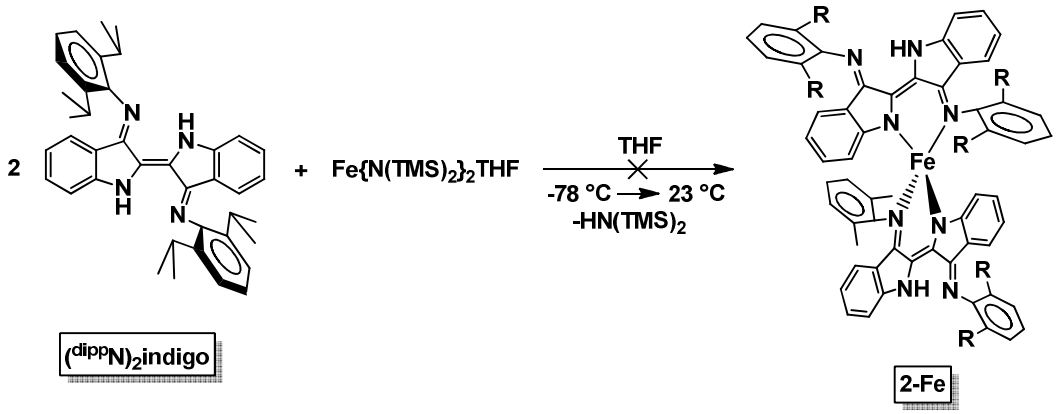

Scheme 5.3. Attempted synthesis of **2-Fe**.

Similar results were observed upon the attempted salt metatheses of $FeCl_2$ with one and two equivs **Li(**^{dipp}**N)$_2$indigo**. Addition of one equiv of **Li(**^{dipp}**N)$_2$indigo** with $FeCl_2$ resulted in a bright green solution with very few resonances observed in the ^{1}H NMR spectrum, which were identified as solvent and very minor amounts of **Li(**^{dipp}**N)$_2$indigo.** Treatment of two equivs of **Li(**^{dipp}**N)$_2$indigo** with $FeCl_2$ resulted in a similarly chaotic ^{1}H NMR spectrum as observed in the reaction of two equivs of **(**^{dipp}**N)$_2$indigo** with Fe{N(TMS)$_2$}$_2$THF.

A potentially advantageous product of the low-yielding ligand synthesis, illustrated in Scheme 5.1, is the mono-condensation product, ^{dipp}**Nindigo.** Since this product was cleanly separated from the reaction mixture, it was also investigated as a potential ligand framework for RH activation. If binding to the metal were to occur through the imine and amine nitrogens, the backbone would still be open for the stabilizing H-bonding interaction as a result of RH activation. Treatment of ^{dipp}**Nindigo** with Fe{N(TMS)$_2$}$_2$THF resulted in a blue/green solution that gave a very

complicated ^{1}H NMR spectrum, containing resonances consistent with a multitude of products.

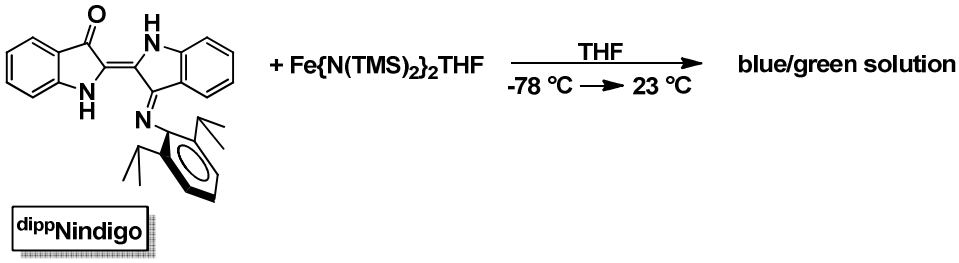

Scheme 5.4. Reaction of ^{dipp}**Nindigo** with Iron.

It is plausible this ligand is prone to generate similar multinuclear chains though binding at the nitrogen and oxygen as was reported in **bpca** chemistry.[24-27]

C. Reactivity of Nindigo ligands with nickel.

Coordination of nickel by various **Nindigo** ligands was targeted by similar methods as described in section **B**. Addition of two equivs of **(^{dipp}N)$_2$indigo** to an equiv of [Ni(NPh$_2$)$_2$]$_2$THF generated a dark green solution that turned navy blue over the course of 12 hours. The proton NMR spectrum revealed the presence of free diphenylamine and numerous resonances in the diamagnetic and paramagnetic regions. While reactivity was observed, as indicated by the production of free amine, it was clear the reaction did not proceed cleanly to afford an isolable product.

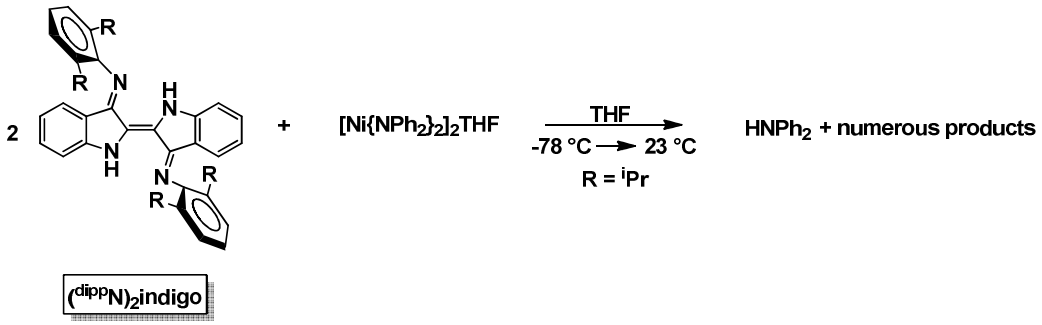

Scheme 5.5. Reaction of one equiv of of **(^{dipp}N)$_2$indigo** per nickel center.

The reaction of one equiv of **(^{dipp}N)$_2$indigo** with $[Ni(NPh_2)_2]_2THF$ resulted in the formation of a dark blue/green solution, and ^{1}H NMR spectroscopy revealed the presence of $HNPh_2$ upon deprotonation of the ligand. A stark contrast between the reactions with one and two equivs of nickel was observed. With two equivs of nickel, very few resonances other than those belonging to free amine and solvent were noted. Upon expansion of the spectrum baseline, ~ 12 resonances in the paramagnetic region were observed. If these resonances belonged to a single product, it was either formed in low concentration, or was not soluble in benzene-d_6. There is literature precedent for coordination of **Nindigo** by two metal centers, as illustrated in Figure 5.6, thus formation of a bis-**(^{dipp}N)$_2$indigo** nickel species (**2-Ni**) is quite plausible.

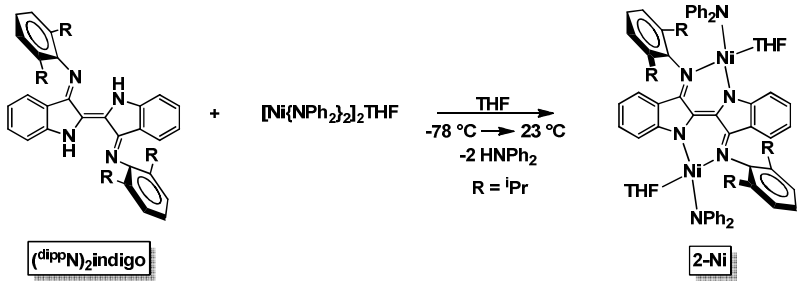

Scheme 5.6. Tentative formulation of (**2-Ni)** in the reaction of **(^{dipp}N)$_2$indigo** with $[Ni(NPh_2)_2]_2THF$.

D. Reactivity of Nindigo with Cobalt.

In an NMR-tube experiment, treatment of **(^{dipp}N)$_2$indigo** with Co{N(TMS)$_2$}$_2$THF in benzene-d_6 produced a brown solution with concomitant solid formation, which was consistent with reports of a previously made **Nindigo**-coordinated di-nuclear cobalt complex.[23] The ^{1}H NMR spectrum revealed the presence of HN(TMS)$_2$ and solvent, which indicated a deprotonation had occurred, however the insolubility of the product made confirmation difficult. It seemed likely that at least one product in this reaction was the dinuclear species, **3-Co**, given the reported reactivity with ligands of this type.[23]

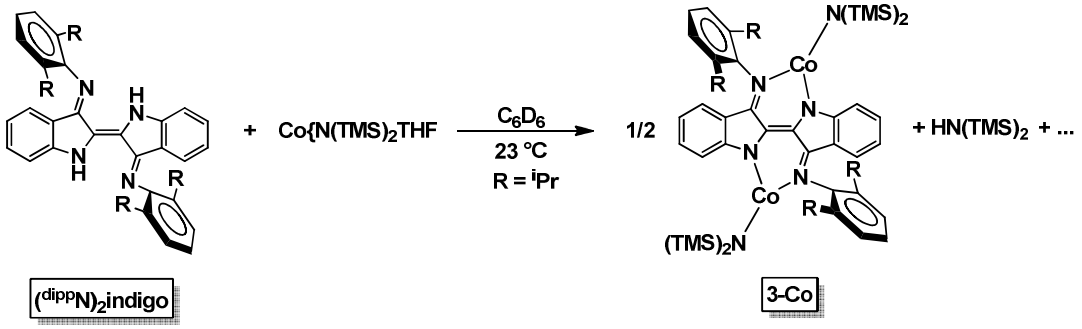

Scheme 5.7. Possible product formed (**3-Co)** in the reaction of of **(^{dipp}N)$_2$indigo** with Co{N(TMS)$_2$}$_2$THF

The reaction of two equivs of **(^{dipp}N)$_2$indigo** with only one equiv of Co{N(TMS)$_2$}$_2$THF resulted in a complicated ^{1}H NMR spectrum, similar to that observed in the analogous reaction with iron. Reactivity of $CoCl_2$ with one and two equivs of the anionic ligand, **Li(^{dipp}N)$_2$indigo,** resulted in similarly unsatisfying observations. Treatment of one equiv of **Li(^{dipp}N)$_2$indigo** with $CoCl_2$ in THF generated a brilliant green solution, and the ^{1}H NMR spectrum revealed the presence

of solvent and a broad singlet at δ = 8.61. The paramagnetic region displayed another 8 resonances that may correlate to a product in low concentration or with limited solubility, which is consistent with observations reported by Caulton.[23]

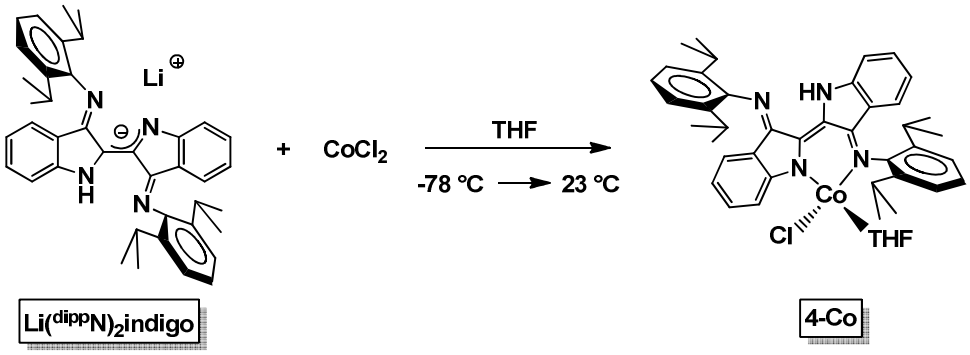

Scheme 5.8. Plausible product (**4-Co)** generated from **Li(**^{dipp}**N)$_2$indigo** and $CoCl_2$

Two equivs of **Li(**^{dipp}**N)$_2$indigo** reacted with $CoCl_2$ to generate another green solution, however the ^{1}H NMR spectrum displayed numerous resonances in the paramagnetic and diamagnetic regions, resembling the results of previous attempts to coordinate two ligands around a metal center.

III. Conclusion

Synthesis of **Nindigo**-coordinated first-row transition metals was targeted by treatment of **(**^{dipp}**N)$_2$indigo** and **Li(**^{dipp}**N)$_2$indigo** with $[M(NR_2)_2]_x$THF (M = Fe, Co; R = $SiMe_3$; x = 1; M = Ni; R = Ph; x = 2). The most promising attempts involved one equiv of **Nindigo** with one or two equivs of metal, while any attempts toward synthesis of a bis-**Nindigo** metal complex resulted in the formation of numerous, unidentifiable products. These observations are consistent with reports by Hicks and

Caulton, who note that **Nindigo** ligands tend to form bimetallic, electron-rich, low-coordinate complexes.[21-23]

Hicks reported failure to generate isolable binuclear species with bulkier **Nindigo** species (R = Me, ^{i}Pr in Fig 5.3), and without crystallographic evidence, it is unknown whether or not **[(^{dipp}N)$_2$indigo]$_2$M** species were generated. It is possible that the bulky substituent, diispropylphenyl, led to a mono-ligand metal complex in some cases. Attempts toward isolation and crystallographic analyses are ongoing, and upon confirmed isolation and characterization of **[(^{dipp}N)$_2$indigo]$_x$M** complexes, H-atom transfer reactions will be examined.

IV. Experimental

A. General Considerations

All reactions and manipulations were carried out under an argon atmosphere using standard Schlenk or glovebox techniques unless stated otherwise. Chlorobenzene was dried over 4 Å sieves and stored under nitrogen. Indigo (95%) was used as received from commercial sources (Aldrich). Diisopropylaniline was distilled prior to use, and DABCO (99%) was sublimed prior to use. Cr{N(TMS)$_2$}(THF)$_2$,[28] Co{N(TMS)$_2$}$_2$THF,[29,30] Fe{N(TMS)$_2$}$_2$(THF),[31] and [Ni{N(Ph)$_2$}$_2$]$_2$THF[32] were prepared according to published procedures. Methylene chloride-d_2 was distilled from and stored over CaH_2. Benzene-d_6 was dried over sodium and stored over 4 Å sieves under nitrogen. All other reagents were commercially available and used without further purification.

^{1}H and ^{13}C{1H}NMR spectra were obtained using Mercury-300, and Inova-400 spectrometers, and chemical shifts are reported relative to benzene-d_6 (^{1}H δ 7.16; ^{13}C{1H} δ 128.39), chloroform-*d* (^{1}H δ 7.16; ^{13}C{1H} δ 128.39) and methylene chloride-d_2 (^{1}H δ 7.16; ^{13}C{1H} δ 128.39).

B. Procedures

1. Bis-diisopropylphenyl Nindigo, (^{dipp}N)$_2$indigo

A 1M toluene solution of $TiCl_4$ (11.4 mL, 11.4 mmol) was added dropwise to a stirred chlorobenzene (75 mL) solution containing DABCO (5.13, 45.6 mmol) and 2,6-diisopropylaniline (1.78 g, 19.06 mmol) at 70 °C. Indigo (2.0 g, 7.62 mmol) was then added under argon and the reaction mixture was heated to reflux for 24 hours. The reaction mixture was filtered hot, allowed to cool, and washed with ether until the washings were colorless. The combined filtrates were evaporated and the crude product was washed with water and ethanol to remove remaining DABCO and diisopropyl aniline. The remaining dark purple solid was suspended in methanol, heated and filtered hot (15 mL x 4) to give 0.800 g (18.1 %) of **3d** as a purple powder. The filtrated from the repeated methanol filtrations contained 0.600 g **(^{dipp}N)indigo** (18.7 %). **(^{dipp}N)$_2$indigo** ^{1}H NMR (CD_2Cl_2): δ 1.03 (d, *J* = 6.9, 12H), 1.22 (d, *J* = 6.9, 12H), 3.11 (septet, *J* = 6.9, 4H), 6.37 (t, *J* = 0.93, 1H), 6.40 (t, *J* = 0.93, 1H), 6.57 (td, *J* = 7.6, 1.0, 2H), 7.06 (t, *J* = 0.93, 1H), 7.08 (t, *J* = 0.93, 1H), 7.22 (td, *J* = 7.7, 1.0, 2H), 7.28 (s, 6H), 9.92 (s, 2H). ^{1}H NMR ($CDCl_3$): δ 1.02 (d, *J* = 5.6, 12H), 1.22 (d, *J* = 5.6, 12H), 3.10 (septet, *J* = 6.9, 4H), 6.38 (d, *J* = 7.3, 2H), 6.55 (t, *J* = 7.3, 2H), 7.02 (d, *J* = 8.2, 2H), 7.18 (t, *J* = 6.9, 2H), 7.25 (br s, 4H) 9.88 (s, 2H).^{13}C{1H} NMR

(CD_2Cl_2): δ = 23.6, 24.1, 29.0, 113.5, 119.3, 120.2, 124.0, 125.7, 125.8, 128.5, 132.1, 139.2, 145.5, 150.2, 159.1. **(^{dipp}N)indigo** ^{1}H NMR ($CDCl_3$): δ 0.97 (d, *J* =6.8, 6H), 1.19 (d, *J* =6.8, 6H), 2.90 (septet, *J* = 6.6, 2H), 6.37 (d, *J* =7.8, 1H), 6.61 (t, *J* = 7.7, 1H), 6.95 (t, *J* = 7.5, 1H), 7.00 (d, *J* = 8.0, 1H), 7.04 (d, *J* = 8.0, 1H), 7.25 (br s, 4 H), 7.44 (t, *J* = 7.6, 1H), 7.8 (d, *J* = 7.7, 1H), 9.26 (s, 1H), 9.60 (s, 1H).

2. Li(bis-diisopropylphenyl Nindigo), Li(^{dipp}N)$_2$indigo

To a 10 mL round-bottom flask charged with 0.100 g (0.238 mmol) of **(^{dipp}N)$_2$indigo** and 0.040 g (0.238 mmol) LiHMDS, was vacuum transferred ~5 mL THF at -78 °C. The reaction was stirred at -78 °C and slowly allowed to warm to 23 °C. After stirring for 1 d, the bright green solution was filtered and removed of all volatiles *in vacuo*. The sticky green solid was triturated with hexanes (3 X 5 mL) to remove excess THF and HMDS to leave a green metallic solid, **Li(^{dipp}N)$_2$indigo,** in 79% yield (0.080 g). ^{1}H NMR (C_6D_6): δ 1.11 (d, *J* = 6.4, 12H), 1.21 (d, *J* = 6.4, 12H), 3.30 (septet, *J* = 6.7, 4H), 6.56 (d, *J* = 8.2, 2H), 6.69 (d, *J* = 8.1, 2H), 6.79 (d, *J* = 7.6, 2H), 6.91 (t, *J* = 7.5, 2H), 6.95 (d, *J* = 7.8, 2H), 7.25 (s, 4H), 11.59 (s, 1H).

3. "1-Fe"

To a 10 mL round-bottom charged with 0.030 g (0.052 mmol) **(^{dipp}N)$_2$indigo** and 0.024 g Fe{N(TMS)$_2$}$_2$THF was added ~5 mL benzene under a nitrogen atmosphere. The intense teal solution was allowed to stir at 23 °C for 1 d. All volatiles were removed *in vacuo,* and triturated with hexanes (3 X 5mL) to remove any residual HMDS. A dark blue/purple solid was isolated (0.040 g) which did not result in observable ^{1}H NMR spectra resonances.

4. "2-Ni"

To a 10 mL round-bottom charged with 0.030 g (0.052 mmol) **(^{dipp}N)$_2$indigo** and 0.041 g (0.052 mmol) [Ni{N(TMS)$_2$}$_2$]$_2$THF was added ~5 mL benzene under a nitrogen atmosphere. The dark blue solution was allowed to stir at 23 °C for 1 d. All volatiles were removed *in vacuo*, and triturated with hexanes (3 X 5mL) to remove any residual HMDS. A dark blue/purple solid was isolated (0.025 g) which did not result in identifiable ^{1}H NMR spectra resonances.

5. "3-Co"

To a J-Young NMR tube was added 0.016 g (0.035 mmol) **(^{dipp}N)$_2$indigo** and 0.020 g (0.035 mmol) Co{N(TMS)$_2$}$_2$THF. Addition of 0.6 mL benzene-d_6 produced a brown solution with concomitant solid formation. No ^{1}H NMR spectral resonances were observed.

6. "4-Co"

To a 10 mL round-bottom flask was added 0.020 g (0.048 mmol) **Li(^{dipp}N)$_2$indigo** and 0.006 g (0.048 mmol) $CoCl_2$. THF (~5 mL) was vacuum transferred at -78 °C, generating a brilliant green solution, and the reaction mixture was allowed to slowly warm to 23 °C. After 1 d, all volatiles were removed *in vacuo*. The crude solid was filtered and washed with benzene (3 X 5 mL) to remove LiCl generated. The solvent was removed *in vacuo* to leave a dark green solid. ^{1}H NMR (C_6D_6): δ -22.40, -17.45, -5.82, -1.90, -1.27, 8.61, 18.59, 20.37.

REFERENCES

(1) Mayer, J. M. *Annu. Rev. Phys. Chem.* **2004**, *55*, 363.

(2) Mader, E. A.; Davidson, E. R.; Mayer, J. M. *J. Am. Chem. Soc*. **2007**, *129*, 5153.

(3) Mayer, J. M.; Mader, E. A.; Roth, J. P.; Bryant, J. R.; Matsuo, T.; Dehestani, A.; Bales, B. C.; Watson, E. J.; Osako, T.; Valliant-Saunders, K.; Lam, W. H.; Hrovat, D. A.; Borden, W. T.; Davidson, E. R. *J. Mol. Catal. A: Chem.* **2006**, *251*, 24.

(4) Mayer, J. M.; Rhile, I. J. *Biochim. Biophys. Acta, Bioenerg.* **2004**, *1655*, 51.

(5) Mayer, J. M.; Rhile, I. J.; Larsen, F. B.; Mader, E. A.; Markle, T. F.; Dipasquale, A. G. *Photosynth. Res.* **2006**, *87*, 21.

(6) Clark, R. J. H.; Cooksey, C. J.; Daniels, M. A. M.; Withnall, R. *Endeavour* **1993**, *17*, 191.

(7) Italia, A. *Tinctoria* **1996**, *93*, 54.

(8) Mellor, C. M. *Color Eng.* **1969**, *7*, 50.

(9) Morita, K. *Kagaku (Kyoto)* **1969**, *24*, 156.

(10) Potsch, W. R. *Melliand Textilber.* **2002**, *83*, E35.

(11) Setsune, J. *Yuki Gosei Kagaku Kyokaishi* **1988**, *46*, 681.

(12) Shinozaki, T. *Sen'i* **1977**, *29*, 145.

(13) Van, S. J. F. *Spectrum (Pretoria)* **1991**, *29*, 15.

(14) Heumann, K. *Ber.* **1890,** *23*, 3043.

(15) Heumann, K. *J. Prakt. Chem.*, **1891,** *43*, 111.

(16) Pfleger, J.; Deutsche Gold & Silber Scheide Anstalt Vorm. Roessler, Germany . 1901.

(17) Blackburn, R. S.; Bechtold, T.; John, P. *Color. Technol.* **2009**, *125*, 193.

(18) Sainsbury, M.; Pt. B ed.; Elsevier: 1997; Vol. 4, p 361.

(19) Quintero, L.; Cardona, S. *Dyna (Medellin, Colomb.)* **2010**, *162*, 371.

(20) Oakley, S. R.; Nawn, G.; Waldie, K. M.; MacInnis, T. D.; Patrick, B. O.; Hicks, R. G. *Chem. Commun. (Cambridge, U. K.)* **2010**, *46*, 6753.

(21) Nawn, G.; Oakley, S. R.; Majewski, M. B.; McDonald, R.; Patrick, B. O.; Hicks, R. G. *Chem. Sci.* **2013**, *4*, 612.

(22) Nawn, G.; Waldie, K. M.; Oakley, S. R.; Peters, B. D.; Mandel, D.; Patrick, B. O.; McDonald, R.; Hicks, R. G. *Inorg. Chem.* **2011**, *50*, 9826.

(23) Fortier, S.; Gonzalez-del, M. O.; Chen, C.-H.; Pink, M.; Le, R. J. J.; Murugesu, M.; Mindiola, D. J.; Caulton, K. G. *Chem. Commun. (Cambridge, U. K.)* **2012**, *48*, 11082.

(24) Kajiwara, T.; Ito, T. *J. Chem. Soc., Dalton Trans.* **1998**, 3351.

(25) Kamiyama, A.; Noguchi, T.; Kajiwara, T.; Ito, T. *Angew. Chem., Int. Ed.* **2000**, *39*, 3130.

(26) Kamiyama, A.; Noguchi, T.; Kajiwara, T.; Ito, T. *Inorg. Chem.* **2002**, *41*, 507.

(27) Yeap, G.-Y.; Ha, S.-T.; Lim, P.-L.; Boey, P.-L.; Mahmood, W. A.; Ito, M.; Sanehisa, S. *Mol. Cryst. Liq. Cryst.* **2004**, *423*, 73.

(28) Bradley, D. C.; Hursthouse, M. B.; Newing, C. W.; Welch, A. J. *J. Chem. Soc., Chem. Commun.* **1972**, 567.

(29) Andersen, R. A.; Faegri, K., Jr.; Green, J. C.; Haaland, A.; Lappert, M. F.; Leung, W. P.; Rypdal, K. *Inorg. Chem.* **1988**, *27*, 1782.

(30) Buerger, H.; Wannagat, U. *Monatsh. Chem.* **1963**, *94*, 1007.

(31) Olmstead, M. M.; Power, P. P.; Shoner, S. C. *Inorg. Chem.* **1991**, *30*, 2547.

(32) Hope, H.; Olmstead, M. M.; Murray, B. D.; Power, P. P. *J. Am. Chem. Soc.* **1985**, *107*, 712.